AFWAL-TR-81-3130

AD-A127378

DEVELOPMENT FEASIBILITY OF MISSILE DATCOM

corporation

MCDONNELL DOUGLAS ASTRONAUTICS COMPANY-ST. LOUIS DIVISION
Saint Louis, Missouri 63166 (314) 232-0232

OCTOBER, 1981
Final Report for Period May, 1980 — May, 1981

APPROVED FOR PUBLIC RELEASE; DISTRIBUTION UNLIMITED.

FLIGHT DYNAMICS LABORATORY
AIR FORCE WRIGHT AERONAUTICAL LABORATORIES
AIR FORCE SYSTEMS COMMAND
WRIGHT-PATTERSON AIR FORCE BASE, OHIO 45433

NOTICE

When government drawings, specifications, or other data are used for any purpose other than in connection with a definitely related government procurement operation, the United States Government thereby incurs no responsibility nor any obligation whatsoever; and the fact that the government may have formulated, furnished, or in any way supplied the said drawings, specifications, or other data, is not to be regarded by implication or otherwise as in any manner licensing the holder or any other person or corporation, or conveying any rights or permission to manufacture, use, or sell any patented invention that may in any way be related thereto.

This report has been reviewed by the Office of Public Affairs (ASD/PA) and is releasable to the National Technical Information Service (NTIS). At NTIS, it will be available to the general public, including foreign nations.

This technical report has been reviewed and is approved for publication.

J. E. Jenkins

J. E. JENKINS
Project Engineer
Flight Control Division

R. O. Anderson

R. O. ANDERSON, Chief
Control Dynamics Branch
Flight Control Division

FOR THE COMMANDER

H. Max Davis

H. MAX DAVIS
Assistant Chief
Flight Control Division

If your address has changed, if you wish to be removed from our mailing list, or if the addressee is no longer employed by your organization please notify AFWAL/FIGC, W-PAFB, OH 45433 to help us maintain a current mailing list.

Copies of this report should not be returned unless return is required by security considerations, contractual obligations, or notice on a specific document.

UNCLASSIFIED

SECURITY CLASSIFICATION OF THIS PAGE (When Data Entered)

REPORT DOCUMENTATION PAGE		READ INSTRUCTIONS BEFORE COMPLETING FORM
1. REPORT NUMBER AFWAL-TR-81-3130	2. GOVT ACCESSION NO.	3. RECIPIENT'S CATALOG NUMBER
4. TITLE (and Subtitle) DEVELOPMENT FEASIBILITY OF MISSILE DATCOM		5. TYPE OF REPORT & PERIOD COVERED May 1980 to May 1981
		6. PERFORMING ORG. REPORT NUMBER
7. AUTHOR(s) Steven R. Vukelich		8. CONTRACT OR GRANT NUMBER(s) F33615-80-C-3605
9. PERFORMING ORGANIZATION NAME AND ADDRESS McDonnell Douglas Astronautics Company-St. Louis P.O. Box 516 St. Louis, Missouri 63166		10. PROGRAM ELEMENT, PROJECT, TASK AREA & WORK UNIT NUMBERS P.E. 62201F Project No. 2403 05 24
11. CONTROLLING OFFICE NAME AND ADDRESS Flight Dynamics Lab (FIGC) AF Wright Aeronautical Laboratories Wright-Patterson Air Force Base, Ohio 45433		12. REPORT DATE October, 1981
		13. NUMBER OF PAGES 304
14. MONITORING AGENCY NAME & ADDRESS(if different from Controlling Office)		15. SECURITY CLASS. (of this report) Unclassified
		15a. DECLASSIFICATION/DOWNGRADING SCHEDULE

16. DISTRIBUTION STATEMENT (of this Report)

Approved for public release; distribution unlimited.

17. DISTRIBUTION STATEMENT (of the abstract entered in Block 20, if different from Report)

18. SUPPLEMENTARY NOTES

19. KEY WORDS (Continue on reverse side if necessary and identify by block number)

Missile Aerodynamics
Aerodynamic Stability
USAF Datcom
Aerodynamic Control

20. ABSTRACT (Continue on reverse side if necessary and identify by block number)

This report summarizes the methods available to predict the aerodynamic static, dynamic, and control characteristics of missiles. The methods selected for Missile Datcom development were based upon a criteria which included ease of use, accuracy, utility over a range of flight conditions and cost effective in their use.

DD FORM 1 JAN 73 1473 EDITION OF 1 NOV 65 IS OBSOLETE

UNCLASSIFIED

SECURITY CLASSIFICATION OF THIS PAGE (When Data Entered)

This report describes the methodology appropriate for the missile designer. An outline of a Missile Datcom handbook is proposed; an automated version is also recommended for development. Those areas presently lacking suitable methodologies are also highlighted.

FOREWORD

This report, "Development Feasibility of Missile Datcom", describes those methods recommended to calculate the static stability, control, and dynamic derivative characteristics of missile configurations. In addition, those areas which require additional methods development are identified.

This work was performed by the McDonnell Douglas Astronautics Company, Box 516, St. Louis, Missouri 63166, under contract number F33615-80-C-3605 with the Air Force Wright Aeronautical Laboratories, Wright-Patterson Air Force Base, Ohio, 45433. The subject contract was initiated under Air Force Flight Dynamics Laboratory Project 2403, Task 24030524 on 15 May 1980 and was effectively concluded in May, 1981. Mr. J. E. Jenkins, AFWAL/FIGC, was the Air Force Project Engineer for the study. Comments may be directed to him at (513) 255-4315, or in writing at the above address.

Copies of this report can be obtained from the National Technical Information Service (NTIS).

This report was submitted in 1981.

TABLE OF CONTENTS

LIST OF ILLUSTRATIONS

LIST OF ILLUSTRATIONS (CONTINUED)

LIST OF ILLUSTRATIONS (CONTINUED)

LIST OF ILLUSTRATIONS (CONTINUED)

LIST OF ILLUSTRATIONS (CONTINUED)

LIST OF TABLES

SECTION 1
INTRODUCTION

Timely design and analysis of missiles requires the use of rapid and accurate analytical procedures to determine their aerodynamic stability, control and drag characteristics. The most complete compendium of methods available is the USAF Stability and Control Datcom, Reference 1. Since it emphasizes aircraft configurations, it does not address the range of geometric and flight condition parameters unique to missiles, such as high angle of attack and bank angle. Although many aerodynamic methods are available in the literature for missile configurations, there is no collection of these techniques in a form suitable for efficient missile design.

This study did determine the feasibility of developing a Missile Datcom. Specifically, the four objectives of this study were as follows:

(a) Determine the range of geometric and flight conditions for which methodology should be specified.

(b) Determine a structure of a handbook and/or computer program which allows rapid and accurate use of available methodology in the missile design environment.

(c) Survey the literature for applicable methodology and determine those areas lacking in appropriate methods and needing further development.

(d) Assess the feasibility, or probability of success, of developing a Missile Datcom and recommend a handbook and/or computer program format.

This report addresses each of these objectives. Throughout the report reference is made to the conceptual, preliminary and point design phases of missile development. The definitions of these phases are as follows:

Conceptual Design - The design process during which the proof of concept is demonstrated. This task demonstrates the feasibility of designing a missile system which performs the tasks required, such as payload carry capability, range, speed and altitude.

Preliminary Design - This stage of the design process explores several variations of a configuration. Trade studies are identified, individual components, such as nose shape and wing type, are analyzed and the impact on system design due to configuration aerodynamics is determined.

Point Design - This is the last major step in the design process prior to hardware development. A baseline configuration is selected and performance characteristics determined. Perturbations to the design are often performed to accommodate changes in subsystem design or to provide an extension of capability.

To be useful, Missile Datcom should apply to all three design phases, but emphasize conceptual and preliminary design.

Since the missile design process is often of shorter duration than that for aircraft, quick and accurate methods are needed. Automation of the techniques fulfills the quickness requirement. However, low analysis costs are also important. These costs include the man-hours required to set-up, execute and interpret the results of the program. The advantage of sophisticated accurate theoretical methodology must be weighed against the costs required to obtain the results. Determining the proper choice between accuracy, efficiency and cost was a goal of this study.

An automated program does not provide the aerodynamicist with the necessary background or methods choices available. A thorough user's manual, or a handbook similar to the USAF Stability and Control Datcom, will supply this additional, yet essential information. Since methods more suitable to accurate design may be difficult to employ in a handbook technique, the choice between alternate methodology and generation of computer-based design charts was also explored.

The methodology collected was assessed based upon the criteria given in Table 1. Ideally, the methods selected should be theoretically based, have minimal parameter inputs, be accurate, and cover a wide range of configuration variables and flight conditions. Since no single method will meet each of these goals, the eight criteria of Table 1 will help identify those techniques that should be retained for the quantitative assessment phase of Missile Datcom development.

TABLE 1 ASSESSMENT CRITERIA

1. METHOD APPROACH	– Theoretical – Semi-Empirical – Empirical
2. EFFICIENCY (HANDBOOK, COMPUTER)	– Number Computations – Complexity of Logic – Number, Type of Inputs – Iterative – Detail of Geometry Required
3. ACCURACY	– Existing Validation – Compatibility with Accuracy Requirements – Sensitivity of Output to Input Accuracy – Derivation Assumptions – Theoretical – Range of Data – Empirical – Geometric Model
4. STATUS	– Current Use in Industry – Handbook Method Available – Method Coded and Used Locally – Does it Need Modification – Is Modification State-of-the-Art
5. RANGE OF APPLICABILITY	– Flight Conditions (Mach, α, β, ϕ) – Geometry
6. UTILITY OF OUTPUT PARAMETERS	– Compatibility with Other Methods – Thoroughness
7. GENERAL UTILITY	– Understandability – Traceability – Modifiability
8. VALIDATION STATUS	– Existing Validation – Data Base Available to Complete Validation

SECTION 2

REQUIREMENTS AND MISSILE DATCOM ARCHITECTURE

2.1 Requirements

To be a useful design tool, Missile Datcom must address those geometric and flight condition requirements of interest to the missile design community. As illustrated in Figure 1, configuration shape is often described by factors beyond the control of the aerodynamicist, such as seeker, warhead size, launching platform or cost. In addition, missile designs are strongly driven by the mission to be performed. As illustrated in Figure 2, the type of mission influences the choice of components which make up the configuration design. The matrix of configurations which satisfy the mission requirements are comprised of both mission and design requirements. The vehicle class (cruise versus intercept) and configuration type (glide, boost-glide or boost sustained) are choices which depend upon the mission to be accomplished, and are usually range or speed dependent. On the other hand, the selection of individual configuration components, such as wing size, body shape, or tail arrangement, arise from both physical (launcher constriants, steering mode or payload size and weight) and mission dependent (propulsion type) requirements. Hence, a range of configurations can be specified which satisfy the mission goals; such a wide range of design variables must be addressed.

Selection of the physical properties and flight conditions most useful to the missile design community was performed through analysis of the world's missile systems. Their characteristics were extracted from "Jane's Weapon Systems" (reference 2), and the experimental data summaries of the "Aeromechanics Survey and Evaluation" report (Reference 3). Design experience obtained from numerous in-house missile programs have also been considered.

The most useful results were obtained through categorizing the data of the Aeromechanics Survey. The types of configurations tested do reflect current trends in missile designs. The classification of results are shown in Figure 3, and were obtained from 1824 separate test summaries. These results indicate that the typical missile design is a body-tail configuration of overall fineness ratio 10. It is tested across the Mach spectrum to approximately 30 degrees angle of attack and the lifting surfaces are straight-tapered with an aspect ratio between one and four. A sharp tangent-ogive is the most common nose shape. Since this typical missile is too specific for design purposes, two sets of requirements evolved from these results,

1) Priority 1 capability, the range of parameters which Missile Datcom must address, and 2) Priority 2 capability, the range of parameters which extend the utility of the method collection, but are not detrimental to the development of Missile Datcom or its usefulness. Coverage of the priority 1 range of conditions was used to determine feasibility of Missile Datcom.

The priority 1 range encompasses 75% of the conditions identified in the Aeromechanics Survey plus additional conditions based upon in-house design experience. This results in the range of conditions given in Table 2. One crucial parameter is Mach number. Mach number limitations vary with altitude, and are primarily driven by structural and thermodynamic considerations. The Mach-altitude boundaries selected are shown in Figure 4. The boundaries are based upon structural requirements, thermodynamic properties of materials, speed required to maintain flight, and effective aerodynamic control. Included on this figure are the requirements for the Reynold's number per foot of length from the 1962 U.S. Standard atmosphere.

2.2 Missile Datcom Architecture

The most common missile aerodynamic analysis technique is "component build-up". A configuration is analytically modeled as a combination of components such as body, wings, tails and inlets. The aerodynamic coefficients of each of the components are estimated, interference effects among them determined and all coefficients summed to determine full configuration aerodynamics. This technique is advantageous in the preliminary or conceptual design process since many configuration components are screened to establish the best configuration.

The structure of Missile Datcom as presented in Table 3 in outline form has been assembled assuming a handbook format and using the "component build-up" approach. A handbook version of Missile Datcom is necessary to supply the detailed documentation necessary for effective use of the methods selected. There are nine sections in the handbook.

Section 1 will include a synopsis of the Missile Datcom methods contained in the entire document. The synopsis gives the user a quick overview of the available methodology and the method limitations.

Section 2 will 1) define the standardized notation used throughout the document, 2) supply equations or charts for calculation of geometric characteristics, such as nose mold line contours, wetted area, planform area, panel local chord, and 3) provide flight condition parameters, such as Reynolds number and speed of sound at altitude.

The remaining sections will contain the method descriptions covering the following areas:

(a) a concise description of the physical phenomena modeled,

(b) a description of the method including equations, tables or charts necessary for its use,

(c) tables or charts which illustrate the accuracy of the method, and

(d) a bibliography of reference documentation or related material.

Since the methods will be automated, approximate equations will also be presented to enable quick hand calculations.

Section 3 through 9 have been structured in a heirarchy of component class, speed regime, and aerodynamic parameter. This heirarchy will minimize redundant explanations, and enables computation of all component forces and moments within one section. This approach also serves as a guide to a modular computer program development.

The notation used in missile design is standardized by usage convention. No known written standard is in use, although "A Compilation of Aerodynamic Nomenclature and Axes Systems", NOLR 1241 (Reference 4) was published some 18 years ago for use in the U.S. Navy. However, the USAF Stability and Control Datcom symbols and nomenclature are in wide use in aircraft design and is recommended for missiles. With few exceptions, this set of nomenclature allows little ambiguity and is applicable to missiles. Some exceptions are: the reference length should be defined as the maximum body diameter/width/height, and the reference area as the area of an equivalent circular section whose diameter is the reference length.

By convention, the body axis system is in primary use in government and industry. This convention should be accepted as the Missile Datcom standard. It is recognized that other axes systems would be preferable for a specific task, and conversion capability among axes systems is required. Static and dynamic axes system conversion equations are recommended for inclusion; reference documentation is given in Reference 4 to 8. It is also convenient to express the relationship between pitch and yaw angle of attack to total angle of attack and bank angle in equation and graphical form. A proposed form of this information is given in Figure 5.

Since missile performance is a result of aerodynamic analysis, it is proposed that suitable data from the 1962 U.S. Standard Atmosphere,

Standard Day, and from the Military Standard 210A/B, non-standard day, be included for ready reference. A typical means of presenting the results is shown in Table 4. Automated atmospheric routines are readily available for computer program use, with an average error of less than 0.5%. The routine in Digital Datcom is an excellent example of the Standard Day routine.

Readily available equations for the geometric characteristics of a missile configuration will facilitate the design process. Computation of wetted area, nose mold line contours, and panel sweep angle are examples of those fundamental relationship that should be included.

Thrust-drag accounting requirements occur when the aerodynamicist and the propulsion engineer derive system performance. The aerodynamicist is responsible for estimating drag. The propulsion engineer, must determine installed engine performance. To avoid a complex bookkeeping task and avoid double accounting of some drag components, the Thrust-Drag Accounting Committee of the JANNAF (Joint Army-Navy-NASA-Air Force) Airbreathing Propulsion Working Group has recommended a standard procedure. This procedure, documented in the "Airbreathing Propulsion Manual", CPIA/M6, Reference 9, is recommended for inclusion.

The Datcom provides useful methods for predicting missile mass and inertial characteristics. This information is recommended for inclusion because of its utility in preliminary design.

The remaining sections of this report will describe Sections 3 through 9 of the Missile Datcom Outline and present the method recommendations.

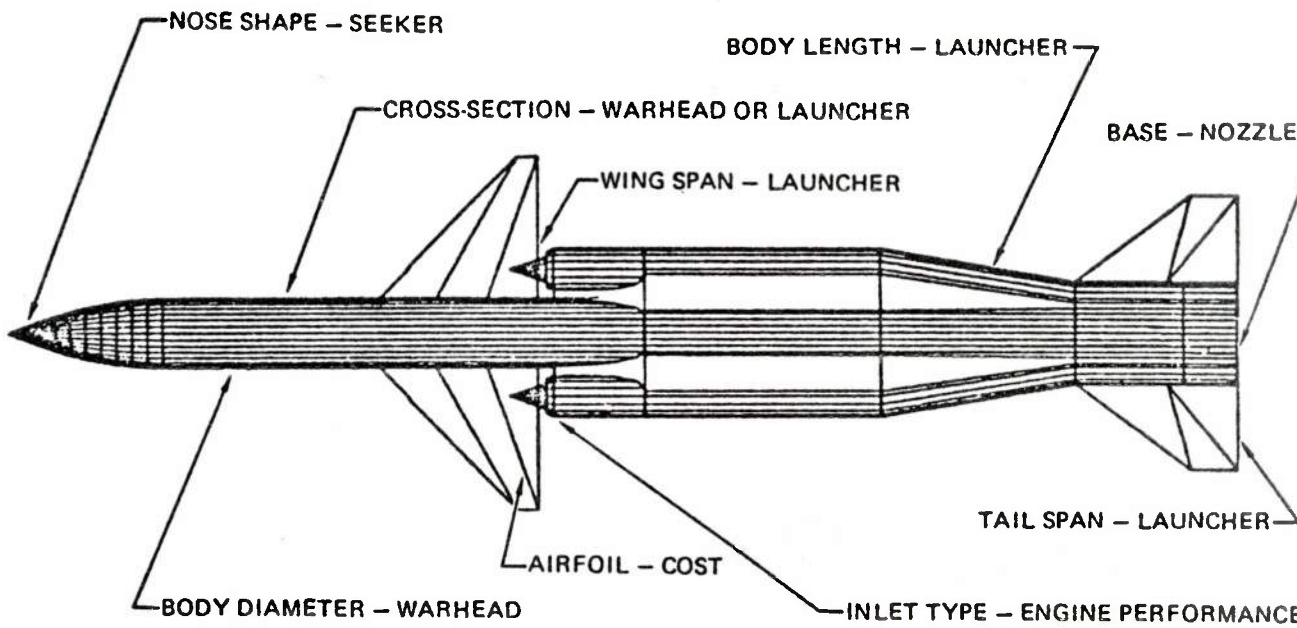

Figure 1. Factors Which Affect Missile Design

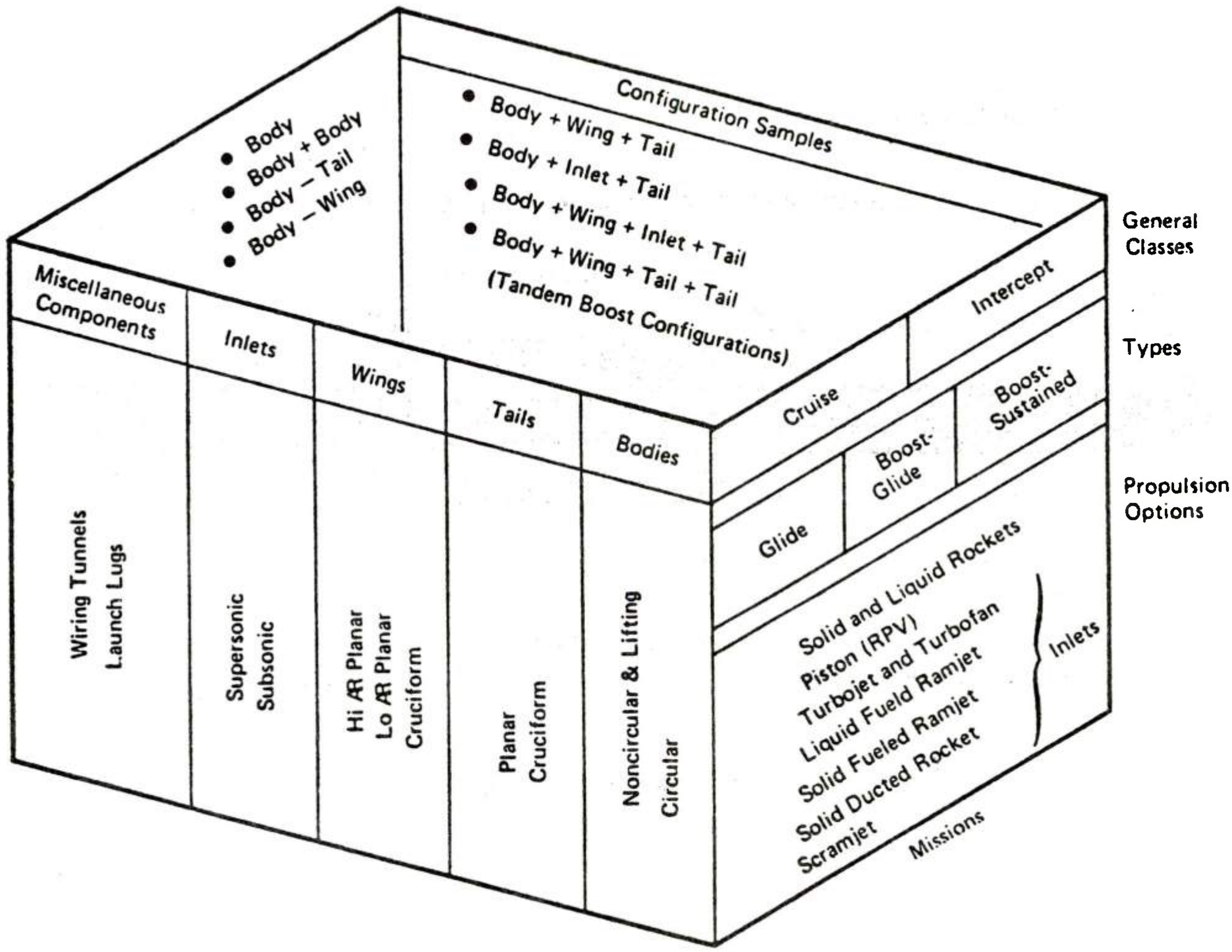

Figure 2. Matrix of Possible Configurations

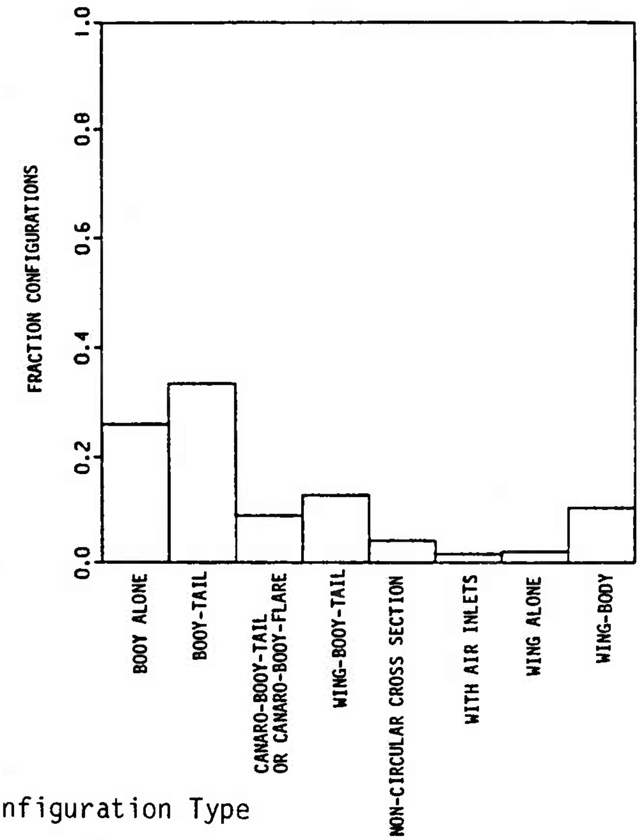

a) Configuration Type

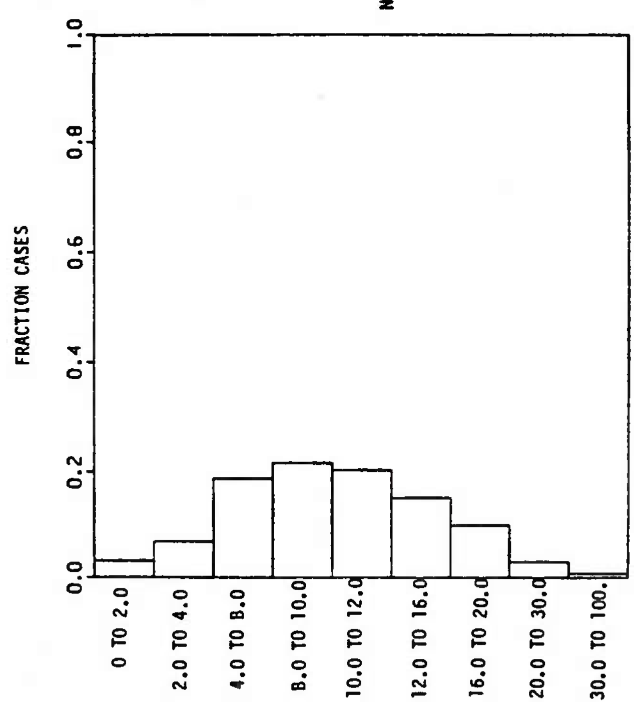

b) Body Fineness Ratio

Figure 3. Aeromechanics Survey Results

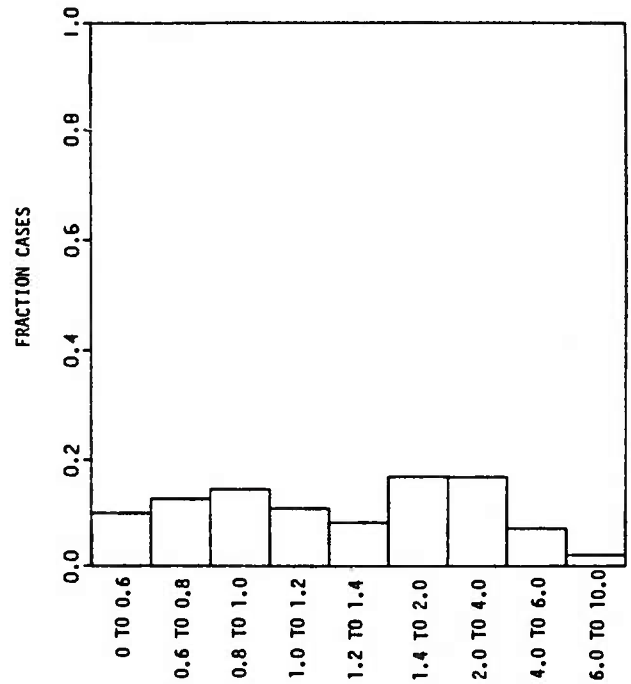

c) Mach Number

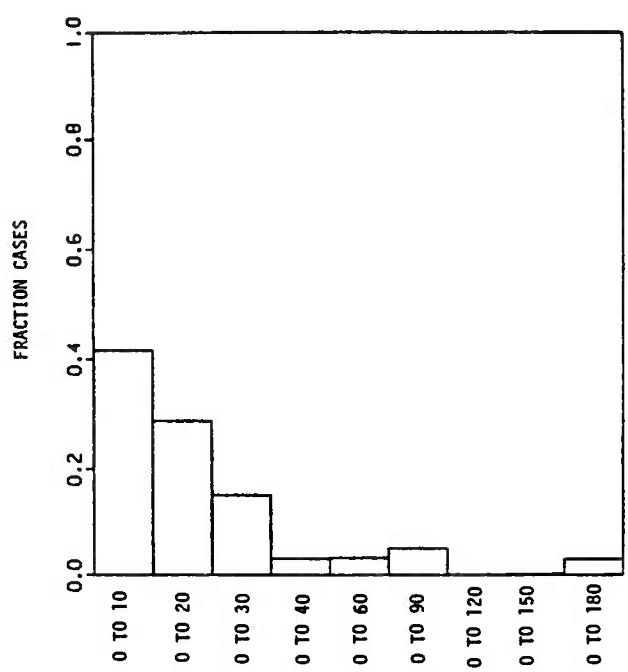

d) Angle of Attack

Figure 3. (Continued)

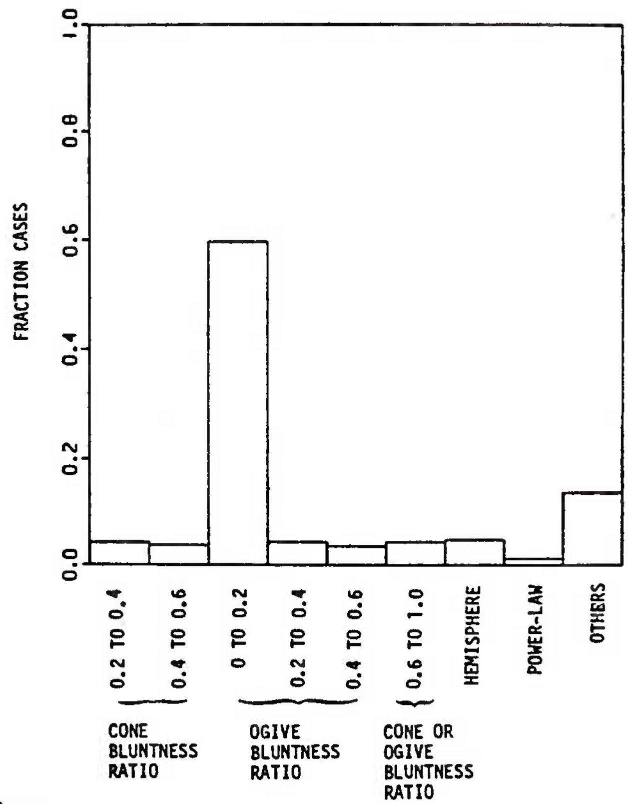

e) Nose Type

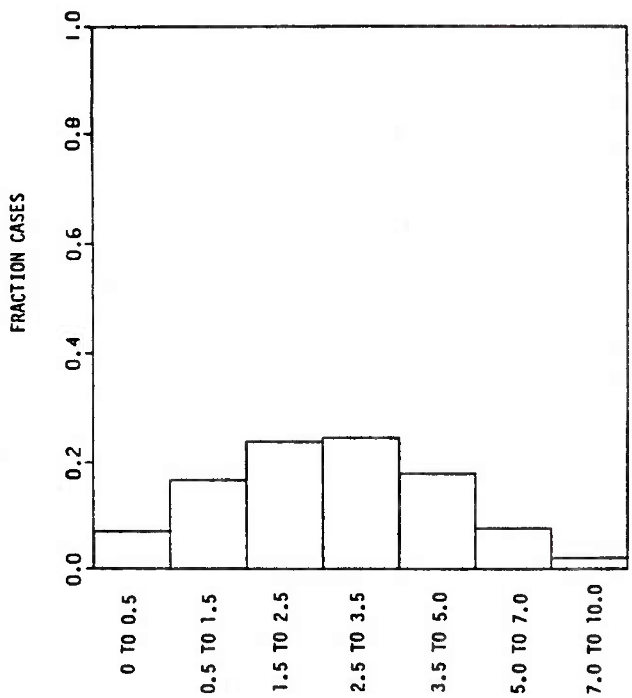

f) Nose Fineness Ratio

Figure 3. (Continued)

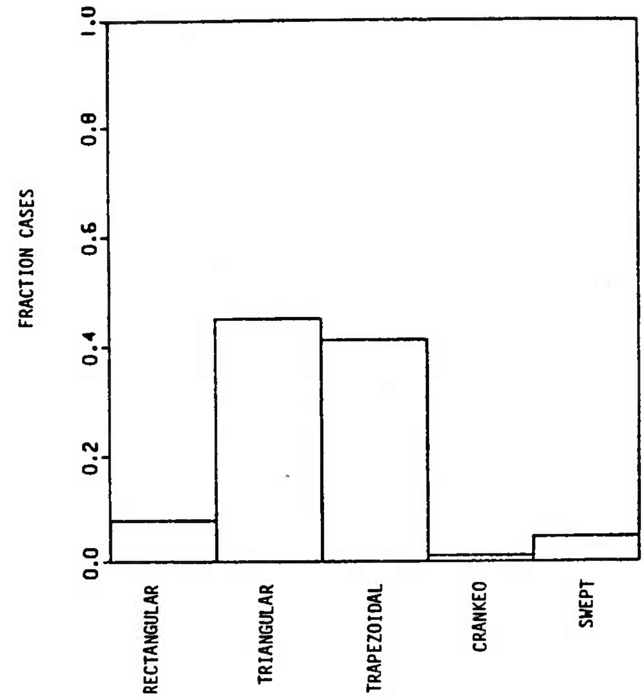

g) Wing Planform

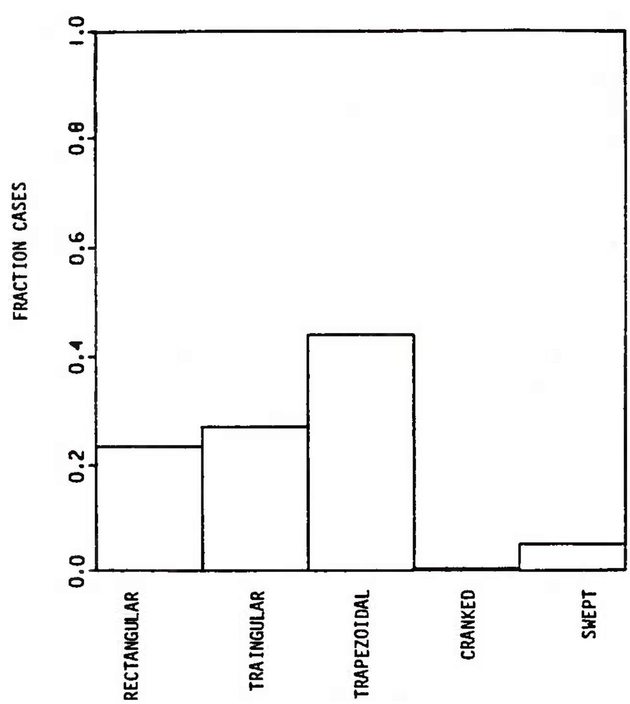

h) Tail Planform

Figure 3. (Continued)

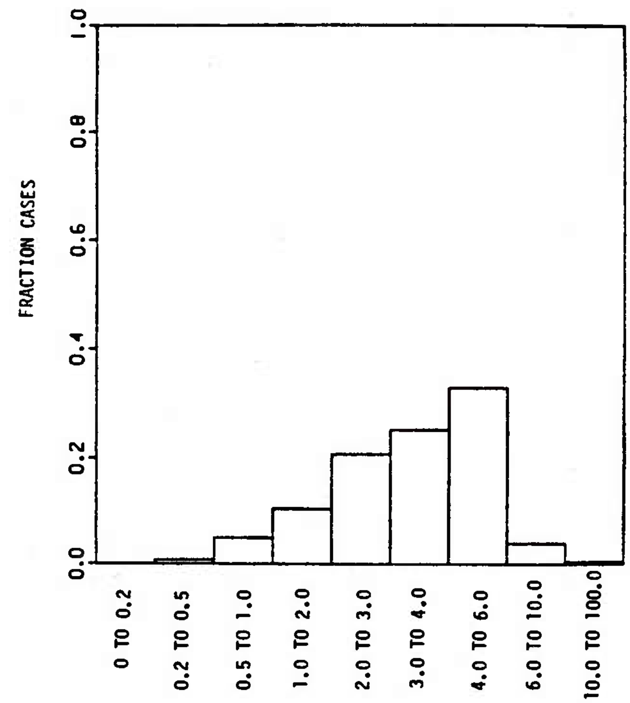

i) Wing b/d

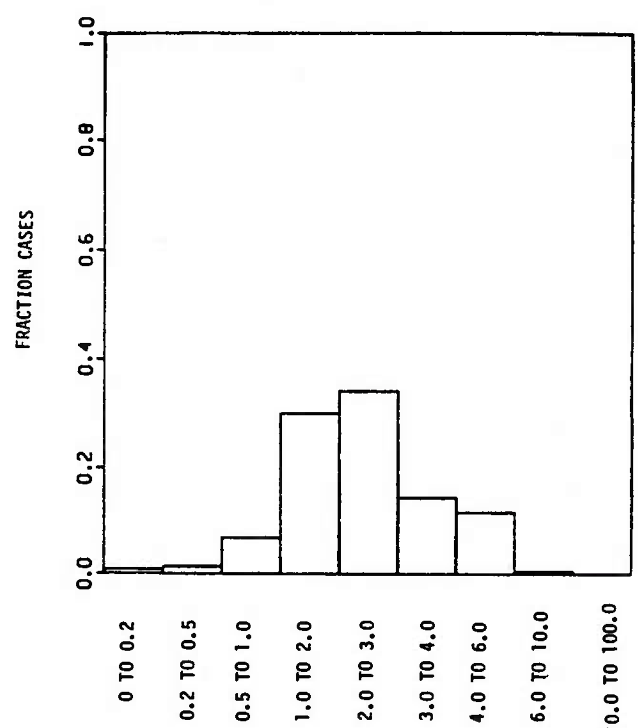

j) Tail b/d

Figure 3. (Continued)

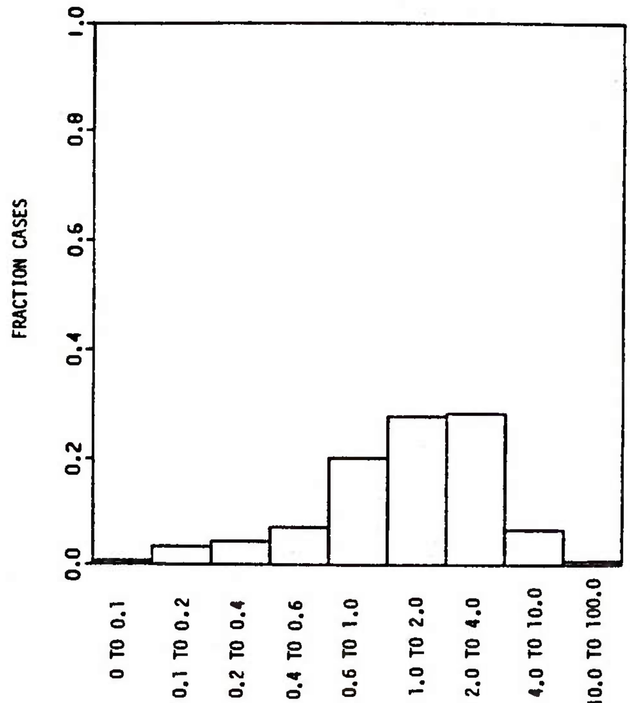

k) Wing Aspect Ratio

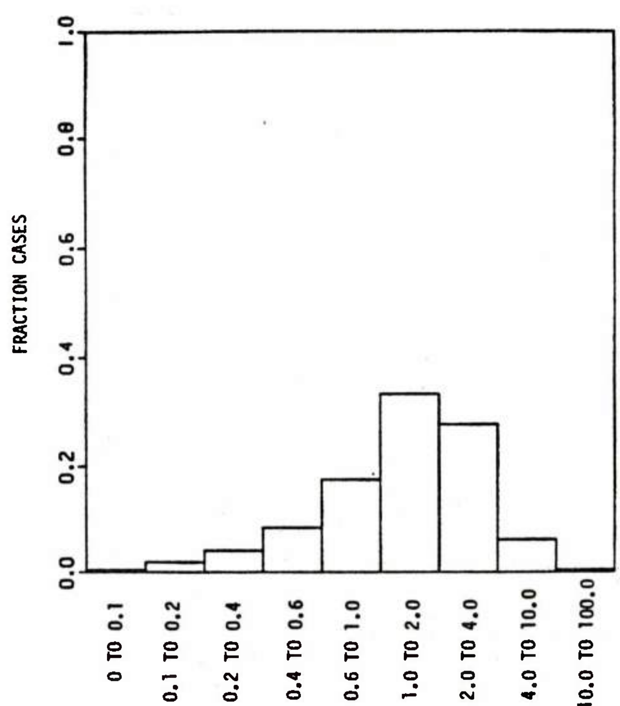

l) Tail Aspect Ratio

Figure 3. (Continued)

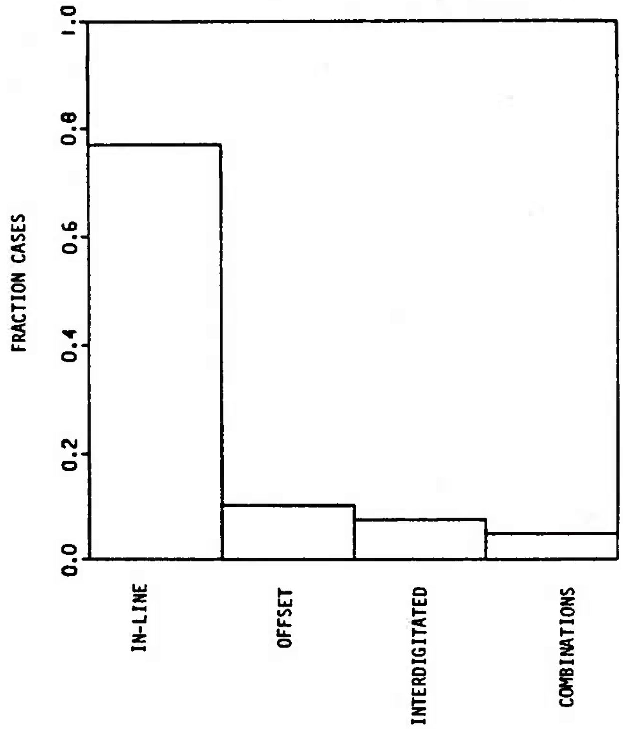

m) Panel Combination

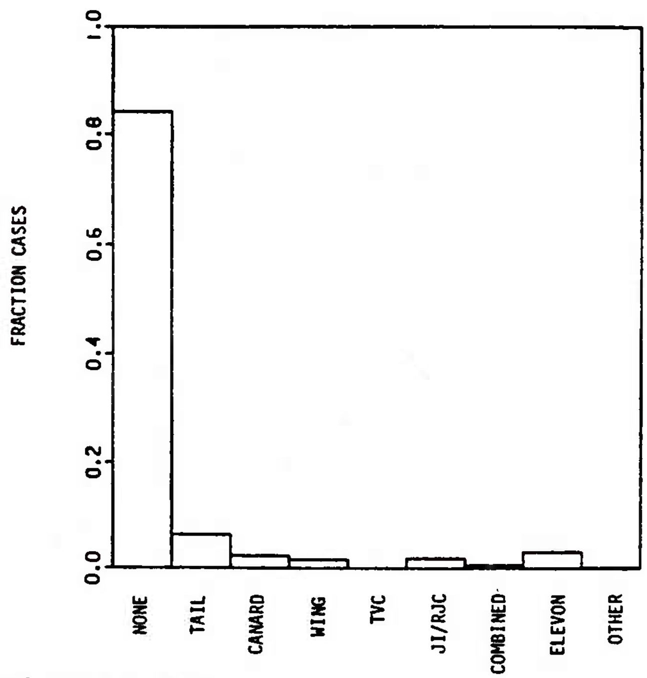

n) Control Device Type

Figure 3. (Continued)

TABLE 2 RANGE OF GEOMETRIC/FLIGHT CONDITIONS

PARAMETER	SYMBOL	PRIORITY 1	PRIORITY 2	SOURCE
ANGLE OF ATTACK, DEG.	α	$-20 \le \alpha \le 30$	$-180 \le \alpha \le 180$	AEROMECHANICS SURVEY AND
ANGLE OF YAW, DEG.	β	$-20 \le \beta \le 20$	$-180 \le \beta \le 180$	WORLD'S MISSILE SYSTEMS
AERODYNAMIC ROLL, DEG.	ϕ	$0 \le \lvert\phi\rvert \le 45$	$0 \le \lvert\phi\rvert \le 180$	
MACH NUMBER	M	$0 \le M \le 6$	$0 \le M \le 10$	
BODY FINENESS RATIO	$(\ell/d)_B$	$6 \le (\ell/d)_B \le 20$	$1 \le (\ell/d)_B \le 30$	
NOSE FINENESS RATIO	$(\ell/d)_N$	$.5 \le (\ell/d)_N \le 5$	$0 \le (\ell/d)_N \le 7$	
FIN EXPOSED SPAN TO DIAMETER	b/d	$1 \le b/d \le 6$	$0 \le b/d \le 10$	
FIN ASPECT RATIO	AR	$0.6 \le AR \le 4$	$0.1 \le AR \le 10$	
FIN PLANFORM		TRIANGULAR TRAPEZOIDAL	ALL	
WING/TAIL ORIENTATION		IN-LINE	ALL	
CONTROL METHOD		ALL MOVEABLE FIN	ALL	
REYNOLDS NUMBER/FT	R_N	$3\text{x}10^5 \le R_N \le 2\text{x}10^7$	$10^3 \le R_N \le 3\text{x}10^7$	MACH-ALTITUDE BOUNDARY
FIN DEFLECTION/INCIDENCE, DEG.	δ	$0 \le \delta \le 30$	$0 \le \delta \le 60$	MISSILE SYSTEM ANALYSIS
ROLL RATE, RAD/SEC.	p	$0 \le \lvert p\rvert \le 1$	$0 \le \lvert p\rvert \le 8$	
PITCH RATE, RAD/SEC.	q	$0 \le \lvert q\rvert \le 1.5$	$0 \le \lvert q\rvert \le 3$	
YAW RATE, RAD/SEC.	r	$0 \le \lvert r\rvert \le 1.5$	$0 \le \lvert r\rvert \le 3$	
FIN DEFLECTION RATE, RAD/SEC.	$\dot{\delta}$	$0 \le \lvert\dot{\delta}\rvert \le 10$	$0 \le \lvert\dot{\delta}\rvert \le 28$	

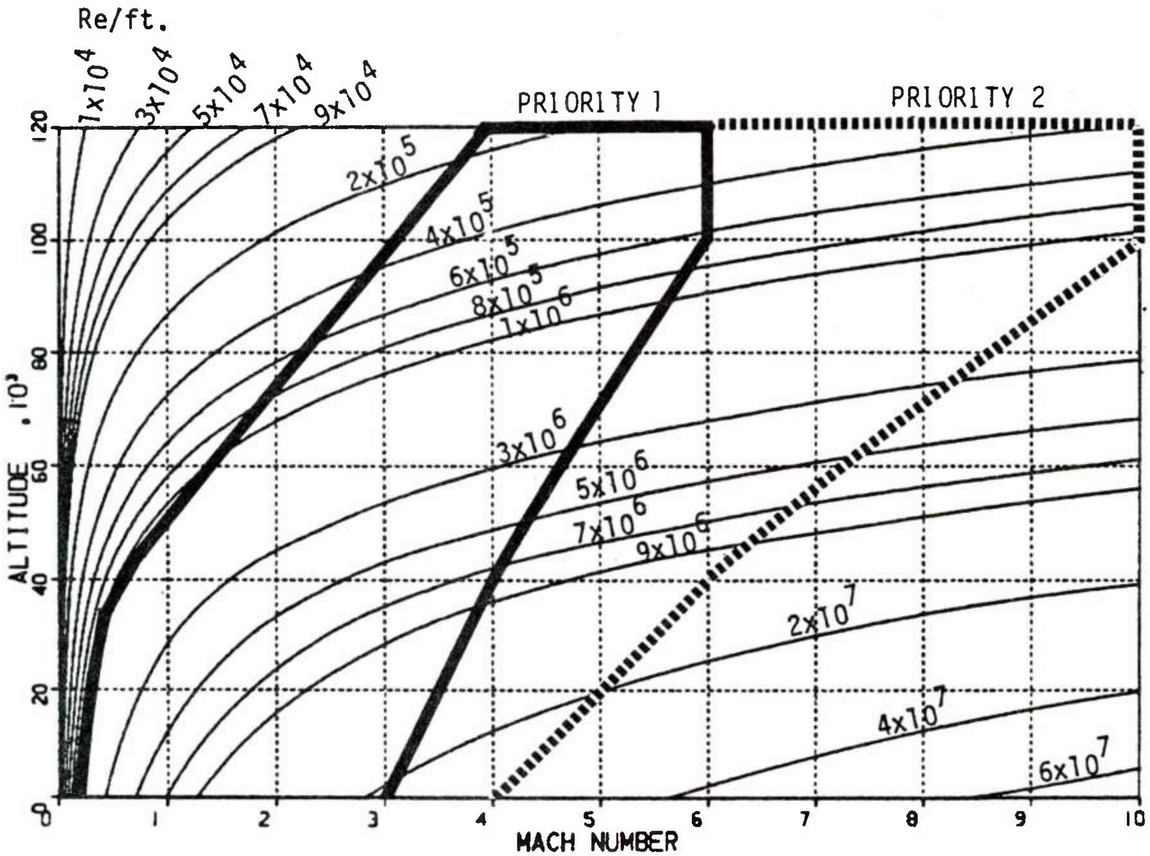

Figure 4. Mach-Altitude-Reynolds Number Requirements for the 1962 Standard Atmosphere

TABLE 3 MISSILE DATCOM OUTLINE

1. INTRODUCTION AND METHODS SUMMARY

2. GENERAL INFORMATION AND EQUATIONS
   - 2.1 NOTATION
   - 2.2 AXES SYSTEMS AND TRANSFER EQUATIONS
   - 2.3 BODY PARAMETERS
   - 2.4 LIFTING SURFACE PARAMETERS
   - 2.5 ENGINE AND INLET PARAMETERS
   - 2.6 SIMPLIFIED EQUATIONS OF MOTION

3. CHARACTERISTICS OF BASIC BODIES
   - 3.1 AXISYMMETRIC BODIES
     - 3.1.1 SUBSONIC
       - 3.1.1.1 AXIAL FORCE
       - 3.1.1.2 NORMAL FORCE
       - 3.1.1.3 PITCHING MOMENT, XAC, XCP
       - 3.1.1.4 ASYMMETRIC VORTEX SHEDDING AT HIGH ALPHA/BETA
     - 3.1.2 TRANSONIC
       - 3.1.2.1 AXIAL FORCE
       - 3.1.2.2 NORMAL FORCE
       - 3.1.2.3 PITCHING MOMENT, XAC, XCP
       - 3.1.2.4 ASYMMETRIC VORTEX SHEDDING AT HIGH ALPHA/BETA
     - 3.1.3 SUPERSONIC/HYPERSONIC
       - 3.1.3.1 AXIAL FORCE
       - 3.1.3.2 NORMAL FORCE
       - 3.1.3.3 PITCHING MOMENT, XAC, XCP
   - 3.2 TWO-AXIS SYMMETRICAL BODIES
     - 3.2.1 SUBSONIC
       - 3.2.1.1 AXIAL FORCE
       - 3.2.1.2 NORMAL FORCE AND SIDE FORCE
       - 3.2.1.3 PITCHING (XAC, XCP), YAWING AND ROLLING MOMENTS
       - 3.2.1.4 ASYMMETRIC VORTEX SHEDDING AT HIGH ALPHA/BETA
     - 3.2.2 TRANSONIC
       - 3.2.2.1 AXIAL FORCE
       - 3.2.2.2 NORMAL FORCE AND SIDE FORCE
       - 3.2.2.3 PITCHING (XAC, XCP), YAWING AND ROLLING MOMENTS
       - 3.2.2.4 ASYMMETRIC VORTEX SHEDDING AT HIGH ALPHA/BETA
     - 3.2.3 SUPERSONIC/HYPERSONIC
       - 3.2.3.1 AXIAL FORCE
       - 3.2.3.2 NORMAL FORCE AND SIDE FORCE
       - 3.2.3.3 PITCHING (XAC, XCP), YAWING AND ROLLING MOMENTS
   - 3.3 ARBITRARY SHAPED BODIES
     - 3.3.1 SUBSONIC
       - 3.3.1.1 AXIAL FORCE
       - 3.3.1.2 NORMAL FORCE AND SIDE FORCE
       - 3.3.1.3 PITCHING (XAC, XCP), YAWING AND ROLLING MOMENTS
     - 3.3.2 TRANSONIC
       - 3.3.2.1 AXIAL FORCE
       - 3.3.2.2 NORMAL FORCE AND SIDE FORCE
       - 3.3.2.3 PITCHING (XAC, XCP), YAWING AND ROLLING MOMENTS
     - 3.3.3 SUPERSONIC/HYPERSONIC
       - 3.3.3.1 AXIAL FORCE
       - 3.3.3.2 NORMAL FORCE AND SIDE FORCE
       - 3.3.3.3 PITCHING (XAC, XCP), YAWING AND ROLLING MOMENTS

TABLE 3 (CONTINUED)

3.4 EFFECT OF PROTUBERANCES
- 3.4.1 SUBSONIC
  - 3.4.1.1 AXIAL FORCE
  - 3.4.1.2 NORMAL FORCE AND SIDE FORCE
  - 3.4.1.3 PITCHING (XAC, XCP), YAWING AND ROLLING MOMENTS
  - 3.4.1.4 ASYMMETRIC VORTEX SHEDDING AT HIGH ALPHA/BETA
- 3.4.2 TRANSONIC
  - 3.4.2.1 AXIAL FORCE
  - 3.4.2.2 NORMAL FORCE AND SIDE FORCE
  - 3.4.2.3 PITCHING (XAC, XCP), YAWING AND ROLLING MOMENTS
  - 3.4.2.4 ASYMMETRIC VORTEX SHEDDING AT HIGH ALPHA/BETA
- 3.4.3 SUPERSONIC/HYPERSONIC
  - 3.4.3.1 AXIAL FORCE
  - 3.4.3.2 NORMAL FORCE AND SIDE FORCE
  - 3.4.3.3 PITCHING (XAC, XCP), YAWING AND ROLLING MOMENTS

3.5 PROPULSION SYSTEM EFFECTS
- 3.5.1 BASE/EXHAUST PLUME
  - 3.5.1.1 SUBSONIC
  - 3.5.1.2 TRANSONIC
  - 3.5.1.3 SUPERSONIC/HYPERSONIC
- 3.5.2 AIRBREATHING INLET AERODYNAMIC CONSIDERATIONS
  - 3.5.2.1 SUBSONIC
  - 3.5.2.2 TRANSONIC
  - 3.5.2.3 SUPERSONIC/HYPERSONIC
- 3.5.3 INLET COVERS
  - 3.5.3.1 SUBSONIC
  - 3.5.3.2 TRANSONIC
  - 3.5.3.3 SUPERSONIC/HYPERSONIC
- 3.5.4 INLET PLUGGED
  - 3.5.4.1 SUBSONIC
  - 3.5.4.2 TRANSONIC
  - 3.5.4.3 SUPERSONIC/HYPERSONIC

4. CHARACTERISTICS OF LIFTING SURFACES

4.1 SECTION CHARACTERISTICS AND DESIGN
- 4.1.1 FLAT PLATE SECTIONS
  - 4.1.1.1 SUBSONIC
  - 4.1.1.2 TRANSONIC
  - 4.1.1.3 SUPERSONIC/HYPERSONIC
- 4.1.2 DOUBLE WEDGE SECTIONS
  - 4.1.2.1 SUBSONIC
  - 4.1.2.2 TRANSONIC
  - 4.1.2.3 SUPERSONIC/HYPERSONIC
- 4.1.3 HEXAGONAL SECTIONS (MODIFIED DOUBLE WEDGE)
  - 4.1.3.1 SUBSONIC
  - 4.1.3.2 TRANSONIC
  - 4.1.3.3 SUPERSONIC/HYPERSONIC
- 4.1.4 CIRCULAR ARC SECTIONS
  - 4.1.4.1 SUBSONIC
  - 4.1.4.2 TRANSONIC
  - 4.1.4.3 SUPERSONIC/HYPERSONIC
- 4.1.5 NACA AIRFOIL SECTIONS
  - 4.1.5.1 SUBSONIC
  - 4.1.5.2 TRANSONIC
  - 4.1.5.3 SUPERSONIC/HYPERSONIC
- 4.1.6 SUPERCRITICAL AIRFOIL SECTIONS
  - 4.1.6.1 SUBSONIC
  - 4.1.6.2 TRANSONIC

TABLE 3 (CONTINUED)

4.1.6.3 SUPERSONIC/HYPERSONIC
4.2 THREE-DIMENSIONAL EFFECTS
4.2.1 STRAIGHT TAPERED SURFACES
4.2.1.1 SUBSONIC
4.2.1.2 TRANSONIC
4.2.1.3 SUPERSONIC/HYPERSONIC
4.2.2 CRANKED SURFACES
4.2.2.1 SUBSONIC
4.2.2.2 TRANSONIC
4.2.2.3 SUPERSONIC/HYPERSONIC
4.2.3 SLEWED SURFACES
4.2.3.1 SUBSONIC
4.2.3.2 TRANSONIC
4.2.3.3 SUPERSONIC/HYPERSONIC
4.2.4 CURVED SURFACES
4.2.4.1 SUBSONIC
4.2.4.2 TRANSONIC
4.2.4.3 SUPERSONIC/HYPERSONIC
4.2.5 VERY LOW ASPECT RATIO SURFACES
4.2.5.1 SUBSONIC
4.2.5.2 TRANSONIC
4.2.5.3 SUPERSONIC/HYPERSONIC

5. INTERFERENCE EFFECTS
5.1 CARRYOVER
5.1.1 BODY / FIN, FIN / BODY
5.1.1.1 SUBSONIC
5.1.1.2 TRANSONIC
5.1.1.3 SUPERSONIC/HYPERSONIC
5.1.2 ADJACENT FIN EFFECT (FIN / FIN)
5.1.2.1 SUBSONIC
5.1.2.2 TRANSONIC
5.1.2.3 SUPERSONIC/HYPERSONIC
5.1.3 BODY / INLET, INLET / FIN
5.1.3.1 SUBSONIC
5.1.3.2 TRANSONIC
5.1.3.3 SUPERSONIC/HYPERSONIC
5.1.4 MULTIPLE BODIES
5.1.4.1 SUBSONIC
5.1.4.2 TRANSONIC
5.1.4.3 SUPERSONIC/HYPERSONIC
5.2 VORTICES
5.2.1 VORTEX STRENGTH AND TRACKING -- BODY
5.2.1.1 SUBSONIC
5.2.1.2 TRANSONIC
5.2.1.3 SUPERSONIC/HYPERSONIC
5.2.2 VORTEX STRENGTH AND TRACKING -- LIFTING SURFACES
5.2.2.1 SUBSONIC
5.2.2.2 TRANSONIC
5.2.2.3 SUPERSONIC/HYPERSONIC
5.2.3 VORTEX STRENGTH AND TRACKING -- INLET
5.2.3.1 SUBSONIC
5.2.3.2 TRANSONIC
5.2.3.3 SUPERSONIC/HYPERSONIC
5.2.4 MULTIPLE VORTEX INTERFERENCE
5.2.4.1 SUBSONIC
5.2.4.2 TRANSONIC
5.2.4.3 SUPERSONIC/HYPERSONIC

TABLE 3 (CONTINUED)

```
6. CONFIGURATION SYNTHESIS
   6.1 BASIC BODY AND INLET/ENGINE
       6.1.1 SUBSONIC
             6.1.1.1 AXIAL FORCE
             6.1.1.2 NORMAL FORCE AND SIDE FORCE
             6.1.1.3 PITCHING (XAC, XCP), YAWING AND ROLLING MOMENTS
             6.1.1.4 ASYMMETRIC VORTEX SHEDDING AT HIGH ALPHA/BETA
       6.1.2 TRANSONIC
             6.1.2.1 AXIAL FORCE
             6.1.2.2 NORMAL FORCE AND SIDE FORCE
             6.1.2.3 PITCHING (XAC, XCP), YAWING AND ROLLING MOMENTS
             6.1.2.4 ASYMMETRIC VORTEX SHEDDING AT HIGH ALPHA/BETA
       6.1.3 SUPERSONIC/HYPERSONIC
             6.1.3.1 AXIAL FORCE
             6.1.3.2 NORMAL FORCE AND SIDE FORCE
             6.1.3.3 PITCHING (XAC, XCP), YAWING AND ROLLING MOMENTS
   6.2 BODY-TAIL OR BODY-WING
       6.2.1 SUBSONIC
             6.2.1.1 AXIAL FORCE
             6.2.1.2 NORMAL FORCE AND SIDE FORCE
             6.2.1.3 PITCHING (XAC, XCP), YAWING AND ROLLING MOMENTS
             6.2.1.4 ASYMMETRIC VORTEX SHEDDING AT HIGH ALPHA/BETA
       6.2.2 TRANSONIC
             6.2.2.1 AXIAL FORCE
             6.2.2.2 NORMAL FORCE AND SIDE FORCE
             6.2.2.3 PITCHING (XAC, XCP), YAWING AND ROLLING MOMENTS
             6.2.2.4 ASYMMETRIC VORTEX SHEDDING AT HIGH ALPHA/BETA
       6.2.3 SUPERSONIC/HYPERSONIC
             6.2.3.1 AXIAL FORCE
             6.2.3.2 NORMAL FORCE AND SIDE FORCE
             6.2.3.3 PITCHING (XAC, XCP), YAWING AND ROLLING MOMENTS
   6.3 BODY-WING-TAIL OR BODY-CANARD-WING-TAIL
       6.3.1 SUBSONIC
             6.3.1.1 AXIAL FORCE
             6.3.1.2 NORMAL FORCE AND SIDE FORCE
             6.3.1.3 PITCHING (XAC, XCP), YAWING AND ROLLING MOMENTS
             6.3.1.4 ASYMMETRIC VORTEX SHEDDING AT HIGH ALPHA/BETA
       6.3.2 TRANSONIC
             6.3.2.1 AXIAL FORCE
             6.3.2.2 NORMAL FORCE AND SIDE FORCE
             6.3.2.3 PITCHING (XAC, XCP), YAWING AND ROLLING MOMENTS
             6.3.2.4 ASYMMETRIC VORTEX SHEDDING AT HIGH ALPHA/BETA
       6.3.3 SUPERSONIC/HYPERSONIC
             6.3.3.1 AXIAL FORCE
             6.3.3.2 NORMAL FORCE AND SIDE FORCE
             6.3.3.3 PITCHING (XAC, XCP), YAWING AND ROLLING MOMENTS

7. CONTROL DEVICES
   7.1 ALL MOVABLE LIFTING SURFACES
       7.1.1 BASIC AERODYNAMICS
             7.1.1.1 SUBSONIC
             7.1.1.2 TRANSONIC
             7.1.1.3 SUPERSONIC/HYPERSONIC
       7.1.2 HINGE MOMENTS
             7.1.2.1 SUBSONIC
             7.1.2.2 TRANSONIC
             7.1.2.3 SUPERSONIC/HYPERSONIC
```

TABLE 3 (CONTINUED)

7.1.3 BENDING MOMENTS
7.1.3.1 SUBSONIC
7.1.3.2 TRANSONIC
7.1.3.3 SUPERSONIC/HYPERSONIC
7.2 PLAIN TRAILING EDGE FLAPS
7.2.1 BASIC AERODYNAMICS
7.2.1.1 SUBSONIC
7.2.1.2 TRANSONIC
7.2.1.3 SUPERSONIC/HYPERSONIC
7.2.2 HINGE MOMENTS
7.2.2.1 SUBSONIC
7.2.2.2 TRANSONIC
7.2.2.3 SUPERSONIC/HYPERSONIC
7.2.3 BENDING MOMENTS
7.2.3.1 SUBSONIC
7.2.3.2 TRANSONIC
7.2.3.3 SUPERSONIC/HYPERSONIC
7.3 JET INTERACTION/REACTION JET CONTROL (JI/RJC)
7.3.1 BASIC AERODYNAMICS
7.3.1.1 SUBSONIC
7.3.1.2 TRANSONIC
7.3.1.3 SUPERSONIC/HYPERSONIC
7.4 THRUST VECTOR CONTROL (TVC)
7.4.1 BASIC AERODYNAMICS
7.4.1.1 SUBSONIC
7.4.1.2 TRANSONIC
7.4.1.3 SUPERSONIC/HYPERSONIC
7.5 SPECIALIZED CONTROL DEVICES
7.5.1 BASIC AERODYNAMICS
7.5.1.1 SUBSONIC
7.5.1.2 TRANSONIC
7.5.1.3 SUPERSONIC/HYPERSONIC
7.5.2 HINGE MOMENTS
7.5.2.1 SUBSONIC
7.5.2.2 TRANSONIC
7.5.2.3 SUPERSONIC/HYPERSONIC
7.5.3 BENDING MOMENTS
7.5.3.1 SUBSONIC
7.5.3.2 TRANSONIC
7.5.3.3 SUPERSONIC/HYPERSONIC
7.6 CONFIGURATION TRIM AERODYNAMICS

8. DYNAMIC DERIVATIVES
8.1 BODY OR BODY-INLET-ENGINE
8.1.1 PITCH DERIVATIVES
8.1.1.1 SUBSONIC
8.1.1.2 TRANSONIC
8.1.1.3 SUPERSONIC/HYPERSONIC
8.1.2 YAW DERIVATIVES
8.1.2.1 SUBSONIC
8.1.2.2 TRANSONIC
8.1.2.3 SUPERSONIC/HYPERSONIC
8.1.3 ROLL DERIVATIVES
8.1.3.1 SUBSONIC
8.1.3.2 TRANSONIC
8.1.3.3 SUPERSONIC/HYPERSONIC
8.2 FIN OR FIN COMBINATIONS
8.2.1 PITCH DERIVATIVES

TABLE 3 (CONTINUED)

8.2.1.1 SUBSONIC
8.2.1.2 TRANSONIC
8.2.1.3 SUPERSONIC/HYPERSONIC
8.2.2 YAW DERIVATIVES
8.2.2.1 SUBSONIC
8.2.2.2 TRANSONIC
8.2.2.3 SUPERSONIC/HYPERSONIC
8.2.3 ROLL DERIVATIVES
8.2.3.1 SUBSONIC
8.2.3.2 TRANSONIC
8.2.3.3 SUPERSONIC/HYPERSONIC
8.3 BODY-WING OR BODY-TAIL
8.3.1 PITCH DERIVATIVES
8.3.1.1 SUBSONIC
8.3.1.2 TRANSONIC
8.3.1.3 SUPERSONIC/HYPERSONIC
8.3.2 YAW DERIVATIVES
8.3.2.1 SUBSONIC
8.3.2.2 TRANSONIC
8.3.2.3 SUPERSONIC/HYPERSONIC
8.3.3 ROLL DERIVATIVES
8.3.3.1 SUBSONIC
8.3.3.2 TRANSONIC
8.3.3.3 SUPERSONIC/HYPERSONIC
8.4 BODY-WING-TAIL OR BODY-CANARD-WING-TAIL
8.4.1 PITCH DERIVATIVES
8.4.1.1 SUBSONIC
8.4.1.2 TRANSONIC
8.4.1.3 SUPERSONIC/HYPERSONIC
8.4.2 YAW DERIVATIVES
8.4.2.1 SUBSONIC
8.4.2.2 TRANSONIC
8.4.2.3 SUPERSONIC/HYPERSONIC
8.4.3 ROLL DERIVATIVES
8.4.3.1 SUBSONIC
8.4.3.2 TRANSONIC
8.4.3.3 SUPERSONIC/HYPERSONIC

9. SPECIALIZED PROBLEMS
9.1 TUMBLING MOTION
9.1.1 PLATES
9.1.1.1 SUBSONIC
9.1.1.2 TRANSONIC
9.1.1.3 SUPERSONIC/HYPERSONIC
9.1.2 CYLINDERS
9.1.2.1 SUBSONIC
9.1.2.2 TRANSONIC
9.1.2.3 SUPERSONIC/HYPERSONIC
9.1.3 CONES
9.1.3.1 SUBSONIC
9.1.3.2 TRANSONIC
9.1.3.3 SUPERSONIC/HYPERSONIC
9.2 SPINNING MOTION
9.2.1 MAGNUS EFFECT
9.2.1.1 SUBSONIC
9.2.1.2 TRANSONIC
9.2.1.3 SUPERSONIC/HYPERSONIC

RELATIONS BETWEEN BODY AXES ANGLES, α AND β, AND TOTAL ANGLE OF ATTACK, α':

$$\beta = -\text{ARCTAN}\,(\text{TAN}\,\alpha' \,\text{SIN}\,\phi)$$
$$\alpha = \text{ARCTAN}\,(\text{TAN}\,\alpha' \,\text{COS}\,\phi)$$
$$\alpha' = \text{ARCTAN}\,\sqrt{\text{TAN}^2\,\alpha + \text{TAN}^2\,\beta}$$

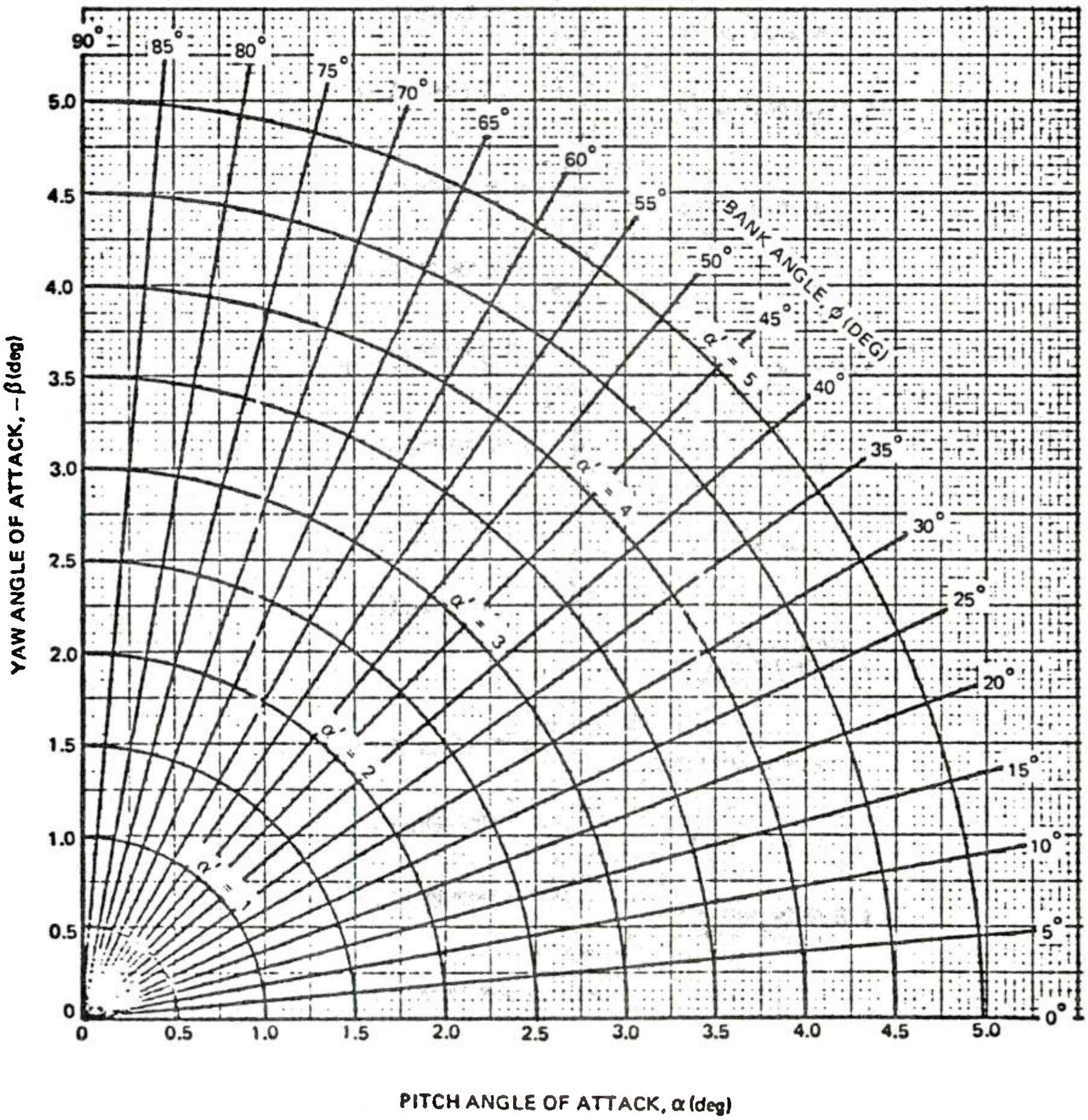

Figure 5. Conversion Between Pitch and Yaw Angle of Attack to Total Angle of Attack

TABLE 4 PRESENTATION OF STANDARD ATMOSPHERE DATA

Altitude (ft)	Pressure (lb/sq ft)	Temperature (deg R)	Speed of Sound (ft/sec)	Density (slugs/cu ft)
0	2.1162E+03	518.67	1116.45	2.3769E-03
5000	1.7609E+03	500.84	1097.09	2.0482E-03
10000	1.4556E+03	483.03	1077.40	1.7556E-03
15000	1.1948E+03	465.22	1057.35	1.4962E-03
20000	9.7327E+02	447.42	1036.93	1.2673E-03
25000	7.8633E+02	429.62	1016.10	1.0663E-03
30000	6.2966E+02	411.84	994.85	8.9069E-04
35000	4.9934E+02	394.06	973.14	7.3820E-04
40000	3.9313E+02	389.97	968.07	5.8728E-04
45000	3.0945E+02	389.97	968.07	4.6227E-04
50000	2.4361E+02	389.97	968.07	3.6392E-04
55000	1.9180E+02	389.97	968.07	2.8652E-04
60000	1.5103E+02	389.97	968.07	2.2561E-04
65000	1.1893E+02	389.97	968.07	1.7767E-04
70000	9.3727E+01	392.25	970.89	1.3920E-04
75000	7.3990E+01	394.97	974.26	1.0913E-04
80000	5.8511E+01	397.69	977.61	8.5710E-05
85000	4.6350E+01	400.42	980.95	6.7434E-05
90000	3.6778E+01	403.14	984.28	5.3147E-05
95000	2.9232E+01	405.85	987.59	4.1959E-05
100000	2.3272E+01	408.57	990.89	3.3182E-05
105000	1.8557E+01	411.29	994.18	2.6285E-05
110000	1.4837E+01	418.38	1002.72	2.0659E-05
115000	1.1912E+01	425.98	1011.79	1.6290E-05
120000	9.6013E+00	433.58	1020.77	1.2900E-05
125000	7.7688E+00	441.17	1029.66	1.0259E-05
130000	6.3094E+00	448.76	1038.48	8.1907E-06
135000	5.1426E+00	456.34	1047.22	6.5650E-06
140000	4.2061E+00	463.92	1055.88	5.2818E-06
145000	3.4517E+00	471.50	1064.47	4.2648E-06
150000	2.8418E+00	479.07	1072.99	3.4557E-06
155000	2.3471E+00	486.64	1081.43	2.8097E-06
160000	1.9419E+00	487.17	1082.01	2.3221E-06
165000	1.6068E+00	487.17		1.9215E-06
170000	1.3297E+00	[illegible]		1.5901E-06
175000	1.1000E+00			[illegible]
180000	9.0836E-01			
185000	7.485[illegible]			
[illegible]				

BEST AVAILABLE COPY

SECTION 3
BODY METHODOLOGY

3.1 INTRODUCTION

This section summarizes those methods available to compute the aerodynamic characteristics of bodies. Those body alone methods chosen for Missile Datcom, summarized in Table 5, are the result of the qualitative assessment criteria given in Table 1. Rationale used in the selection of these recommended techniques, as well as available alternate methodology are discussed in the following paragraphs.

The most complete compendium of methodology available is for axisymmetric bodies. Theoretical analysis is greatly simplified over more complex shapes. The large quantity of experimental results also allows for more rapid and accurate analysis. Since Max Munk first derived the potential flow over pointed, slender bodies of revolution, other authors have developed more sophisticated techniques which allow accurate analysis for more realistic configuration shapes. With high speed computers being almost common-place, the mathematically complex methods are being used more often for design.

The capability exists to determine the inviscid normal force and pitching moment characteristics of axisymmetric bodies across the Mach spectrum. At subsonic speeds the Neumann Potential Flow process of simulating a body by a series of source-sink pairs and applying the condition of zero flow velocity normal to the body surface is well known. At supersonic speeds, the work of Van Dyke, Syvertson and Dennis, and Lavender in solving the inviscid Euler equations are recognized as great strides in analytical prediction capability. The transonic speed regime has been more elusive, having been solved just recently by Klopfer and Chaussee in a manner suitable for engineering design purposes through numerical solution of the unsteady Euler equations. Although theoretical methods can be identified at all speed regimes, use of all these methods is not desirable for Missile Datcom. Neumann Potential Flow is a large computer program which is costly, and requires significant geometry detail. The solution of the unsteady Euler equations in the transonic Mach regime is an iterative solution, shown to utilize 3900 seconds computer time per case on a CDC 7600. Although these methods are attractive, they are not the quick and inexpensive methods desirable for Missile Datcom. Generation of design charts is, however, an acceptable way of using these techniques.

Available methods were assembled through extensive literature searches of the Defense Technical Information Center (DTIC), the National Aeronautics and Space Administration (NASA) and the McDonnell Douglas Corporation libraries and the archive journals and meeting papers of the American Institute of Aeronautics and Astronautics (AIAA). The reports selected were categorized by subject and screened according to the required range of geometry and flight conditions. This process identifies most of the state-of-the-art prediction methods.

Of primary consideration is the method type: theoretical, semi-empirical, or empirically derived. Theoretical or semi-empirical techniques are desirable because they provide greater capability than empirically derived methods. Since method extrapolation is often required, the techniques with a theoretical base can often be extrapolated without great loss in accuracy. Empirical methods using cruvefits of test results generally do not follow any rationale physical phenomena, but are chosen for convenience. Hence, theoretical or semi-empirical techniques are preferred if the accuracy, range of applicability, and ease of use of the methods are acceptable. Empirical techniques are not completely excluded. A proper mix of the method types will allow analysis of a large range of the selected requirements.

3.2 AXIAL FORCE

Configuration stability and control is of importance in configuration design but vehicle drag (axial force) is the determining factor in assessing the ability of a configuration to deliver its payload to the target. Since the body is a major component, its axial force must be predicted accurately.

The body axial force is comprised of friction drag, nose pressure/wave drag, interference, boattail pressure/wave drag, base drag and protuberance drag. The Mach number variation of the major contributors are shown in Figure 6. The following paragraphs describe the recommended and available methods for each component.

Skin Friction Drag - Van Driest Method II is recommended for skin friction at all Mach numbers. The method requirements for skin friction are based upon the expected range of Reynolds number and Mach number. These ranges are set by the vehicle flight profiles, as well as a typical wind tunnel model size and test conditions.

The classic means of evaluating skin friction is to use flat plate results and apply correction factors for three-dimensional flow or compressibility. Of the many skin friction methods available, only the Blasius laminar flow theory is considered theoretical; the remaining methods are equations which model experimental results. Many of the smooth skin friction methods used are summarized in Table 6. The Mach-Reynolds number capability of each of these methods are shown in Figures 7 and 8. The methods in Figure 8 are presented assumming no compressibility correction. The characteristic length of one foot is representative of a fin panel mean geometric chord for a full scale vehicle; the ten foot characteristic length is representative of a body. The turbulent Sommer and Short T', Van Driest methods I and II, and Spalding and Chi techniques are shown to be candidate for further review; Van Driest has been shown to be superior to others in its class and is the recommended automated approach. Since the Van Driest method is an iterative technique, the Blasius and Schoenher methods are chosen for handbook use. These methods are given in Table 7. For Reynolds numbers near $5x10^5$ per foot (comparable to high altitude), a laminar boundary layer will transition to turbulent. A suitable method for the transition regime assumming an adiabatic wall, is given in Reference 32 and is as follows:

1. Determine the transition Reynolds number

$$R_{e_{TRA}} = e^{.22M} \times 10^6$$

2. Compute laminar Reynolds number

$$R_{e_{lam}} = R_{e_{TRA}} [1-(0.67/A)^{1.25} R_{e_{TR}}^{-.375}]$$

where, $A = 0.036 - .00128M - .00072M^2$

3. Compute turbulent Reynolds number

$$R_{e_{TUR}} = R_e - R_{e_{LAM}}$$

where R_e is Reynolds number based on the characteristic length at freestream conditions.

4. Compute total friction of component

$$C_{f_{TR}} = (C_{f_{lam}} R_{e_{lam}} + C_{f_{tur}} R_{e_{tur}})/R_e$$

This technique can be used for each component of the configuration.

Heat transfer effects can be included by using the relationship

$$R_{e_{TR}} = R_{e_{TR}} \left[\frac{1-(T_w/T_{aw})_{CRIT}}{T_w/T_{aw}-(T_w/T_{aw})_{CRIT}} \right]^{1/2}$$

where $(T_w/T_{aw})_{CRIT}$ is a function of Mach number and given in either Dunn and Lin, Reference 20, or Van Driest and Boison, Reference 23. Note that the Eckstrom and Eckert methods handle transition; these methods are recommended alternates.

Eaton, Reference 33, uses the empirical results of Chapman and Kester, Reference 34. These data are limited to low supersonic Mach numbers and were, therefore, excluded.

Skin Friction Compressibility Correction - The Hoerner method is recommended. A correction due to compressibility at Mach number is commonly used to utilize incompressible values of skin friction at compressible speeds. For methods without heat transfer, Hoerner (Reference 36) presents the commonly used formulas, which are as follows:

Laminar Body Layer -

$$\frac{C_f}{C_{f_i}} = (1. + 0.045M^2)^{-4}$$

Turbulent Boundary Layer -

$$\frac{C_f}{C_{f_i}} = (1+0.15M^2)^{-.58}$$

The turbulent boundary layer relationship of Datcom, Figure 4.2.3.1-68, is also recommended.

Surface Roughness Correction - The Clutter method is recommended. Clutter, Reference 18, presents charts of skin friction coefficient as a function of Mach number, Reynolds number and surface roughness (sample given in Figure 9) using a modified form of the Prandtl and Schlichting Method (Reference 31). Datcom presents a table, shown in Table 8, which equates surface type to an equivalent sand roughness. From this admissable roughness height, a critical Reynolds number is determined from Datcom Figure 4.1.5.1-27. This Reynolds number is then used to compute skin friction using data for a smooth, turbulent flat plate.

Friction is a more significant effect at subsonic speeds since it is a greater percentage of the vehicle drag. However, it should not be ignored at supersonic speeds. It is recommended that the Clutter friction method be used. It is essentially an extension of the Van Driest II technique. Since this method requires iteration, it is more amenable to automation. For a handbook, it is recommended that the Datcom technique be employed because of its simplicity.

Subsonic Nose Pressure Drag - The Hoerner "form factor" correlation is recommended. At subsonic and transonic speeds, the zero-lift drag terms of pressure and friction drag are normally presented as a multiplier to the friction coefficient (C_f), sometimes referred to as a "form factor". Experimental observation quantifies pressure drag as a direct function of C_f and thickness to chord ratio (t/c) as follows:

Flow	Pressure Drag
2-Dimensional	$60\ (\frac{t}{c})^3\ C_f$
3-Dimensional	$7\ (t/c)^3\ C_f$

In addition, a correction is applied to C_f since the local flow over the surface is at a higher speed than free-stream (from the Bernoulli principle). Theoretically, it can be shown that the increase in C_f is as shown below:

FLOW	INCREASE IN C_f DUE TO q
2-Dimensional	2 (t/c) for $(\frac{X}{C})_{max} = 0.3$
	1.2 (t/c) for $(\frac{X}{C})_{max} = 0.5$
3-Dimensional	$1.5\ (t/c)^{1.5}$

Hence, by summation, the following formulas are applicable at subsonic speeds:

2-Dimensional:

$$\frac{C_{D_0}}{C_f} = [1+1.2\ (\frac{d}{L})^{1.5} + 7\ (\frac{d}{L})^3]\ \frac{S_{wet}}{S_{ref}}$$

3-Dimensional:

$$\frac{C_{D_0}}{C_f} = [1+1.5\ (\frac{d}{L})^{1.5} + 7\ (\frac{d}{L})^3]\ \frac{S_{wet}}{S_{ref}}$$

Although Datcom presents what appears to be a radically different formula for 3-D flow

$$\frac{C_{D_0}}{C_f} = [1+0.0025\ (\frac{L}{d}) + \frac{60}{(L/d)^3}]\ \frac{S_{wet}}{S_{ref}}$$

closer inspection however shows the results from both methods are nearly the same for body fineness ratios greater than six.

Transonic Nose Pressure/Wave Drag - Chaussee and empirical techniques are recommended. Since knowledge of the pressure distribution over a body is required to compute pressure drag, it is difficult to obtain such information for general body shapes without the use of test results or complex computer programs. The "form factor" techniques previously described easily solve this difficulty.

Wave drag can be handled theoretically using the variety of techniques shown in Table 9. Transonic wave/pressure drag is classically evaluated through use of empirical correlations of cones, tangent ogives and hemisphere shapes such as those given in References 37-42. Since nose bluntness can be

accounted for through addition of the blunt nose cap drag to that of a sharp nose, less the increment of the unblunted cap, a series of design charts are available (MDAC-HB Reference 32) for a wide variety of cone and ogive shapes with varying degrees of nose bluntness, form Mach 0.5 to 5.0, and nose fineness ratios of 1.5 to 5.0 (Figure 10). Chaussee, Reference 43, performed the same task through numerical solution of the unsteady Euler equations in the transonic speed regime (Figure 11). The results are given in Table 10 as a function of nose bluntness ratio, fineness ratio and Mach number. Use of the Chaussee data with the empirical results for tangent ogives should accurately define the transonic wave/pressure drag for this common nose shape.

Supersonic Nose Wave Drag - The second-order shock-expansion technique is recommended. At supersonic speeds it is shown in Reference 14, and Figure 12, that modified Newtonian theory applied to hemispheres is accurate to low supersonic speeds. Since nose shape generality is desirable, the use of modified Newtonian theory with the second-order shock expansion method (Reference 44) appears to be an excellent choice. As will be shown later, second-order shock expansion is an excellent technique compared to other theories for predicting normal force and center of pressure. Hence, this one method can be used to evaluate three separate aerodynamic parameters, C_N, X_{CP}, C_{D_W}, that are related by the pressure distribution.

Other methods available for ogive and cone nose shapes are shown in Figures 13 and 14. The data presented in the Martin-Marietta CAMS program (Reference 45) shown in Figure 15 is very complete; wave/pressure drag from NACA A52H28 (Reference 46) has been correlated for the 3/4-power, L-D Haack, conical and tangent ogive shapes. These methods are selected as alternates to the theoretical second-order shock method recommended.

Note that these methods only address axisymmetric geometries. There is no technique available to estimate wave/pressure drag of arbitrary-shaped configurations. The only non-circular methods available are for elliptic shaped configurations. Datcom provides a correction to wave drag due to body ellipticity and Jorgensen (Reference 47) has derived an expression from slender-body theory for constant elliptic cross section cones. These methods are given in Figure 16. Arbitrarily-shaped configurations must be analyzed through use of a "paneling" code such as Supersonic/Hypersonic Arbitrary Body Program (S/HABP), Reference 48, whose inclusion is beyond the scope and intent of Missile Datcom.

Boattail wave/pressure drag - The empirical results of Payne are recommended. The effect of boattails or flares is perhaps the greatest gap in methodology. In spite of the volume of test data available on the subject, and reported by P. R. Payne (Reference 53), most of the published results treat specialized configurations. Data was available to permit construction of parametric design charts of conical and circular arc boattails, from Mach 0.6 to Mach 1.3 for the range of parameters in Figure 17. Since many missile configurations employ boattailing, and as much as 30% of a configuration zero-lift drag can be attributable to the afterbody, an accurate means are required to estimate boattail pressure drag (and the effect on base pressure drag. The Payne results are available for pressure/wave drag and base drag, and their use is recommended in this speed regime. Though the range of applicability is for $(d_b/d_m)^2$ greater than 0.5, this does cover the great percentage of boattail designs considered for missile configurations. Since results are not available at subsonic speeds, it seems appropriate to use the Datcom approach of determining a separation point on the afterbody and assume full base drag over the remaining boattail area.

Moore, Reference 51, suggests the use of Wu and Aoyoma theoretical technique (Reference 54), where

$$C_p\,(X) = -\frac{2}{5}\,\frac{(x_1 - C)}{\sqrt{(\gamma+1)}\;M_\infty^{2/3}}\left[\frac{1}{25}\;\frac{(x_1 - C)^2}{(\gamma+1)\;M_\infty^{2/3}} - \frac{1 - M_\infty^2}{(\gamma+1)\;M_\infty^2}\right]^{1/2} - \left(\frac{dR}{dx}\right)^2$$

Here, x_1 is measured from the shoulder of the boattail and

$$C^2 = 25\,(\gamma+1)\,M_\infty^{2/3}\left\{\frac{1}{2}\;\frac{1 - M_\infty^2}{(\gamma+1)\;M_\infty^2} + \left[\frac{5}{4}\left(\frac{1 - M_\infty^2}{(\gamma+1)\;M_\infty^2}\right)^2 + \frac{2}{M_\infty^{2/3}}\left(\frac{1 - M_\infty^2}{(\gamma+1)\;M_\infty^2}\right)\left(\frac{3\;dR/dx}{2\;\sqrt{\gamma+1}}\right)^{2/3} + \left(\frac{3\;dR/dx}{2M_\infty\;\sqrt{\gamma+1}}\right)^{4/3}\right]^{1/2}\right\}$$

The pressure distribution so determined is integrated over the boattail to determine pressure drag. This method is limited to the range from Mach 0.8 to 1.2. To assure method continuity, the Payne results are preferred over this theoretical technique.

Although the results presented by John Jack, Reference 55, and shown in Figure 18, were performed using theoretical techniques in supersonic flow,

the second-order shock expansion method has been shown to given reasonably good accuracy and can handle a wide variety of configurations.

The design chart methods for wave drag at supersonic speeds are not recommended for automation, but they are extremely useful for handbook computations. Use of the nose wave drag and boattail wave drag results must however be corrected for afterbody length; the afterbody pressure distribution is a function of nose length. The Datcom design chart, given in Figure 19, handles this difficulty.

Base Drag - Empirical correlations are recommended. The methods available to evaluate base drag are shown in Figure 20. At subsonic speeds, the empirically derived Hoerner result

$$C_{D_b}=0.029\left(\frac{d_b}{d}\right)^3/\sqrt{C_{D_f}}$$

is used by many because of its simplicity. Moore proposed an approach which incorporates an angle of attack effect, shown in Figure 21. This method has the advantage of being simple to apply and is quantitatively verified at zero angle of attack. The Love (Reference 57) results shown in Figure 22 serve as an excellent data source. Aiello, Reference 58, presents empirically derived tables of base drag due to angle of attack, but are limited in the range $1.5 \leq M \leq 2.75$ and $0 \leq \alpha \leq 30$ degrees.

These methods are for non-boattailed bodies. It is recommended that the angle of attack influence given by Moore and Aiello be used to develop a unified method across the Mach regime. Search of the literature has determined that there are sufficient results available to perform the following method development tasks:

1. Effect on base drag due to Reynolds number for laminar boundary layers; if the flow ahead of the base is turbulent, no effect on base drag is shown,
2. Effect on base pressure due to body fineness ratio; for ℓ/d greater than 5, in supersonic flow, the forebody effect can be neglected, and
3. Effect of base pressure due to boattailing at supersonic speeds.

Some methods to determine these effects have been developed in Reference 32. It is also recommended that the Datcom methodology of Section 4.6 be included to account for jet effects.

Boattail Wave Drag Due To Jet Effects - The method of Payne is recommended. A body which has a jet exhausting from the base will experience an entrainment effect of the jet exhaust over the aft body. The body pressure distribution shown schematically in Figure 23 is altered depending upon the nozzle area fraction of the base. The qualitative variation of boattail pressure drag, given in Figure 24, illustrates a typical variation due to jet velocity. At u_j/u_o of unity, the boattail pressure distribution is unaltered, hence this point should correspond to the true pressure drag. As jet velocity is increased, the jet flow acts like a flow sink, thereby increasing the local flow speed over the afterbody and increasing the boattail drag. Since little results are available in the region $u_j/u_o=1$ to $M_j=1.0$, it is assumed that boattail drag varies linearily; limited experimental results do reflect a linear trend. As the jet velocity exceeds sonic flow, a number of second-order phenomena take place which are configuration dependent. Generally, exhaust pluming will become the dominant characteristic as jet velocity is further increased, acting like a source and reducing boattail flow velocity, hence, reducing boattail drag. In the extreme, this pluming will completely cancel the entrainment effect and cause a negative boattail drag.

A theoretical method for evaluating this effect was presented by Payne, Reference 53. For a conical boattail, the change in pressure drag to entrainment is

$$\Delta C_{D_{\beta E}} = (K/2)\,(u_{jo}/u_o - 1)\,\Phi$$

where K = entrainment ratio, 0.0415 at low speeds

u_{jo} = jet "core" velocity

u_o = free-stream velocity

and

$$\Phi = \frac{2\beta\tan\theta}{\hat{r}^2_{max}}\left\{\frac{1}{1+\beta^2\tan^2\theta}\left[\sqrt{(1+\beta^2\tan^2\theta)\hat{r}^2_{max} - 2\,\hat{r}_{max} + 1} - \beta\tan\theta\right] + \frac{1}{(1+\beta^2\tan^2\theta)^{1.5}}\left[\sinh^{-1}\left(\frac{(1+\beta^2\tan^2\theta)\,\hat{r}_{max} - 1}{\beta\tan\theta}\right) - \sinh^{-1}(\beta\tan\theta)\right]\right\}$$

where $\beta = \sqrt{1-M^2}$

θ = boattail angle

$\hat{r}_{max} = r_{max}/r_s$

Protuberance drag - Recommend Hoerner compilation. Probably the most comprehensive compilation of drag data and methods assembled is that by Sighard Hoerner in his book "Fluid-Dynamic Drag" (Reference 36). The method presented in Section V, "Drag of Surface Imprefections", is comprehensive enough to allow the missile designer to quickly and accurately estimate the drag effect of joints, steps or surface waviness. A significant protuberance of interest to the missile designer is that due to launch lugs, or shoes, which attach the missile to the launcher. Limited test results for standard lugs were presented in AIAA Paper 72-969 (Reference 59). It is recommended that selected data compilations from Hoerner be used to allow the designer to perform drag analysis of surface imperfections or protuberances suitable for missile design purposes.

Axial Force At Angle of Attack - The methods for evaluating C_A (or C_D) at angle of attack range from an Allen and Perkins theoretical equation to empirical curve fits. The Jorgensen technique (Reference 47) is simple to apply, but is only approximate because it assumes that C_A varies as the axial component of dynamic pressure. The CAMS prediction code (Reference 45) uses the induced drag equation

$$C_{D_i} = \sin 2\alpha \sin \frac{\alpha}{2} + \eta C_{d_c} \sin^3\alpha \frac{S_P}{S_{REF}}$$

from Allen and Perkins and Datcom at subsonic and transonic speeds. This method can be reduced, through inspection to

$$C_{D_i} = C_L \sin \alpha$$

Limited results from the report "Analysis of Datcom Methods as Applied to Modern Configurations", Reference 60, shows this equation to be superior to Jorgensen's result at moderate angles of attack. Some authors have instead chosen the relation

$$C_{D_i} = C_L \tan\alpha$$

The CAMS technique at supersonic speeds has modified this method empirically to

$$C_{D_i} = C_L \tan\alpha[1+K\ (0.566 + 0.111M)\ (1.15-0.075\ F_A/F_N)]$$

where K is a modification factor which is a function of angle of attack.

Another empirical technique is also attributable to Martin-Marietta (Reference 58). The non-linear axial force, from Mach 0.6 to 1.3, is an empirical function of Mach number and angle of attack.

$$C_A = C_{A_0} + f\ (M, \alpha)$$

where $f(M,\alpha)$ is given in Figure 25. The few comparisons with test results are observed to be quite good. A good approximation is obtained at higher supersonic speeds by specifing C_A to be invariant with angle of attack. This characteristics is quite common for bodies.

The techniques for estimating body axial force at angle of attack are primarily empirically based. It is recommended that empirical results be utilized at angles of attack greater than approximately 20 degrees. Use of the Allen and Perkins and Jorgensen results are preferred at the lower angles of attack. The method recommendations are given in Table 11.

3.3 BODY NORMAL FORCE AND PITCHING MOMENT

In most methods the normal force on a missile body is assumed to be composed of potential and viscous components. This technique is used extensively, is simple to apply, and models the vortex separation phenomena at high angles of attack.

Subsonic Inviscid Lift and Pitching Moment - Empirical and the Allen and Perkins methods are recommended. In 1924, Max Munk, Reference 61, derived the potential flow normal force of pointed slender bodies of revolution (based on maximum cross-sectional area)

$$C_{N_p} = (K_2-K_1)\ \sin\ (2\alpha)$$

where (K_2-K_1) is the virtual mass coefficient difference between transverse and axial motion for ellipsoids of revolution computed from Lamb, Reference

62. Ward, Reference 63, examined Munk's hypothesis and determined that the resulting force vector should be inclined down-stream by an angle $\alpha/2$ to the vertical. Hence, normal force in potential flow became

$$C_{N_p} = (K_2-K_1) \sin (2\alpha) \cos (\alpha/2)$$

This work was extended by Allen and Perkins, Reference 64, 65, and 66, when they derived the potential normal force equation for blunt-based bodies,

$$C_{N_p} = (K_2-K_1) \frac{S_b}{S} \sin (2\alpha) \cos (\tfrac{\alpha}{2})$$

The potential pitching moment was also presented, being

$$C_{m_p} = (K_2-K_1) \left[\frac{V-S_b(\ell-X_M)}{SD} \right] \sin (2\alpha) \cos (\alpha/2)$$

Using a trigonometric identity, the normal force becomes

$$C_{N_p} = 2 (K_2-K_1) \sin\alpha\cos\alpha\cos (\alpha/2) \frac{S_b}{S}$$

Nielsen (Reference 12) has shown that for a slender body with a blunt base, slender-body potential theory derives C_{N_α} as 2.00 per radian, based on base area. If C_{N_α} is known for a body, then the potential normal force and pitching moment become

$$C_{N_p} = C_{N_\alpha} \sin\alpha\cos\alpha\cos (\alpha/2)$$

$$C_{mp} = C_{N_\alpha} \left[\frac{V-S_b(\ell-X_M)}{SD} \right] \sin\alpha\cos\alpha\cos (\alpha/2)$$

Hence, one is able to approximate the potential normal force and pitching moment of a body through simple modification of the slender-body result.

Many empirical techniques exist that are curve-fits of specific data bases. The well-known empirical techiques are those of Martin-Marietta Company (MMC) and by Baker of AEDC. The MMC results, given in Reference 58, and the Baker methods of Reference 74 do provide for excellent prediction as long as the configuration being analyzed lies within the data base. These data may be useful for analysis of selected configurations at transonic speeds, but the methods are not recommended because of their questionable extrapolation capability.

Since the Allen and Perkins potential normal force and pitching moment results were derived using the simplifying assumption of long-pointed forebodies, many authors have strived to obtain much better results for "realistic" configurations.

At subsonic speeds, Moore (Reference 51) correlated data from projectiles to evaluate the body normal force slope by summation of the nose, afterbody and boattail components,

$$C_{N_\alpha} = (C_{N_\alpha})_N + (C_{N_\alpha})_A + (C_{N_\alpha})_{BT}$$

where $(C_{N_\alpha})_N$ is evaluated from empirical data, $(C_{N_\alpha})_A$ is evaluated from the theoretical calculations of Wu and Aoyoma (Reference 54), and $(C_{N_\alpha})_{BT}$ is an empirical correlation. One must resort to empirical results at subsonic and low transonic speeds since there are no easily applied methods to compute potential flow at these speeds other than the Allen result. The well-known Neumann Potential Flow (References 90 and 91) and Woodward (Reference 92) computer codes supply excellent results at low angles of attack, but are large, costly and mathematically complex. Their inclusion is considered outside the scope of Missile Datcom.

<u>Transonic inviscid lift and pitching moment</u>. Klopfer and Chaussee and empirical are recommended. The method of Wu and Aoyoma in determining transonic theoretical normal force slope and aerodynamic center is based on small perturbation theory. Application to blunter nose shapes raises doubts as to the methods applicability. Chaussee and Klopfer (Reference 93) have numerically solved the three-dimensional flow about axisymmetric bodies and the computed pressure profile nearly reproduced test results. Since this procedure requires an iteration scheme, the technique is extremely costly (3900 sec. computer time on a CDC 7600) and not desirable as a module in an automated Missile Datcom. Parametric results are available which provide theoretical solutions in the transonic Mach regime.

The range of applicability of the Klopfer results are shown in Figure 26. The results were curve-fit with quadratic polynominals, similar to the one shown in Figure 27. The terms of the polynominals are Mach number dependent and are presented in Tables 12 and 13 for normal force slope and pitching moment slope, respectively. This scheme was used because of the extreme cost in generating points for the interpolation tables. Correlations with test data have been shown to be quite good. The body fineness ratio range investigated is smaller than desirable, and the range of nose bluntness ratios, from 0.025 to 0.5, are limited. However, it is felt that these results are important enough to warrant inclusion since they do cover the lower body fineness ratio range.

As shown in Figure 28, these results do supplement the higher afterbody fineness ratio empirical results of Aiello and Bateman (Reference 58) and Krieger (Reference 49). Extrapolation outside of the nose fineness ratio and afterbody length ranges covered should be determined. The effect of nose bluntness is limited. It is anticipated that incremental nose bluntness effects can be summed to sharp-nosed profiles, as was described earlier for wave drag, to obtain the effects of nose bluntness. This was performed in the Krieger compilation with success.

Moore suggests computing pitching moment slope using the relationship

$$C_{M_\alpha} = -[(C_{N_\alpha})_N\ (X_{CP})_N + (C_{N_\alpha})_A (X_{CP})_A + (C_{N_A})_{BT} (X_{CP})_{BT}$$

where $(X_{CP})_N$ and $(X_{CP})_{BT}$ are evaluated using slender-body theory,

$$(X_{CP})_N = \ell_N - \frac{(VOL)_N}{\pi R^2_{ref}}$$

$$(X_{CP})_{BT} = \ell - \frac{(VOL)_{BT}}{\pi R^2_{ref}}$$

and $(X_{CP})_A$ is evaluated using the theoretical result from Wu and Aoyoma. No serious fault can be seen using this technique at subsonic speeds. At transonic and supersonic speeds more accurate results are required. Use of empirical results, with Klopfer and Chaussee theoretical solutions, are recommended at transonic speeds.

Inviscid Lift and Pitching Moment - Supersonic - Second-order shock-expansion and modified Newtonian are recommended. The range of applicability of the various supersonic theories are shown in Figure 29. Since several techniques are available, method selection was based primarily on method accuracy and the fundamental theory used in its development.

At supersonic speeds, Van Dyke, Reference 94 and 95, derived a second-order solution for axial flow and cross-flow. He found that solutions for the cross-flow equations could only be obtained for conical flow, so a refinement of the first-order approximations were necessary. He proposed the Hybrid Theory which combines first-order cross flow developed by Tsien with second-order axial flow. Other attempts to solve the potential equations resulted in the Method of Characteristics, Tangent-Cone and the Shock-Expansion Techniques. The Method of Characteristics is the most exact technique but requires computer solutions. Taylor and Maccoll, Reference 70, formulated a numerical solution to the shock wave equations proposed by Rankine, where

the position of the Mach wave and the pressure over a cone in supersonic flow were determined. Kopal, Reference 97, and the Ames Research Staff extended this work in NACA Report 1135 (Reference 98) . The Generalized Shock Expansion method was extended by Syvertson and Dennis, Reference 44, to cover a much larger Mach regime. Fenter, Reference 99, developed the Modified Second-Order Shock Expansion technique for use with ogive cylinder configurations. Newtonian Impact Theory was developed by assuming that the shock wave lies on the body surface, attainable at very high (hypersonic) Mach numbers; this method has been modified to include a pressure relief due to flow centrifugal force over a curved surface. Some quantitative comparisons with test results are shown in Figure 30.

In general, the Second-Order Shock Expansion method performs better and is far superior to the Allen and Perkins result, since it can adequately handle more arbitrary shaped surfaces. It is available in automated form from many sources. Datcom Figures 4.2.1.1-21 and 4.2.2.1-23, Figures 31 and 32, summarize these results for both cones and tangent ogives; the test results for Figure 30 have been reported in NACA 1328 by Syvertson and Dennis, Reference 44. An extensive summary chart is not readily available for the Hybrid Theory, because of its limitation that the body surface slope be less than the Mach wave angle (see Figure 33).

The second-order shock expansion method requires an attached shock, and therefore cannot handle the effects of nose bluntness. The method proposed by Moore, Reference 131, is recommended. It uses Newtonian theory over the blunted cap and a pressure matching criteria from perturbation theory.

The effect of boattails or flares can be handled using the Second-Order Shock Expansion Theory for supersonic flow, through its accuracy has not been thoroughly examined. Empirical boattail results at supersonic speeds are also given in Datcom (Figure 4.2.1.1-22a), shown in Figures 34 and 35; their use in a handbook is ideally suited with data of Figures 31 and 32. At subsonic and transonic speeds one must resort to empirically derived equations or charts. Moore, Reference 51, and Krieger, Reference 49, correlated a large collection of test data and then applied the correlation

$$(C_{N_\alpha})_{BT} = (C_{N_\alpha})'_{BT} \left[1 - \left(\frac{d_B}{d_r}\right)^2\right] \frac{\pi}{4} \frac{d^2}{S} \text{ (1/degree)}$$

where $(C_{N_\alpha})'_{BT}$ is the boattail increment obtained as a polynominal function. These results should be adequate for missile design.

<u>Viscous Lift and Pitching Moment</u> - Allen and Perkins is recommended. Allen and Perkins surmised that an inclined body of revolution experiences a cross flow which is the result of viscous flow about the body. The viscous cross flow acting on an incremental section of the body is assumed to be produced from the cross-section drag coefficient, Cd_c, which is a function of Reynolds Number. This incremental normal force is

$$\Delta C_{N_{VIS}} = Cd_c \; d \sin^2 \alpha \; \Delta X / S_b$$

Integration of this equation along the body, assuming Cd_c is constant, results in

$$C_{N_{VIS}} = Cd_c \frac{A_P}{S} \sin^2\alpha$$

and

$$C_{M_{VIS}} = Cd_c \frac{A_P}{S} \left(\frac{X_M - X_C}{D}\right) \sin^2\alpha$$

Allowance must be made for finite body lengths. Goldstein (Reference 73) determined a reduction factor, η, shown in Figure 35 for this purpose. Baker (Reference 74) and Aiello (Reference 58) later modified η at transonic speeds. Hence, the Allen and Perkins results became

$$C_N = (K_2 - K_1) \frac{S_b}{S} \sin(2\alpha) \cos(\alpha/2) + \eta Cd_c \frac{A_P}{S} \sin^2\alpha$$

$$\left.\begin{aligned} C_M = {} & (K_2 - K_1)\left[\frac{V - S_b(\ell - X_M)}{SD}\right] \sin(2\alpha)\cos(\alpha/2) \\ & + \eta \, Cd_c \frac{A_P}{S} \left[\frac{X_M - X_C}{D}\right] \sin^2\alpha \end{aligned}\right\}$$

as p. 317 Eq (8-36) (red book)

Several methods are available to determine η at transonic speeds. All have been derived by assuming a Mach number variation in Cd_c, several of which are shown in Figure 37. A particular η and Cd_c combination cannot be recommended at transonic speeds, but must be determined quantitatively. All applicable methods must be assessed for accuracy before a choice is made.

Hill, Reference 75, pointed out that the flow external to the boundary layer is potential in nature, so the body model must include the exterior of the boundary layer. Kelly, Reference 76, called the use of a constant C_{d_c} alcng the body length inappropriate; he took the results by Schwabe, Reference 77, and derived the Impulsive Flow Analogy, where the development of cross flow on a body is analogous to the time dependent development of cross flow force of a cylinder set in motion from rest. The flowfield is assumed to be developing along the body length, being analogous to time. In 1966, Sarpkaya (Reference 78) modified the data of Schwabe to remove the inertia effects. The results are shown in Figure 38. Perkins and Jorgensen (Reference 79) and Mello (Reference 80) did extensive studies of the pressure and normal force distributions over bodies and found that the cross flow drag rose steadily and then declined to a steady state value, a trend similar to the Schwabe results. The result of Kelly's refinements became

$$C_N = (K_2-K_1)\,\frac{S_b}{S}\sin(2\alpha)\cos(\alpha/2) + \int_{nose}^{tail} C_{d_c}\, d\, \sin^2\alpha\, dX$$

This method should be quantitatively assessed as an alternate technique.

In NOL TR 73-225 (Reference 89), Darling proposed modifying the cross flow drag along a missile body, as shown in Figures 39 and 40, by accounting for upstream influence of the base, the effect of nose axial pressure gradient, and base influence at transonic speeds. This method is also worth further review because of its more rigorous approach.

Datcom (Section 4.2.1.1) presents a method by which the viscous effect is applicable over only that portion of the body aft of X_0, the position of maximum negative change in cross-section area. This technique, though simple, is too elementary compared to other available methods. The accuracy is dependent upon the choice of X_0, and is subject to wide interpretation. This method was shown to be less accurate than other available techniques (Reference 60), and is not recommended.

Since the viscous cross flow methods derived from Allen and Perkins use the flow past an infinite cylinder to model the effect of viscous normal force, it is expected that such models will be most accurate in the higher angle of attack range. The time dependency noted by Kelly should serve as an excellent analogy to the formation of the vortex patterns shown in Figure 41.

Jorgensen, References 47, 86, and 87, has used the method of Allen and Perkins to develop a technique valid for slender bodies through 180 degrees angle of attack. This method adjusts the inviscid and viscous components by a factor (C_n/C_{n_0}), which is the local cross-flow force ratioed to that for an infinite cylinder. Even though most cross-sectional shape experimental investigations have been conducted at subsonic speeds, this method is useful at speeds where (C_n/C_{n_0}) has been developed from theory. This has been done for elliptical cross-section and can be performed for arbitrarily-shaped sections using Newtonian theory. The integral form of Jorgensen's equations

$$C_N = \frac{\sin 2\alpha \cos(\alpha/2)}{A_r} \int_o^{\ell} \left(\frac{C_n}{C_{n_o}}\right)_{SB} \frac{dA}{dx}\, dx + \frac{2\eta C_{d_n} \sin^2\alpha}{A_r} \int_o^{\ell} \left(\frac{C_n}{C_{n_o}}\right)_{Newt} r\, dx$$

$$C_m = \frac{\sin 2\alpha \cos(\alpha/2)}{A_r X} \int_o^{\ell} \left(\frac{C_n}{C_{n_o}}\right)_{SB} \frac{dA}{dx} (x_m - x)dx + \frac{2\eta C_{d_n} \sin^2\alpha}{A_r X} \int_o^{\ell} \left(\frac{C_n}{C_{n_o}}\right)_{Newt} r(x_m - x)dx$$

allow for variation in body shape along its length, making it a far more useful tool in missile design. Other methods for handling more arbitrarily shaped configurations are summarized below.

Baker (Reference 74) has empirically modified the Jorgensen pitching moment result to bring the method in line with results of his data base. He has used the equation

$$C_M = C_{M_{JORGENSEN}} + Z_{MAX}\, \overline{\delta}\, \left(\frac{\ell/d}{10}\right)^2$$

Figure 42 presents those parameters used by Baker in his analysis. This method is also recommended for further consideration in the transonic Mach regime.

Arbitrary Shaped Bodies - No specific method is recommended. As can be expected, there are no simple techniques available to predict normal force or pitching moment of general body configurations at any Mach number. The most comprehensive method available is proposed by Jorgensen in NASA TN-D-6996 and NASA TN-D-7228 (References 47 and 86), where the Allen and Perkins method is extended through use of correction factors to the potential and viscous terms of C_N and C_m. The equations relevant to Jorgensen's technique are presented in Figure 43 as given in Datcom. Note that the terms $(C_N/C_{N_{cir}})_{SB}$ and $(C_N/C_{N_{cir}})_{NT}$ correct the potential and viscous terms due to body ellipticity. These equations assume that the body cross-section is uniformly elliptic from nose to tail. Other results available for $(C_N/C_{N_{cir}})$ are presented in Figure 44 from Jorgensen. A logical extension of this method is to permit the body cross-section shape to vary along the body length. The C_N and C_m equations transformed in this manner were previously shown. Jorgensen provided a thorough discussion of this concept in NASA TR R-474, Reference 87, and provided comparisons with test results; the samples of which are shown in Figure 45. As anticipated, fair agreement with test was obtained at the higher angles of attack. This is expected since the viscous contribution is derived from cross-flow drag results.

Another means of using the Jorgensen method has been to substitute the experimental cross-flow drag coefficient for the particular shape. However, the shapes available (presented in Figure 46) have only been experimentally investigated at subsonic speeds. Examples of other configurations tested are shown in Figure 47, indicating the probability of a limited data base for arbitrary shaped slender bodies. Since no comprehensive summary of results have been collected, the Jorgensen method is constrained to circular and elliptical configurations at the higher Mach numbers by virtue of data availability.

A second subsonic method used for bodies of revolution and elliptical cross-section bodies is similar to that derived using the concept of vortex lift of thin wings by Polhamus, commonly referred to as the Polhamus Suction Analogy (Reference 102), and empirically extended in Datcom. The

method, outlined in Figure 48, has been observed to fairly represent the lift of elliptical shaped bodies with a power law planform shape. However, a more unified approach, such as Jorgensen's method is preferred.

Williams, Reference 108, presented a method based upon theory and experiment ot predict the aerodynamics of elliptical lifting body geometries, similar to that shown in Figure 49. Application of the technique to other similar configurations is not known. The method requires knowledge of the configuration pressure distribution to derive pressure drag. The method of Jorgensen should perform equally well yet have a wider range of configuration applicability.

A number of lifting bodies at subsonic speeds have been included in the Datcom. The types of configurations shown in Figure 50 have enabled the Datcom authors to develop empirically based methodology. These configurations are applicable to missile design, and inclusion of the Datcom techniques are recommended. Unfortunately, methodology at supersonic speeds is not available, although programs similar to S/HABP are ideally suited to such designs.

In the design environment, the S/HABP code is perhaps the most inexpensive technique presently available. It does however, require experience in use and methods choice to obtain good results, and often requires "calibration" to a known, similar configuration. Figure 51 presents a pressure method selection rationale (Reference 110) to reduce this "calibration" time.

A promising technique still in development is that being performed by Purvis at NSWC, White Oak Laboratory. It is designed to allow static and dynamic aerodynamic prediction of non-axisymmetric geometries. This computer program will allow the aerodynamic estimation of general body shapes, but having the advantage of allowing the user to build a complex geometry using a minimal number of inputs. This multi-Mach program is considered a significant advance in prediction capability. None the less, it is not recommended that such complex codes be inserted in an automated Missile Datcom. There are many other codes available, such as APAS from Rockwell, Woodward from NASA, and PANAIR (Reference 109) from Boeing, and referencing the available methodology and data comparisons such as that in Reference 111, is a significant benefit of Missile Datcom which will enhance and not detract from its usefulness.

Asymmetric Forces - No method is recommended. The cross flow methods all strive to model the flowfield of a body at angle of attack. As illustrated in Figure 41, experimental observations show two symmetric vortices forming at the lower angles of attack. As the angle of attack is increased the pattern changes to a Bernard-Von Karman vortex street. At much higher angles of attack a new phenomena develops, originally termed "phantom yaw", in which the flowfield shows unsteadiness and the vortex patterns switch between sides of the body and exhibit large forces perpendicular to the plane of the velocity vector. In theory, the time integral of these forces should be zero, but characteristics such as wind tunnel flow angularity, model surface imperfections or alignment, cause the vortices to favor one side of the configuration. Formation of the leeside flow unsteadiness disappears when the cross flow Mach number exceeds approximately 0.5 and its occurance is a function of nose bluntness, nose cone semi-apex angle and presence of vortex producers such as strakes. Since this phenomena is due to the boundary layer separating on the leeside of the body, boundary layer blowing has also been used to alleviate the effect. The work of Wardlaw (References 81 and 82), Fleeman (Reference 83), Reding (Reference 84) and Dahlem (Reference 85) have presented semi-empirical and empirical techniques to model this phenomena.

For practical use in the missile design community, the following are recommended for inclusion:

- A summary for the current state-of-the-art in prediction methodology
- A summary of available experimental results
- A concise description of the phenomena
- A selected method which enables an approximation to the magnitude of the forces/moments that are possible.

It is recommended that one of the methods outlined above be evaluated to determine its suitability for inclusion. No specific method is recommended.

TABLE 5 RECOMMENDED BODY METHODOLOGY

COMPONENT \ MACH NUMBER REGION	SUBSONIC	TRANSONIC	SUPERSONIC
NOSE WAVE DRAG	-	CHAUSSEE & EMPIRICAL	2ND ORDER SHOCK EXPANSION & MODIFIED NEW-TONIAN
BOATTAIL WAVE DRAG	-	EMPIRICAL	2ND ORDER SHOCK EXPANSION
SKIN FRICTION DRAG	VAN DRIEST II		
BASE DRAG AND JET EFFECTS	EMPIRICAL		
INVISCID LIFT AND PITCHING MOMENT	EMPIRICAL + ALLEN & PERKINS	KLOPFER & CHAUSSEE + EMPIRICAL	2ND ORDER SHOCK EXPANSION & MODIFIED NEW-TONIAN
VISCOUS LIFT AND PITCHING MOMENT	ALLEN & PERKINS CROSSFLOW		
AXIAL FORCE AT ANGLE OF ATTACK	ALLEN & PERKINS	EMPIRICAL	JORGENSEN + EMPIRICAL

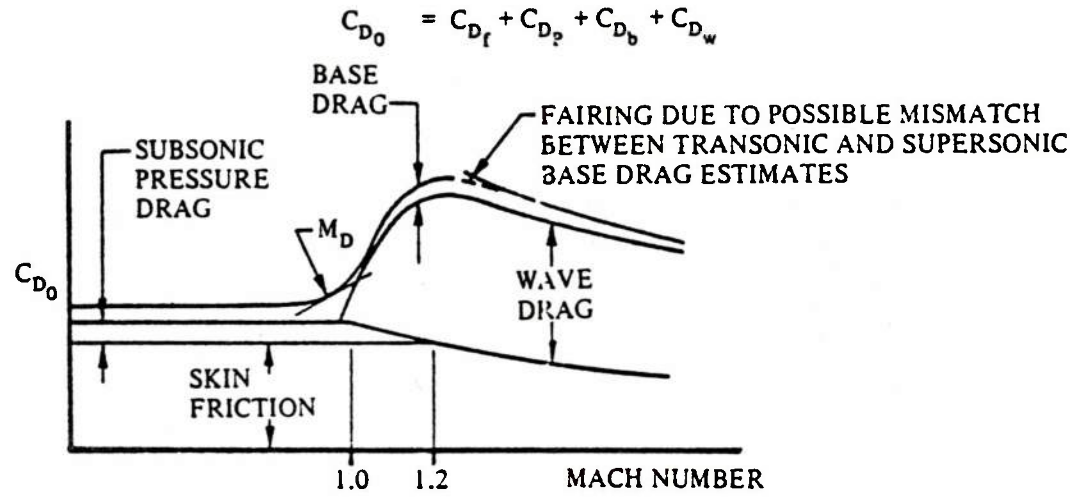

Figure 6. Variation of Zero-Lift Drag Components due to Mach Number

TABLE 6 SUMMARY OF SKIN FRICTION METHODS

THEORY (Refs)	BOUNDARY LAYER FLOW CONDITIONS	R_e RANGE	HEAT TRANSFER	MACH RANGE	TEMP. RANGE
SOMMER & SHORT T* [13]	TURBULENT	$R_e < 5 \times 10^7$	YES	$0 < M < 10$	
VAN DRIEST I [16]	TURBULENT	$5 \times 10^5 < R_e < 10^9$	NO	$0 < M < 10$	
VAN DRIEST II [16]	TURBULENT	$5 \times 10^5 < R_e < 10^9$	YES	$0 < M < 10$	
NIKURADSE [11]	TURBULENT	$1.7 \times 10^6 < R_e < 18 \times 10^6$	NO	$(1/2)M^2 << 1$	
SCHULTZ-GRUNOW [11]	TURBULENT	$10^5 < R_e < 10^9$	NO	$(1/2)M^2 << 1$	
SCHOENHER [11]	TURBULENT	$10^5 < R_e < 5 \times 10^7$	NO	$(1/2)M^2 << 1$	
PRANDTL-SCHLICHTING [11]	TURBULENT	$R_e < 10^9$	NO	$(1/2)M^2 << 1$	
PRANDTL [11]	TURBULENT	$5 \times 10^5 < R_e < 10^7$	NO	$(1/2)M^2 << 1$	
ECKSTROM (LMSC) [26]	LAMINAR & TURBULENT	$M/R_e^{1/2} < .01$	YES	$M/R_e^{1/2} < .01$	$T < 3{,}000°R$
VON KARMAN [11,13]	TURBULENT	$10^5 < R_e < 5 \times 10^7$	NO	$(1/2)M^2 << 1$	
ECKERT REF. TEMP. [19]	LAMINAR & TURBULENT	$10^5 < R_e < 10^9$	YES	$M^3/R_e^{1/2} << 1$	CONST. WALL TEMP.
SPALDING & CHI [15]	TURBULENT	$5 \times 10^5 < R_e < 10^9$	YES	$0 < M < 15$	$.05 < T_W/T_\infty < 30$
BLASIUS [11]	LAMINAR	$10^5 < R_e < 2 \times 10^6$	NO	$(1/2)M^2 << 1$	
HILL [27]	TRANSITION	$10^5 < R_e < 10^9$	NO		

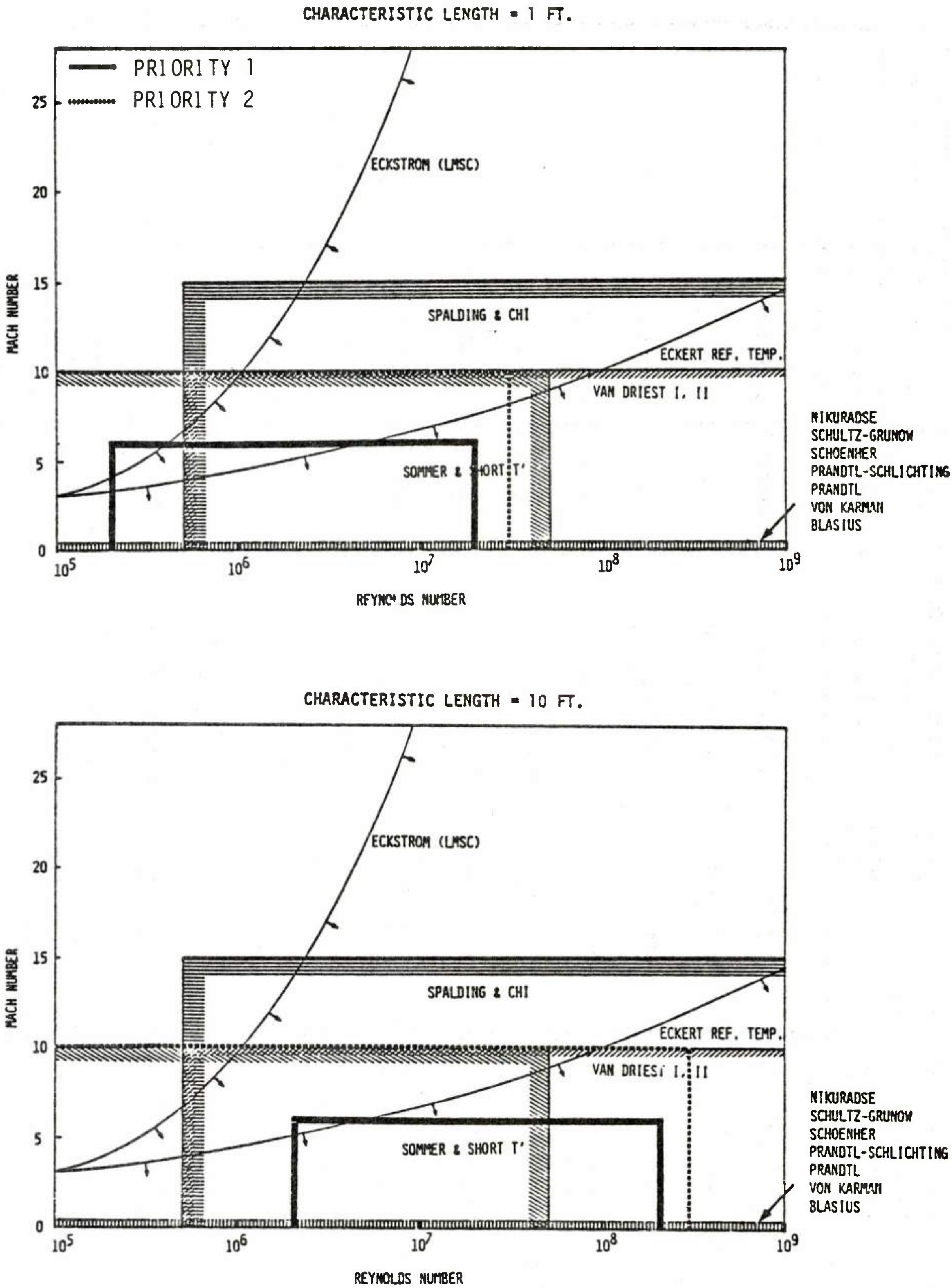

Figure 7. Applicability of Friction Methods

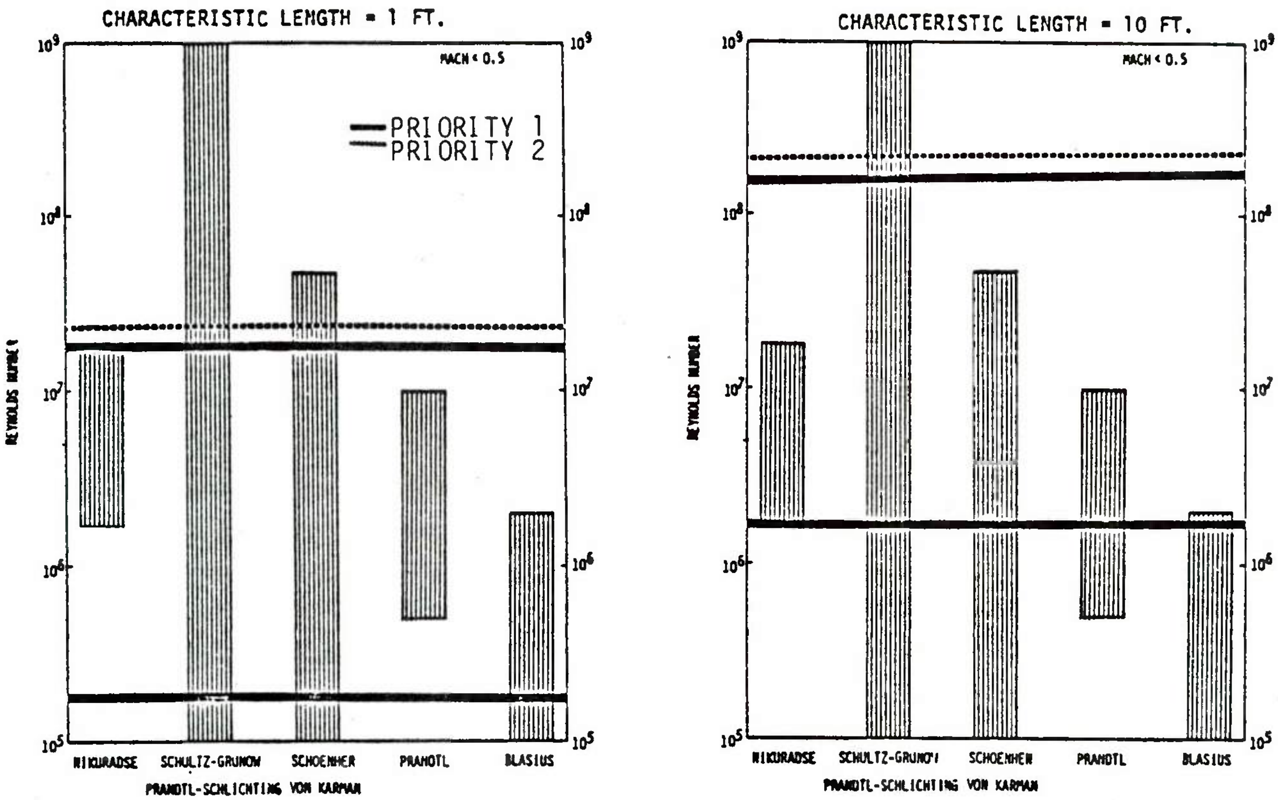

Figure 8. Applicability of Incompressible Friction Methods

TABLE 7 RECOMMENDED METHODS FOR SKIN FRICTION

Van Driest II Theory

(Requires iteration for solution)

$$A = [1/2\,(\gamma - 1)M^2/(T_W/T_\infty)]^{1/2}$$

$$B = [1 + .5\,(\gamma - 1)M^2]/(T_W/T_\infty) - 1$$

$$\alpha = (2A^2 - B)\,(B^2 + 4A^2)^{-1/2}$$

$$\beta = B(B^2 + 4A^2)^{-1/2}$$

$$C_F = [(.242\,(\sin^{-1}\alpha + \sin^{-1}\beta)/[A(T_W/T_\infty)^{1/2} \log R_e C_F - .5\,(1 + 2w)\log \frac{T_W}{T}]\,]^2$$

$$C_f = [.558/A(\sin^{-1}\alpha + \sin^{-1}\beta)C_F]/[.558/A\,(\sin^{-1}\alpha + \sin^{-1}\beta) + 2\sqrt{C_F}(T_W/T_\infty)^{1/2}]$$

Schoenher Theory

$$C_F = (4.13 \log R_e C_F)^{-2}$$

Blasius Laminar Theory

$$C_F = 1.328\; R_e^{-1/2}$$

$$C_f = .664\, R_e^{-1/2}$$

$$\delta/\ell = 5.78\, R_e^{-1/2}$$

$$\delta^*/\ell = 1.73\, R_e^{-1/2}$$

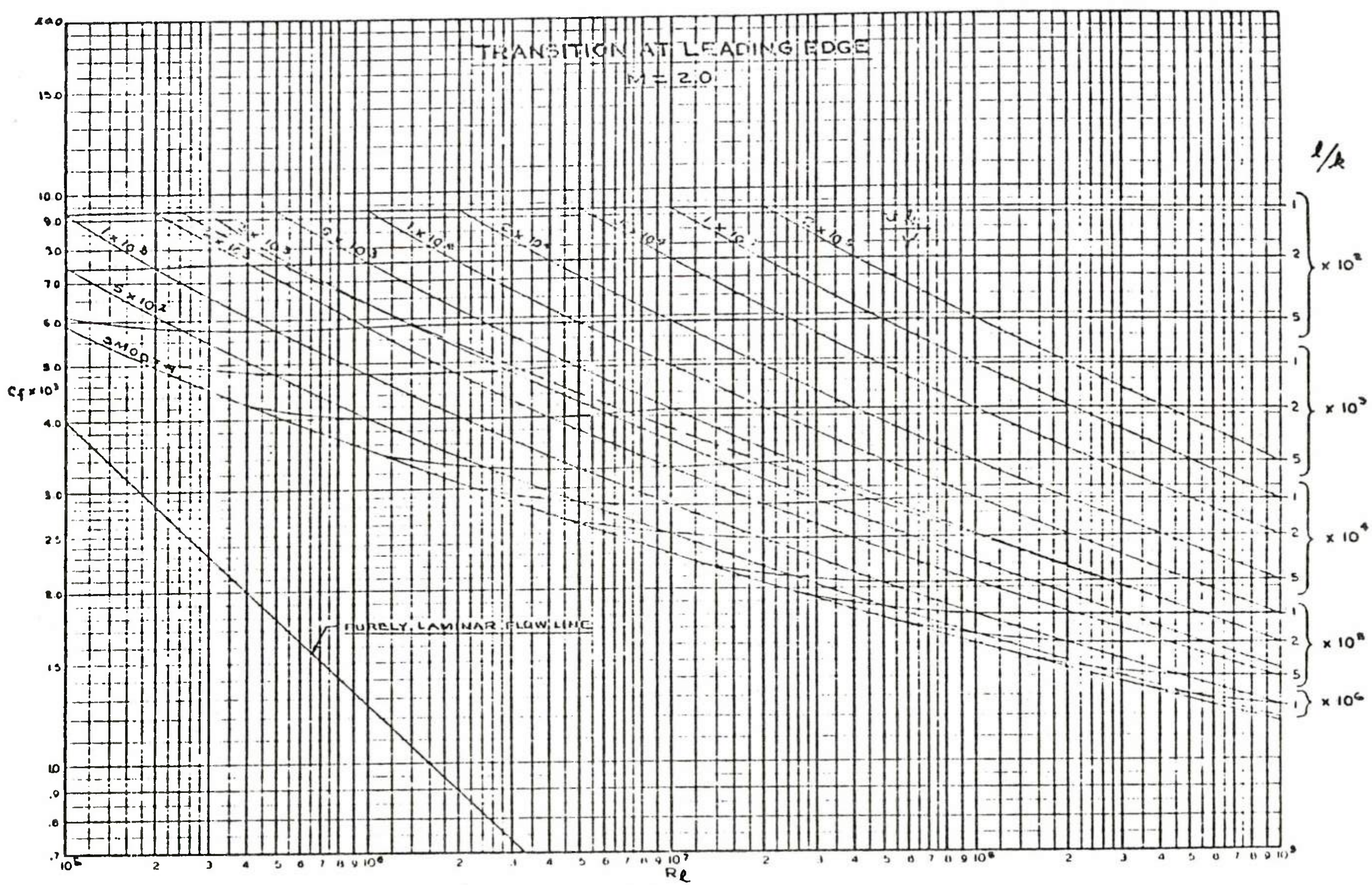

Figure 9. Sample Presentation of Clutter Results

TABLE 8 DATCOM EQUIVALENT SAND ROUGHNESS

Type of Surface	Equivalent Sand Roughness k (inches)
Aerodynamically smooth	0
Polished metal or wood	$0.02 - 0.08 \times 10^{-3}$
Natural sheet metal	0.16×10^{-3}
Smooth matte paint, carefully applied	0.25×10^{-3}
Standard camouflage paint, average application	0.40×10^{-3}
Camouflage paint, mass-production spray	1.20×10^{-3}
Dip-galvanized metal surface	6×10^{-3}
Natural surface of cast iron	10×10^{-3}

TABLE 9 RECOMMENDED WAVE/PRESSURE DRAG METHODS

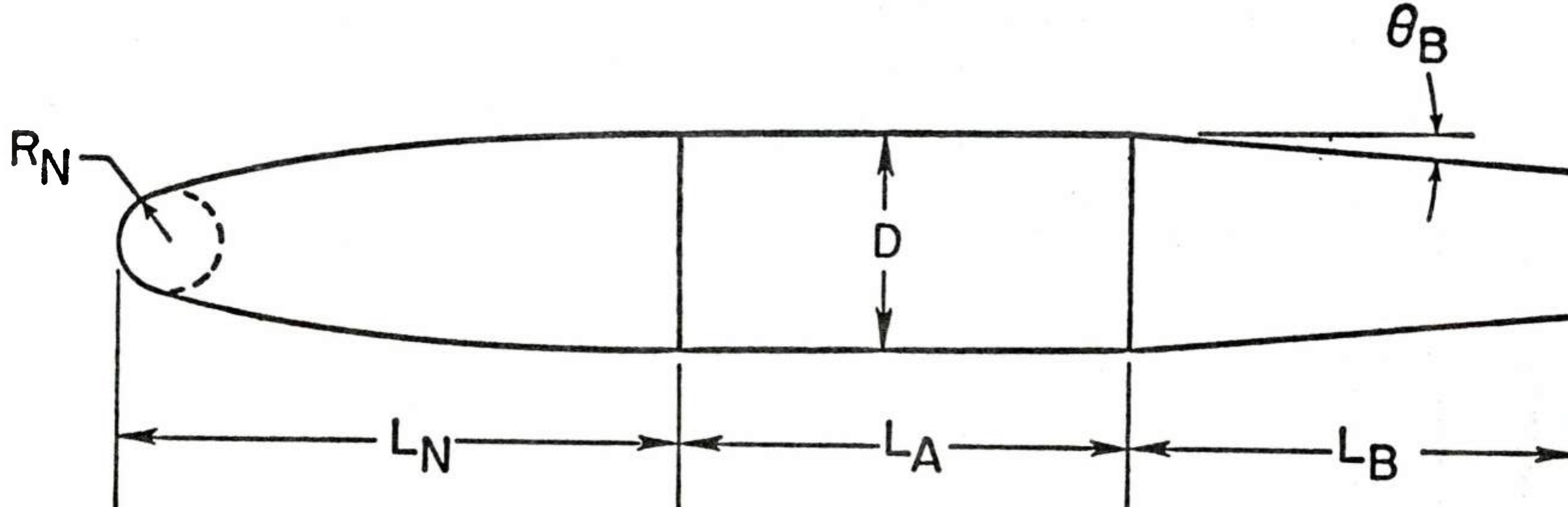

M	NOSE	AFTERBODY	BOATTAIL
0 → 0.6	DATCOM OR HOERNER		
0.6 → 1.4	CHAUSSEE	(NONE)	DTNSRDC JET ON/OFF
1.4 → 6.0	SECOND-ORDER SHOCK EXPANSION PLUS MODIFIED NEWTONIAN		

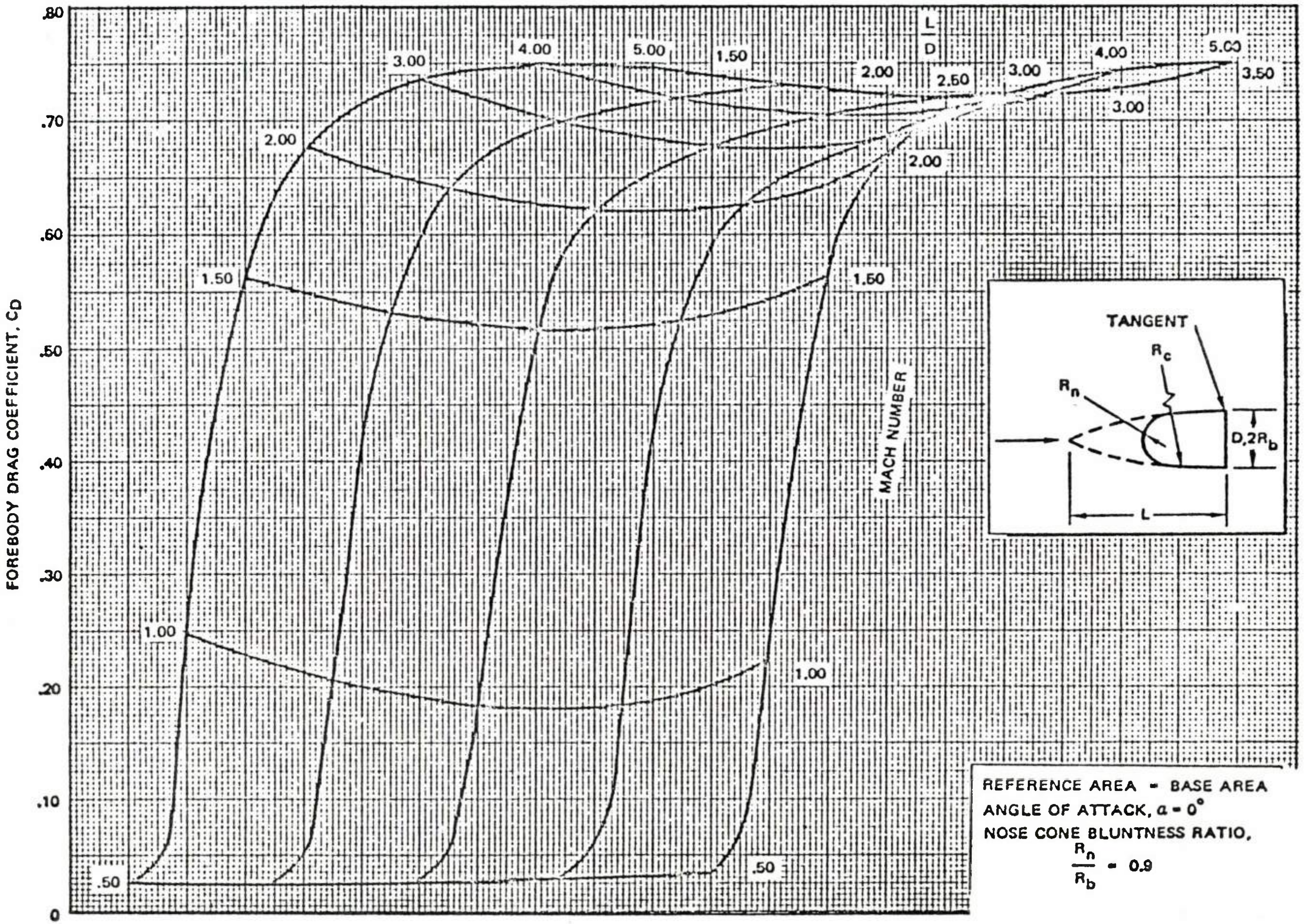

Figure 10 Sample Presentation of MDAC-HB Results

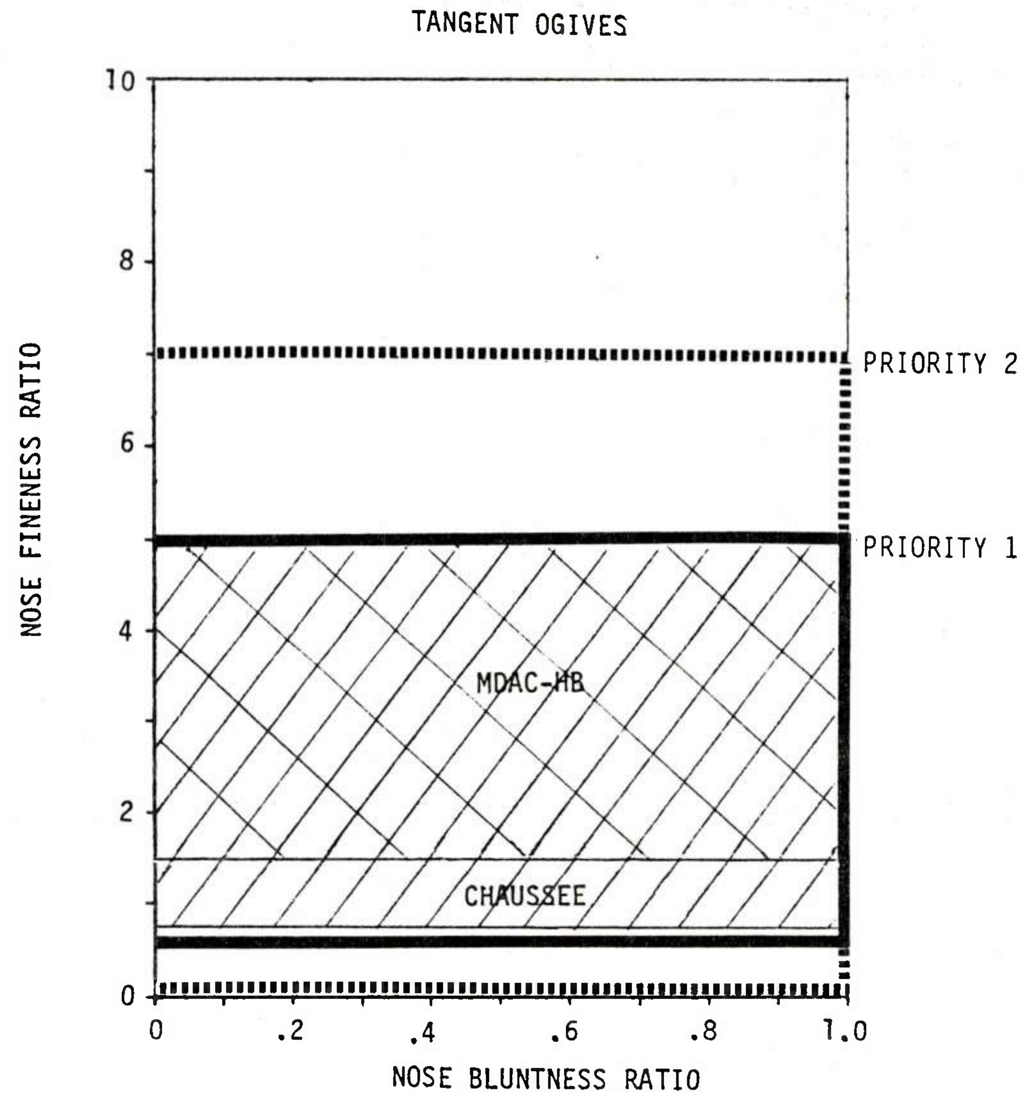

Figure 11. Transonic Nose Wave Drag Tangent Ogives

TABLE 10 CHAUSSEE PRESSURE/WAVE DRAG AT TRANSONIC SPEEDS

L_n/R_b \ R_n/R_b	.0	.1	.2	.3	.4	.5	.6	.7	.8	1.0
		M_∞ = .8								
1.5	.422	.290	.198	.130	.089	.065	.060	.058	.060	.08
2.0	.290	.200	.130	.081	.051	.040	.040	.045	.055	.08
2.5	.210	.140	.088	.051	.030	.020	.022	.031	.042	.08
3.0	.151	.101	.065	.035	.020	.018	.022	.031	.042	.08
4.0	.100	.070	.040	.020	.010	.010	.020	.031	.042	.08
6.0	.068	.041	.020	.007	.006	.010	.020	.031	.042	.08
8.0	.050	.029	.012	.007	.006	.010	.020	.031	.042	.08
10.0	.041	.020	.008	.007	.006	.010	.020	.031	.042	.08
		M_∞ = .95								
1.5	.518	.400	.311	.250	.211	.190	.180	.180	.184	.278
2.0	.395	.295	.223	.175	.144	.130	.123	.238	.150	.278
2.5	.262	.200	.150	.115	.091	.080	.081	.091	.121	.278
3.0	.198	.150	.110	.075	.055	.047	.048	.065	.108	.278
4.0	.130	.091	.061	.042	.040	.031	.048	.065	.108	.278
6.0	.080	.049	.038	.032	.031	.031	.048	.065	.108	.278
8.0	.040	.031	.021	.028	.028	.031	.048	.065	.108	.278
10.0	.025	.020	.015	.020	.021	.031	.048	.065	.108	.278
		M_∞ = 1.05								
1.5	.67	.541	.441	.365	.335	.310	.291	.285	.300	.410
2.0	.505	.409	.339	.290	.260	.240	.229	.223	.240	.410
2.5	.390	.321	.270	.230	.202	.180	.170	.170	.200	.410
3.0	.302	.250	.210	.180	.160	.145	.135	.130	.175	.410
4.0	.211	.175	.140	.115	.100	.095	.100	.121	.175	.410
6.0	.105	.085	.067	.055	.051	.061	.082	.120	.175	.410
8.0	.040	.035	.030	.030	.038	.050	.077	.120	.175	.410
10.0	.025	.025	.025	.025	.025	.040	.070	.120	.175	.410
		M_∞ = 1.2								
1.5	.820	.652	.552	.497	.470	.451	.435	.425	.435	.565
2.0	.640	.521	.450	.404	.374	.350	.335	.333	.355	.565
2.5	.468	.411	.370	.333	.302	.281	.270	.280	.320	.565
3.0	.350	.319	.290	.263	.245	.231	.230	.240	.302	.565
4.0	.225	.205	.190	.175	.170	.170	.180	.211	.290	.565
6.0	.095	.092	.095	.100	.109	.121	.151	.205	.290	.565
8.0	.040	.040	.050	.060	.070	.105	.145	.204	.290	.565
10.0	.025	.025	.030	.041	.055	.095	.140	.204	.290	.565

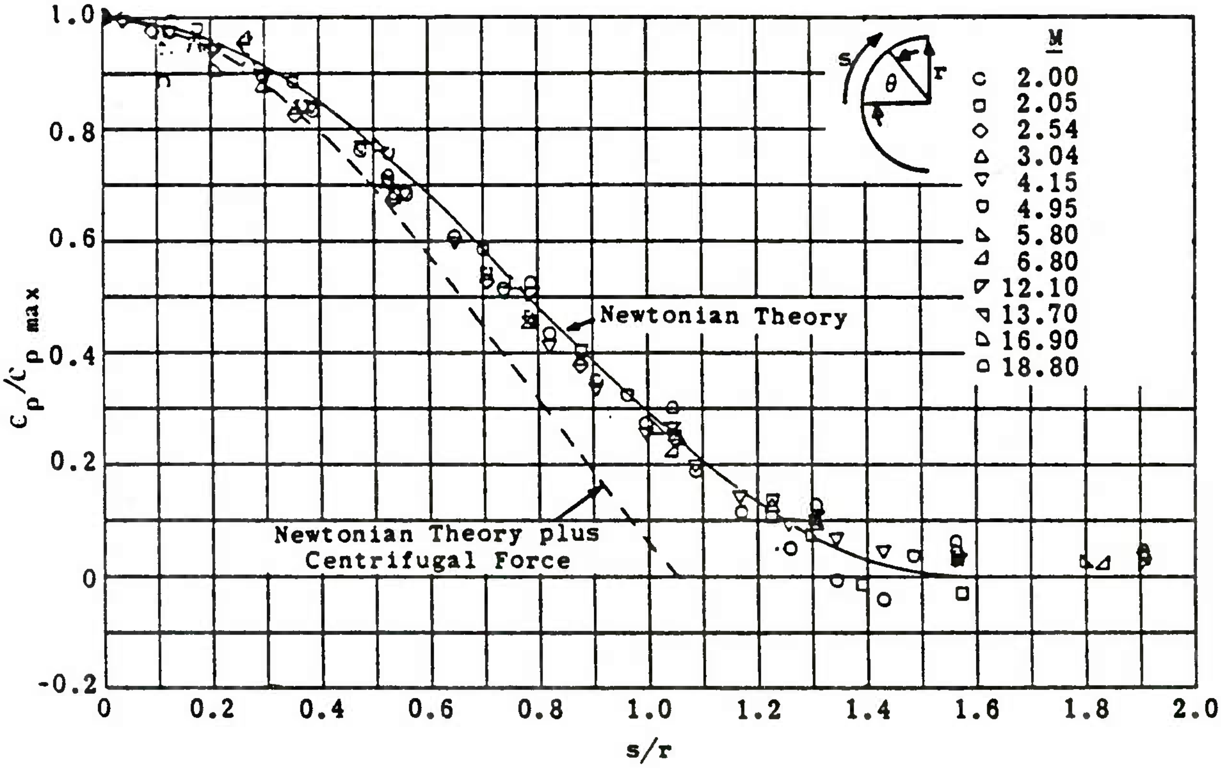

Figure 12. Comparison of Newtonian Theory with Test Results

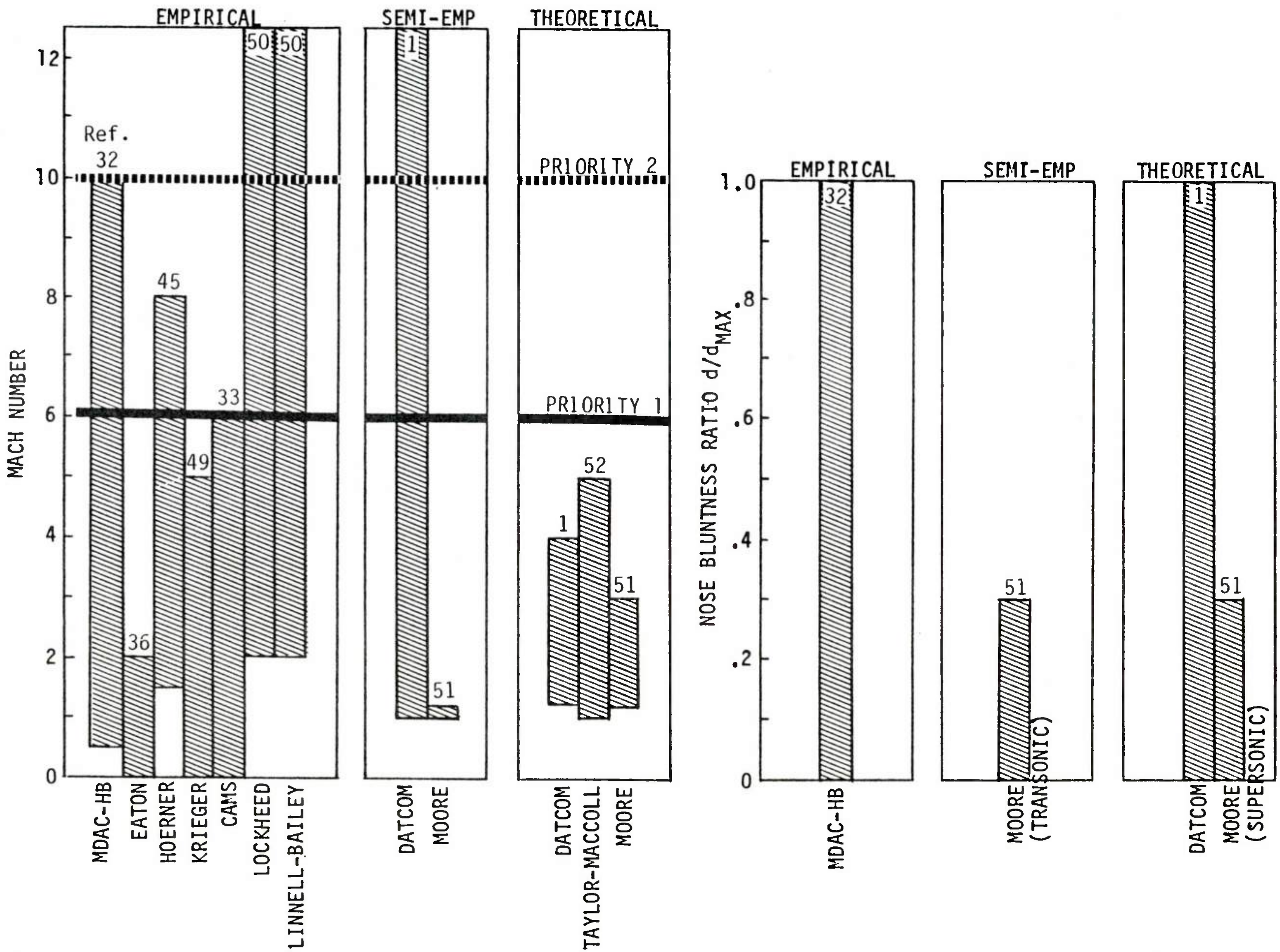

Figure 13. Cone Pressure/Wave Drag Methods Summary

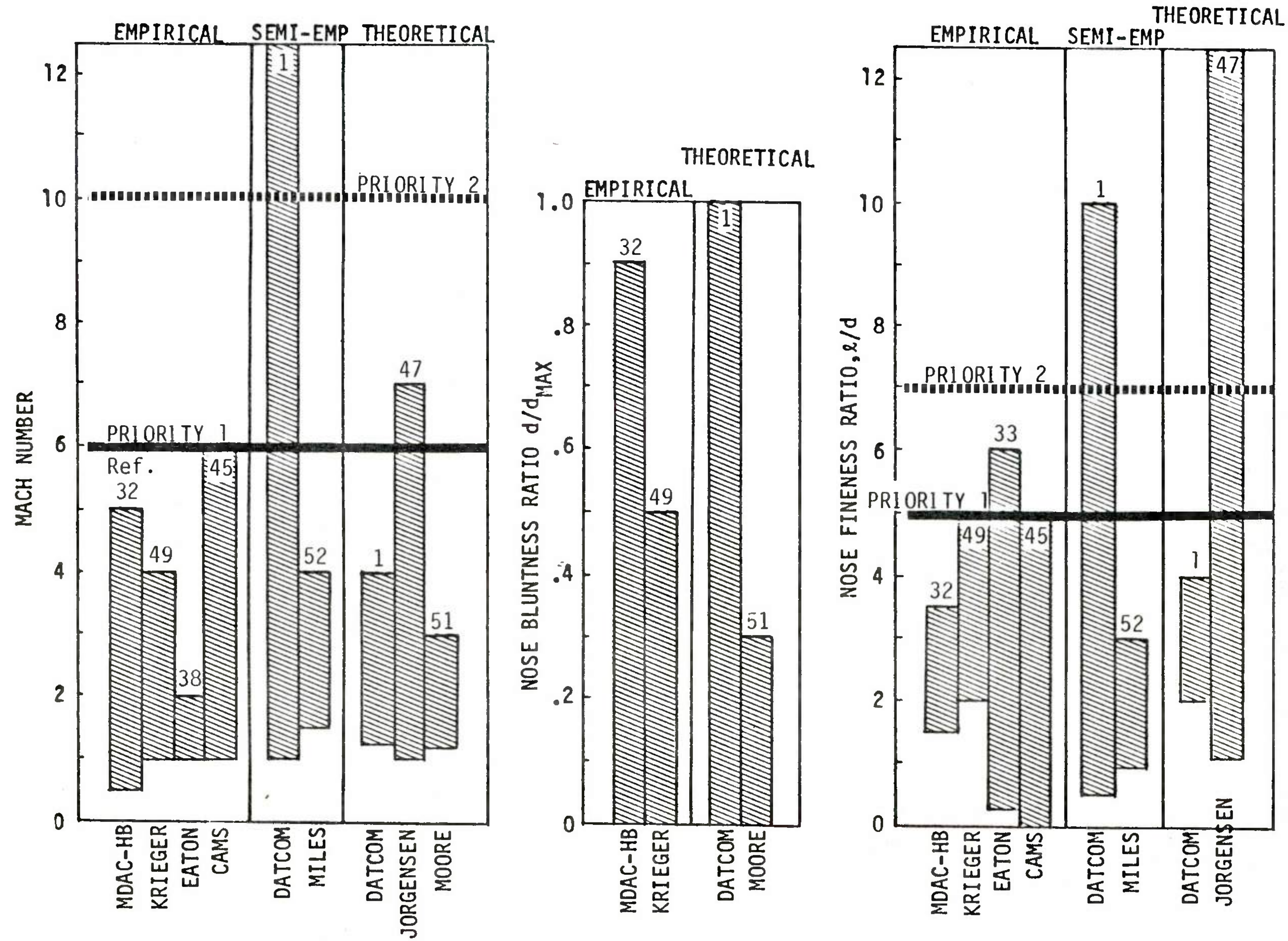

Figure 14. Tangent Ogive Pressure/Wave Drag Methods Summary

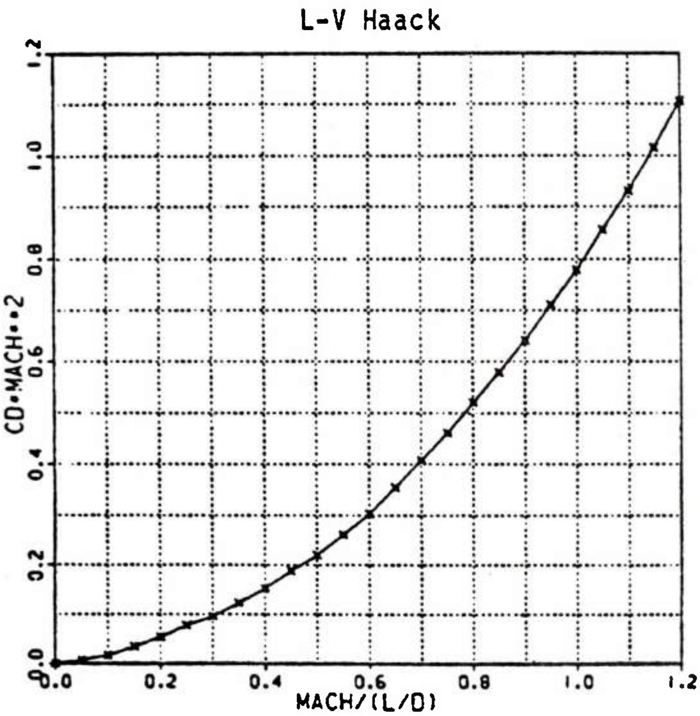

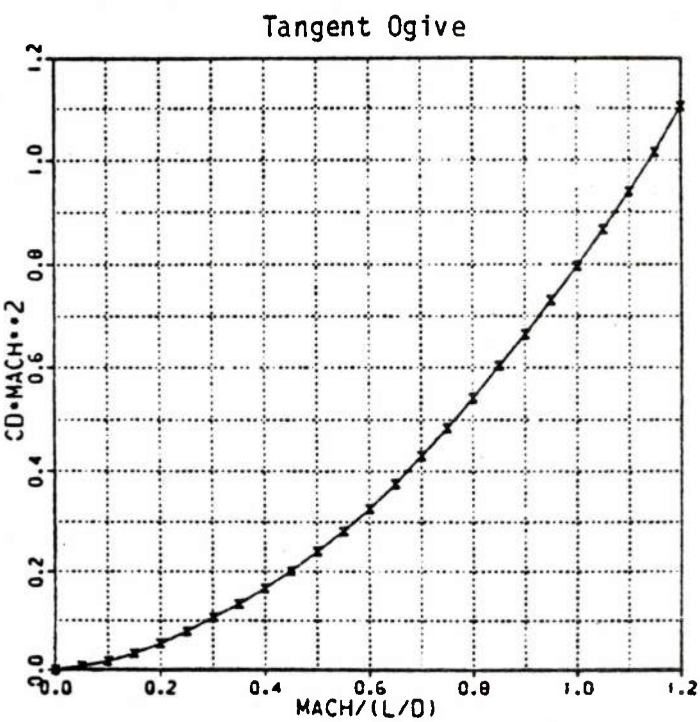

Figure 15. Sample Results of CAMS Wave Drag Correlation

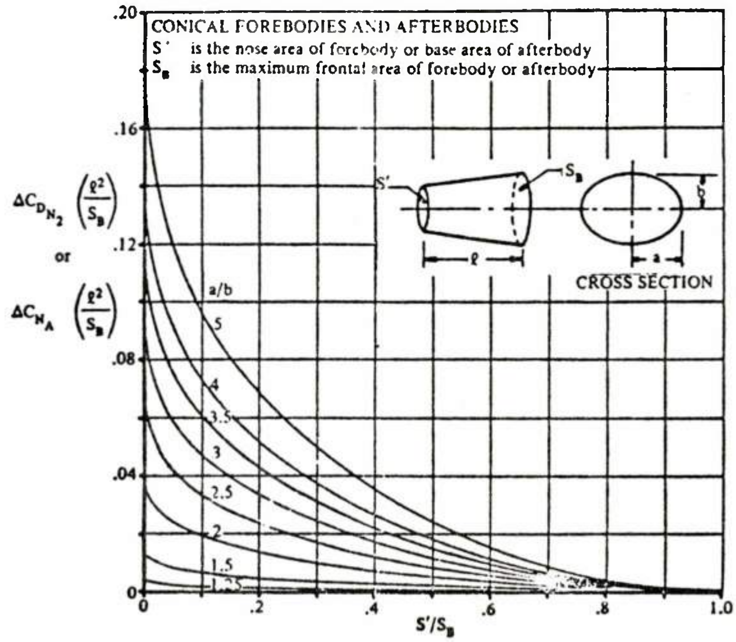

a) Datcom increment applied to circular sections

$$C_{A_W} = a\,b\,(2\lambda+1) + \beta^2 a\,b\left[3\,a\,b\lambda^2 + \frac{3}{2}(a^2+b^2)\,\lambda - \frac{1}{2}\,(a-b)^2 + \frac{1}{2}\,a\,b\right]$$

$$+ a^2\,b^2\left[(\gamma+1)\frac{M_\infty^4}{\beta^2} - (2+M_\infty^2)\,\lambda + \left(\frac{1}{4}\,M_\infty^2 - 1\right)\frac{a^2+b^2}{2\,a\,b}\right]$$

$$+ M_\infty^2\,a^2\,b^2\left[\frac{3}{8}\,\frac{a^2+b^2}{a\,b} - (\lambda+1) + \frac{3}{2}\,\frac{ab}{a^2-b^2}\log\,\frac{a}{b}\right]$$

$$\lambda = \log\frac{4}{\beta\,(a+b)} - 1\,, \quad \beta = \sqrt{M_\infty^2 - 1}$$

b) Jorgensen theoretical method

Figure 16. Wave Drag of Elliptical Sections

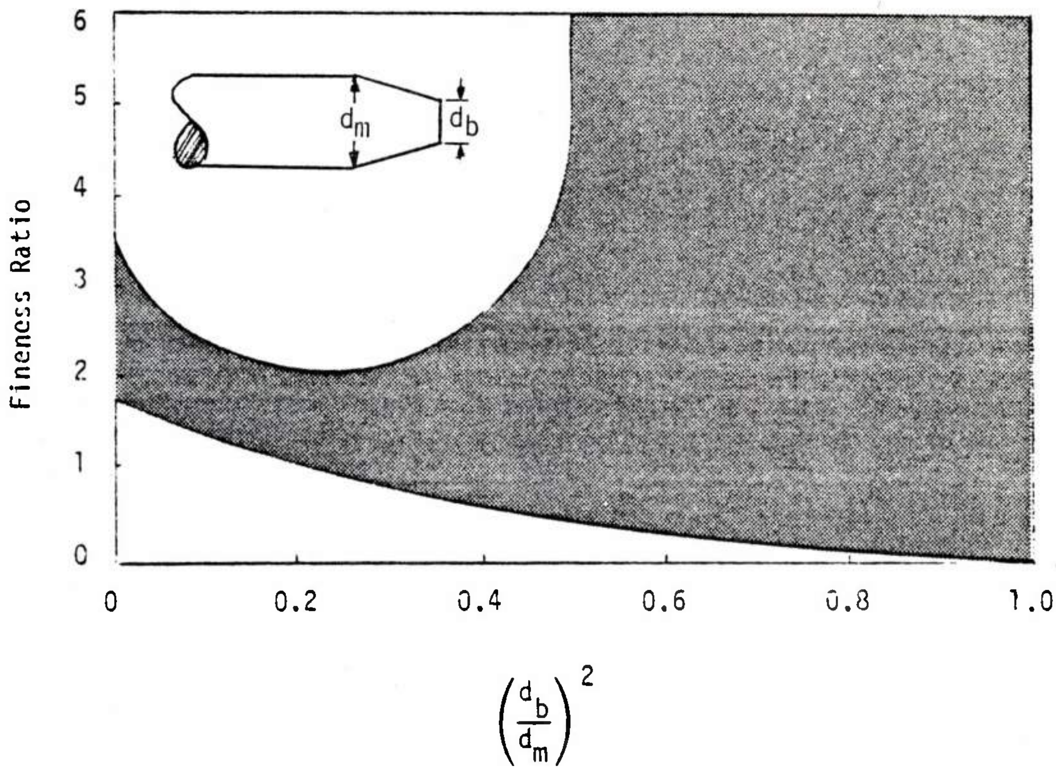

Figure 17. Applicability of Payne Data Correlations

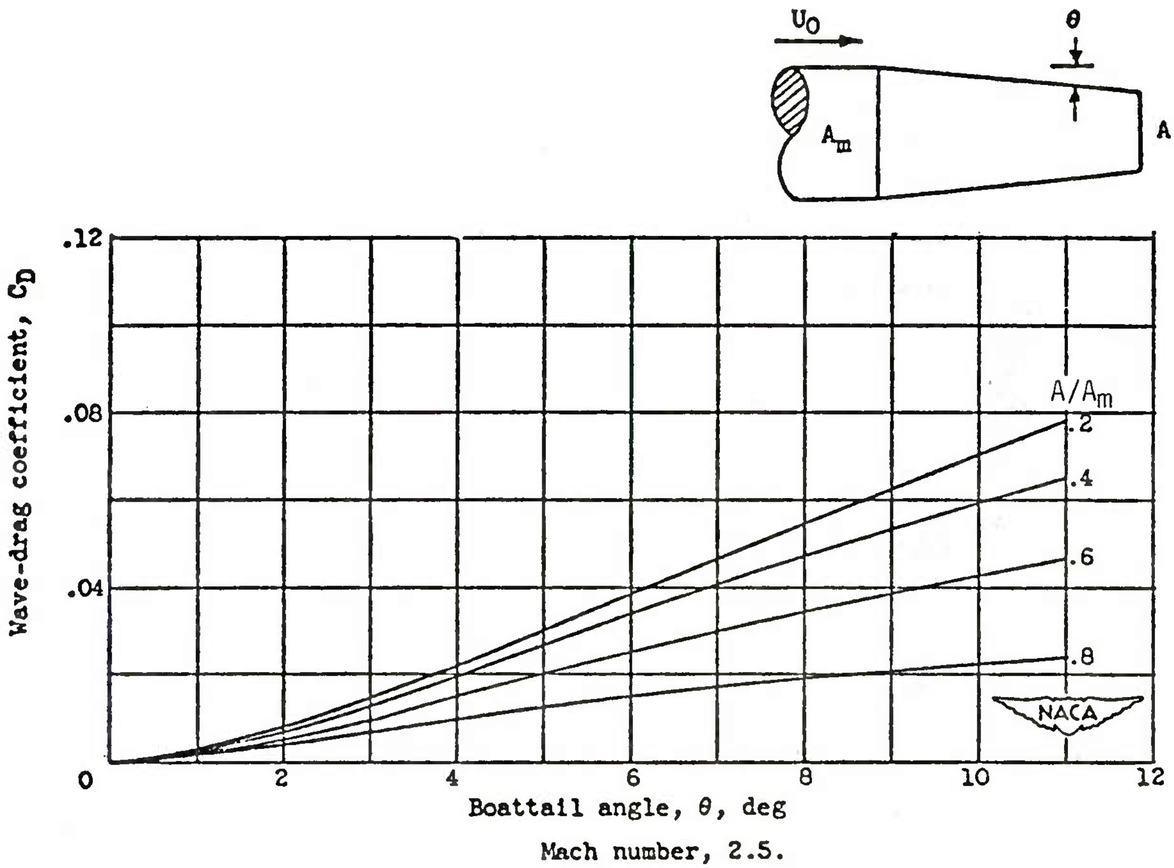

Figure 18. Jack Theoretical Wave Drag of Boattails

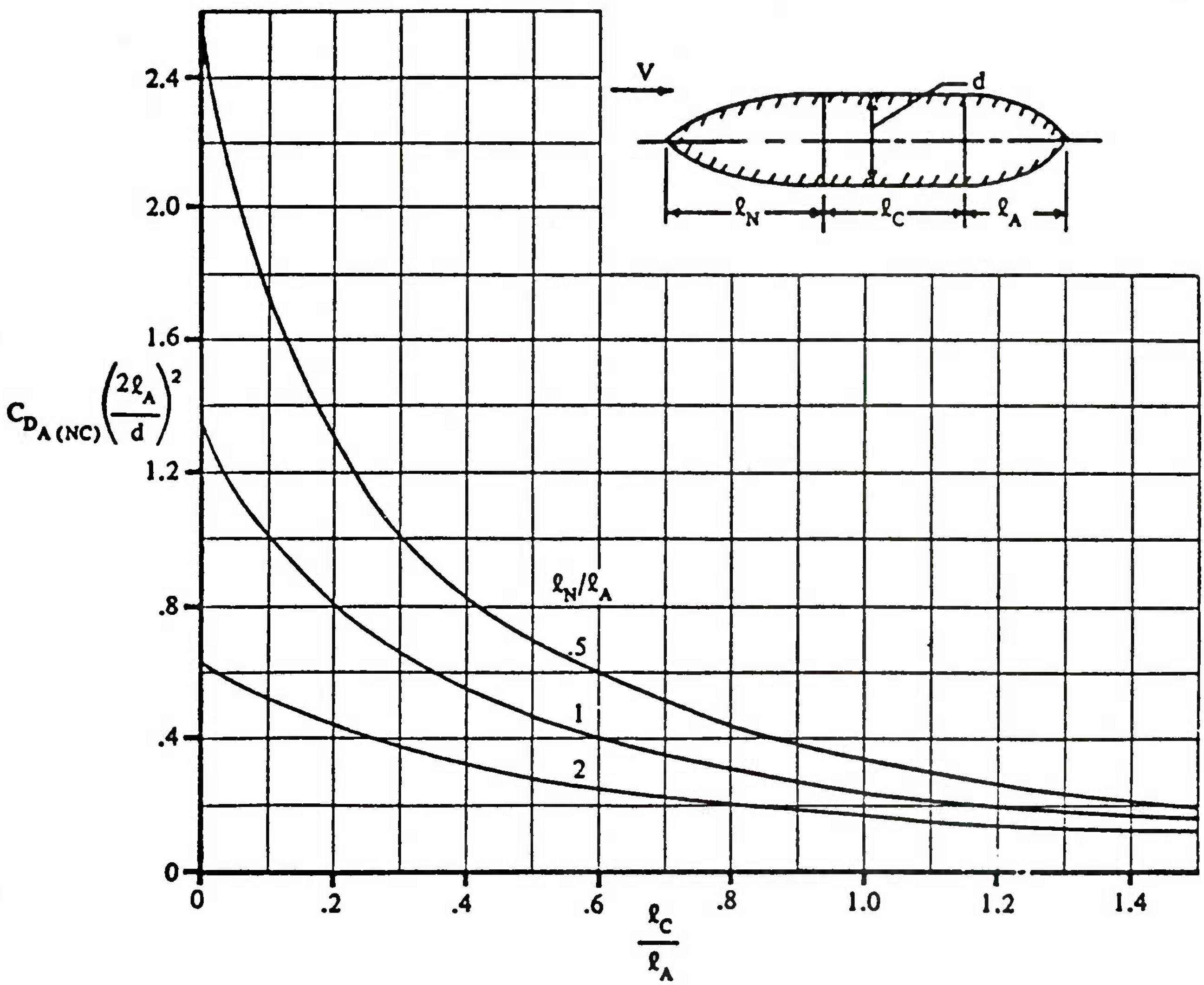

Figure 19. Datcom Charts for Determining Interference Drag

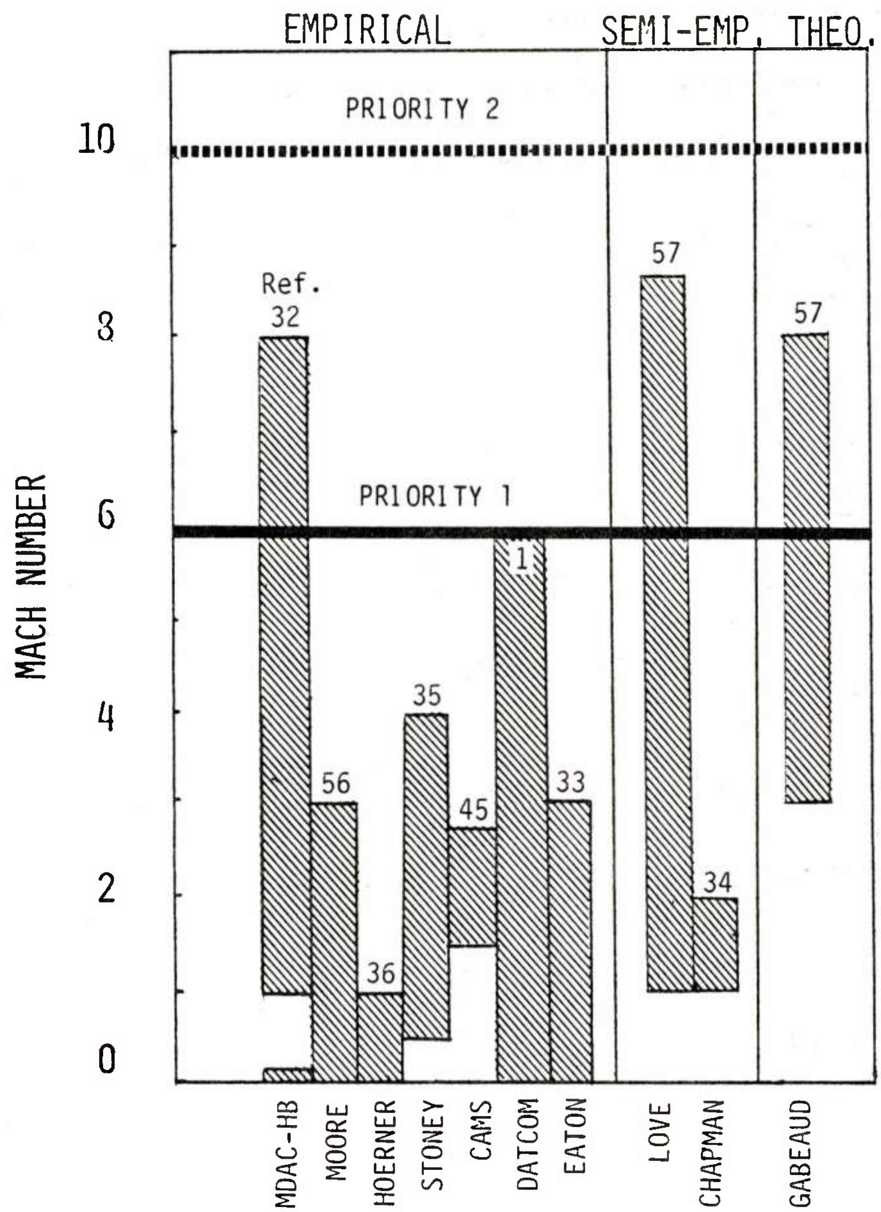

Figure 20. Base Drag Methods Summary

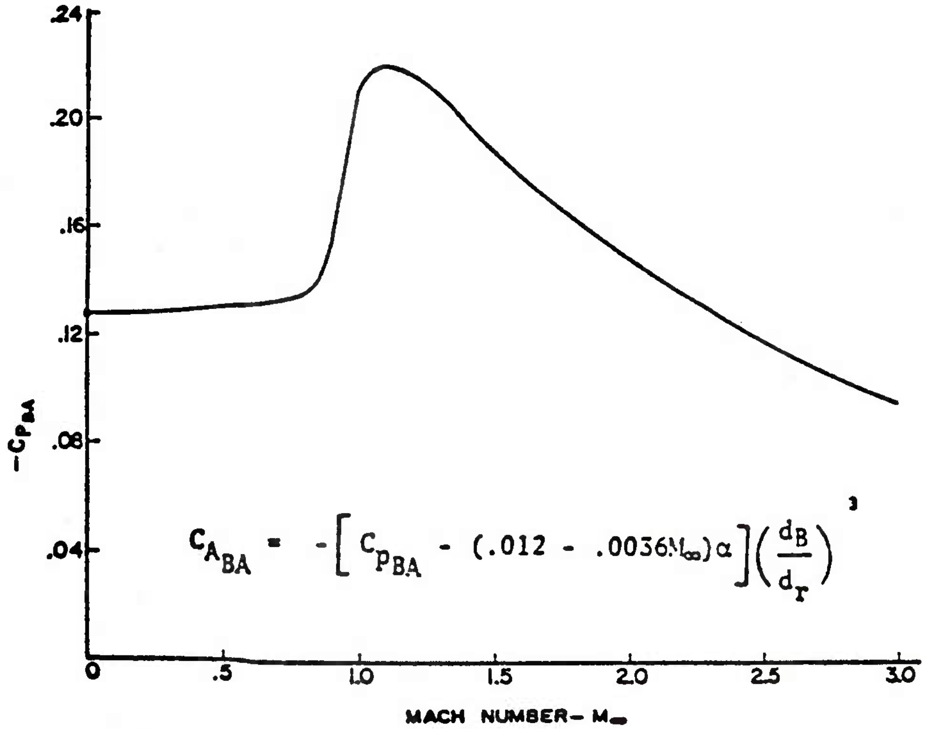

Figure 21. Moore Base Drag Method

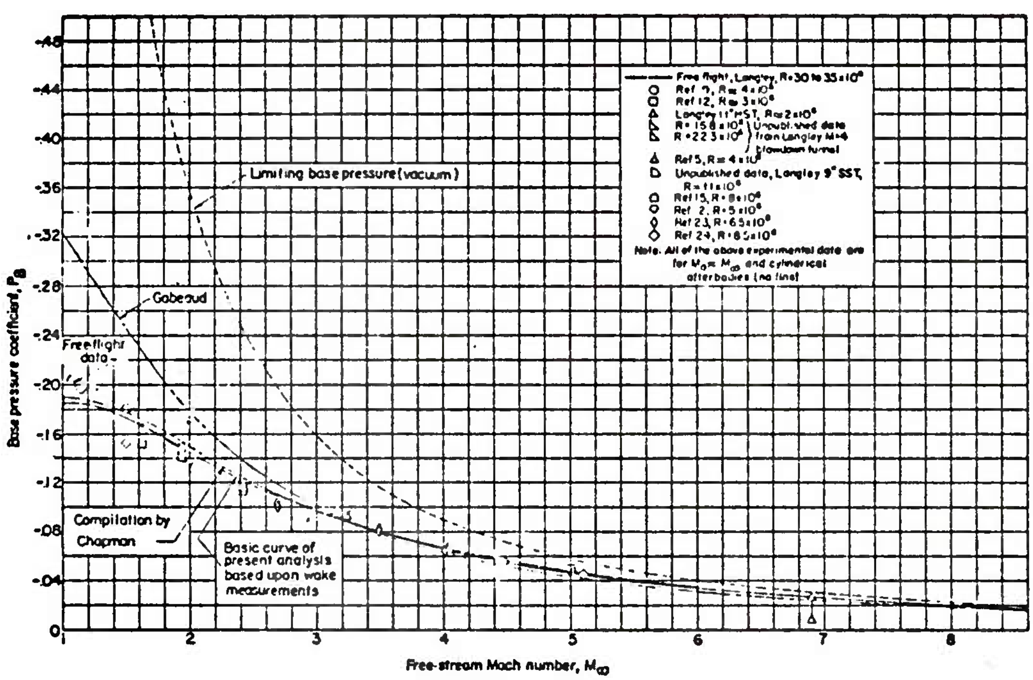

Figure 22. Compilation by Love, NACA 3819

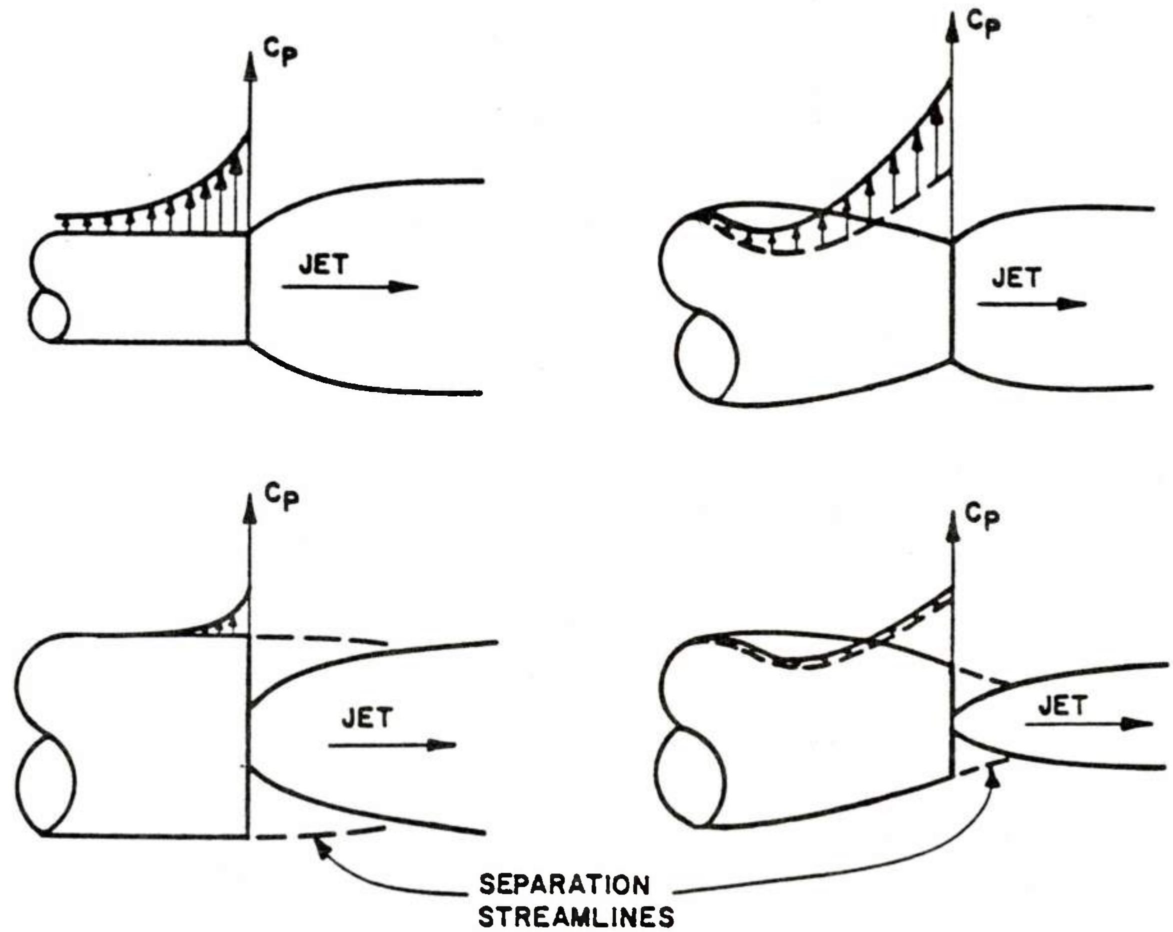

Figure 23. Influence of Nozzle Diameter on Aft Body Pressure Distributions

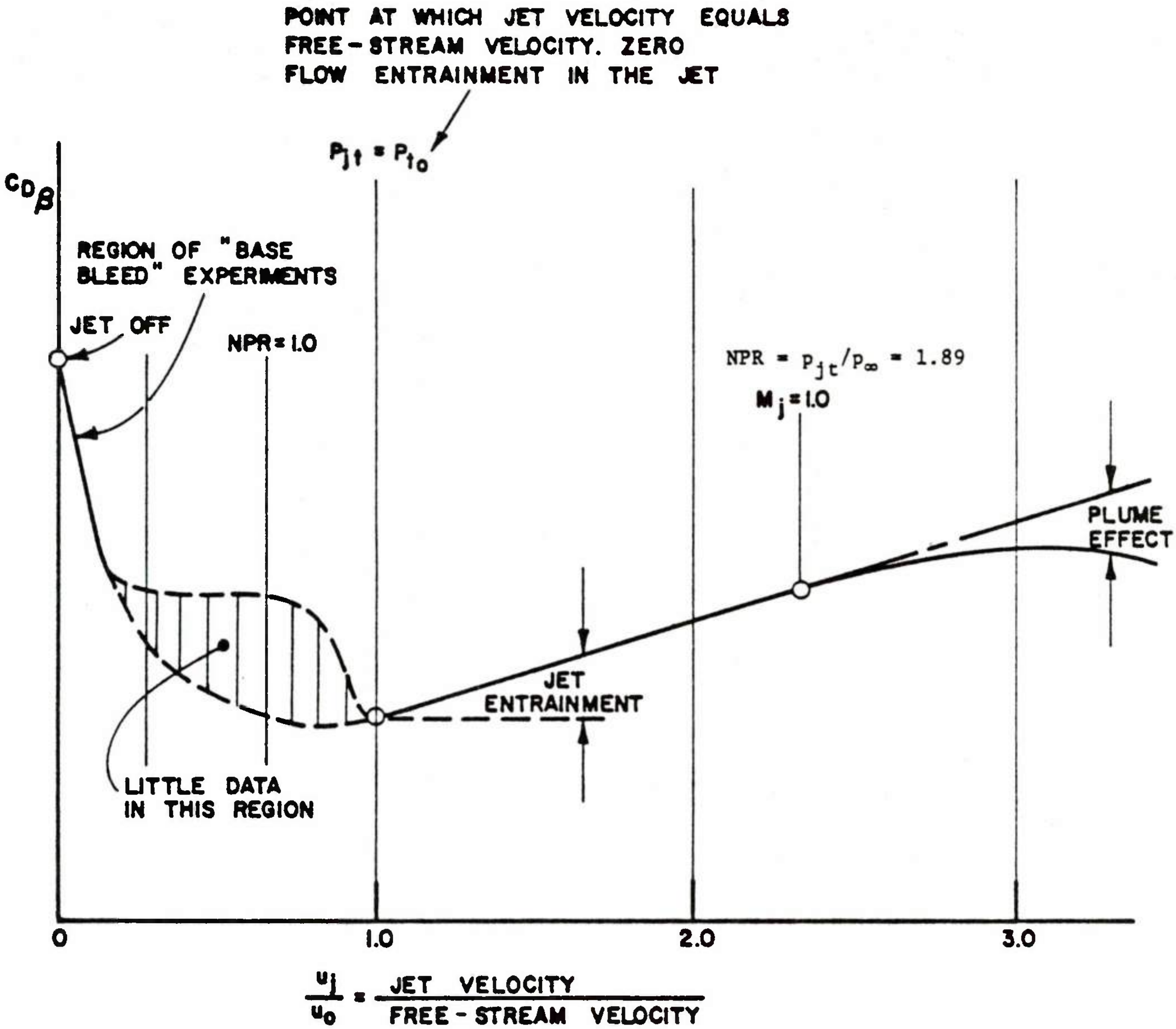

Figure 24. Effect of Jet on Afterbody Wave Drag

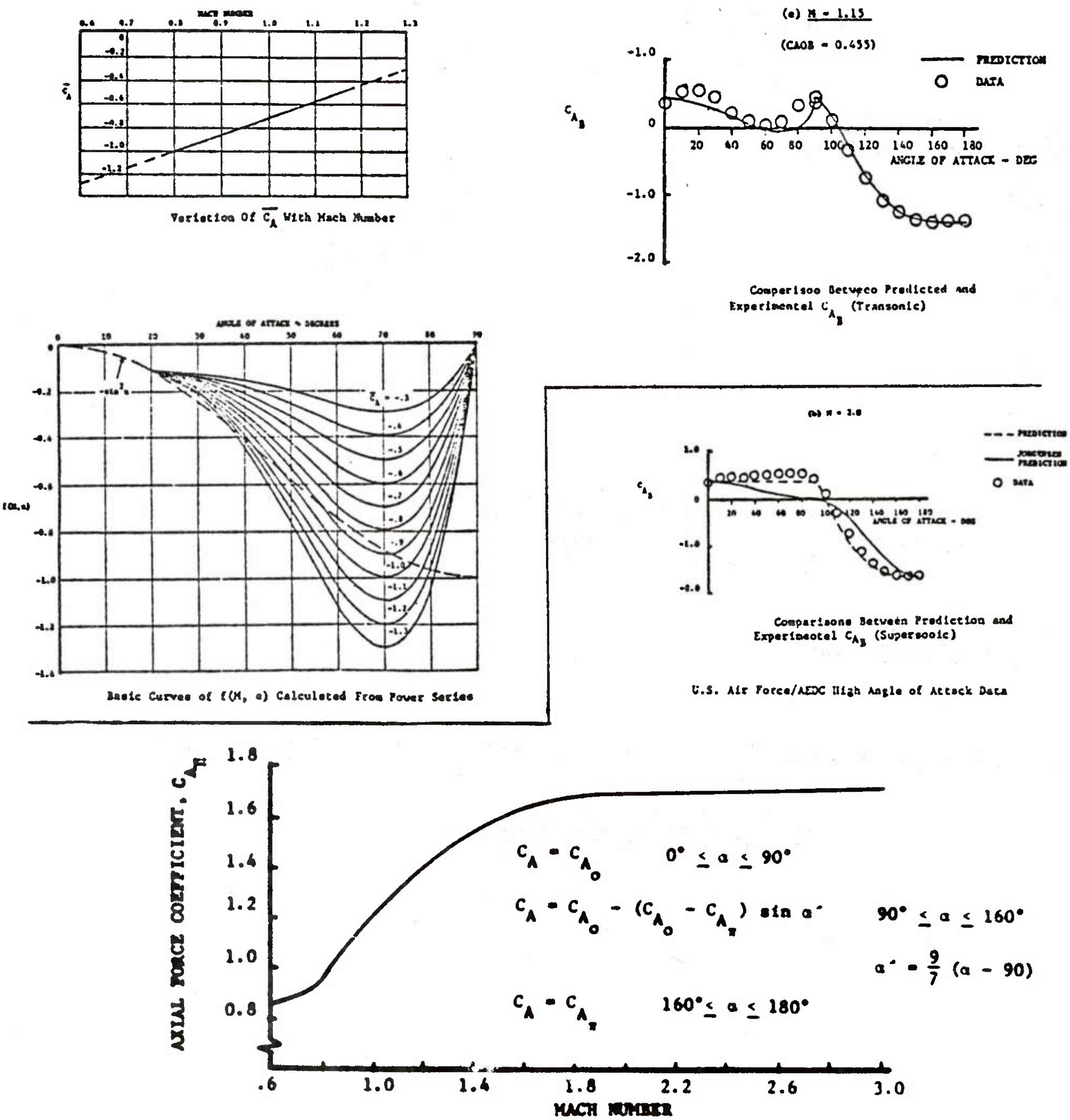

Figure 25. Aiello Empirical Axial Force at Angle of Attack

TABLE 11 METHOD RECOMMENDATIONS FOR AXIAL FORCE AT ANGLE OF ATTACK

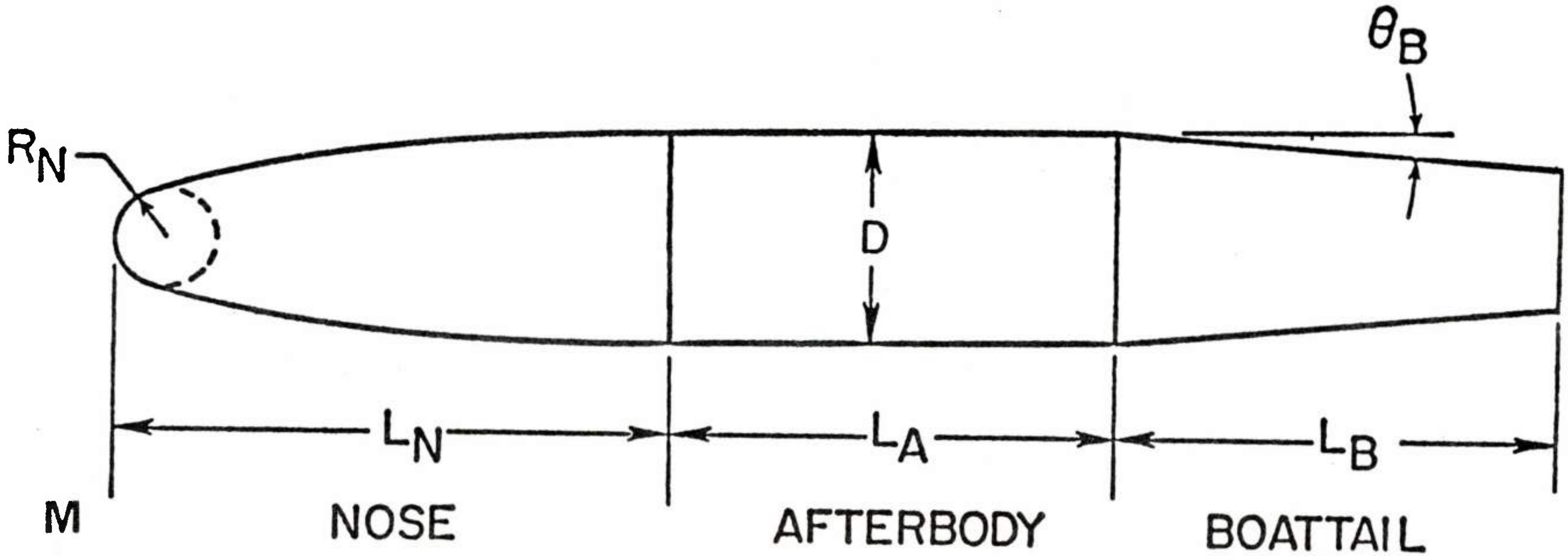

M	
0 → 0.6	ALLEN AND PERKINS
0.6 → 1.4	EMPIRICAL
1.4 → 6.0	JORGENSEN / EMPIRICAL

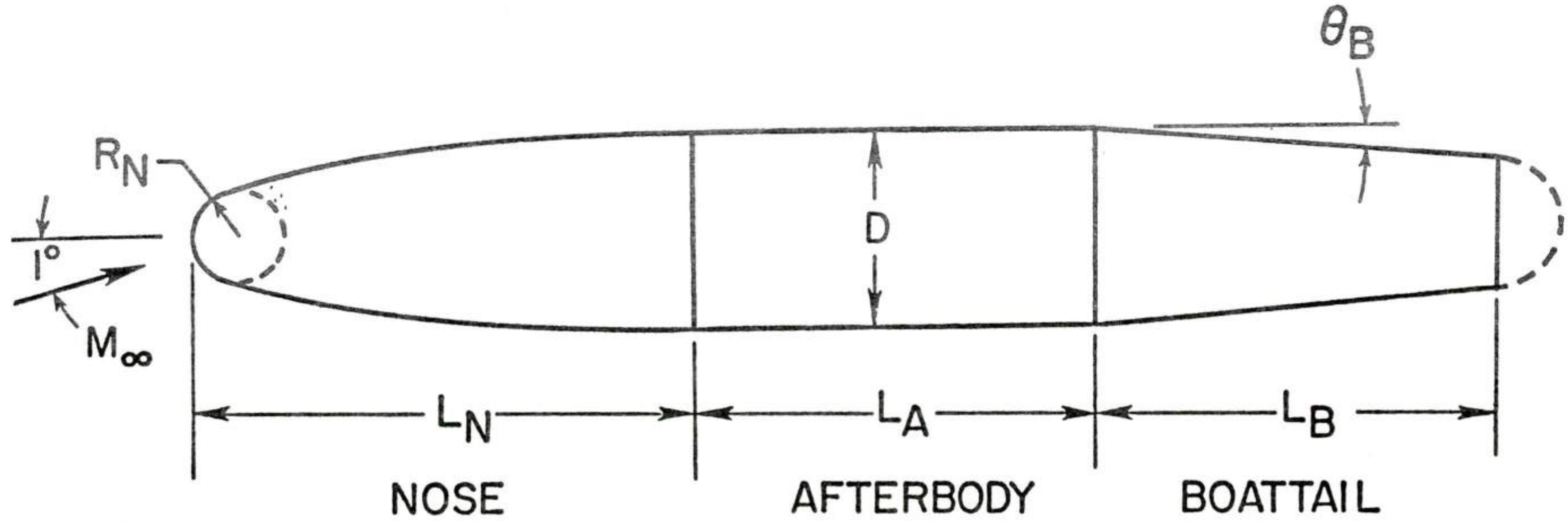

PARAMETER RANGE:

$$0.75 \leq M_\infty \leq 1.2$$
$$0.025 \leq R_N/D \leq 0.5$$
$$1.5 \leq L_N/D \leq 5.0$$
$$0 \leq L_A/D \leq 5.0$$
$$0 \leq L_B/D \leq 2.0$$
$$0° \leq \theta_B \leq 10°$$

Figure 26. Limitations of Klopfer and Chaussee Results

$$
\begin{aligned}
C_{N\alpha} = {} & (C_{N\alpha})_o + \left(\frac{\partial C_{N\alpha}}{\partial \bar{R}_N}\right)_o \Delta\bar{R}_N + \left(\frac{\partial C_{N\alpha}}{\partial \bar{L}_N}\right)_o \Delta\bar{L}_N + \left(\frac{\partial C_{N\alpha}}{\partial \bar{L}_A}\right)_o \Delta\bar{L}_A + \left(\frac{\partial C_{N\alpha}}{\partial \bar{\theta}_B}\right)_o \Delta\bar{\theta}_B \\
& + \left(\frac{\partial^2 C_{N\alpha}}{\partial \bar{R}_N^2}\right)_o (\Delta\bar{R}_N)^2 + \left(\frac{\partial^2 C_{N\alpha}}{\partial \bar{R}_N \partial \bar{L}_N}\right)_o \Delta\bar{R}_N \Delta\bar{L}_N + \left(\frac{\partial^2 C_{N\alpha}}{\partial \bar{R}_N \partial \bar{L}_A}\right)_o \Delta\bar{R}_N \Delta\bar{L}_A + \left(\frac{\partial^2 C_{N\alpha}}{\partial \bar{R}_N \partial \bar{\theta}_B}\right)_o \Delta\bar{R}_N \Delta\bar{\theta}_B \\
& + \left(\frac{\partial^2 C_{N\alpha}}{\partial \bar{L}_N^2}\right)_o (\Delta\bar{L}_N)^2 + \left(\frac{\partial^2 C_{N\alpha}}{\partial \bar{L}_N \partial \bar{L}_A}\right)_o \Delta\bar{L}_N \Delta\bar{L}_A + \left(\frac{\partial^2 C_{N\alpha}}{\partial \bar{L}_N \partial \bar{\theta}_B}\right)_o \Delta\bar{L}_N \Delta\bar{\theta}_B \\
& + \left(\frac{\partial^2 C_{N\alpha}}{\partial \bar{L}_A^2}\right)_o (\Delta\bar{L}_A)^2 + \left(\frac{\partial^2 C_{N\alpha}}{\partial \bar{L}_A \partial \bar{\theta}_B}\right)_o \Delta\bar{L}_A \Delta\bar{\theta}_B + \left(\frac{\partial^2 C_{N\alpha}}{\partial \bar{\theta}_B^2}\right)_o (\Delta\bar{\theta}_B)^2
\end{aligned}
$$

where $\bar{R}_N = R_N/(R_N)_{max.}$; $\bar{L}_N = L_N/(L_N)_{max.}$; $\bar{L}_A = L_A/(L_A)_{max.}$;
$\bar{\theta}_B = \theta_B/(\theta_B)_{max.}$ and M_∞, L_B are constants.

Figure 27. Polynominal Representation of Klopfer and Chaussee Results

TABLE 12 KLOPFER AND CHAUSSEE COEFFICIENTS, C_N

COEFFICIENTS FOR THE QUDRATIC INTERPOLATION FORMULA FOR THE NORMAL-FORCE-CURVE SLOPES FOR THE ENTIRE BODY WITH A ONE CALIBER BOATTAIL

		Free Stream Mach Number M_∞			
		0.75	0.90	0.95	1.20
Linear Terms	$(C_{N\alpha})_o$	1.578	1.454	1.534	2.177
	$(\partial C_{N\alpha}/\partial \bar{R}_N)_o$	-.625	-.445	-.575	.361
	$(\partial C_{N\alpha}/\partial \bar{L}_N)_o$	.296	.017	.039	-.462
	$(\partial C_{N\alpha}/\partial \bar{L}_A)_o$	..107	.008	.338	-.649
	$(\partial C_{N\alpha}/\partial \bar{\theta}_B)_o$	-1.920	-1.945	-1.897	-.827
Quadratic Terms	$(\partial^2 C_{N\alpha}/\partial \bar{R}_N^2)_o$	-.331	.319	.476	-.701
	$(\partial^2 C_{N\alpha}/\partial \bar{R}_N \partial \bar{L}_N)_o$	-.685	-.821	1.032	-.090
	$(\partial^2 C_{N\alpha}/\partial \bar{R}_N \partial \bar{L}_A)_o$	.041	-.814	-.290	-.126
	$(\partial^2 C_{N\alpha}/\partial \bar{R}_N \partial \bar{\theta}_B)_o$	-.778	-1.332	-.889	-.712
	$(\partial^2 C_{N\alpha}/\partial \bar{L}_N^2)_o$	-.278	-.816	-.832	.128
	$(\partial^2 C_{N\alpha}/\partial \bar{L}_N \partial \bar{L}_A)_o$	-.703	.240	.439	.773
	$(\partial^2 C_{N\alpha}/\partial \bar{L}_N \partial \bar{\theta}_B)_o$	-.451	1.084	.767	.562
	$(\partial^2 C_{N\alpha}/\partial \bar{L}_A^2)_o$	-.089	.297	-.296	1.376
	$(\partial^2 C_{N\alpha}/\partial \bar{L}_A \partial \bar{\theta}_B)_o$	.632	.930	.038	.535
	$(\partial^2 C_{N\alpha}/\partial \bar{\theta}_B^2)_o$	.083	1.465	1.663	.104

where $\bar{R}_N = R_N/(R_N)_{max}$; $\bar{L}_N = L_N/(L_N)_{max}$; $\bar{L}_A = L_A/(L_A)_{max}$;
$\bar{\theta}_B = \theta_B/(\theta_B)_{max}$

TABLE 13 KLOPFER AND CHAUSSEE COEFFICIENTS, C_m

COEFFICIENTS FOR THE QUADRATIC INTERPOLATION FORMULA FOR THE PITCHING-MOMENT-CURVE SLOPE FOR THE ENTIRE BODY WITH A ONE CALIBER BOATTAIL

		Free Stream Mach Number M_∞			
		0.75	0.90	0.95	1.20
Linear Terms	$(C_{M\alpha})_o$	.515	1.591	1.420	-1.319
	$(\partial C_{M\alpha}/\partial \bar{R}_N)_o$	2.856	2.804	3.639	.160
	$(\partial C_{M\alpha}/\partial \bar{L}_N)_o$	-1.280	-.714	-1.721	-7.349
	$(\partial C_{M\alpha}/\partial \bar{L}_A)_o$	2.875	3.514	2.122	4.583
	$(\partial C_{M\alpha}/\partial \bar{\theta}_B)_o$	8.482	9.478	9.951	2.927
Quadratic Terms	$(\partial^2 C_{M\alpha}/\partial \bar{R}_N^2)_o$	1.544	-2.282	-1.431	4.682
	$(\partial^2 C_{M\alpha}/\partial \bar{R}_N \partial \bar{L}_N)_o$	11.199	12.480	6.177	-1.214
	$(\partial^2 C_{M\alpha}/\partial \bar{R}_N \partial \bar{L}_A)_o$	-.549	2.947	2.823	-15.080
	$(\partial^2 C_{M\alpha}/\partial \bar{R}_N \partial \bar{\theta}_B)_o$	3.903	6.767	8.013	10.845
	$(\partial^2 C_{M\alpha}/\partial \bar{L}_N^2)_o$	-.269	4.265	5.151	7.352
	$(\partial^2 C_{M\alpha}/\partial \bar{L}_N \partial \bar{L}_A)_o$	6.172	1.643	-.611	-3.682
	$(\partial^2 C_{M\alpha}/\partial \bar{L}_N \partial \bar{\theta}_B)_o$	14.263	4.686	1.562	-9.186
	$(\partial^2 C_{M\alpha}/\partial \bar{L}_A^2)_o$	-.006	-2.660	-.135	-4.087
	$(\partial^2 C_{M\alpha}/\partial \bar{L}_A \partial \bar{\theta}_B)_o$	7.463	4.803	7.536	-5.228
	$(\partial^2 C_{M\alpha}/\partial \bar{\theta}_B^2)_o$	.489	-7.698	-9.178	8.201

where $\bar{R}_N = R_N/(R_N)_{max}$; $\bar{L}_N = L_N/(L_N)_{max}$; $\bar{L}_A = L_A/(L_A)_{max}$

$\bar{\theta}_B = \theta_B/(\theta_B)_{max}$

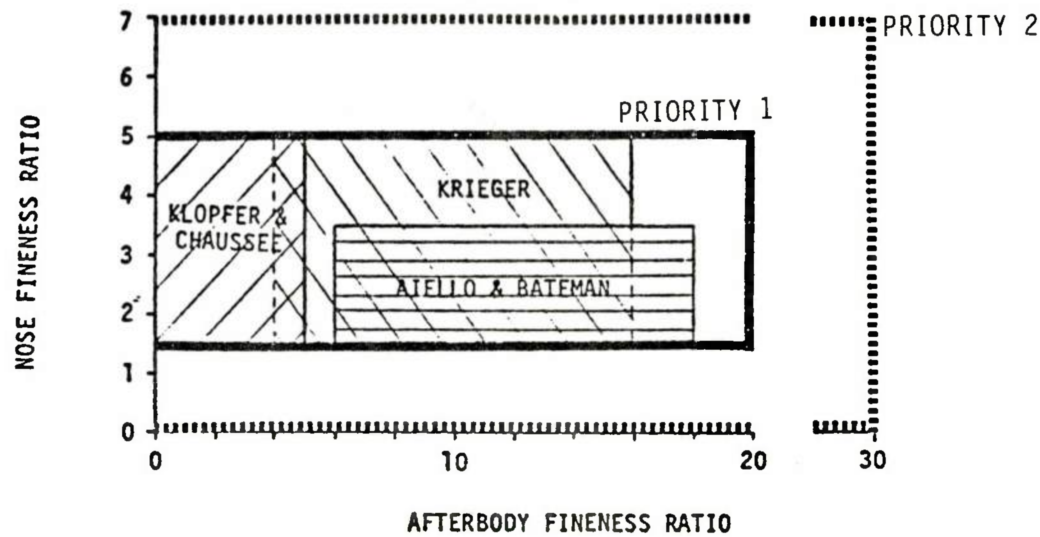

Figure 28. Transonic Capability-Ogive-Cylinder Bodies

Method	Refs	Mach Range	Angle of Attack Range	Configuration
Neumann Potential Flow	90, 91	Subsonic	Linear to Low α	Arbitrary Slender and Blunt Bodies
Van Dyke Hybrid	94	Transonic – Supersonic ($1.2 \lesssim M_\infty \lesssim 4$)	Linear	Slender Bodies
Second-Order Shock Expansion	44	Supersonic ($1.5 \lesssim M_\infty \lesssim 6$)	0° for Pressure; Linear for Stability Coefficients	Slender Bodies
Method of Characteristics	100, 101	Supersonic – Hypersonic	0°	Slender Bodies with Sharp or Blunt Noses
Tangent Cone	48	Supersonic – Hypersonic	Linear to Low α	Slender Bodies
Modified Newtonian Impact	48	Supersonic – Hypersonic ($M_\infty \gtrsim 2$)	Linear and Nonlinear (0° to 180°)	Arbitrary Blunt Bodies

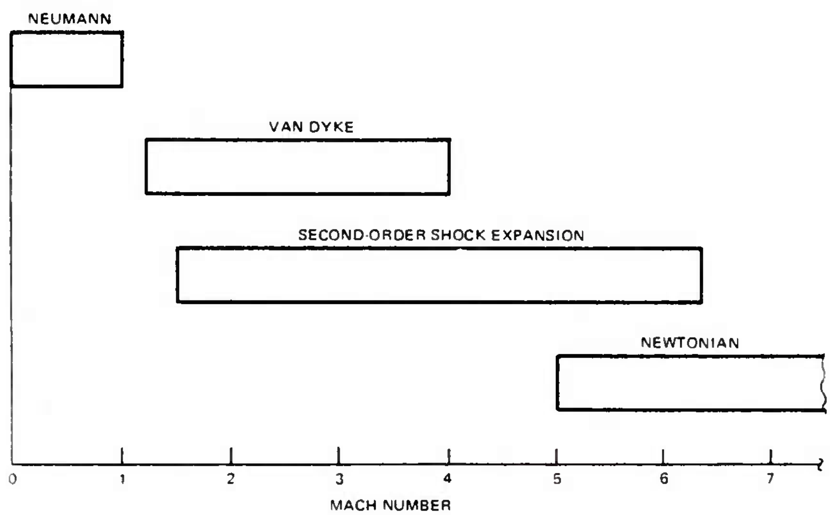

Figure 29. Qualitative Capability of Supersonic Theories

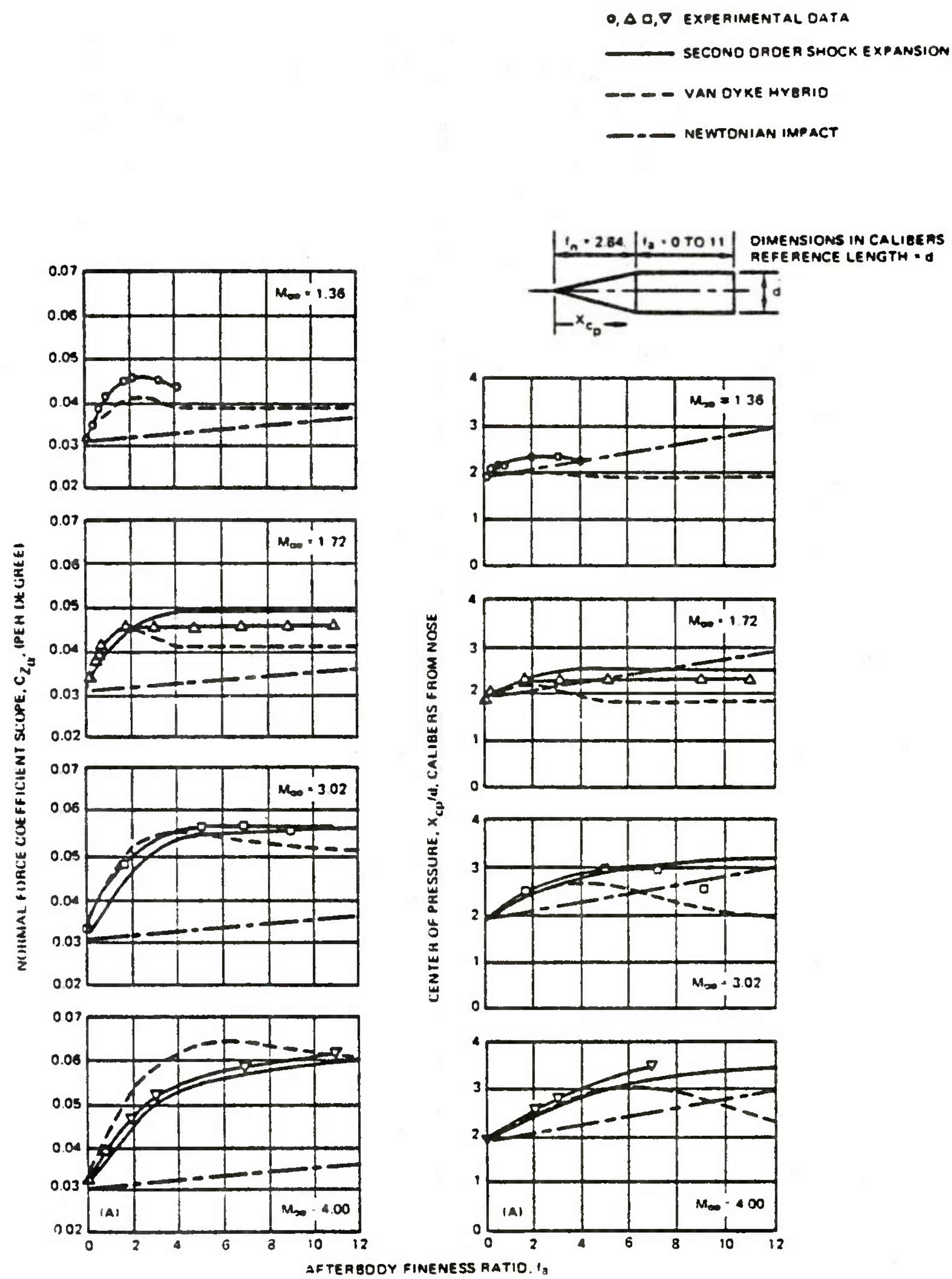

Figure 30. Comparison of Supersonic Methods

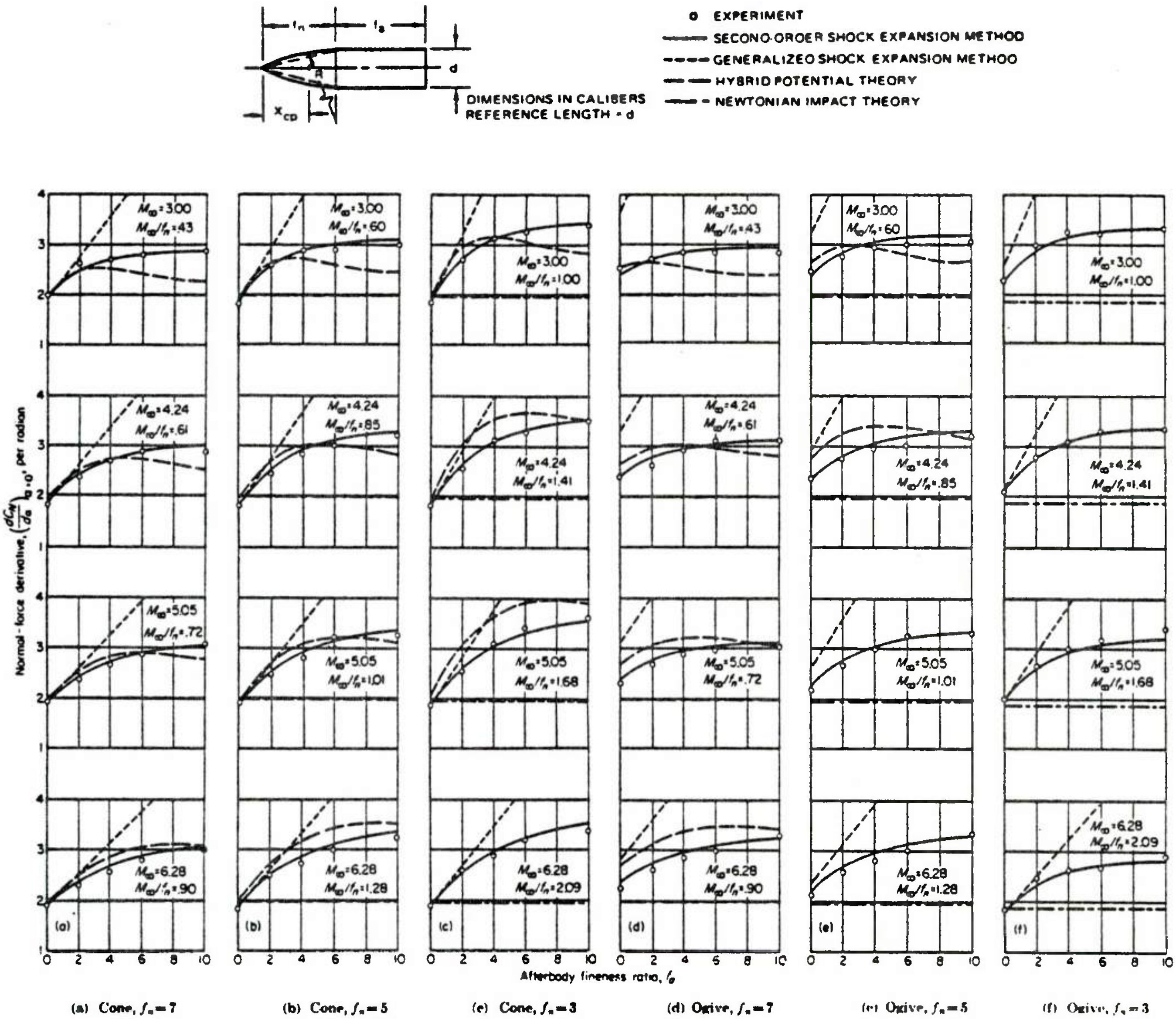

Figure 30. (continued)

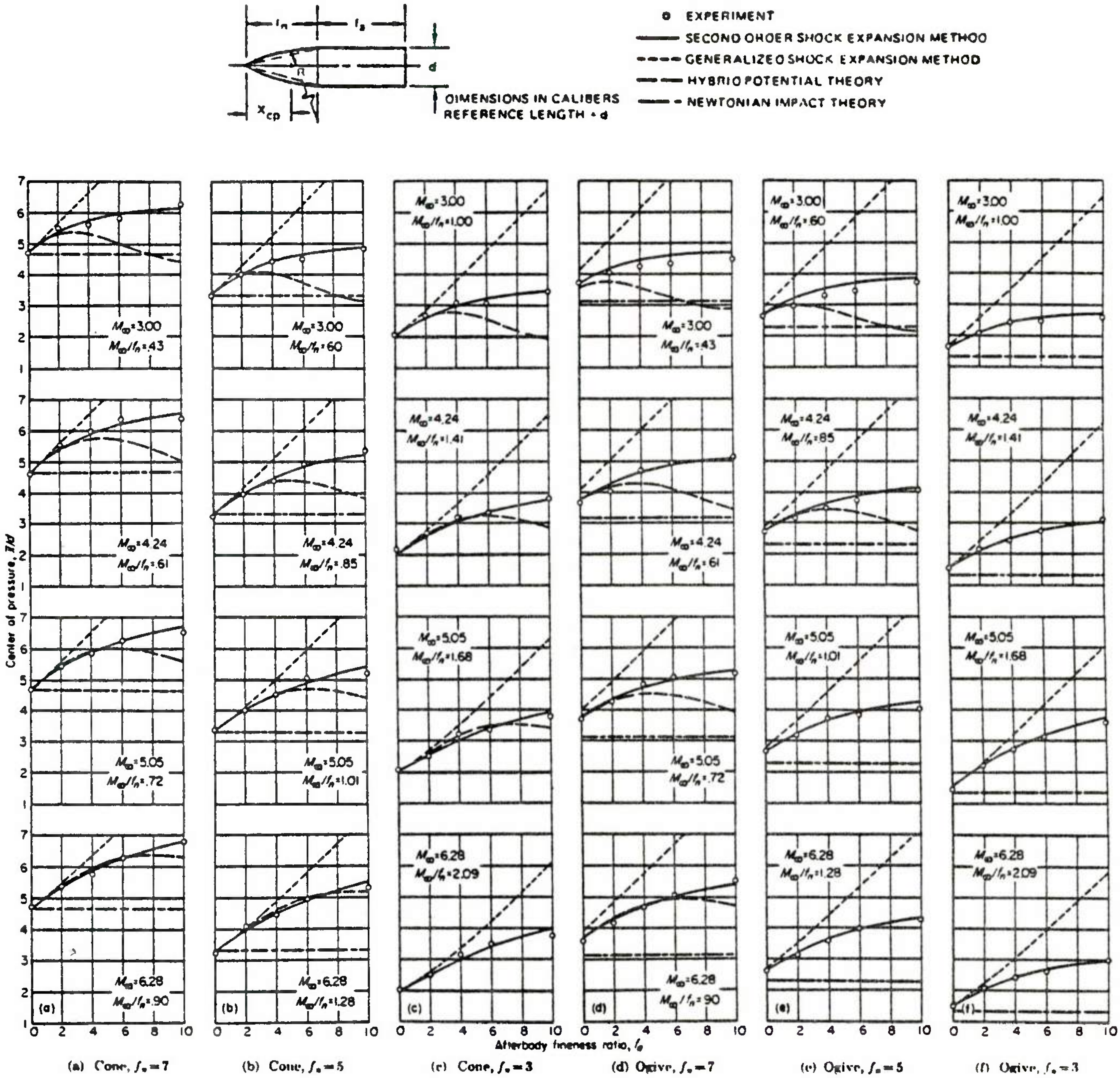

Figure 30. (continued)

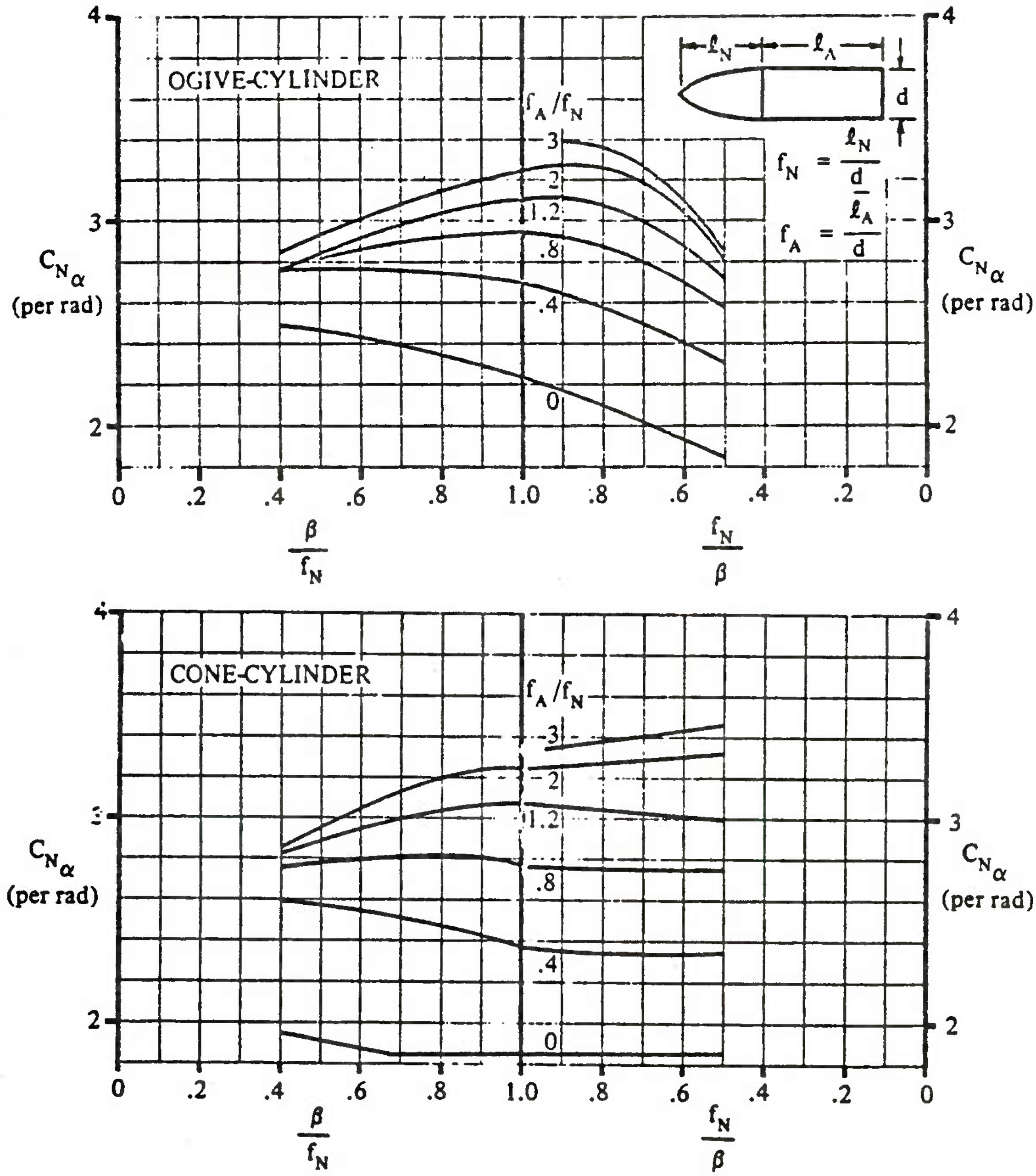

Figure 31. Datcom Design Charts Based on Second-Order Shock Expansion-C_{N_α}

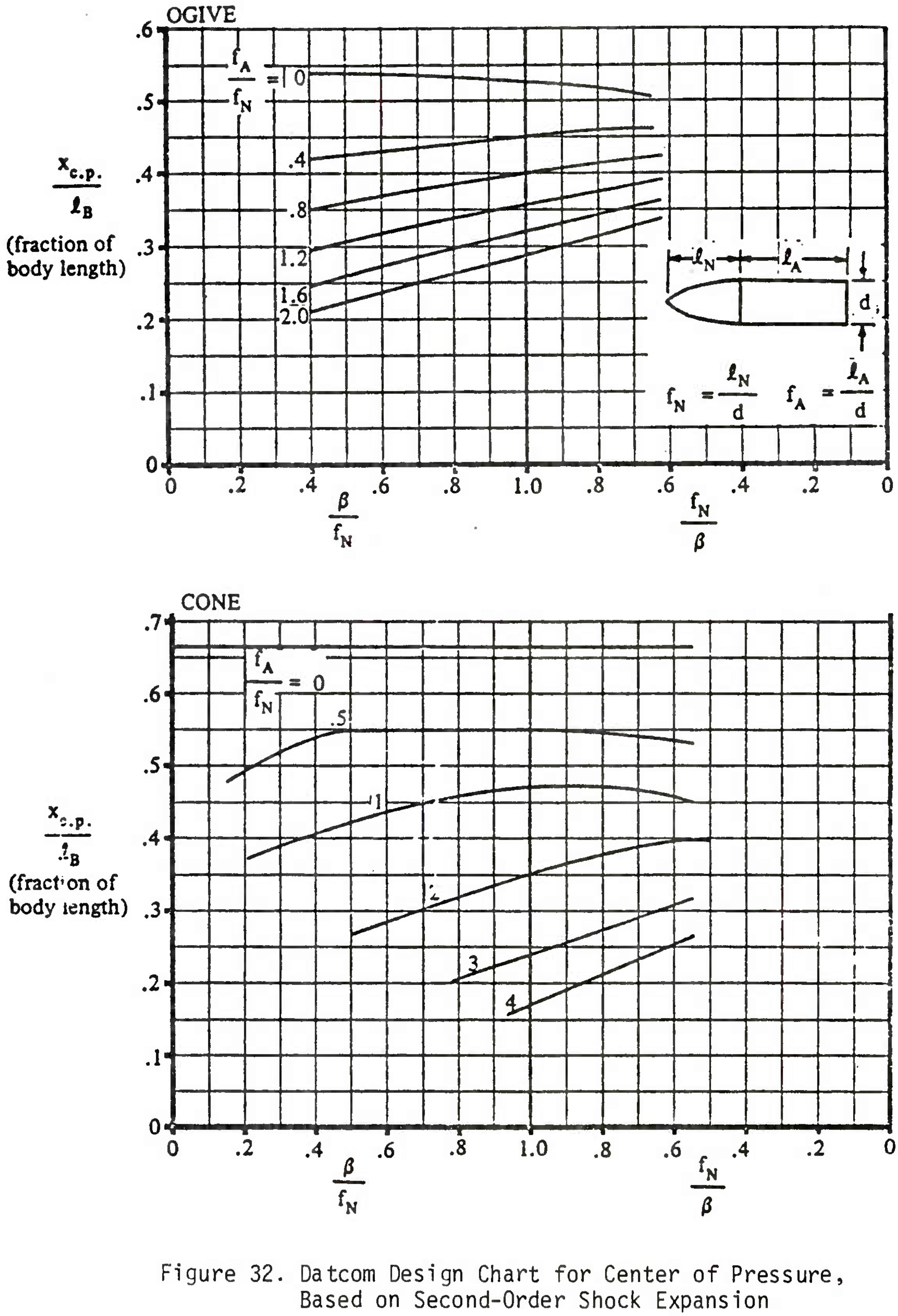

Figure 32. Datcom Design Chart for Center of Pressure, Based on Second-Order Shock Expansion

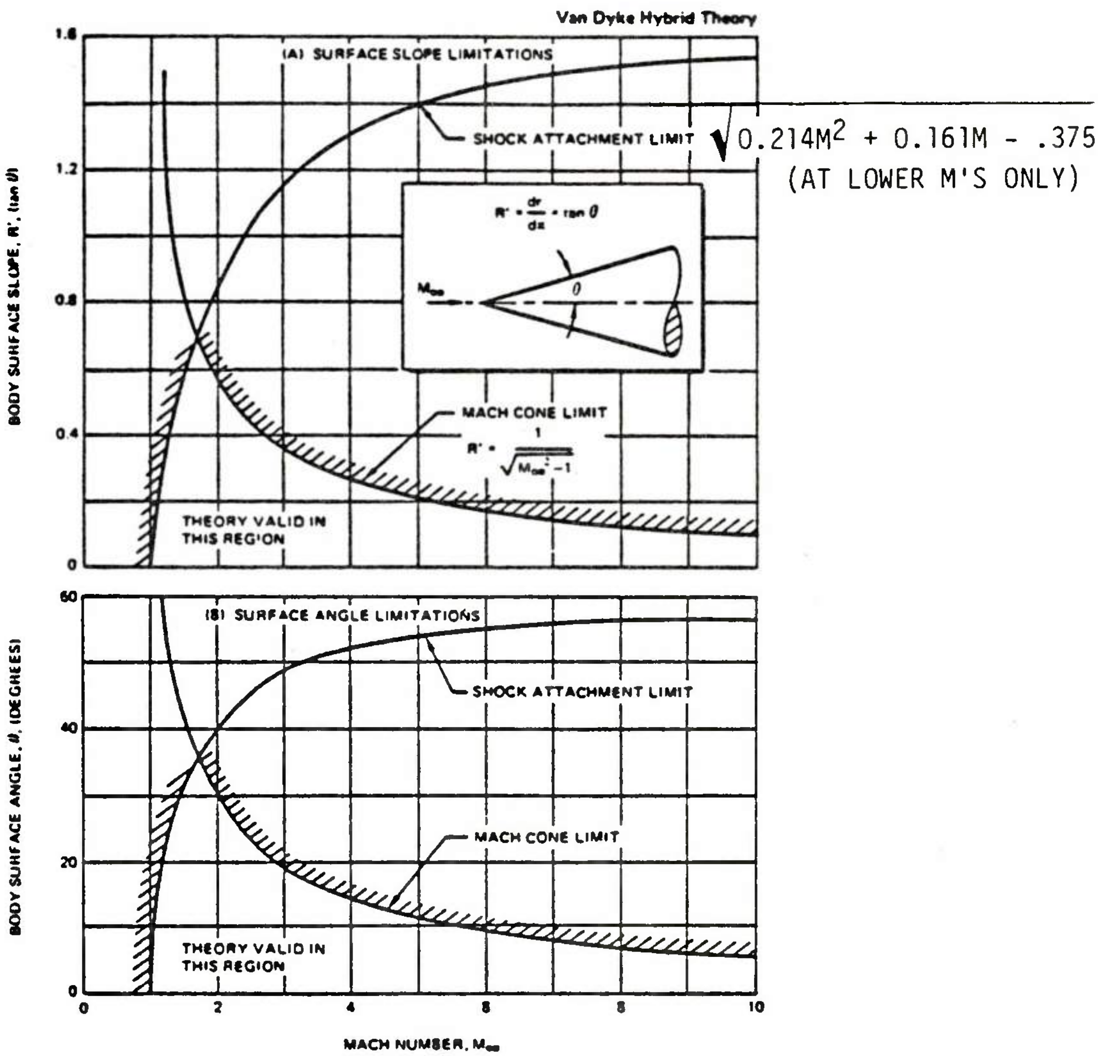

Figure 33. Limitations of Van Dyke Hybrid Theory

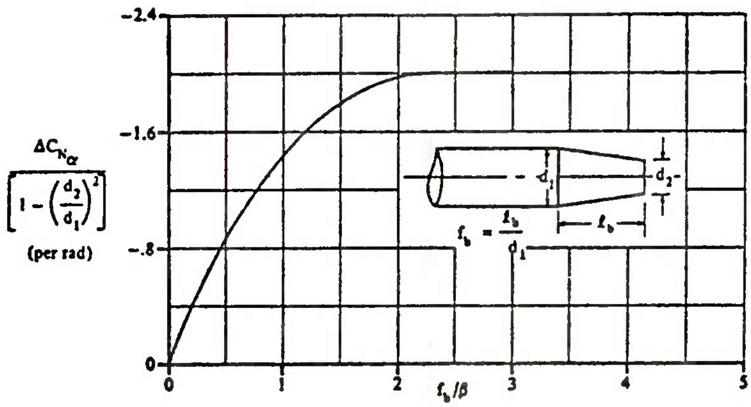

Figure 34. Datcom Supersonic Boattail C_{N_α} Correlation

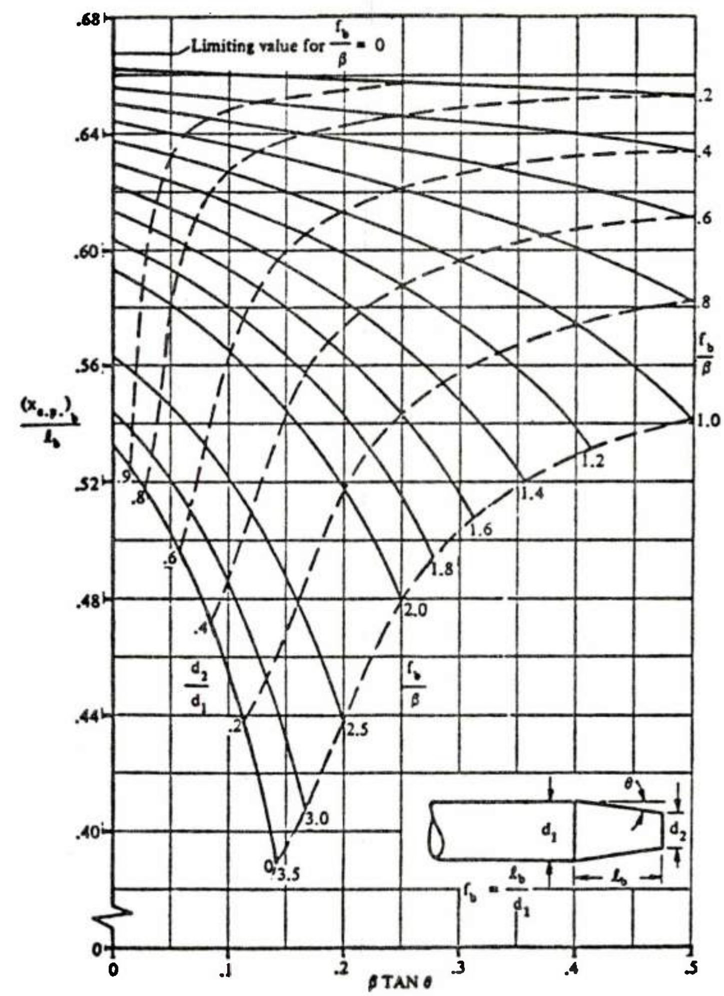

Figure 35. Datcom Center of Pressure of Boattails

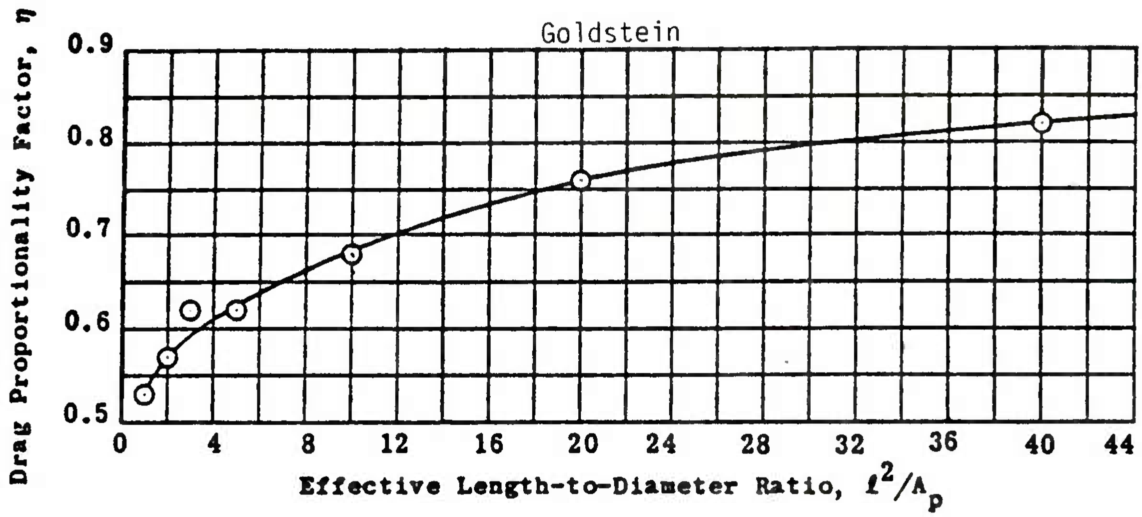

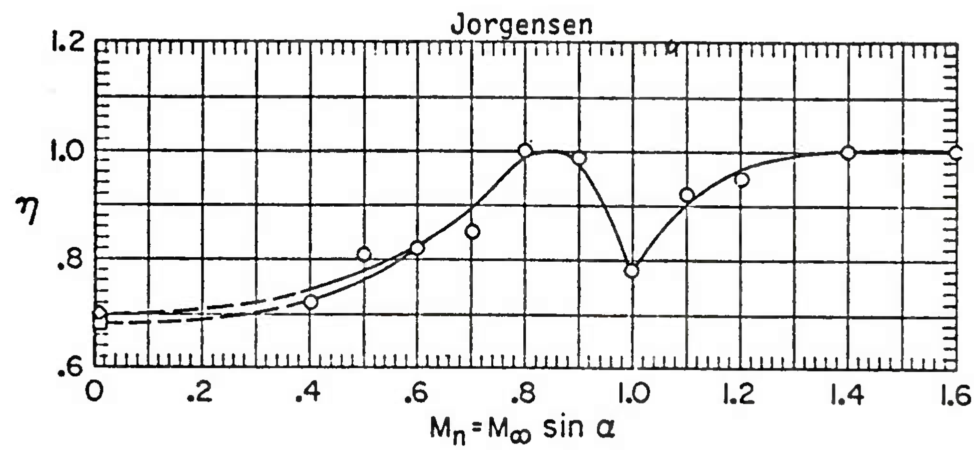

- Baker's Transonic Fairing

  $\eta = \eta^* + [(1-\eta^*)/2]\,[1 + \tanh\{(M-1)\,(15/M^4)\}]$

  η^* - From Goldstein's result

- Martin Marietta (MMC) Transonic Fairing

  $\eta = B_o \eta^* + B_1$

  $B_o = -9.0741 + 31.1111\, M_C - 30.5556\, M_C^2 + 9.2593\, M_C^3$

  $B_1 = 10.0741 - 31.1111\, M_C + 30.5556\, M_C^2 - 9.2593\, M_C^3$

Figure 36. Cross-Flow Drag Proportionality Factor Methods

1. USAF DATCOM Ref. (1)
2. MOORE (NSWC) (51)
3. BAKER (AEDC) (75)
4. JORGENSEN (NASA) (47,87,88)
5. AIELLO (MMC) (58)
6. KRIEGER (MDAC) (49)
7. EATON (DTMB) (33)
8. SAFFELL (NSRDC) (33)
9. MACHA (TEXAS A&M) (89)

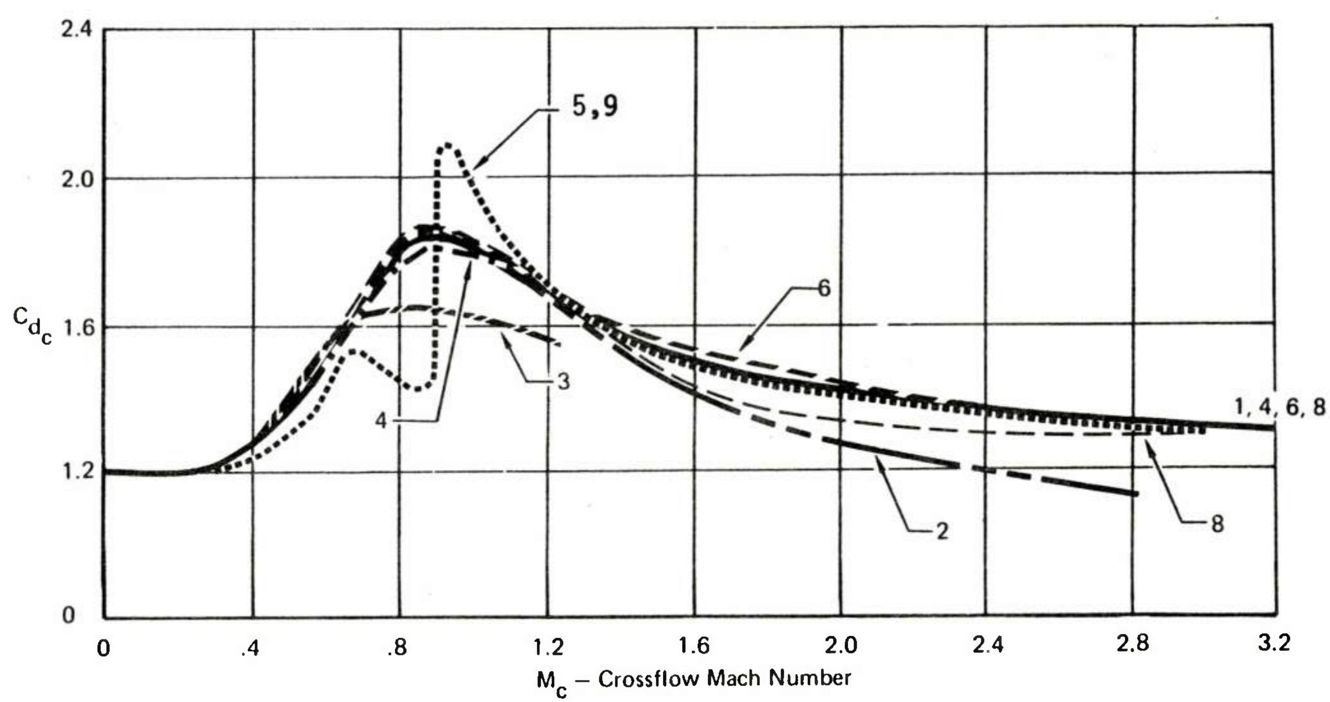

Figure 37. Comparison of Cross-Flow Drag Results

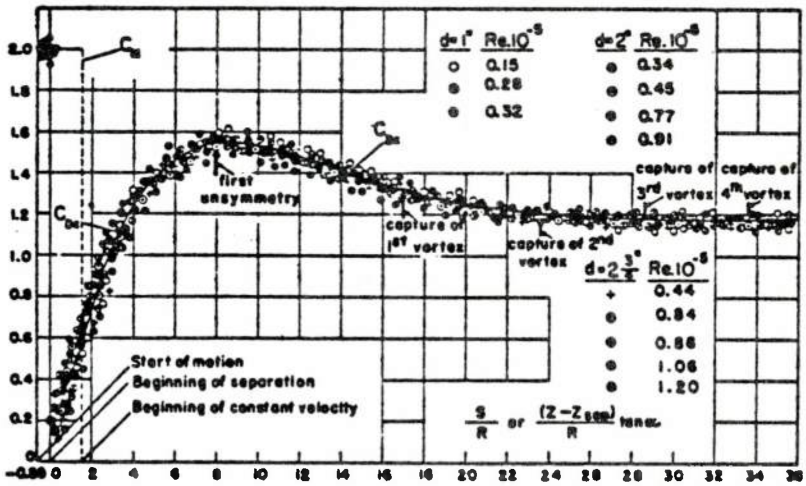

Figure 38. Sarpkaya Reduction of Schwabe's Results

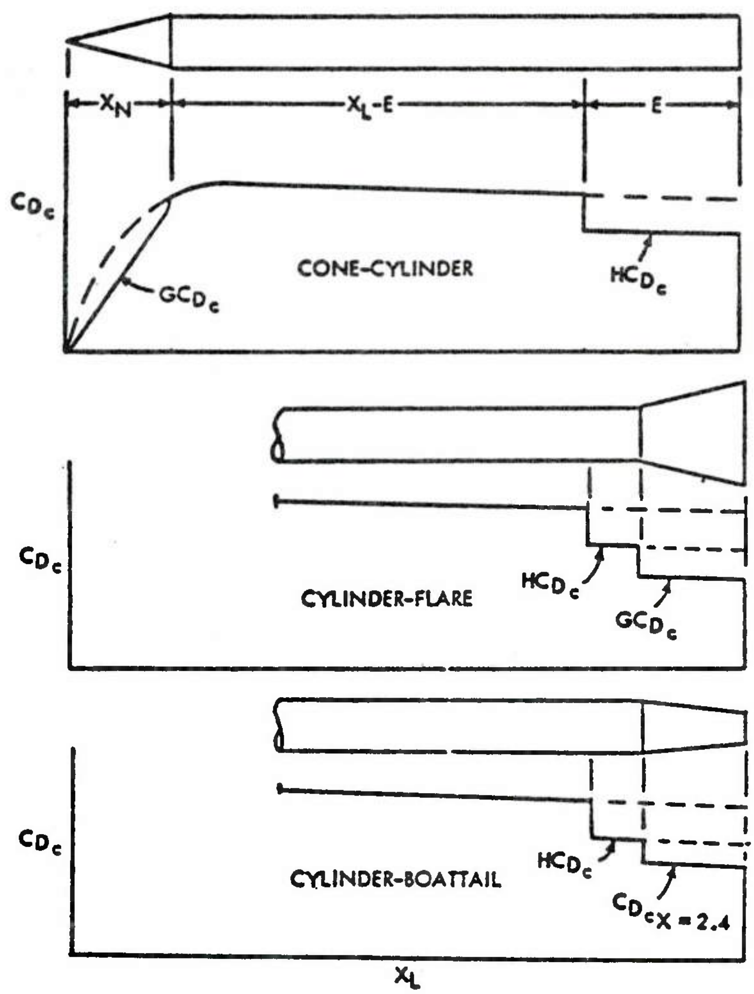

Figure 39. Variation of Cross-Flow Drag Used by Darling

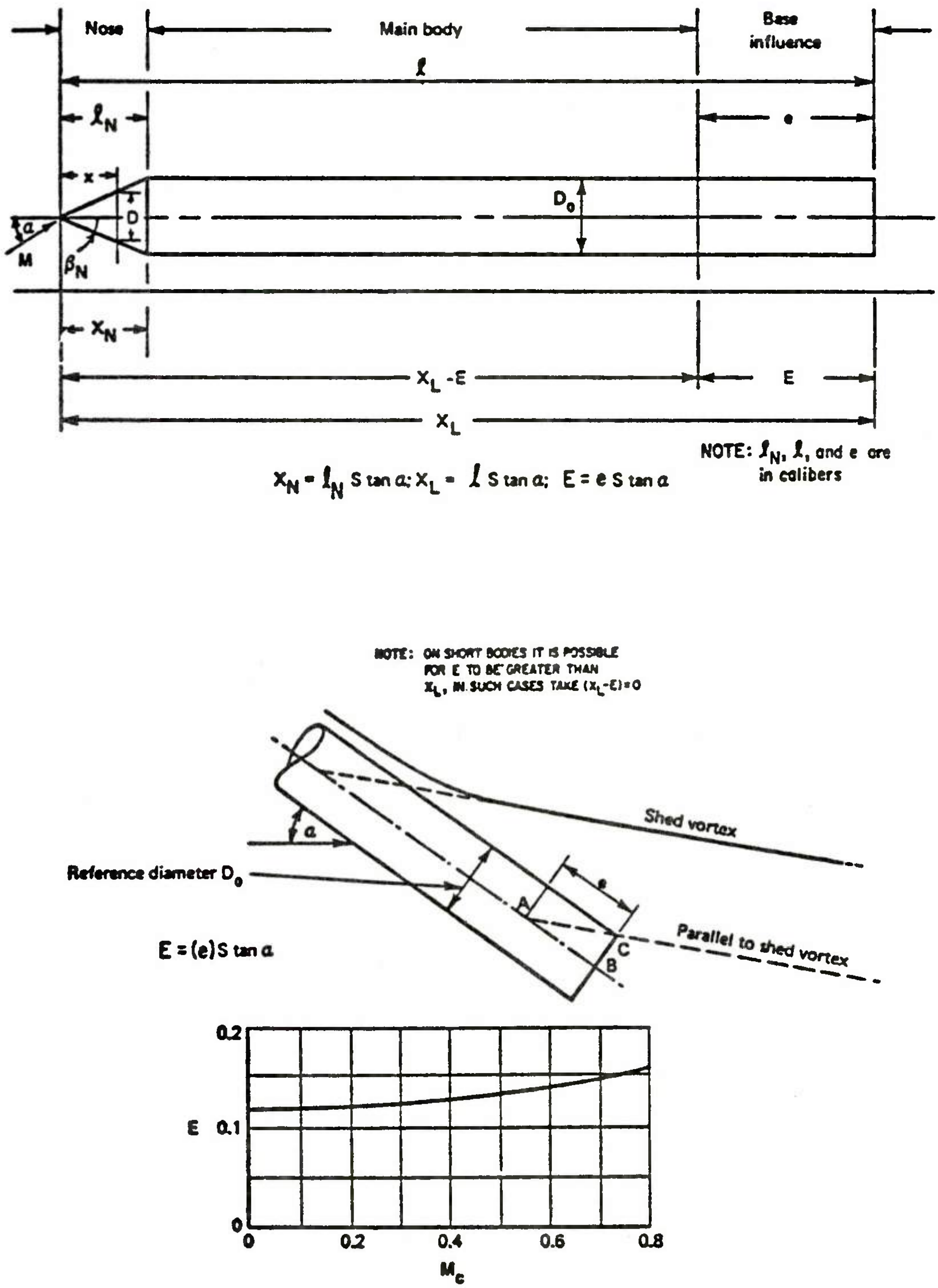

Figure 40. Correction Terms Cross-Flow Drag Presented by Darling

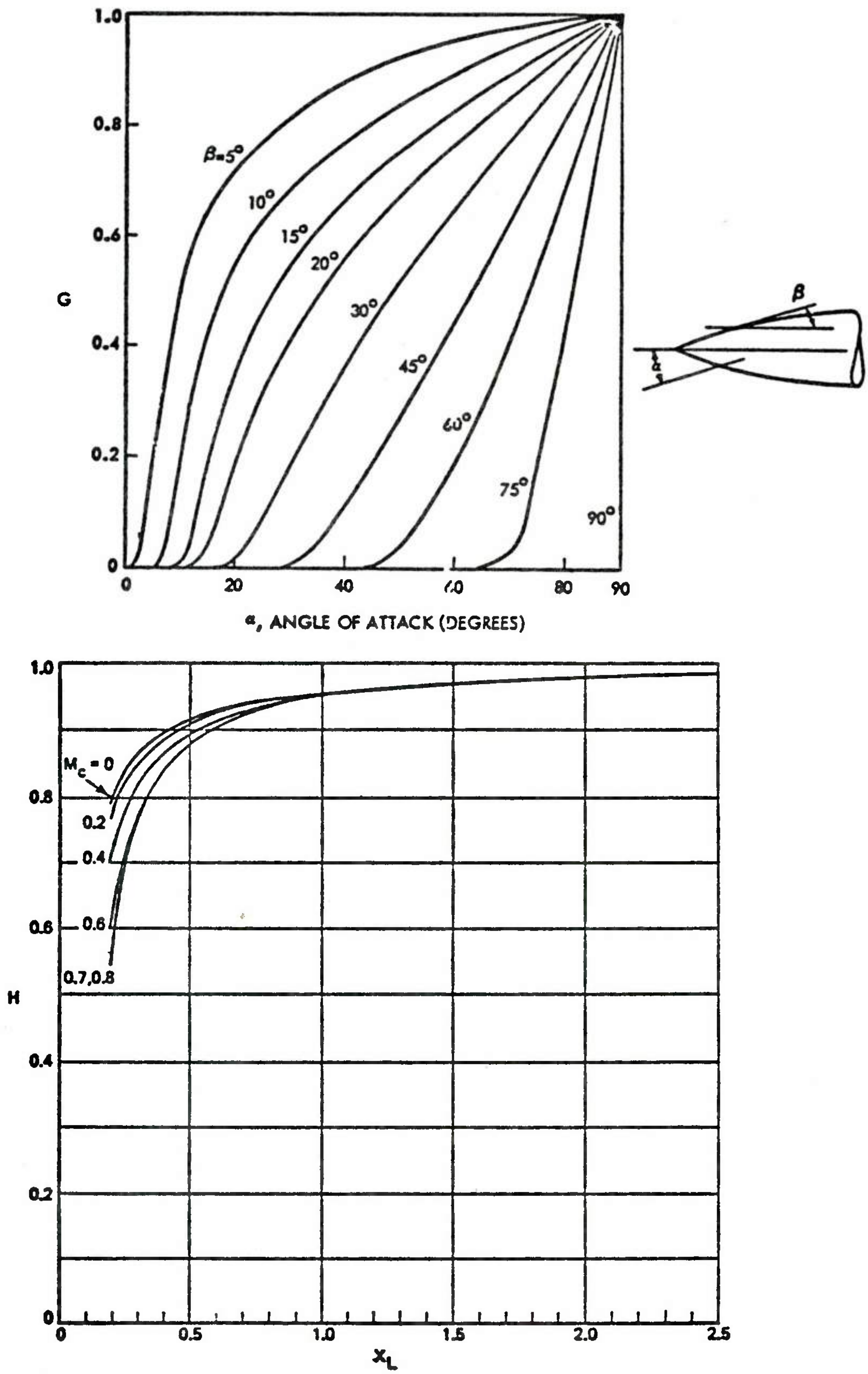

Figure 40. (continued)

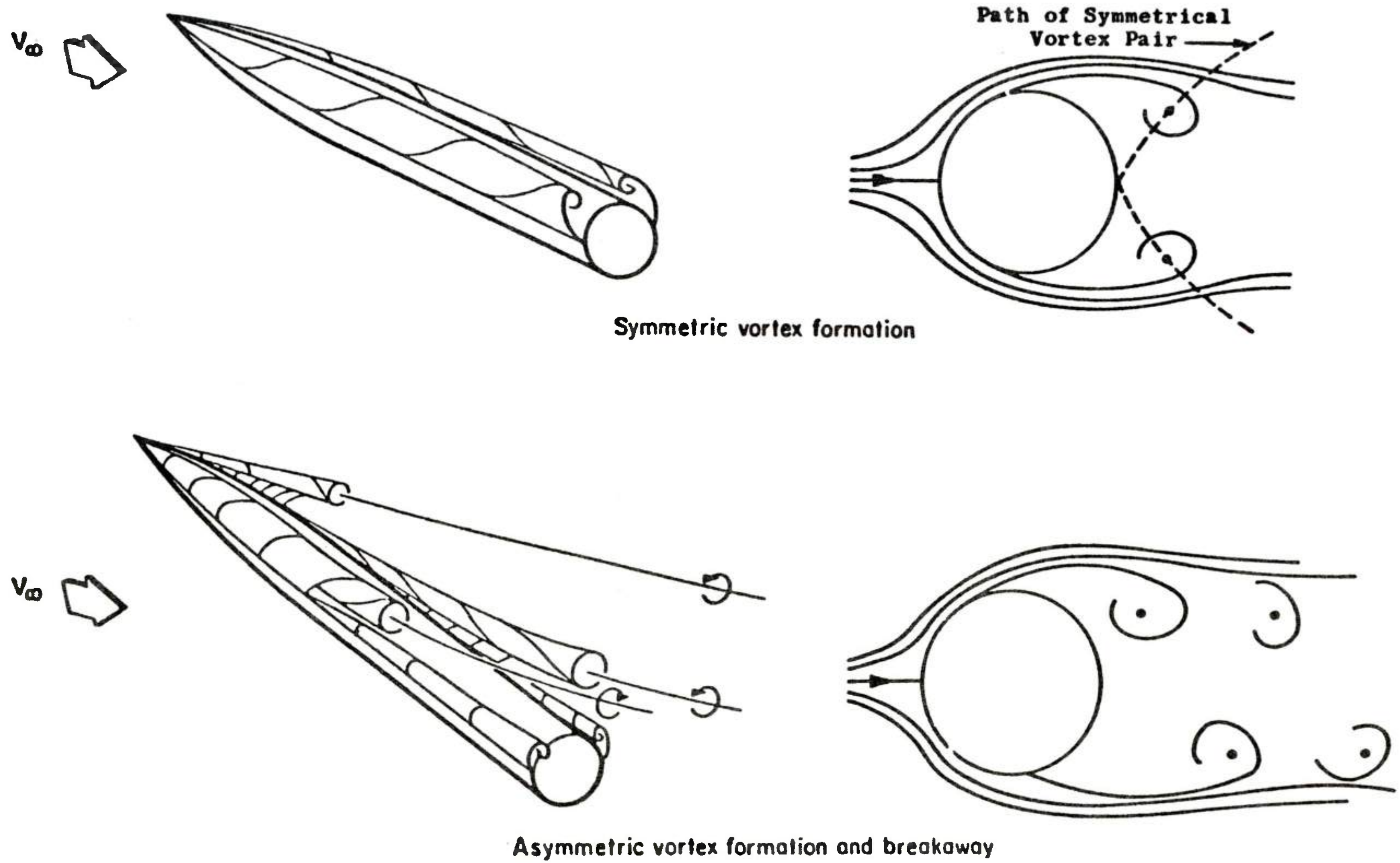

Figure 41. Vortex Formation for a Body at Incidence

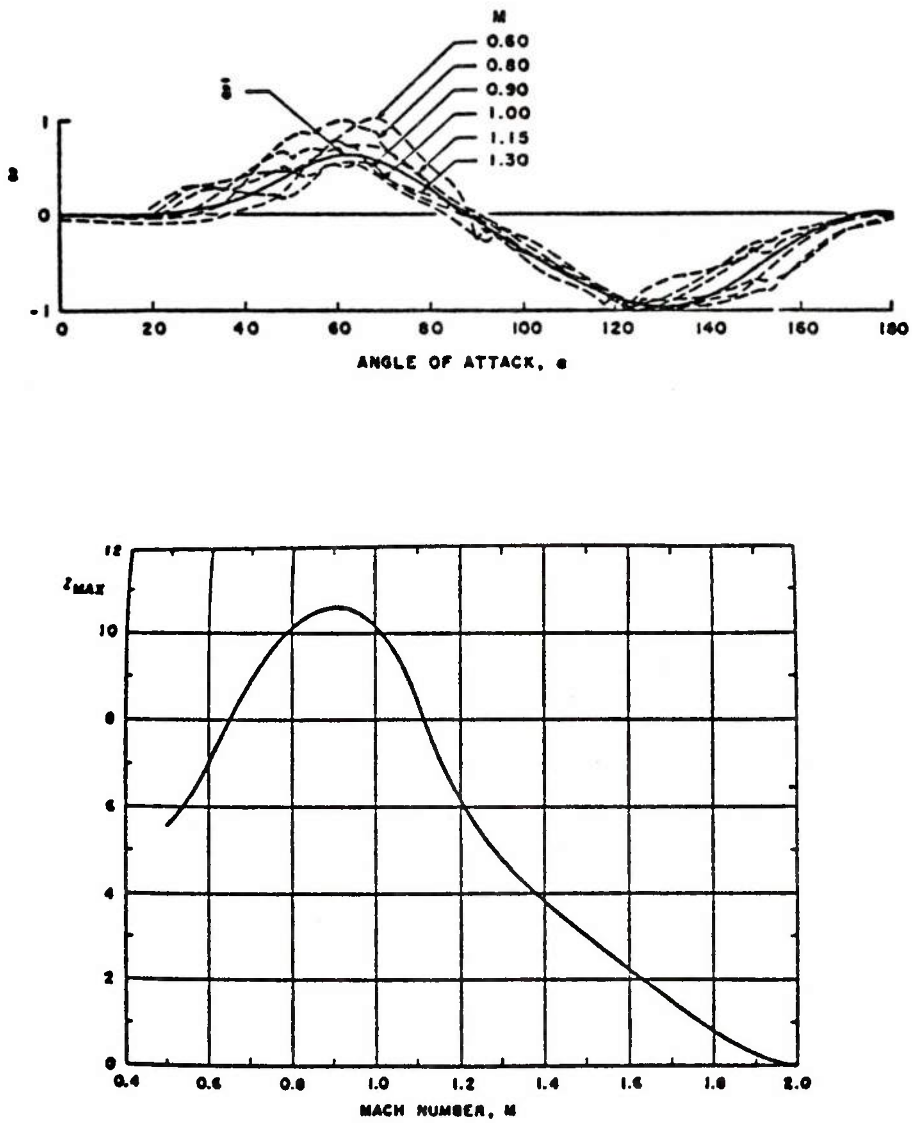

Figure 42. Baker's Correction Factor to Jorgensen's Pitching Moment Relation

$$C_N = \left(\frac{C_N}{C_{N_{cir}}}\right)_{SB} \left(\frac{S_b}{S} \sin 2\alpha' \cos \frac{\alpha'}{2}\right) + \left(\frac{C_N}{C_{N_{cir}}}\right)_{NT} \left(\eta c_{d_c} \frac{S_p}{S} \sin^2 \alpha'\right)$$

$$C_m = \left(\frac{C_N}{C_{N_{cir}}}\right)_{SB} \left[\frac{V_B - S_b(\ell_B - x_m)}{Sd}\right] \sin 2\alpha' \cos \frac{\alpha'}{2} + \left(\frac{C_N}{C_{N_{cir}}}\right)_{NT} \eta c_{d_c} \frac{S_p}{S} \left(\frac{x_m - x_c}{d}\right) \sin^2\alpha'$$

When the major axis (a) is perpendicular to the cross-flow velocity.

$$\left(\frac{C_N}{C_{N_{cir}}}\right)_{NT} = \frac{3}{2}\sqrt{\frac{a}{b}} \left\{ \frac{-b^2/a^2}{\left(1 - \frac{b^2}{a^2}\right)^{3/2}} \log_e\left[\frac{a}{b}\left(1 + \sqrt{1 - \frac{b^2}{a^2}}\right)\right] + \frac{1}{1 - \frac{b^2}{a^2}} \right\}$$

When the minor axis (b) is perpendicular to the cross-flow velocity,

$$\left(\frac{C_N}{C_{N_{cir}}}\right)_{NT} = \frac{3}{2}\sqrt{\frac{b}{a}} \left[\frac{a^2/b^2}{\left(\frac{a^2}{b^2} - 1\right)^{3/2}} \tan^{-1}\left(\sqrt{\frac{a^2}{b^2} - 1}\right) - \frac{1}{\frac{a^2}{b^2} - 1} \right]$$

$$\left(\frac{C_N}{C_{N_{cir}}}\right)_{SB} = \frac{a}{b}\cos^2\phi + \frac{b}{a}\sin^2\phi$$

ϕ is the angle of bank of the body about its longitudinal axis; $\phi = 0$ with the major axis horizontal, and $\phi = 90^\circ$ with the minor axis horizontal.

Figure 43. Jorgensen Method for Elliptical Bodies, as Given in Datcom

CROSS SECTION	NEWTONIAN THEORY		MOD. NEWT. THEORY FOR $C_{p_{stag}} = 1.8$		MEASURED		
	C_{d_n}	C_n / C_{n_o}	C_{d_n}	C_n / C_{n_o}	C_{d_n}	C_n / C_{n_o}	REF.
	1.33	1.00	1.20	1.00	1.20	1.00	11
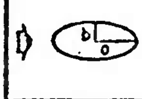 a/b = 2	0.94	0.50	0.85	0.50	0.70	0.41	12, 13
a/b = 4	0.59	0.22	0.53	0.22	0.35	0.15	12
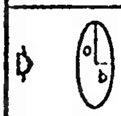 a/b = 2	1.65	1.75	1.49	1.75	1.60	1.89	13, 14
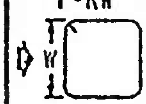 r = kw, k = 0.0	2.00	1.33	1.80	1.33	2.05	1.51	12
k = 0.02	1.97	1.33	1.78	1.33	2.00	1.48	13
k = 0.08	1.89	1.26	1.70	1.26	1.65	1.22	15
k = 0.24	1.68	1.14	1.51	1.14	1.12	0.85	15
k = 0.50	1.33	1.00	1.20	1.00	1.20	1.00	11

NOTE: ALL C_{d_n}'s IN TABLE ARE BASED ON WIDTH OF CROSS SECTION, NOT EQUIVALENT d.

Figure 44. Some Newtonian Theory Results of Jorgensen

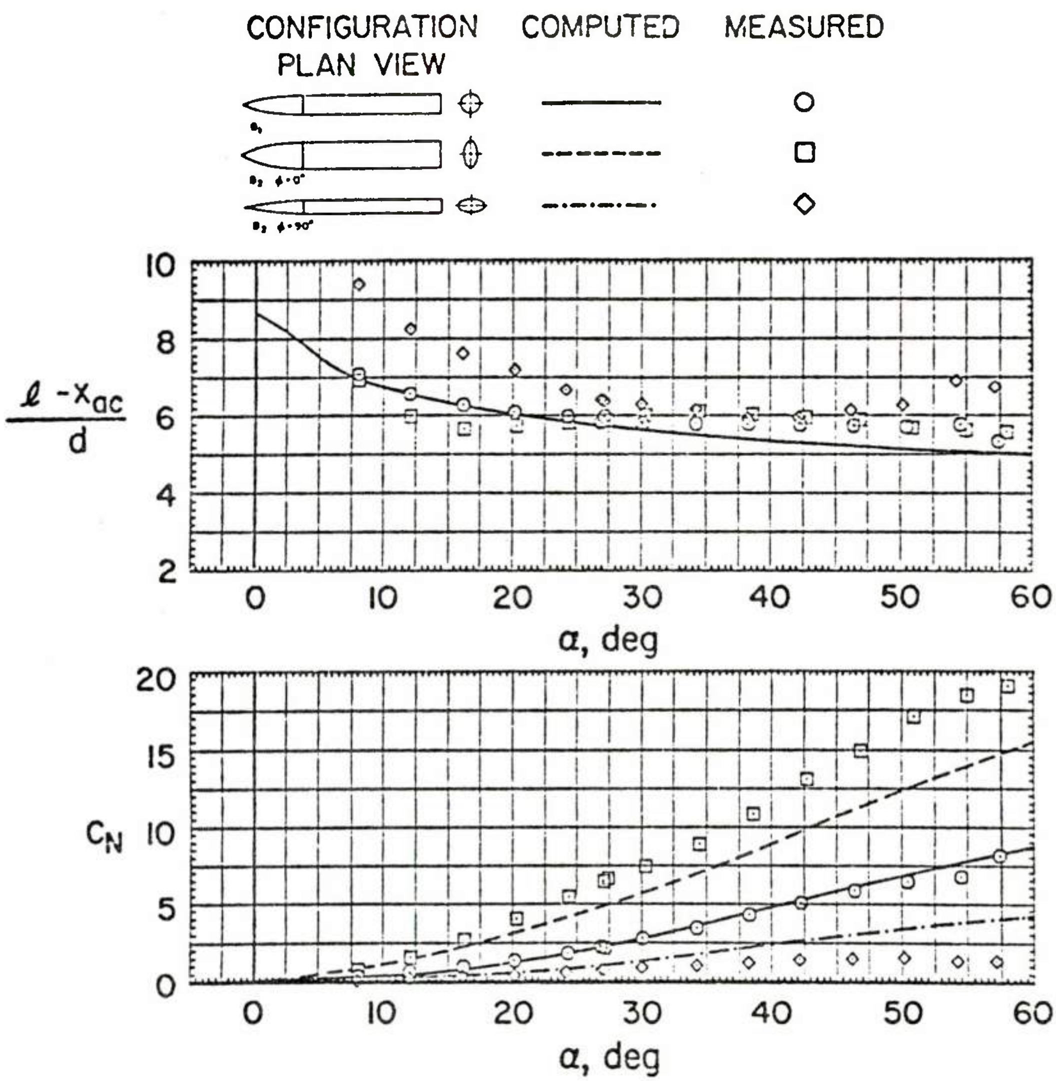

$M_\infty = 0.6$, Re = $6.5\text{X}10^5$

Figure 45. Jorgensen Integral Form Method Comparison to Data

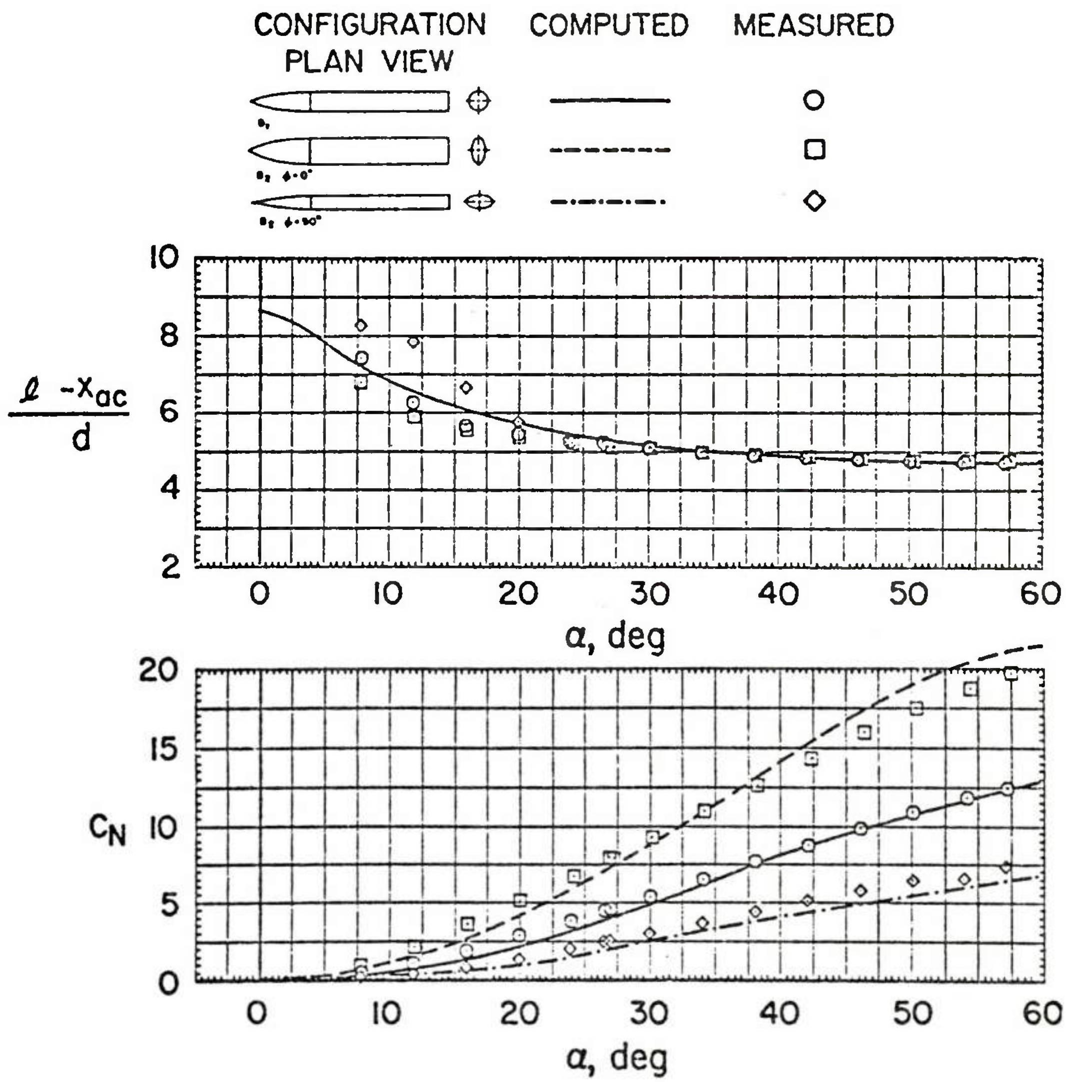

$M_\infty = 2.0$, Re $= 3.8 \times 10^5$

Figure 45. (continued)

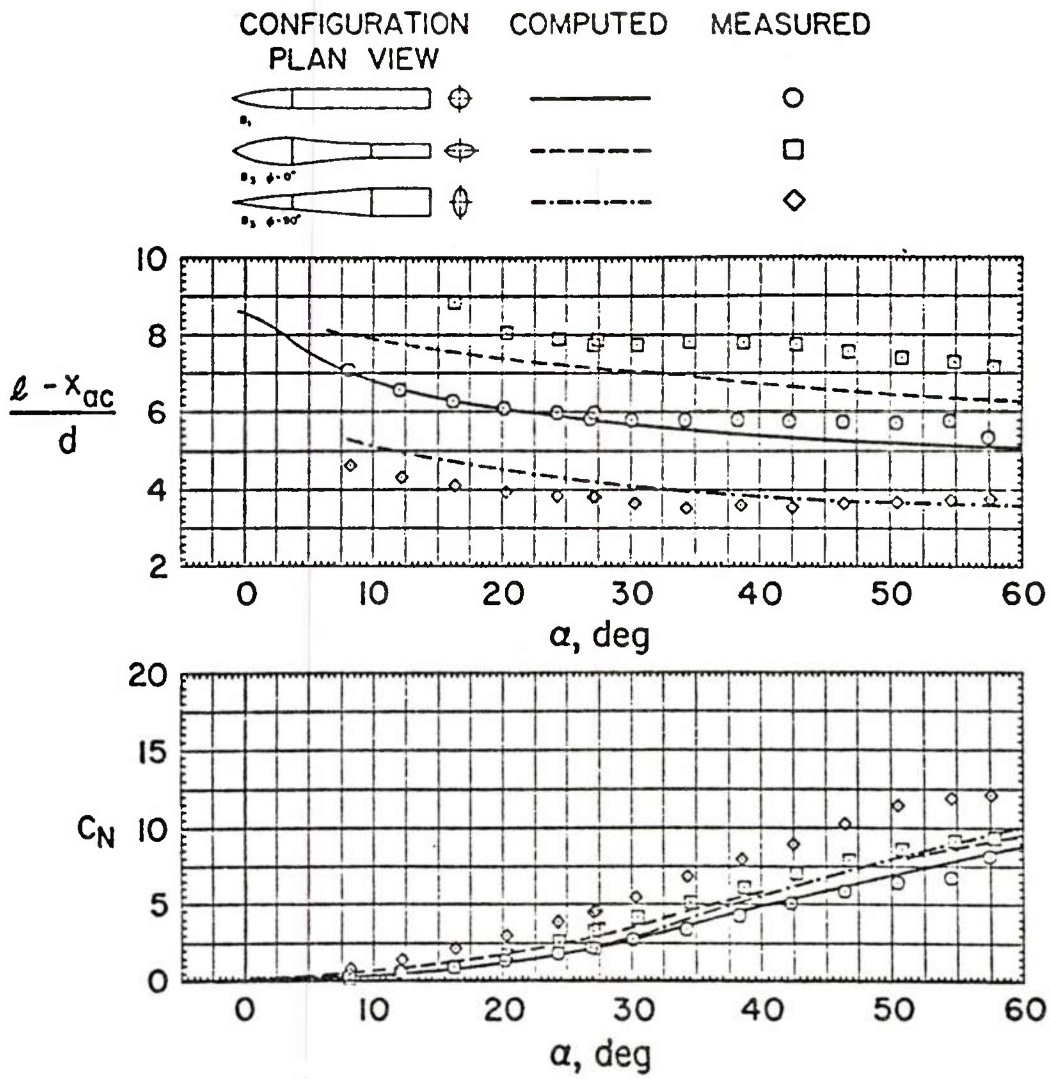

$M_\infty = 0.6$, Re = 6.5×10^5

Figure 45. (continued)

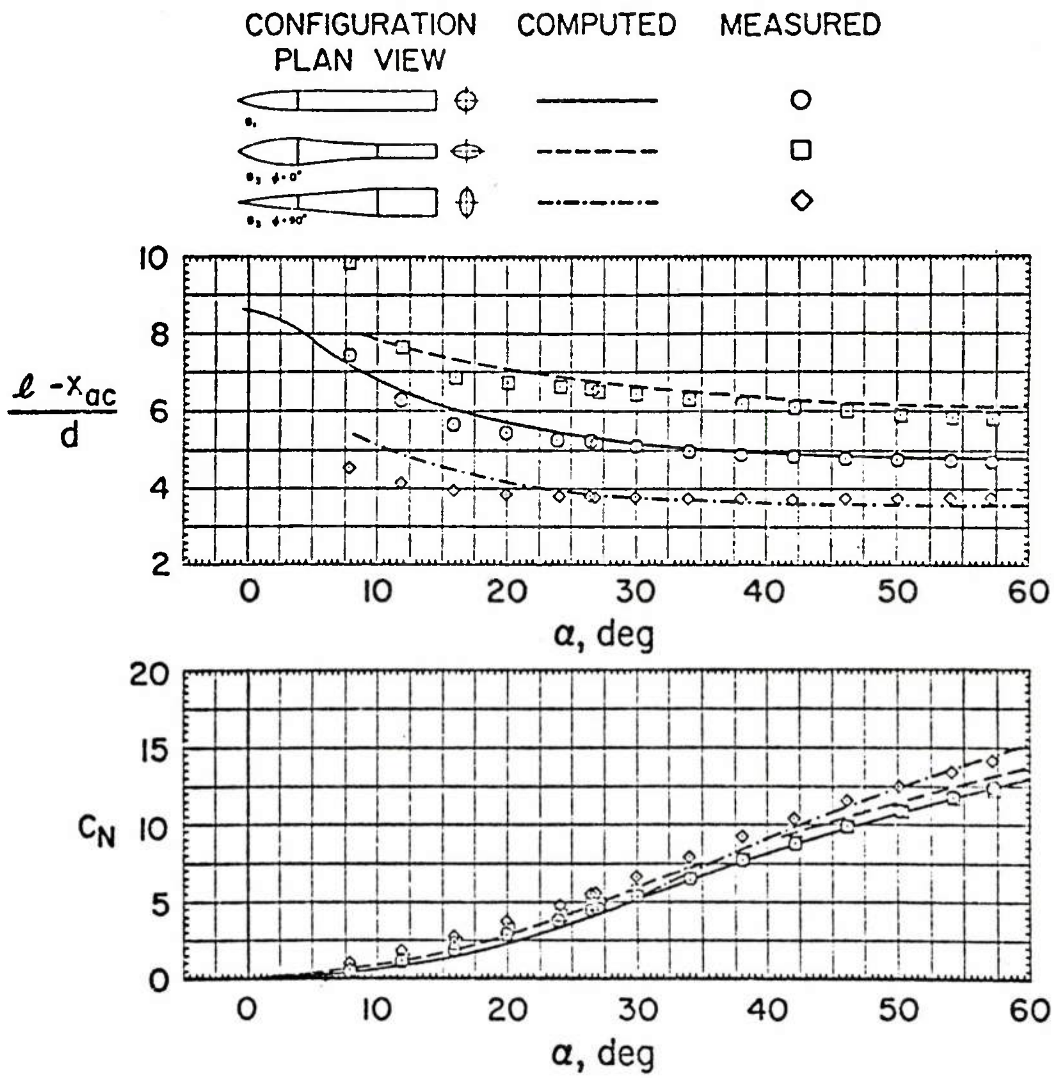

$M_\infty = 2.0$, Re $= 3.8 \times 10^5$

Figure 45. (continued)

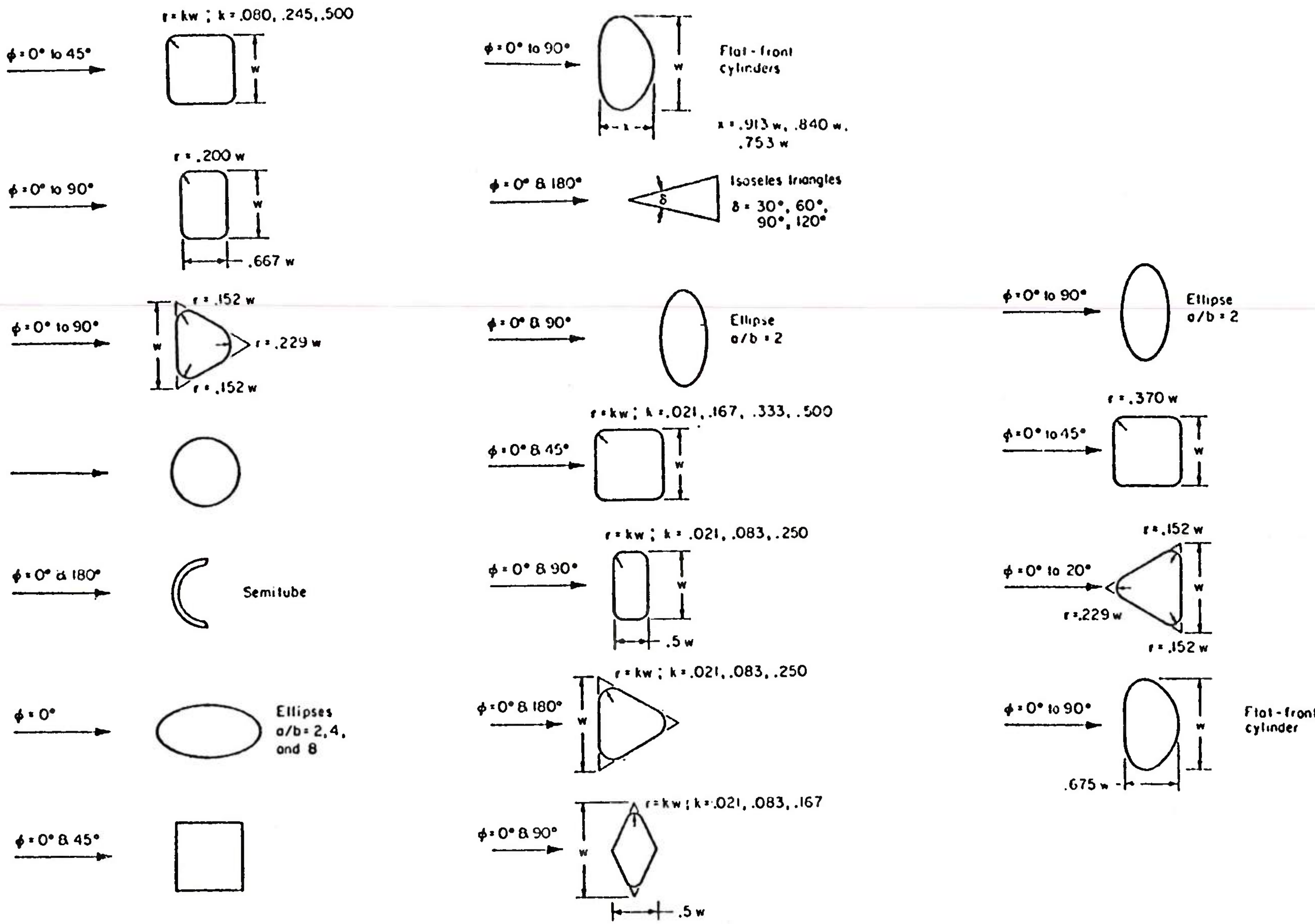

Figure 46. Other Shapes Experimentally Investigated at Subsonic Speeds

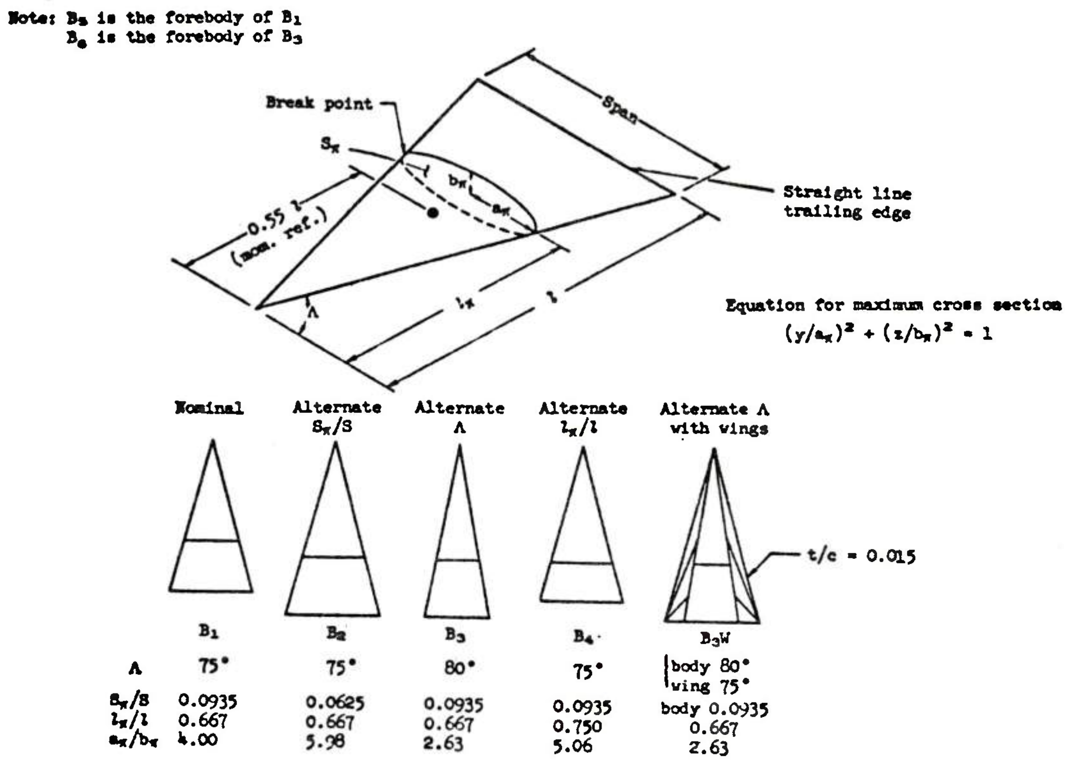

a) NASA TN D-6821

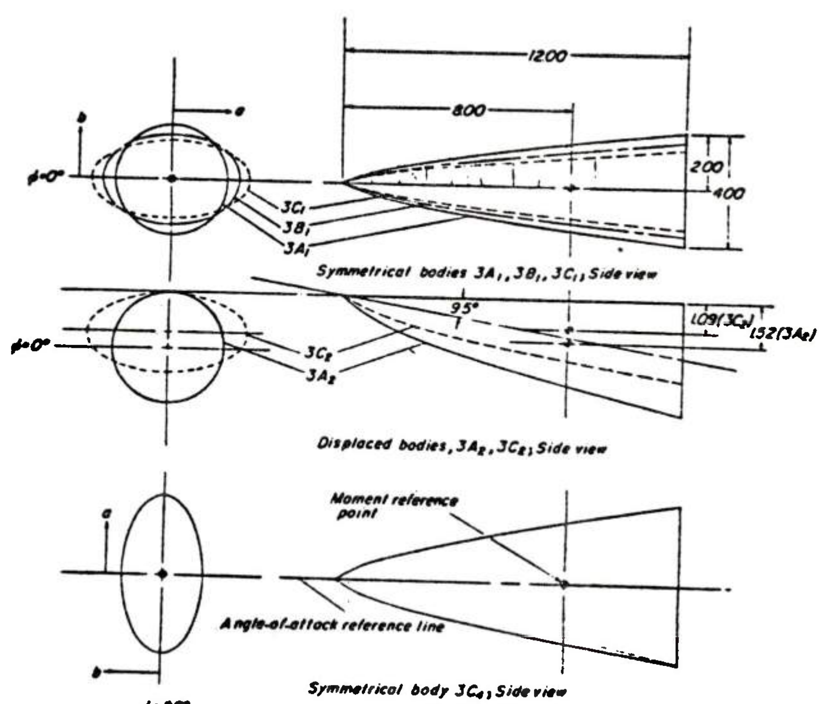

b) NASA TN D-2622

Figure 47. Example Results for General Shaped Bodies

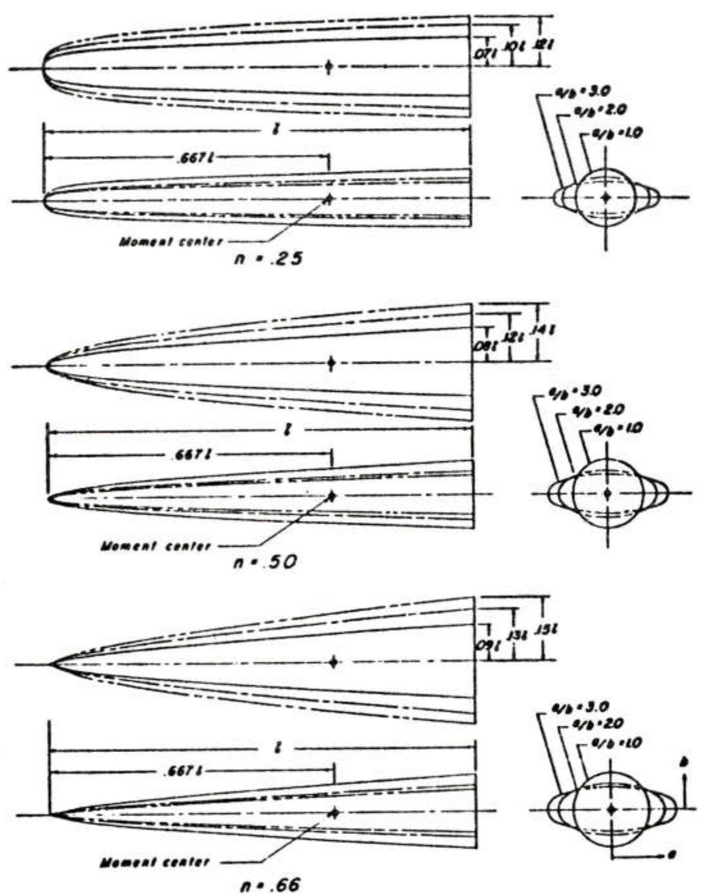

c) NASA TN D-3203

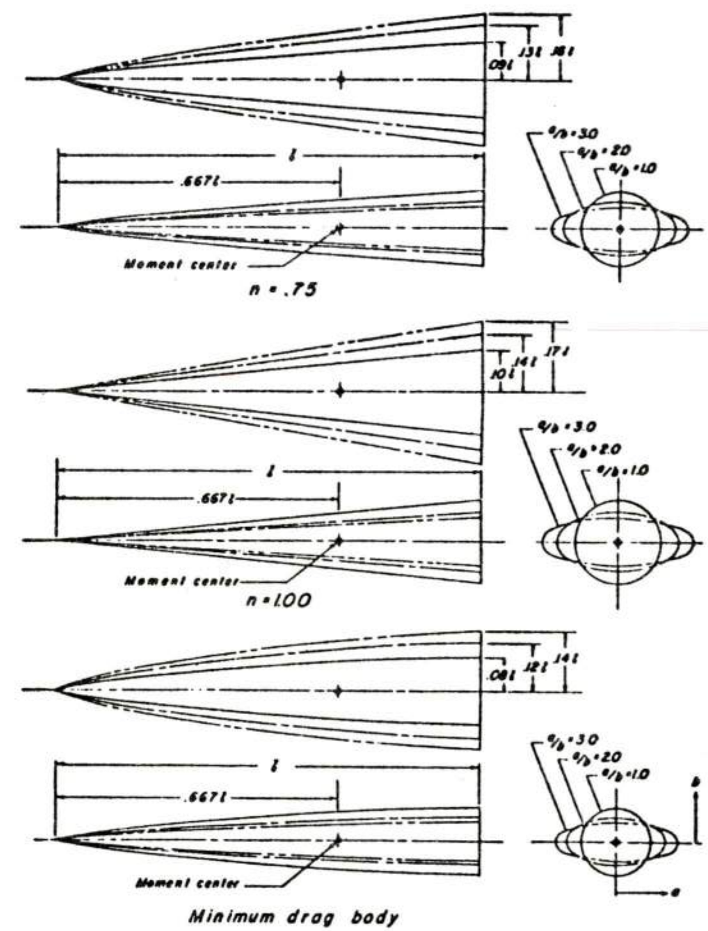

d) NASA TN D-3539

Figure 47. (continued)

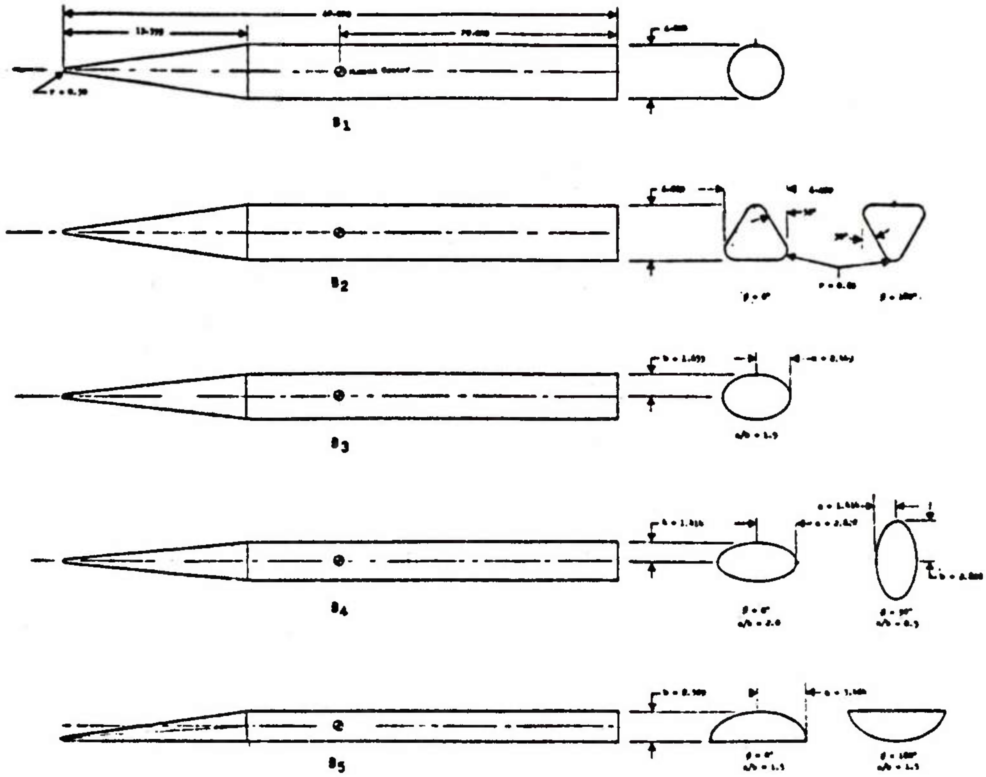

e) NASA TN D-1620

Figure 47. (continued)

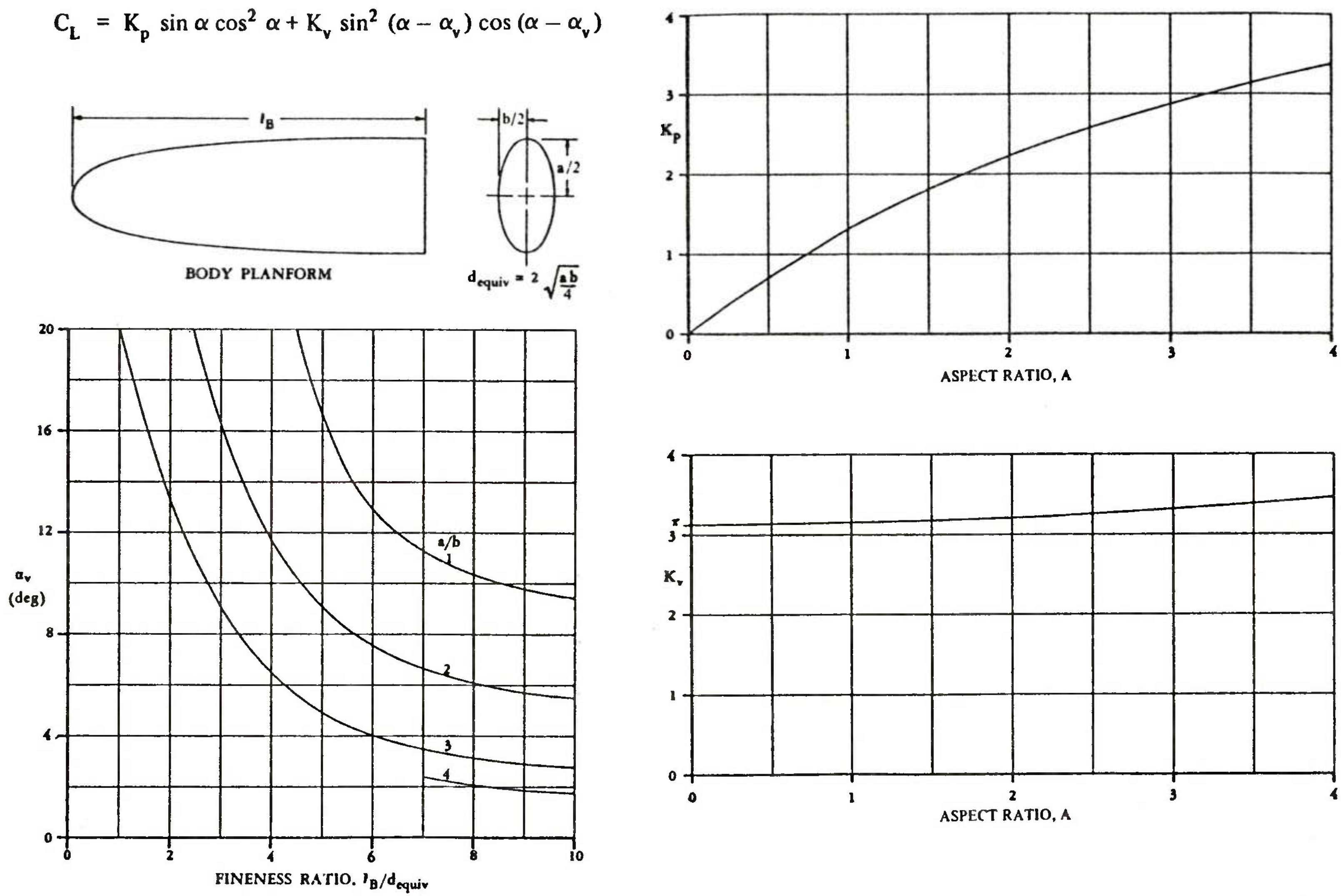

Figure 48. Datcom Version of Polhamus Suction Analogy for Bodies

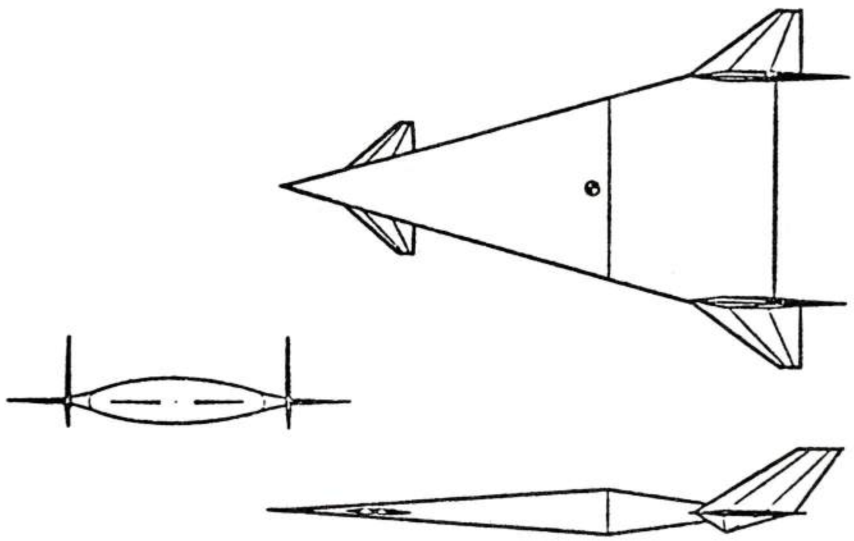

$$C_L = C_1 \sin\alpha + C_2 \sin^2\alpha$$

$$M \lesssim 1.0 \quad \begin{cases} C_1 = \dfrac{\pi AR}{2} - 0.355\ \beta^{0.45} AR^{1.45} \\ C_2 = 0 \end{cases}$$

$$\begin{array}{l} M > 1.0 \\ \beta < \dfrac{4}{AR} \end{array} \quad \begin{cases} C_1 = \dfrac{\pi AR}{2} - 0.153\ \beta AR^2 \\ C_2 = \text{linear interpolation with respect to } \beta \text{ from} \\ \quad C_2 = 0 \quad \text{at} \quad \beta = 0 \quad \text{to} \\ \quad C_2 = e^{[0.955-(4.35/M)]} \quad \text{at} \quad \beta = \dfrac{4}{AR} \end{cases}$$

$$\begin{array}{l} M > 1.0 \\ \beta \geq \dfrac{4}{AR} \end{array} \quad \begin{cases} C_1 = \dfrac{4.17}{\beta} - 0.13 \\ C_2 = e^{[0.955-(4.35/M)]} \end{cases}$$

Figure 49. Geometry Investigated by Williams

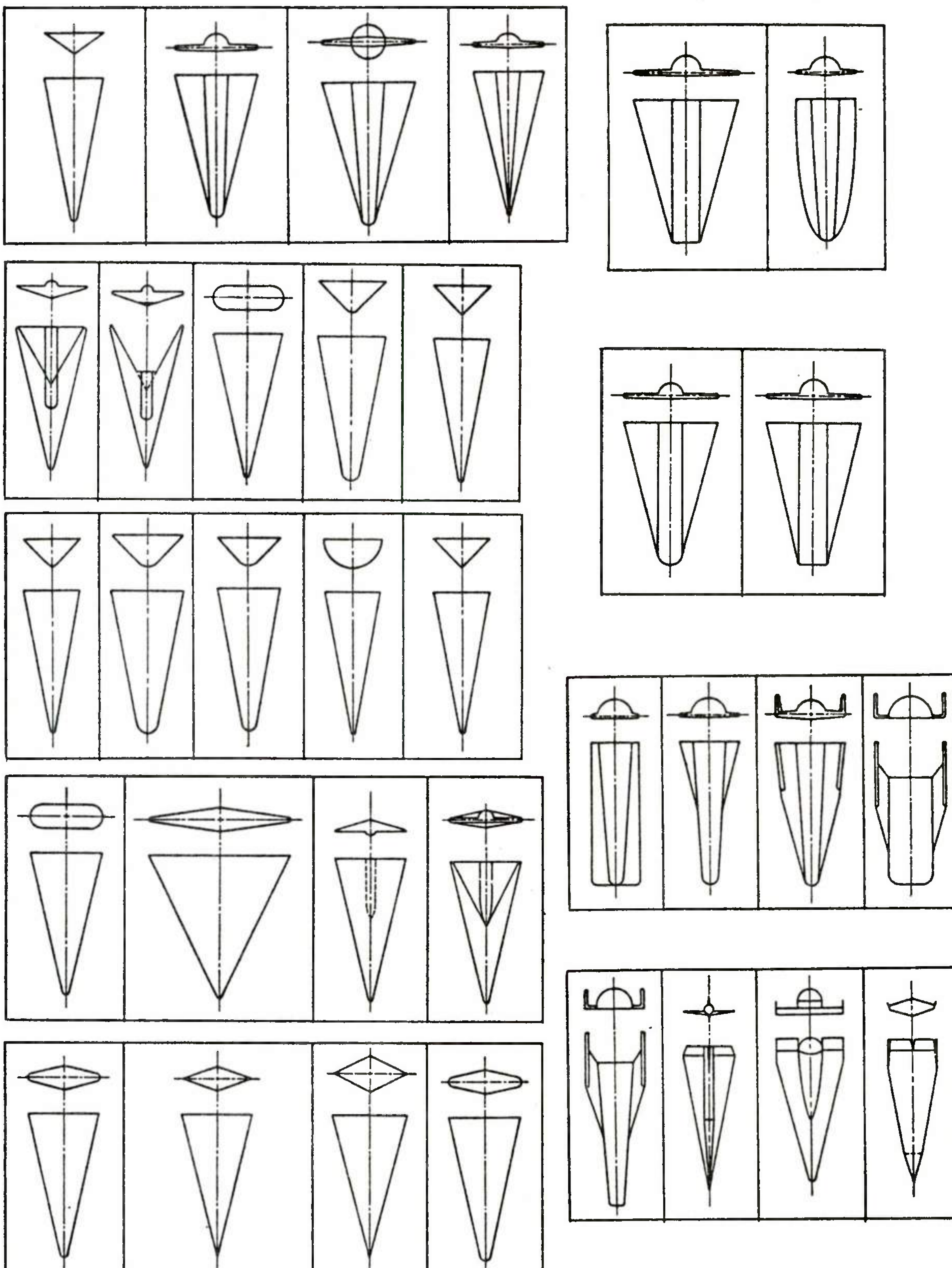

Figure 50. Datcom Subsonic Lifting Body Configurations

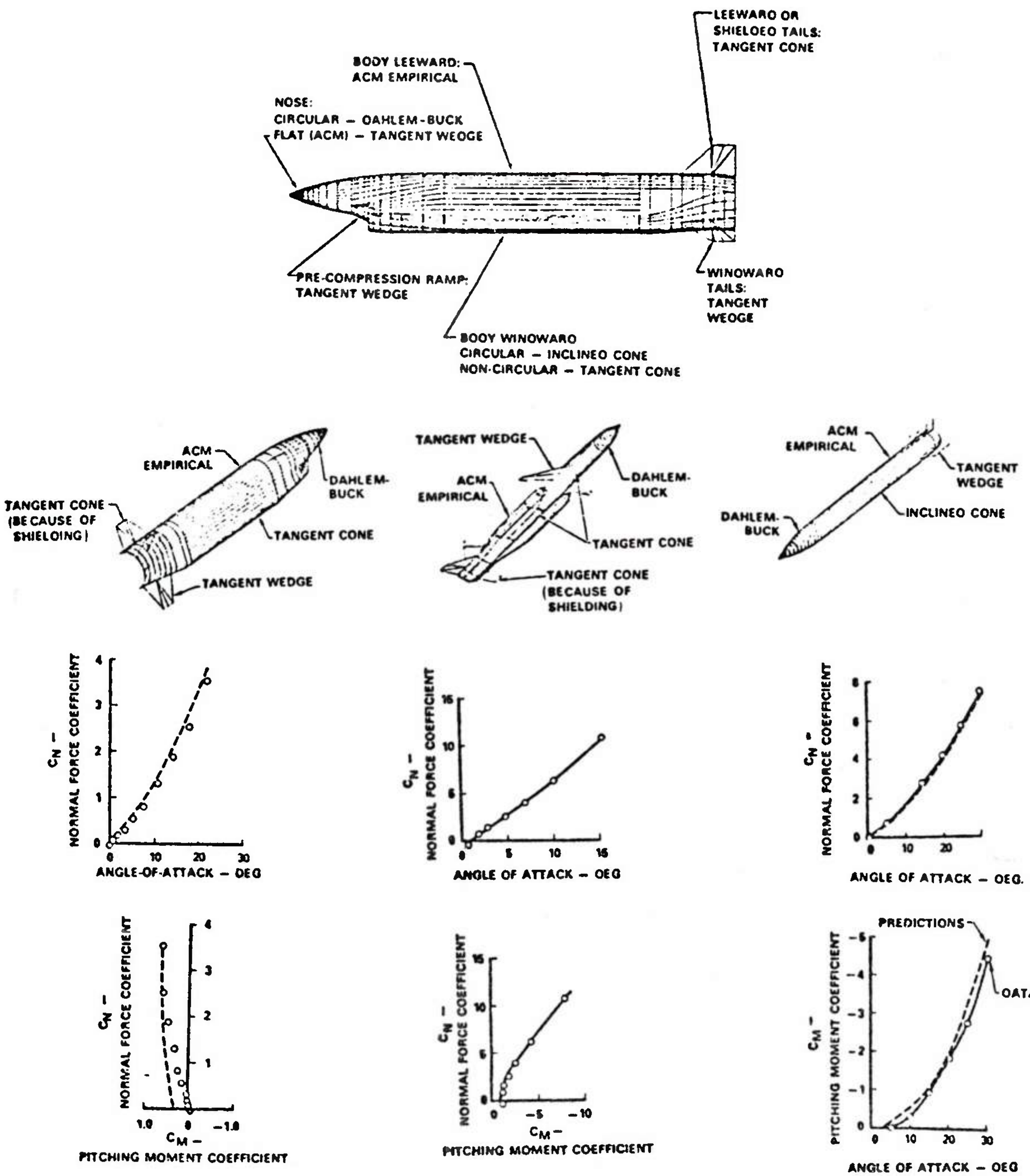

Figure 51. Pressure Method Selection Criteria for S/HABP

SECTION 4
LIFTING PANEL ALONE METHODOLOGY

4.1 INTRODUCTION

Tail surfaces on a missile serve the primary purpose of stability and control. In some instances, the design requirements specify altitude and/or maneuverability levels which cannot be met with only a body-tail configuration; wings then are required to increase the configuration normal force. As described in Section 2 of this report, a significant number of missile designs have much lower aspect ratio surfaces than those commonly used in aircraft. Missile aspect ratios normally range from one-half to four. Additionally, the most common surface types are trapezoidal and triangular panels. The following paragraphs describe the methodologies available for analysis for missile-class fin panels. Table 14 summarizes the recommendations. Since Datcom is specifically oriented to aircraft, and lifting surfaces dominate the aerodynamic characteristics, it is not surprising that the majority of the lifting surface methods recommended are those of Datcom. The methods presented in this section assume a panel referenced axis system, analogous to the body-axis system, where the longitudinal axis is oriented along the root chord. Hence, deflection or incidence of the panel is analogous to angle of attack.

Total fin axial force is assumed to be the sum of zero angle of attack drag and drag at angle of attack. The zero angle of attack drag (C_{A_0}) is computed as the sum of friction drag, pressure drag for sharp edged fins, leading edge drag due to rounding or bluntness, and trailing edge drag. For friction drag, methods which more accurately model the two-dimensional flow characteristics of fins are suggested. These are the equivalent skin friction chord approach by Vondrasek and the Barkhem method that approximates strip-integration for straight-tapered fins.

A good fin pressure drag method is that of Moore. It may be selected because of its versatility as a theoretical method. However, this technique requires a computer program which will allow fin "paneling" and integration procedures. It may provide results similar to that of the Datcom which is easiest to apply.

The Datcom method is selected for sharp-nosed pressure drag and leading edge bluntness drag.

For fins at angle of attack, the Datcom method is recommended due to its completeness in addressing various types of fins from subsonic to supersonic speeds.

4.2 AXIAL FORCE

Determination of fin drag for missile configurations has developed along lines unique to missile requirements. Missile fins are typically designed for efficient operation at high speeds, and have section characteristics designed to have low drag, provide adequate control, and meet the requirements of manufacturing relatively small panels in a cost effective manner. Drag reduction is usually more important than lift efficiency. This situation has led to fin design considerably different than typical airplane wings which emphasize lift performance in the subsonic and transonic regions. Missile fin planform characteristics tend to be low aspect ratio and simple in shape, such as triangles, rectangles and trapezoids. Section characteristics such as twist and camber are very seldom used. Airfoil sections usually are flat plate, wedges, or biconvex in shape and have relatively sharp leading and trailing edges. Therefore, the development of drag methods for typical missile fins has been characterized by these traits and have concentrated on the supersonic speed regime.

A component build-up approach to fin drag is typically used which accounts for the following parameters:

$$C_{A_{FIN}} = C_{A_F} + C_{A_{Wave}} + C_{A_{LE}} + C_{A_{TE}} + C_{A_\alpha}$$

where C_{A_F} - fin friction drag

$C_{A_{Wave}}$ - fin wave/pressure drag

$C_{A_{LE}}$ - fin leading-edge drag

$C_{A_{TE}}$ - fin trailing-edge drag

C_{A_α} - fin drag due to angle of attack

These component methodologies will be discussed for subsonic, transonic, and supersonic speed regimes.

Fin Skin Friction - Recommend the use of Van Driest II. The approach used to calculate fin skin friction is similar to that of bodies. Flat plate skin friction coefficients are used and corrected for three-dimensional flow and compressibility. The Van Driest Method II is the most comprehensive method in relation to the requirements, but is an iterative technique and

therefore requires computer solution. The Schultz-Grunow and Schoenher methods are recommended for handbook application. For mixed laminar and turbulent flow, the transition-criteria presented in Section 3 is suggested when applicable to a fin.

Flow over a wing surface is more two-dimensional than over a body. This results in lower local Mach numbers and, therefore, lower skin friction drag relative to bodies at the same conditions. The two-dimensional characteristics of fin flow has led to the development of methods to determine average panel skin friction coefficients. Table 15 summarizes three of these methods for fully turbulent flow. The Butler method divides the fin into strips using the local skin friction coefficient based on a mean local chord Reynolds number. Eaton reduces the flat plate skin friction coefficient by an empirical Mach number dependent term and a Reynolds number based on the wing mean geometric chord. Barkhem proposes a method for triangular or tapered fins that improves upon the equivalent chord approaches. His formula was developed by correlating taper ratio (λ) and Reynolds number to values calculated by complete integration using the Prandtl flat-plate turbulent skin friction formula. For the Reynolds number range of 10^5 to 10^9 the formula agrees within 0.2% with the strip-integrated values.

Another attempt to improve accuracy is presented by Vondrasek in Reference 118. She observed that for a limited Reynolds number range, $\log_{10}C_{fi}$ (incompressible) was approximately linear with $\log_{10}Re$. By simplifying the incompressible friction coefficient equation to the expression

$$c_{f_i} = .0261/R_e^{.1372}$$

she was able to integrate to find the average skin friction coefficient of a straight-tapered fin in terms of exposed root chord (C_{R_E}) and exposed taper ratio (λ_E). The equivalent skin friction chord (c*) was determined to be

$$c_* = c_{R_E}\left[\frac{1.8628}{2}\,\frac{1-\lambda_E^2}{1-\lambda_E^{1.8628}}\right]^{1/.1372}$$

which was shown to apply at all Reynolds numbers in subsequent investigations.

The above skin friction coefficients apply to flat plates with no pressure gradient and uniform temperature. When applied to fins of finite thickness, regions of nonuniform pressure and temperature exist and change the coefficients. A "form factor" approach similar to that described in Section 3 is also used for fins. Hoerner, Reference 36, related subsonic pressure and friction drag for slender airfoil sections by combining the friction and pressure contributions due to thickness. The change in velocity because of flow displacement results in increased dynamic pressure over the fin. The differential is approximately 2(t/c) for maximum thickness located at 30% chord. The pressure drag originates along the afterbody of the fin and was found experimentally to vary as $60(t/c)^4$. Hoerner's relationship for a position of maximum thickness at 30% chord is

$$\frac{C_{Do}}{C_f} = 1 + 2\ t/c + 60\ (t/c)^4$$

Examination of experimental data for a maximum thickness at 50% chord resulted in a viscous term of 1.2 (t/c). This has been combined with the above equation into

$$C_{Do}/C_f = [1 + (2 + K)\ (t/c) + 60\ (t/c)^4]\ \frac{S_{wet}}{S_{ref}}$$

where $K = 4\ [0.3 - (x/c)_{max}]$ and assumed linearly valid between $(x/c)_{max}$ of 0.3 to 0.5.

Datcom refined Hoerner with the following equation,

$$C_{D_0} = C_f\ [1 + L\ (\frac{t}{c}) + 100\ (\frac{t}{c})^4\ ]\ R_{L.S.}\ \frac{S_{wet}}{S_{ref}}$$

The L term is identical to the (2+K) term from Hoerner. A lifting-surface correlation factor which accounts for increased Reynolds number length due to spanwise flow has been added from Reference 119. The correction factor, $R_{L.S.}$, is shown in Figure 52. This factor was empirically derived from wing data having round-nosed airfoil sections. The solid lines are used for conventional straight-tapered wings, and for outboard panels of non-straight-tapered wings; the dashed lines are for use on the inboard section of a cranked wing. For transonic and supersonic flow Datcom defines the friction drag as

$$C_{D_f} = C_f \left[1 + L\left(\frac{t}{c}\right)\right] \frac{S_{wet}}{S_{ref}} \qquad \text{Transonic} \qquad C_{D_f} = C_f\ \frac{S_{wet}}{S_{ref}} \qquad \text{Supersonic}$$

The wave drag term is computed separately. The Reynolds number characteristic length is the mean aerodynamic chord of the fin. Compressibility functions for laminar and turbulent flow (C_f/C_{f_i}) are the same as described for the body.

These methods are reasonably accurate techniques for determining fin friction drag. The methods developed to increase accuracy are recommended. These are the equivalent skin friction chord (c*) technique of Vondrasek and the Barkhem method that approximates a strip-integration for straight-tapered fins. The methods are valid for low to moderate angles of attack. The lack of methods at high angle of attack is not important because at high angles of attack skin friction is a small contribution to drag.

<u>Fin Pressure C_{A_0} - Subsonic</u> - Pressure drag arises from the inability to obtain full pressure recovery of flow over a fin due to shocks or boundary layer displacement. At subsonic speeds this drag is usually small compared to friction drag, however, it becomes the dominant contributor at transonic and supersonic speeds. The empirical methods described for subsonic fin skin friction were formulated by relating friction to pressure drag. Datcom presents a procedure for analyzing non-straight-tapered planforms by treating each component indivually then summing the results.

<u>Fin Pressure or Wave C_{A_0} - Transonic</u> - The transonic regime is characterized by regions of mixed subsonic-supersonic flow over the airfoil. This is shown in Figure 53 and results in a significant drag rise. The pressure drag contribution results from losses through the shock on the wings. The mixed flow pattern is not readily amenable to theoretical treatment.

Hoerner describes the application of similarity parameters to transonic fin analysis. Interactions from a variety of fin parameters such as sweep, fin thickness, maximum thickness location, taper ratio, aspect ratio and leading edge characteristics affect fin drag. Thus, even similarity parameters were found difficult to correlate with data. Datcom uses von Karman similarity laws to show fin drag proportional to $(t/c)^{5/3}$. Empirical data has been correlated in Figure 54 as a function of aspect ratio and thickness-to-chord ratio for unswept wings and round-nosed airfoils. A swept fin drag curve is constructed by modifying the unswept values for peak drag, peak drag Mach number, and drag divergence Mach number (where $\partial C_D/\partial M=0.10$) by the following relationships:

$$C_{D_{w_{peak}}}\Big|_{\Lambda_{c/4}=n} = C_{D_{w_{peak}}}\Big|_{\Lambda_{c/4}=0} (\cos n)^{2.5}$$

$$M_{C_{D_{w_{peak}}}}\Big|_{\Lambda_{c/4}=n} = \frac{M_{C_{D_{w_{peak}}}}\Big|_{\Lambda_{c/4}=0}}{(\cos n)^{1/2}}$$

$$M_{D}\Big|_{\Lambda_{c/4}=n} = \frac{M_{D}\Big|_{\Lambda_{c/4}=0}}{(\cos n)^{1/2}}$$

Moore also uses the Datcom approach for transonic fin wave drag. Other techniques that are applicable to the transonic regime are basically supersonic methods and will be discussed as such.

Fin Pressure or Wave C_{A_0} - Supersonic - Several methods exist for the computation of fin supersonic pressure drag. Most of these are theoretical and have been derived from linear supersonic theory as applied to straight-tapered planforms. The approximations of linear theory and the relative simplicity of the assumed geometric shapes have allowed exact solutions to be obtained. The basic approach is presented in Figure 55 which shows the common types of airfoil sections and the two dimensional and conical flow regions established on typical planforms in supersonic flow. Several zero lift drag solutions have been formulated with these models using linear theory and are summarized in Figure 56. It should be noted that these results assume complete supersonic flow over the fin. In reality, the Mach number variation on the fin results in certain regions of sonic flow in the leading and trailing edge portions of the fin. When experimental values are compared to a typical theoretical curve the theory will over-predict drag in these areas because the bow shock actually detaches resulting in sonic flow.

Some of the finite wing solutions are summarized in Figure 57 through 59. The angle of attack dependency (α terms) are also included. The equations of Figure 58 are derived from second-order theory assuming an attached shock. The pressure drag varies as the square of the thickness ratio for a given cross-sectional shape. The R.A.S. Data Sheets also provide drag equations for three types of airfoils, Figure 58. Carafoli in Reference 128 used oblique shock wave and expansion theory to compute the drag on various supersonic profiles; Figure gives the expressions (including angle of attack terms) for several profiles.

The equations from linear theory are adequate for determining trends of fin wave drag. As already mentioned, sonic flow regions over portions of the fin do result in experimental trends that do not match theoretical "peaks". The Datcom method is obtained from linear theory for the two-dimensional case. For sharp-nosed airfoils the expressions for wave drag are,

$$C_{D_w} = \frac{K}{\beta}\left(\frac{t}{c}\right)^2_{eff}\frac{S_{bw}}{S_{ref}}$$

for supersonic fin leading, $(\beta\cot\Lambda_{LE_{bw}}) \geq 1$, and

$$C_{D_w} = K\cot\Lambda_{LE_{bw}}\left(\frac{t}{c}\right)^2_{eff}\frac{S_{bw}}{S_{ref}}$$

for subsonic fin leading edge, $(\beta\cot\Lambda_{LE_{bw}} < 1)$.

The variations in fin thickness ratio and planform are accounted for by defining the effective thickness ratio. This effective thickness ratio is defined by

$$\left(\frac{t}{c}\right)_{eff} = \frac{\left[\int_0^{b/2}\left(\frac{t}{c}\right)^2 c_{bw}\,dy\right]^{1/2}}{\left(\frac{S_{bw}}{2}\right)^{1/2}}$$

which is solved by numerical integration. The constant factor K is defined for specific sharp-nosed airfoil sections shown in Figure 60. For fins with variable thickness ratios the K factor is defined by the average chord. Linear theory shows the drag due to camber to be exactly equal to the drag due to thickness at zero angle of attack. Thus, fins with flat bottoms have additional drag due to camber over symmetrical fins of the same thickness.

Eaton's approach is similar to Datcom. He assumes the fins are constant thickness to chord, thin $(t/c \leq 0.04)$, symmetrical, and have a maximum thickness at 50 percent chord. With these assumptions he uses an expression similar to that of Datcom,

$$(C_{D_w})_W = K_{w_W}\left(\frac{t}{c}\right)_W^2\left(\frac{S_W}{S_R}\right)N_W$$

The factor K_{w_W} is defined as

$$K_{w_W} = (C_{d_w})_W\left(\frac{1}{\beta}\right) \qquad \text{for } \lambda \leq 0.15$$

$$K_{w_W} = (C_{d_w})_W\,(AR_{W_e}) \qquad \text{for } \lambda < 0.15$$

The values of $(C_{d_w})_w$ are given in Figures 61 and 62, respectively.

The R.A.S. Data Sheets, Reference 129, present a series of theoretical fin wave drag charts. Figure 63 is an example for a double-wedge airfoil with zero taper. The charts present variations in maximum thickness location and taper ratios for double-wedge and parabolic airfoil sections. As previously discussed, these values will not be accurate near the cusped peaks due to sonic flow over portions of the fin.

Moore, Reference 131, suggests two techniques supersonically. From Mach 1.2 to 2.5 he suggests using linear theory combined with Modified Newtonian to handle blunt leading edge flow regions. From Mach 2.5 to 8.0 he has suggested the use of a tangent wedge strip theory that is currently in development. For the linear theory method, he assumes a thin airfoil which is symmetric, has no camber, and is either a biconvex or a modified double wedge section. The procedure requires integration by numerical quadrature of the equation

$$C_D = \frac{8}{S_w}\int_0^{b/2}\int_{c(x_l)}^{c(y)} C_p(x,y)\,w(x,y)\,dx\,dy \qquad \text{where } C_p(x,y) = -2\phi_x(x,y,0)$$

For each flow region on the panel the perturbation velocity is defined by the individual surface slope of that local element. This simplifies the integration into a form that is easily performed for simple wing planforms. The airfoil surface slopes, although assumed constant within an elemental area, can vary between elements in either the spanwise or chordwise direction.

Leading/trailing edge bluntness effects - The methods described for fin pressure/wave drag applies to fins with sharp leading and trailing edges. When fin edges are blunt, additional methodology must be applied in the nose vicinity because the assumptions of perturbation theory are not valid. The change in drag due to bluntness is modeled by computing a leading edge drag term that is added to the total drag.

At supersonic speeds Moore applies Modified Newtonian Theory to blunt leading edges and has derived the following expression for leading edge axial force,

$$C_{A_{LE}} = \frac{4R_{avg}bC_{p0}\cos^2\Lambda_l}{S_{ref}}\left[\sin\epsilon_u - \frac{\sin^3\epsilon_u}{3}\right] \qquad \text{where} \qquad R_{avg} = \frac{(r_{LE})_r + (r_{LE})_t}{2}$$

The C_{p_0} terms is the stagnation pressure behind a normal shock such that

$$C_{p0} = \frac{2}{\gamma M_\infty^2}\left[\left(\frac{(\gamma+1)M_\infty^2}{2}\right)^{\gamma/(\gamma-1)}\left(\frac{\gamma+1}{2\gamma M_\infty^2-(\gamma-1)}\right)^{1/(\gamma-1)}-1\right]$$

The term ε is the angle where Newtonian theory and perturbation theory match as shown in Figure 64 and assumes that first order perturbation pressure coefficients are computed at ε=15° and the flow is allowed to expand to the matching point. The leading edge radii are also allowed to vary with span.

Datcom presents design charts for a cylindrical leading-edge pressure correlation from Crosthwait, Reference 132, which is shown in Figure 65, and valid at subsonic and supersonic speeds. In equation form, the relationship is

$$C_{D_{LE}} = \left[\frac{2r_{LE_{bw}}\left(\dfrac{b_{bw}}{\cos\Lambda_{LE_{bw}}}\right)}{S_{ref}}\right] 1.28 \; \frac{M^3\cos^6\Lambda_{LE_{bw}}}{1+M^3\cos^3\Lambda_{LE_{bw}}}$$

Datcom suggests using the leading edge radius at the average chord point for variable radii fins. This approach has been substantiated over a Mach number range from 0.5 to 8.0 and for sweep angles from 0 to 75°.

The Datcom or Moore methods are suggested for use due to their completeness and demonstrated applicability in conjunction with sharp-nosed pressure methods.

Moore provides methodology for fin trailing edge separation drag. When the trailing edge is either sufficiently blunt or the surface slope sufficiently large, the boundary layer will separate near the trailing edge. This situation results in increased drag due to an equivalent rear-facing step that exhibits two-dimensional base drag characteristics. Moore has taken the experimental supersonic blunt wing data of Chapman, Reference 134, as a function of Mach number and applied it to fins. This incremental drag is presented in Figure 66. The curve was extrapolated from Mach 0.0 to 1.1 based on three-dimensional base pressure trends.

Drag due to lift - Additional axial force components can be generated when a fin is at angle of attack. Several methods exist to determine drag contribution due to lift. Saffell, Reference 135, suggests that the change in drag due to angle of attack be approximated by resolving a flat plate normal to the flow by the following expression:

$$\Delta C_{D_{T-\alpha}} + \Delta C_{D_{T-\delta}} = C_{D_{FP}} \left[\frac{S_T \sin(\alpha + \delta)}{S_{REF}} \right]$$

The flat plate drag coefficient normal to flow is presented in Figure 67. This technique is limited to $0 \leq \beta A \leq 10$ and is quoted as valid to 180° angle of attack.

Datcom expresses the drag increment in terms of drag due to lift. The subsonic drag due to lift expression is,

$$C_{D_L} = \frac{C_L^2}{\pi A e} + \Delta C_{D_L} + f(\theta)$$

The first term defines drag due to lift resulting from induced drag and viscous drag. Induced drag depends on spanwise fin loading distribution and results from the rearward rotation of the lift vector produced by the fin trailing-vortex system. The viscous drag due to lift results from boundary-layer changes over the fin resulting in an effective increase in profile area. The C_L term is fin lift coefficient and the span-efficiency factor, e, is

$$e = \frac{1.1 \left(C_{L_\alpha}/A\right)}{R\left(C_{L_\alpha}/A\right) + (1 - R)\pi}$$

The factor R is the leading-edge-suction parameter, defined as the ratio of actual leading-edge suction to theoretical. This factor, is shown in Figure 68 as a function of Reynolds number based on leading-edge-radius, Mach number, aspect ratio and leading edge sweep angle. For fins with sharp

leading edges, R=0. These factors were derived for fins with relatively high aspect ratios (greater than 2.0), taper ratios from 0.0 to 0.713, and leading edge sweep angles between 19.1° and 63.4°.

For cranked fins, ΔC_{D_L} represents the drag due to lift resulting from a breakdown in leading-edge suction (rounded edges are assumed) when separation occurs. This term is an empirical correlation. The span efficiency factor, e, for the cranked fin is determined by an effective leading-edge-suction parameter (R') for the inner and outer panels such that

$$R' = R_i(\eta_B) + R_o(1 - \eta_B)$$

Fin twist is accounted for in the f(Θ) term for which charts are used. The empirical factors v and w are related to induced drag such that

$$C_{D_L} = \frac{C_L^2}{\pi A e} + C_L \theta \, c_{\ell_\alpha} v + \left(\theta \, c_{\ell_\alpha}\right)^2 w$$

The w dependent term is for a zero-lift drag increment due to twist.

At transonic speeds Datcom determines drag due to lift of conventional trapezoidal planforms of symmetrical section using transonic similarity parameter charts, such as Figure 69. This approach is used due to the lack of data at transonic speeds. The method covers the following range of parameters,

$$0 \le AR \tan \Lambda_{LE} \le 3.0$$

$$0.5 \le AR\,(t/c)^{1/3} \le 2.0$$

$$-4 \le \beta^2/(t/c)^{2/3} \le 2$$

At supersonic speed Datcom suggests that fins be classified as a function of whether the Mach number component normal to the leading edge is subsonic or supersonic. If the fin has a supersonic leading edge, the spanwise pressure loading will be constant due to two-dimensional flow. Subsonic leading edges can vary from no suction to full suction depending on the subsonic component normal ot the leading edge. Two-dimensional flow regions can be modeled by linear or shock-expansion theory to determine drag due to lift. Three-dimensional flow regions have varying span loading and

thus also have a vortex drag contribution. Datcom gives the two-dimensional value of drag due to lift from linear theory as

$$C_{D_L} = \frac{\beta C_L^2}{4}$$

The supersonic fin drag due to lift method is given by the relationship

$$\frac{C_{D_L}}{C_L^2} = \left[\pi A \frac{C_{D_L}}{C_L^2} \frac{p}{1+p}\right]\left(\frac{1}{\pi A}\right)\left(\frac{1+p}{p}\right)$$

The term in the first bracket is shown in Figure 70. The term p is a wing geometry parameter which is basically a wing area fraction. Comparisons with data were made over the following ranges of fin parameters,

Round Leading Edge	Sharp Leading Edge
$1.313 \leq A \leq 4.0$	$1.5 \leq A \leq 3.5$
$35^\circ \leq \Lambda_{LE} \leq 73^\circ$	$0 \leq \Lambda_{LE} \leq 71^\circ$
$0 \leq \lambda \leq 0.5$	$0 \leq \lambda \leq 1.0$
$0.237 \leq p \leq 0.502$	$0.333 \leq p \leq 0.995$
$0.271 \leq \frac{b_w}{2\ell} \leq 1.00$	$0.333 \leq \frac{b_w}{2\ell} \leq 1.070$

The variation in surface pressure forces over a fin at angle of attack or deflection has been determined from linear theory. The techniques shown in Figure 57 include terms that represent the influence of angle of attack on fin pressure drag. It is suggested that the results of linear theory at angle of attack be evaluated in conjunction with experimental data to determine the accuracy of the method. Otherwise, the Datcom approach to induced drag is recommended due to its completeness. The Datcom technique should be evaluated quantitatively for the range of typical missile fin parameters to determine the limits of applicability to missile fins at angle of attack.

Sufficient methodologies exist to compute fin axial force characteristics for typical missile planforms and airfoil sections. The method described do not include interference effects. Such interference effects on drag are usually considered small and are often neglected.

4.3 NORMAL FORCE AND PITCHING MOMENT

This section describes the methods available to evaluate the linear and nonlinear normal force and pitching moment of isolated lifting surfaces.

Many of the techniques use design charts to facilitate calculation; where appropriate the relevant equations are presented. Calculation of fin alone C_N or C_m is often suitable for hand calculation.

Subsonic Normal Force - At subsonic speeds, the most comprehensive and experimentally verified straight-tapered method used is the lifting line theory derived by Lowry and Polhamus, Reference 136, and shown in Figure 71. The Lowry-Polhamus formula is considered valid over the following ranges:

$$M \leq 0.8$$
$$t/c \leq 10\%$$

An input requirement to this method is the determination of the section lift-curve-slope. For NACA airfoil sections, tables and experimental results are available in Datcom or "Theory of Wing Sections," Reference 137. Using the Kutta-Joukowski hypothesis of finite velocity at the wing trailing edge yields the theoretical method in Figure 71, and plotted in Figure 72 (bottom) with θ_{TE} of 20 deg (the upper limit of the method). Since this method over-predicts due to viscous effects, experimental results are used to correct the theoretical result. The revised section lift-curve-slope equation is shown in Figure 71, and the correction factor is given in Figure 72.

Although the Multhopp (Reference 138) lifting surface theory is highly accurate, it is also difficult to apply. It has, however, been automated for straight-tapered surfaces by Moore, Reference 139, in the U.S. Navy Approximate Aerodynamic Prediction Code, and is most useful for low aspect ratio panels typical to missiles. Assuming the computing cost of this technique is reasonably low, and the method routine size is kept within the required computer field length limitations, its inclusion is suggested as an excellent choice since it can also be used for non-striaght tapered surfaces.

The method more suitable to handbook application, and found to be fairly accurate to low aspect ratio panels is the Lowry-Polhamus method. It has been extended by Spencer, Reference 140, to include double-delta panels ($A \leq 3$) through calculation of an effective half-chord sweep angle. This area weighted sweep angle is used in the Lowry-Polhamus formula.

Transonic Normal Force - Only empirical curve-fits are available. The most comprehensive technique available transonically is the empirically derived method outlined in Datcom, Section 4.1.3.2. Datcom

classifies wing panels as types "A" or "B". Thick, unswept panels show the variation given in Figure 73 for a type "A" wing, whereas thin, low aspect ratio panels common to missiles follow the trend for type "B". This method is a fairing of results obtained at five distinct Mach numbers: subsonic (Mach 0.6), the force break Mach number (M_{fb}), Figures 74 and 75 , two determined from Figure 76 (M_a,M_b); and supersonically at Mach 1.4, where

$$M_a = M_{fb} + 0.07$$
$$M_b = M_{fb} + 0.14$$

The lift-curve slope at M_{fb} is determined from Figure 71, and

$$(C_{L_\alpha})_{M_a} = (1 - \frac{a}{c})\, C_{L_{\alpha fb}}$$
$$(C_{L_\alpha})_{M_b} = (1 - \frac{b}{c})\, C_{L_{\alpha fb}}$$

The user is then required to fair the results according to wing type. The Royal Aeronautical Society data sheets, S.01.03.04, present transonic fairings, shown in Figure 77. These charts present inviscid theoretical flat plate values of lift-curve slope at subsonic and supersonic speeds for taper ratios from zero to unity. The accuracy of the supersonic values has been shown to be within $\pm$10%; accuracy at subsonic speeds are not available. The transonic fairings are suggested and not experimentally verified. Aside from empirical data results available from Aiello (Reference 58), Baker (Reference 75), Nielsen (Reference 144) and Stallings (Reference 58) ard Lamb (Reference 142) for selected fin designs, no complete method is available.

There are no generally accepted techniques for non-straight tapered panels, though Datcom presents a correlation at Mach 1.0 for lift-curve-slope to be used as a fairing guideline.

Supersonic Normal Force - There are more supersonic techniques available because it is possible to simplify the flow model. Hoewver, they all reduce to a form of linearized lifting surface theory. Moore in Reference 142 has described in detail a technique for straight tapered, thin, uncambered surfaces for several flow conditions. General forms of these relations, from NACA TN 2114, Reference 143, are given in Figure 78. Five conditions for which the airfoil pressure distribution are computed are shown. The applicable angle of attack range is unknown. However, linear thoery is often valid

to moderate angles of attack. Datcom presents these theoretical results in chart form, Figure 79. Regions where theoretical solutions have been obtained are shown in Figure 80 and are as follows:

Region of Supersonic L. E. and T. E.	NACA TN 2114
Region of Subsonic L. E. and Supersonic T. E.	NACA TR 970
Region of tip-root and tip-tip interactions	Douglas SM-13480
Region of Subsonic L. E. and T. E.	NACA TR 1050
Region of $A\beta \leq 0.25$ and $\sigma \leq 1.0$	NACA TR 835
where $\sigma = 0.25\ [A(1+\lambda)\tan\Lambda_{LE}]$	
Region of $A\beta \leq 0.25$ and $\sigma \geq 1.0$	ARC R&M 2888 and NACA TN 3105

Datcom has combined this vast amount of theoretical work into the easily used design charts of Datcom Section 4.1.3.2, Figure 4.1.3.2-56. The qualitative range of applicability for the Datcom figure is shown in Figure 81. Note that the R.A.S. data sheets (Figure 77) will have the same upper limit of validity shown in Figure 81, but the ordinate will be half-chord sweep anlge; the lowest limit is $\Lambda_{C/2}=0$ for all aspect ratios. Figure 82 graphically illustrates the conversion from half-chord to leading edge sweep angles. It is evident that greater coverage is obtained at the lower aspect ratios of interest through usage of the Datcom design charts. Hence, the Datcom design charts are recommended for handbook use.

Thin airfoil theory has been assumed in development of the Datcom charts. When the leading edge is nearly sonic, thickness effects cause the shock to detach with a resultant loss of normal force. The correction factor to account for this condition is presented in Figure 83. One of the unique applications of the Datcom design charts occurs through use of the reversibility theorem in supersonic flow, Reference 150. This theorem can be summarized as--"the normal-force-slope of a panel in forward flight is the same as the normal-force-slope of the same panel in reverse flight at the same Mach number." Hence, it is implied that swept forward panels can be handled using the theoretical results presented.

Figures 84 through 88 present Datcom methods for non-straight-tapered panels of interest. The results of Squire, Reference 151 and Figure 88, define a technique for the little-used ogee or gothic shapes.

Normal Force at Angle of Attack - There are four approaches used to determine wing normal force at angle of attack: (1) fairing from the linear range to 90 degrees angle of attack, (2) computing non linear lift from the cross-flow concept, (3) variations of Polhamus suction analogy, and (4) empirical curvefits of test results. Techniques 1, 2 and 4 use the fin normal force at 90 degrees angle of attack through empirical data correlation; the results given in Datcom, Eaton (Reference 33) and Aiello (Reference 58) are shown in Figure 89. It should be noted that the results of Aiello (Figure 89-C) correlate better with Datcom (Figure 89-a subsonically, and Datcom Figure 4.1.3.3-60a supersonically). The Mach number idependency assumption by Eaton is suspect since it is not observed to occur for planforms of interest to Missile Datcom.

Since normal-force-slope is easily determined, and normal force in normal flow is fairly well described, the modeling an intermediate angles of attack become the challenge. The Datcom technique (Approach 1) uses the relationship

$$C_N = C_{N\alpha}\frac{\sin 2\alpha}{2} + C_{N_{\alpha\alpha}} \sin\alpha \left|\sin\alpha\right|$$

for straight-tapered panels at subsonic and supersonic speeds. At subsonic speeds $C_{N_{\alpha\alpha}}$ is a function of $C_{L_{MAX}}$; at supersonic speeds $C_{N_{\alpha\alpha}}$ is a function of the Mach detachment angle of attack. Some degree of empiricism cannot be avoided and this method seems to be a sound approach. The disadvantage is the lack of methods in the range $0.6 \leq M \leq 1.4$. The alternate cross-flow approach

$$C_N = C_{N_\alpha}\frac{\sin 2\alpha}{2} + C_{dc}\sin^2\alpha$$

does not adequately handle such phenomena as fin stall and shock detachment, since the data base deriving C_{d_c} is based on only normal flow, i.e., panel stalled or shock detached at all speeds. Empirically derived curves of C_L versus angle of attack are given in Datcom, and presented in Figures 90

and 91, for double-delta and gothic or ogee planforms at subsonic speeds. Results are also available from NASA TN D-5661, Reference 152; one chart from this report is shown in Figure 92. These results were generated by employing the modified Multhopp approach on a series of panels to generate design charts at subsonic speeds. Limitations on these design charts are as follows:

Mach Number	Prandtl-Glauert Compressibility Rule	
Trailing-Edge Sweep	Zero	
Inboard Panel Sweep	Outboard Panel Sweep	Taper Ratio
55° to 85°	50°	0.1 to 0.5
0° to 85°	60°	0.1 to 0.5
0° to 85°	72°	0.1 to 0.5

This report also includes results for the following aerodynamic parameters: C_L, X_{ac}, C_{ℓ_p}, C_{m_q}, and C_{L_q}.

Experimental results for sharp delta wings at low angles of attack show that the flow separates from the leading edge and rolls up into two spiral vortex sheets. Acceleration of the flow in this manner produces lift. The results of flow separation at the leading edge is called potential lift, and the effect of the spiral vortex is termed vortex lift. These effects are shown in Figure 93. It is assumed that the leading edge suction force produced in potential flow is the same as the pressures required to maintain flow equilibrium and attached flow. The resulting force is then equal to the theoretical leading edge suction force (C_S) and is perpendicular to the leading edge. This Polhamus Suction Analogy concept (References 102, 153, and 154) has received much attention since it attempts the invsicid plus viscous modeling. The potential-flow normal force and lift are

$$C_{L,p} = K_p \sin\alpha \cos^2\alpha$$

$$C_{L,p} = C_{N,p} \cos\alpha$$

and the viscous (suction force) is

$$C_{L,v} = K_v \sin^2\alpha \cos\alpha$$

and K_p and K_v are derived from the modified Multhopp theory (Reference 155) for triangular panels. This theory was found to agree well with test data at very low speeds to 25 degrees angle of attack for aspect ratio panels less than two. The method was also extended by Lamar (Reference 156), among others, to deduce leading-edge and side-edge vortex lift factors for application to straight tapered panels. The normal force (lift) of a panel is represented as

$$C_L = K_p \sin\alpha \cos^2\alpha + K_{v,le} \sin^2\alpha \cos\alpha + K_{v,se} \sin^2\alpha \cos\alpha$$

$$C_m = K_p \sin\alpha \cos\alpha \frac{\bar{x}_p}{c_{ref}} + K_{v,le} \sin^2\alpha \frac{\bar{x}_{le}}{c_{ref}} + K_{v,se} \sin^2\alpha \frac{\bar{x}_{se}}{c_{ref}}$$

where $K_{v,LE}$ is that given above for triangular panels and for panels with subsonic leading edges, and sonic trailing edges

$$m = B \cot\Lambda$$

$$c_t' = \frac{c_t}{b/2} \cot\Lambda$$

$$S_{ref} = \frac{b^2}{2} \tan\Lambda \left[c_t' + (1 - m)/2\right]$$

For rectangular panels

$$K_{v,se} = \frac{8}{\pi A \sqrt{M^2 - 1}}$$

Charts at subsonic speeds were given by Polhamus in Reference 157 for selected fins.

Lecat and Rietschlin of Grumman Aerospace developed "Goniometric Aerodynamics," Reference 158, and achieved good correlations through modification of the Polhamus K_p and K_v formulations. A planform shape parameter, p, given in Figure 94, simplified the formulation for general shaped surfaces to

$$K_p = \frac{4\pi}{\tan\phi + \sqrt{\tan^2\phi_M + \dfrac{\sin^2\phi_M}{p_M^{*2}} + 4\beta^2}}$$

$$K_v = \left[K_p - K_p^2 \frac{\tan\phi_M}{4\pi}\right] \sqrt{1 + \tan^2\phi_M}$$

$$K_v = \frac{K_p}{\cos\phi} \cos\gamma, \qquad \sin\phi = \tan\gamma\,[\tan(\gamma + \phi)]$$

Subsonic

$$2p^* \tan \phi = \tan \psi$$
$$\psi_M = \psi$$
$$p_M^* = p^*$$

Transonic

$$p_M^* = \frac{p^*}{1 - \frac{\tan \phi_M}{2 \tan \phi}} \qquad \tan \psi_M = 2p_M^*(\tan \phi - \tan \phi_M)$$

Supersonic

$$p_M^* = p^* \, (2 \tan \phi / \tan \phi_M)$$
$$\tan \psi_M = 2 \tan \psi (1 - \tan \phi / \tan \phi_M)$$

The authors claim accuracy with this technique, but use of this method for a wide range of shapes should be evaluated before it is chosen for implementation, because it is not well known within the industry. Oberkampf, Reference 159, extended the vortex concept to 60 degrees angle of attack using the following formulation

$$C_N(\alpha) = [Kp \sin\alpha \cos\alpha + Kv \sin^2\alpha] \sqrt{\cos \frac{2\pi}{5} \frac{\alpha}{\alpha_s}}$$
$$\text{for } 0 \leq \alpha \leq \alpha_s$$
$$C_N(\alpha) = \zeta \, C_N(\alpha_s) + \frac{\lambda A}{5} \, C_N(\alpha - \alpha_s)$$
$$\text{for } \alpha_s \leq \alpha \leq 2\alpha_s$$
$$C_N(\alpha) = (\zeta + \frac{\lambda A}{5} \, C_{N(\alpha_s)})$$
$$\text{for } 2\alpha_s < \alpha$$

where,

$$\zeta = 0.7 + 0.3M^2 \qquad (M < 1)$$
$$\alpha_s = \frac{1.3}{\sqrt{1 + A} \, (1.5 + \lambda)}$$
$$Kp = 1.45 \, A - 0.17 \, A^2$$
$$Kv = \pi(1 + \frac{\lambda}{1 + A}) \text{ for } A < 3$$
$$C_N \, (\alpha, A, \lambda)\Big|_{M_\infty} = \frac{1}{\beta} \, C_N \, (\alpha, A, \lambda)\Big| \, M = 0$$

Bradley, Reference 160 and Figure 95, has devised a method where the leading edge suction force is computed across the span. Hence, the vortex lift is

$$C_{L_V} = [\sum(\frac{C_{tn}}{\cos \Lambda n}) + Cy - \sum(C_{Tm} \tan \Lambda_n)] \cos \alpha$$

where C_{T_n} and C_y are computed from lifting-surface theory. Therefore,

$$C_L = Kp \sin\alpha \cos^2\alpha + (K_{V_{LE}} + K_{V_{TiP}}) \sin^2\alpha \cos\alpha$$

$$\text{and} \quad K_{V_{LE}} = \frac{\partial}{\partial \sin^2\alpha} \left(\frac{\sum C_{Tn}}{\cos \Lambda_n}\right)$$

$$K_{V_{Tip}} = \frac{\partial}{\partial \sin^2\alpha} \left(Cy - \sum C_{Tn} \tan \Lambda_n\right)$$

This technique has shown remarkable accuracy to 30 degrees angle of attack. Like the Grumman method, these methods should be verified for missile-type lifting surfaces and general accuracy.

There is a large body of test results (References 161 through 165, for example) which have explored the use of wraparound fins. For those launchers which limit the span of fins attached to the body, this type of fin is ideal. Experience has shown that at low angles of attack the aerodynamic characteristics are the same as that for an equivalent flat panel. There are no theoretical methods available to analyze wraparound fins at angle of attack. Reference to experimental results are required.

There is a large body of panel alone empirical results available, due primarily to the efforts of Baker (Reference 74), Nielsen (Reference 141), Hill (Reference 166), and Stallings and Lamb (Reference 142). The Stallings and Lamb paper presented at the AIAA 19th Aerospace Sciences Meeting in January 1981, is a good summary of the available results. The available data cover the following ranges of conditions:

Taper Ratio	0.0 to 1.0
Aspect Ratio	0.5 to 2.0
Mach Number	0.6 to 3.0
Angle of Attack	0 to 60 deg

The data consists of normal force, longitudinal center of pressure, and lateral center of pressure. Although these results do not quite cover the range of panel aspect ratios or Mach numbers required, they do cover the transonic Mach regime, which has been shown to be a difficult analysis area. It is recommended that these results be considered for use in Missile Datcom.

Pitching Moment - Pitching moment methods exist for each of the Mach regimes specified for normal force above. The Datcom contains an extensive compendium of generally accepted methodology which utilizes the procedures and theories applied for normal force. It is appropriate to select the pitching moment technique which has been developed using the same derivation assumptions for normal force. The method sources for the recommended normal force methods apply for pitching moment as well.

Pitching Moment at Angle of Attack - The panel aerodynamic center can be evaluated theoretically at subsonic and supersonic speeds. Datcom has correlated section center of pressure for the double wedge, modified double wedge and circular-arc sections due to angle of attack, as shown in Figure 96. In addition, Datcom design charts derived through integration of the theoretical pressure distribution on the panel are shown in Figure 97. An empirical method is also presented in Figure 97 at transonic speeds through correlation of aspect ration and thickness-to-chord-ratio. The Datcom methods are of sufficient detail and it is recommended that they be employed for handbook use. If selection of the Multhopp (subsonic) or pressure region (supersonic) theories are chosen for automation, it is recommended that the results be integrated to obtain pitching moment or center of pressure. Use of the empirical results available are also recommended for determining the effects of angle of attack in the transonic Mach regime. It is recommended that results of the Polhamus Suction Analogy method be quantified for low aspect ratio panels.

TABLE 14 RECOMMENDED LIFTING SURFACE METHODOLOGY

COMPONENT / MACH NUMBER REGION	SUBSONIC	TRANSONIC	SUPERSONIC
INVISCID LIFT AND PITCHING MOMENT	LOWRY-POLHAMUS OR LIFTING SURFACE THEORY	EMPIRICAL	LINEAR THEORY
VISCOUS LIFT AND PITCHING MOMENT	DATCOM	EMPIRICAL	DATCOM
PRESSURE OR WAVE C_{A_0}	DATCOM	EMPIRICAL	LINEAR THEORY OR DATCOM
SKIN FRICTION DRAG	VAN DRIEST II		
LEADING EDGE BLUNTNESS DRAG	EMPIRICAL		DATCOM
TRAILING EDGE SEPARATION DRAG	EMPIRICAL		
C_A AT ANGLE OF ATTACK	EMPIRICAL + DATCOM		

TABLE 15 FIN SKIN FRICTION METHODS

SKIN FRICTION COEFFICIENT (FLAT PLATE)	SOURCE	MACH NUMBER	REYNOLDS NUMBER CHARACTERISTIC LENGTH
$C_{F_c} = \frac{0.49}{F_c} \Big/ \log_{10}\left(\frac{F_\delta}{F_c} Re\right)^{2.625}$ $F_\delta = 1 + 0.056M^2$ $F_c = \sqrt{1 + 0.2M^2}$	DUTLER	.2-2.8	Local Mean Chord
$C_{f_W} = \left(\frac{0.455}{\log(Re)_W^{2.58}}\right) - \left(0.0004\ M\right)$	EATON	0-3.0	$\bar{c}_W = \left(\frac{c_{r_W}}{2}\right)(1 + \lambda_W)$
$c_f = \frac{0.472}{\left({}^{10}\log Re\ \frac{1+\lambda}{2}\right)^{2.58}}\left[1 - \frac{(1-\lambda)^4(4.55 - 0.27 \cdot {}^{10}\log Re)}{100}\right]$	BARKHEM	0-3.0	Exposed root chord-C_r 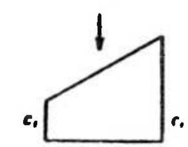 $\lambda = \frac{c_t}{c_r}$ $(c_r > c_t)$

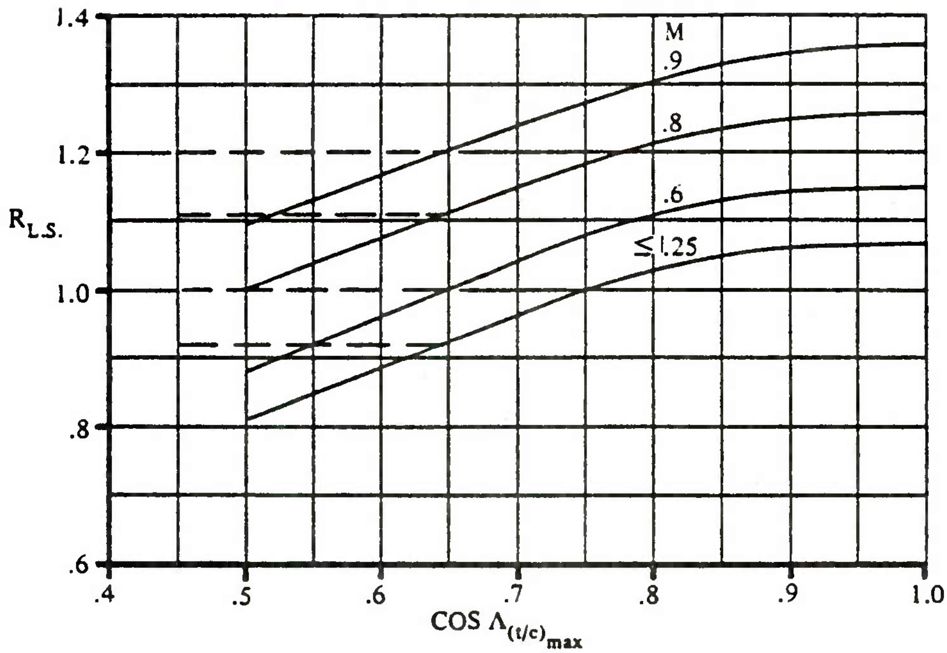

Figure 52. LIFTING-SURFACE CORRELATION FACTOR FOR SUBSONIC MINIMUM DRAG

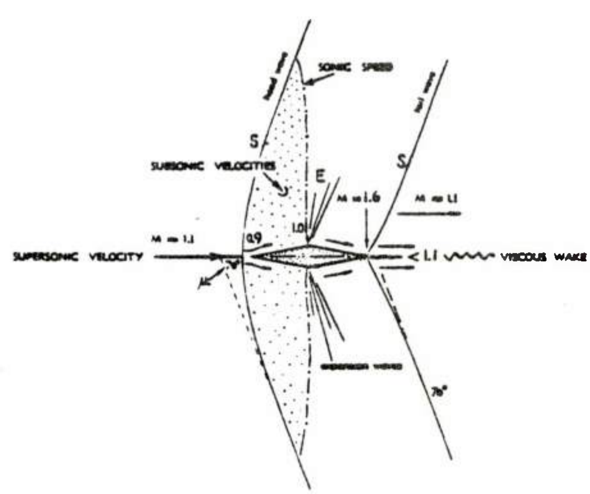

Figure 53. MIXED FLOW REGIONS AT TRANSONIC SPEEDS

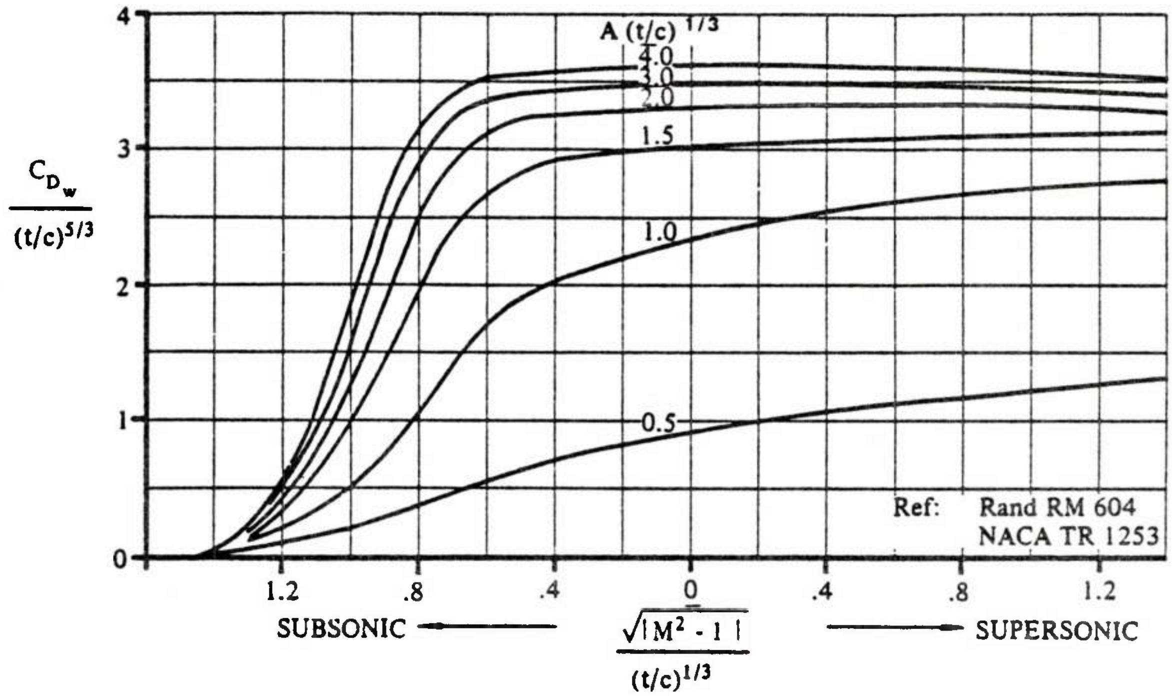

Figure 54. TRANSONIC ZERO-LIFT WING WAVE DRAG FOR UNSWEPT WINGS AND ROUND-NOSE AIRFOILS

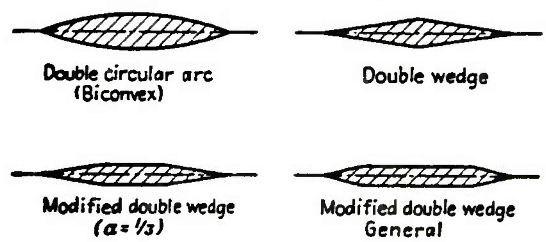

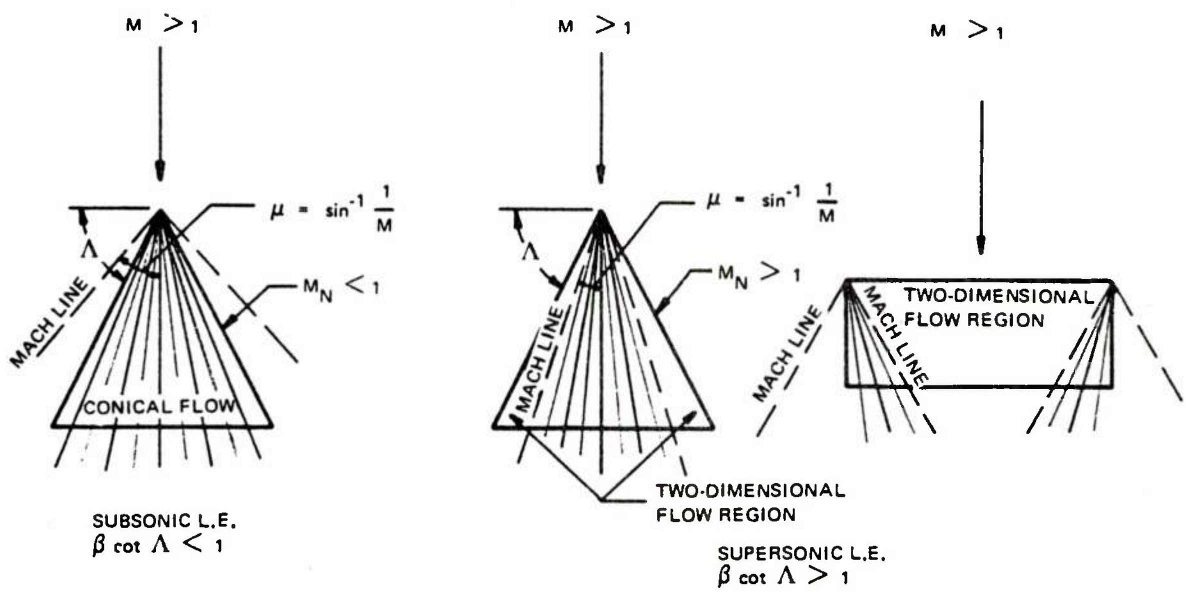

Figure 55. SUPERSONIC FLOW REGIONS OVER FINS

PLANFORM	SECTION	WAVE-DRAG SOLUTION (ZERO LIFT)	
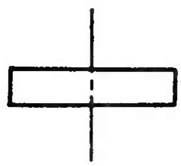		Bonney	Ref. 120
		Bonney	Ref. 120
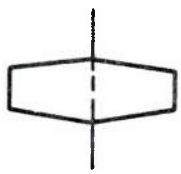		Puckett & Stewart Beane	Ref. 121 Ref. 122
		Beane	Ref. 122
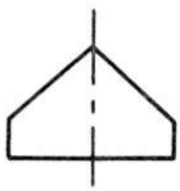		Puckett Margolis	Ref. 123 Ref. 124
		Beane	Ref. 122
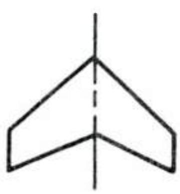		Puckett & Stewart Margolis Bishop & Cane	Ref. 121 Ref. 124 Ref. 125
		Jones Beane Bishop & Cane	Ref. 126 Ref. 122 Ref. 125
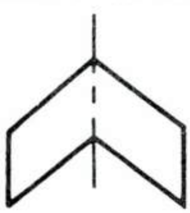		Bishop & Cane	Ref. 125
			
			
		Bishop & Cane	Ref. 125
			
			

Figure 56. SUMMARY OF FINITE WING SOLUTIONS

Type	Flat plate	Flat plate	Airfoil	Airfoil
R	Infinite	Finite	Infinite	Finite (untapered)
C_D	$\frac{4\alpha^2}{B} + C_{D_f}$	$\frac{4\alpha^2}{B}\left(1 - \frac{1}{2RB}\right) + C_{D_f}$	$\frac{K_1\tau^2}{B} + \frac{4\alpha^2}{B} + C_{D_f}$	$\frac{K_1\tau^2\phi(RB)}{B} + \frac{4\alpha^2}{B}\left[1 - \frac{1}{2RB}\left(1 - \frac{2C_2}{C_1}A'\right)\right] + C_{D_f}$

RB	$\phi(RB)$	RB	$\phi(RB)$
0	0	0.5	0.90
0.2	0.55	0.6	0.96
0.3	0.70	0.75	0.99
0.4	0.82	1.0	1.00

R=Aspect Ratio

$B = [M^2-1]^{1/2}$

Figure 57. Aerodynamic Characteristics for Supersonic Airfoils - Bonny

	TYPE 1	TYPE 2	TYPE 3
	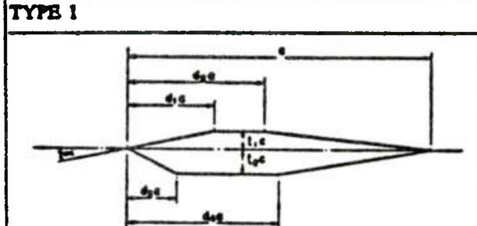	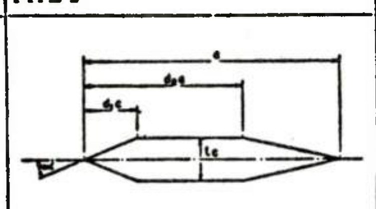	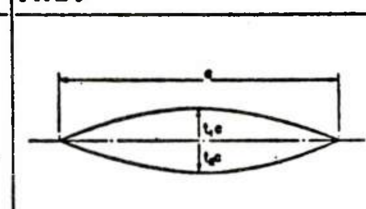
C_{Dw}	$C_1\left[t_1^2\left(\frac{1}{d_1} + \frac{1}{1-d_2}\right) + t_2^2\left(\frac{1}{d_3} + \frac{1}{1-d_4}\right)\right] + 2C_1\alpha^2$ $+ C_2\left[t_1^2\left(\frac{1}{d_1^2} - \frac{1}{(1-d_2)^2}\right) + t_2^2\left(\frac{1}{d_3^2} - \frac{1}{(1-d_4)^2}\right)\right]$ $- 3C_2\alpha\left[t_1^2\left(\frac{1}{d_1} + \frac{1}{1-d_2}\right) - t_2^2\left(\frac{1}{d_3} + \frac{1}{1-d_4}\right)\right]$	$C_1\frac{t^2}{2}\left(\frac{1}{d_1} + \frac{1}{1-d_2}\right) + 2C_1\alpha^2$ $+ C_2\frac{t^3}{4}\left(\frac{1}{d_1^2} - \frac{1}{(1-d_2)^2}\right)$	$\frac{16}{3}C_1(t_1^2 + t_2^2) + 2C_1\alpha^2$ $- 16C_2\alpha(t_1^3 - t_2^3).$

$$C_1 = \frac{2}{\sqrt{(M^2-1)}}$$

$$C_2 = \frac{\frac{\gamma+1}{2}M^4 - 2(M^2-1)}{(M^2-1)^2}.$$

Figure 58. Supersonic Airfoil Section Data - R.A.S. Data Sheets

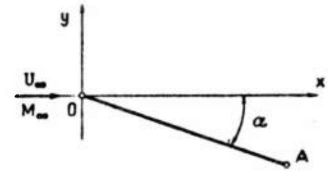

$$C_d = C_l \tan\alpha \approx \alpha C_l \quad \mu_2 = \tfrac{1}{2}\frac{C_l}{\cos\alpha} \approx \tfrac{1}{2} C_l.$$

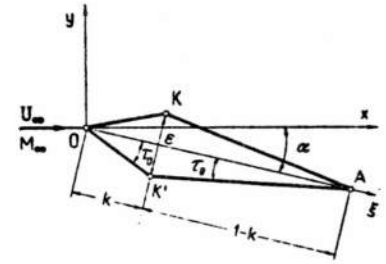

$$C_d = \left[k(C_{pl}^{(a)}\tau_{al} + C_{pu}^{(a)}\tau_{au}) + (1-k)(C_{pl}^{(a)}\tau_{al} + C_{pu}^{(a)}\tau_{au})\right]\cos\alpha$$

$$\approx \frac{4}{\sqrt{M_\infty^2-1}}\left[\alpha^2 + \frac{\varepsilon^2}{4k(1-k)} + \frac{1}{2}\left(\frac{\gamma+1}{4}\right)^2 m^2 M_\infty^2\left(\alpha^4 + \frac{3\alpha^2\varepsilon^2}{2k(1-k)}\right.\right.$$

$$\left.\left. + \frac{\varepsilon^4(1-3k+3k^2)}{16k^2(1-k)^3}\right)\right] \mp \frac{(\gamma+1)m^2\varepsilon^2(1-2k)}{8k^2(1-k)^2},$$

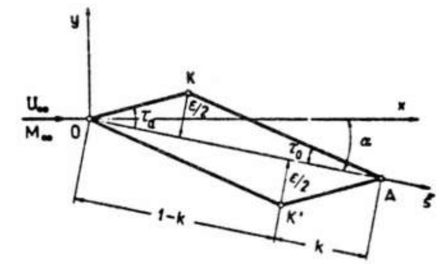

$$C_d = \left[(1-k)(C_{pl}^{(a)}\tau_{al} + C_{pu}^{(a)}\tau_{au}) + k(C_{pl}^{(a)}\tau_{al} + C_{pu}^{(a)}\tau_{au})\right]\cos\alpha$$

$$\approx \frac{4}{\sqrt{M_\infty^2-1}}\left[\alpha^2 + \tfrac{1}{2}\left(\frac{\gamma+1}{2}\right)^2 m^2 M_\infty^2\left(\alpha^4 + \frac{3\alpha^2\varepsilon^2}{2k(1-k)} - \frac{\alpha\varepsilon^3(1-k)}{2k^2(1-k)^2}\right.\right.$$

$$\left.\left. + \frac{\varepsilon^4(1-3k+3k^2)}{16k^3(1-k)^3}\right)\right],$$

$$\tau_{au} = -\alpha+\tau_a, \quad \tau_{au} = -\alpha-\tau_0, \quad \tau_{al} = \alpha+\tau_0, \quad \tau_{al} = \alpha-\tau_a,$$

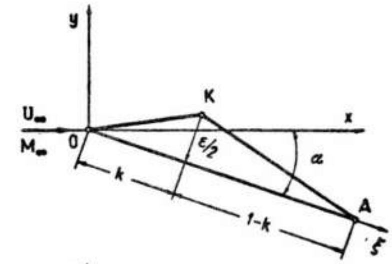

$$C_d = \left[C_{pl}^{(a)}\alpha + kC_{pu}^{(a)}\tau_{au} + (1-k)C_{pu}^{(a)}\tau_{au}\right]\cos\alpha$$

$$\approx \frac{2}{\sqrt{M_\infty^2-1}}\left\{2\alpha^2 + \frac{\varepsilon^2}{k(1-k)} + \frac{1}{2}\left(\frac{\gamma+1}{4}\right)^2 m^2 M_\infty^2\left[\alpha^4 + k\left(\alpha - \frac{\varepsilon}{k}\right)^4\right.\right.$$

$$\left.\left. + (1-k)\left(\alpha + \frac{\varepsilon}{1-k}\right)^4\right]\right\} - \frac{(\gamma+1)m^2\varepsilon^2}{2k(1-k)}\left[3\alpha - \frac{\varepsilon(1-2k)}{k(1-k)}\right],$$

$$\tau_{al} = \alpha, \quad \tau_{au} = -\alpha+\tau_0, \quad \tau_{au} = -\alpha-\tau_a.$$

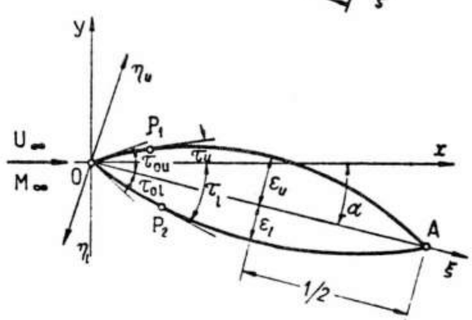

$$C_d = -\frac{\cos^2\alpha}{4\sqrt{M_\infty^2-1}}\left(\frac{1}{\varepsilon_u}H_{u2} + \frac{1}{\varepsilon_l}H_{l2}\right) - 8(\gamma+1)m^2(\varepsilon_u^2-\varepsilon_l^2)\cos^3\alpha\tan\alpha$$

$$\approx \frac{4}{\sqrt{M_\infty^2-1}}\left\{\alpha^2 + \tfrac{8}{3}(\varepsilon_u^2+\varepsilon_l^2) + \tfrac{1}{2}\left(\frac{\gamma+1}{4}\right)^2 m^2 M_\infty^2\left[\alpha^4 + 16\alpha^2(\varepsilon_u^2+\varepsilon_l^2)\right.\right.$$

$$\left.\left. + \tfrac{128}{5}(\varepsilon_u^4+\varepsilon_l^4)\right]\right\} - 8(\gamma+1)m^2(\varepsilon_u^2-\varepsilon_l^2)\alpha,$$

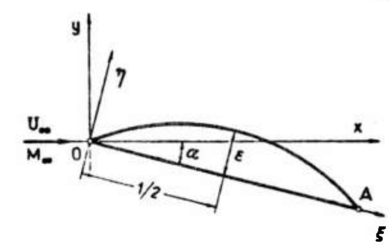

$$C_d = C_{pl}^{(0)}\sin\alpha - \frac{\cos^2\alpha}{4\varepsilon\sqrt{M_\infty^2-1}}H_{u2} - 8(\gamma+1)m^2\varepsilon^2\cos^3\alpha\tan\alpha$$

$$\approx \frac{4}{\sqrt{M_\infty^2-1}}\left[\alpha^2 + \tfrac{8}{3}\varepsilon^2 + \tfrac{1}{2}\left(\frac{\gamma+1}{4}\right)^2 m^2 M_\infty^2(\alpha^4 + 16\alpha^2\varepsilon^2 + \tfrac{128}{5}\varepsilon^4)\right]$$

$$- 8(\gamma+1)m^2\varepsilon^2\alpha,$$

Figure 59. Supersonic Airfoil Characteristics - Carafoli

SHARP-NOSED AIRFOILS

Basic Wing Airfoil Section	K	Section
Biconvex	$\frac{16}{3}$	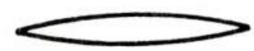
Double Wedge	$\frac{c/x_t}{1 - x_t/c}$	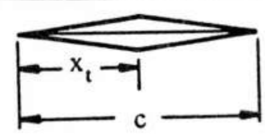
Hexagonal	$\frac{c\,(c - x_2)}{x_1\, x_3}$	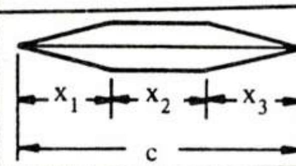

Figure 60. Sharp-Nosed Airfoil Thickness Factor

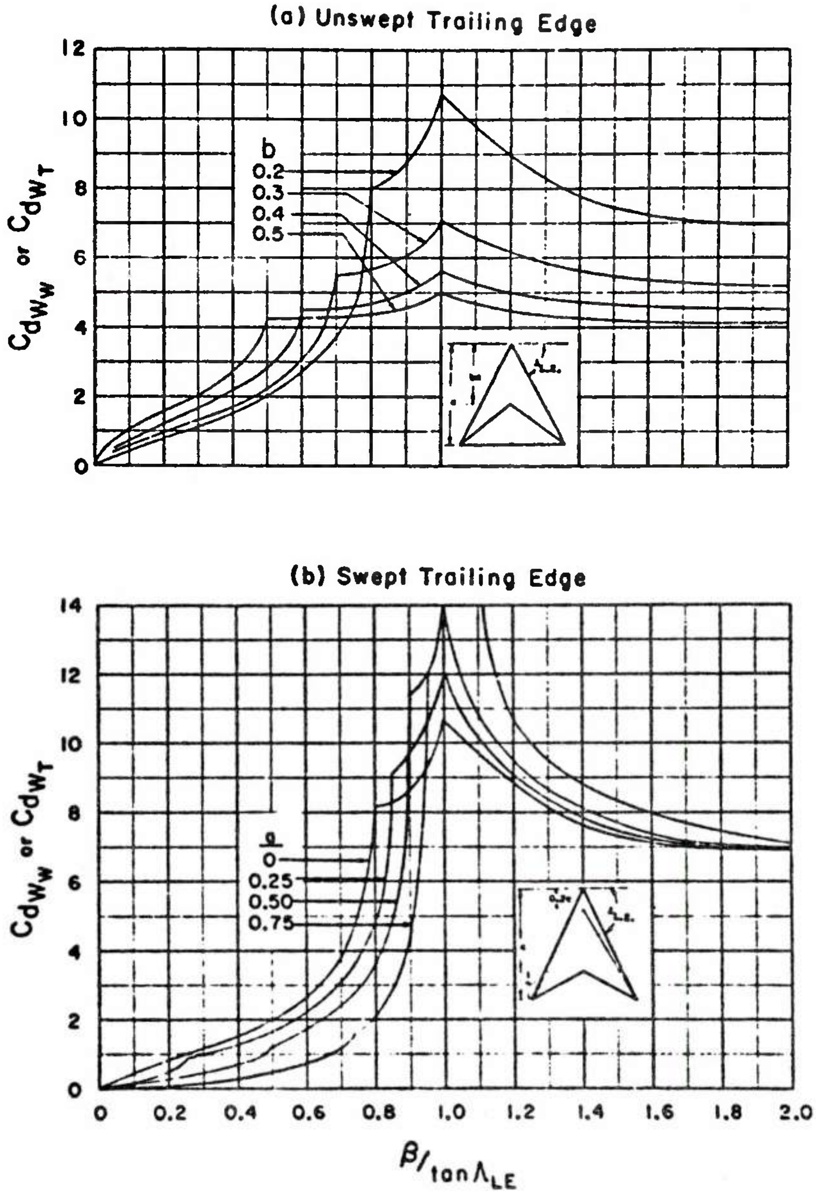

Figure 61. Wave Drag of Zero Taper Ratio Lifting Surfaces (Wings or Tails) ($\lambda_W = 0.15$)

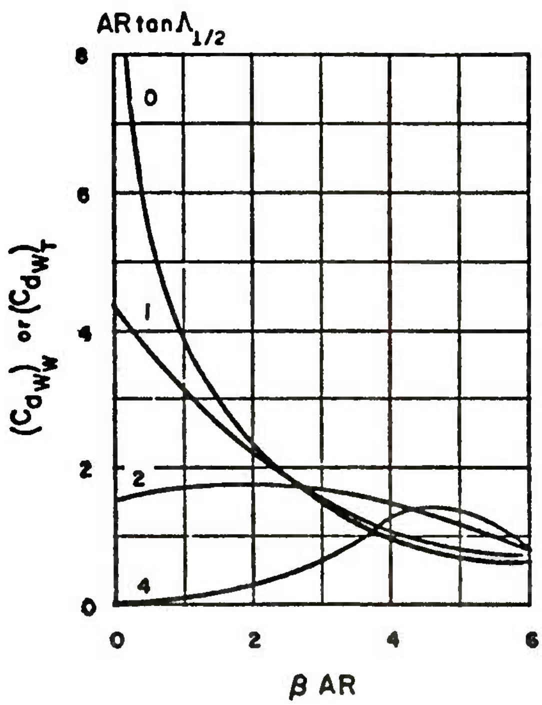

Figure 62. Wave Drag of Lifting Surfaces (Wings or Tails) Whose Taper Ratio is Greater Than 0.15

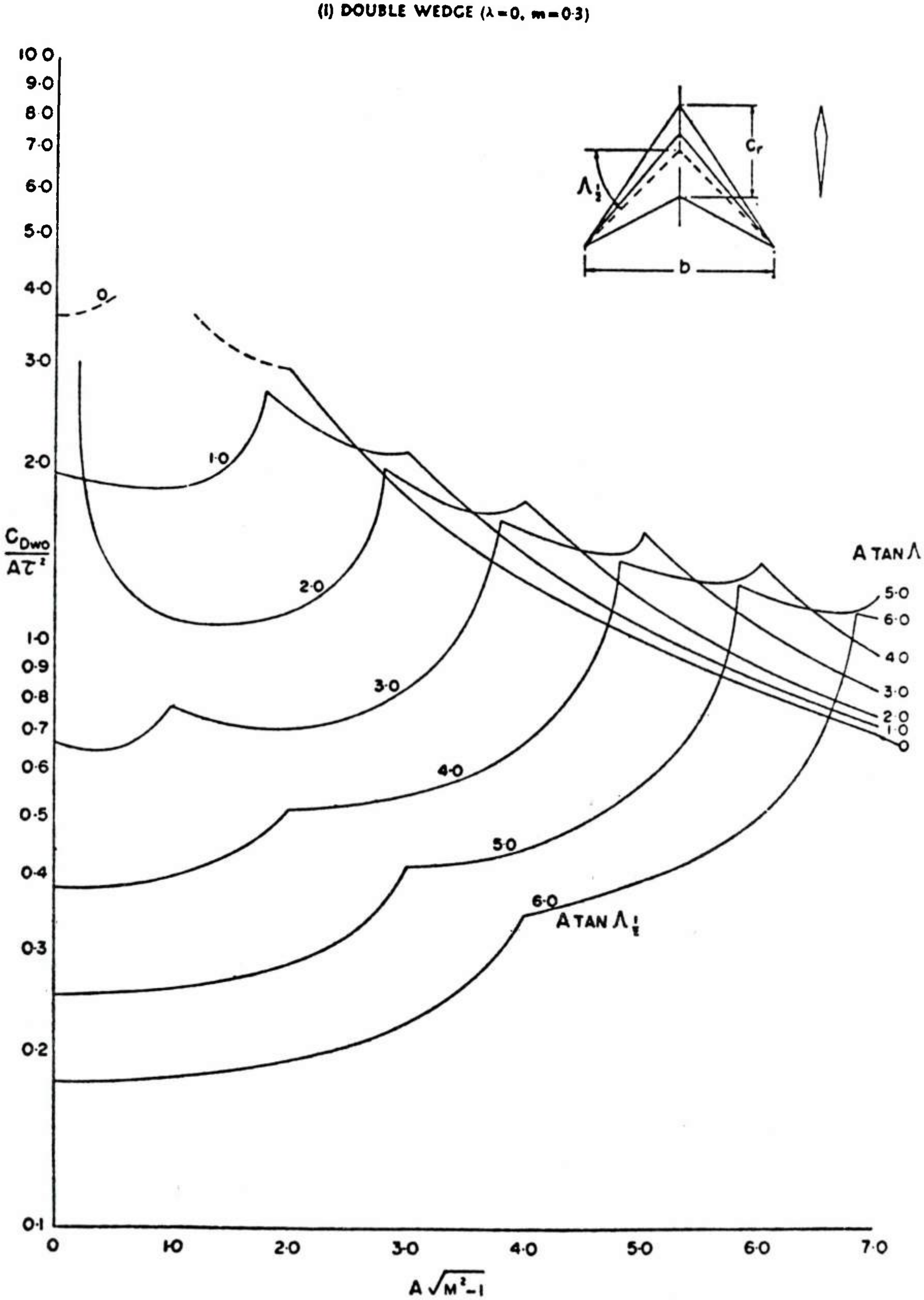

Figure 63. Fin Theoretical Wave Drag - R.A.S. Data Sheets

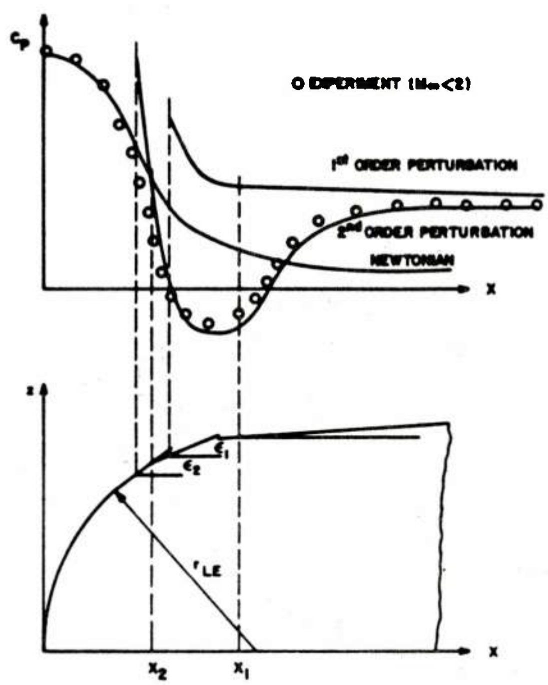

Figure 64. **Combined Newtonian and perturbation theory for a blunt leading edge.**

$$C_{D_{LE}}\left[\frac{S_{ref}}{2r_{LE_{bw}}\left(\frac{b_{bw}}{\cos\Lambda_{LE_{bw}}}\right)}\right] = 1.28\ \frac{M^3\cos^6\Lambda_{LE_{bw}}}{1 + M^3\cos^3\Lambda_{LE_{bw}}}$$

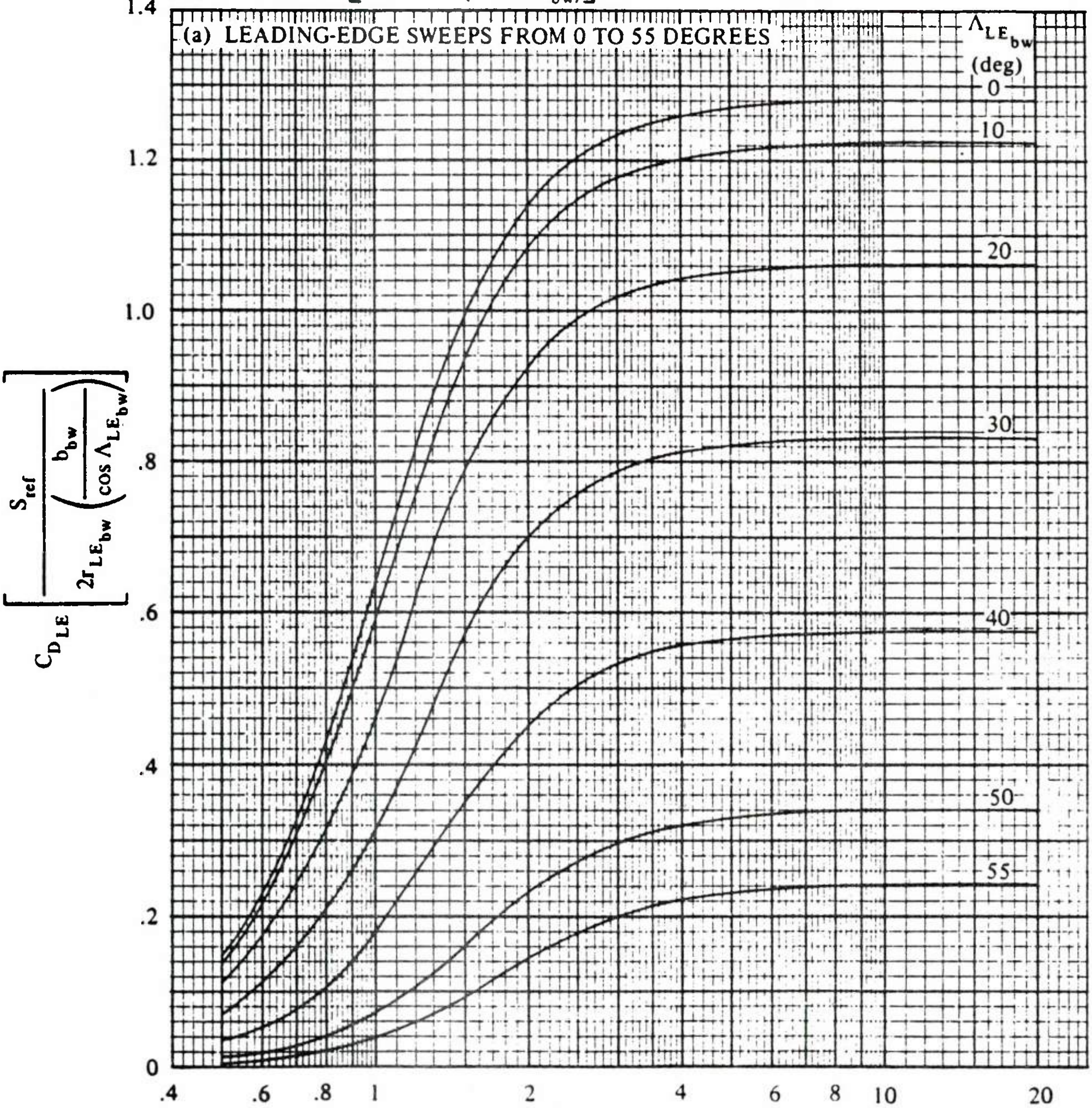

Figure 65. CORRELATION OF CYLINDRICAL LEADING-EDGE PRESSURE DRAG COEFFICIENTS

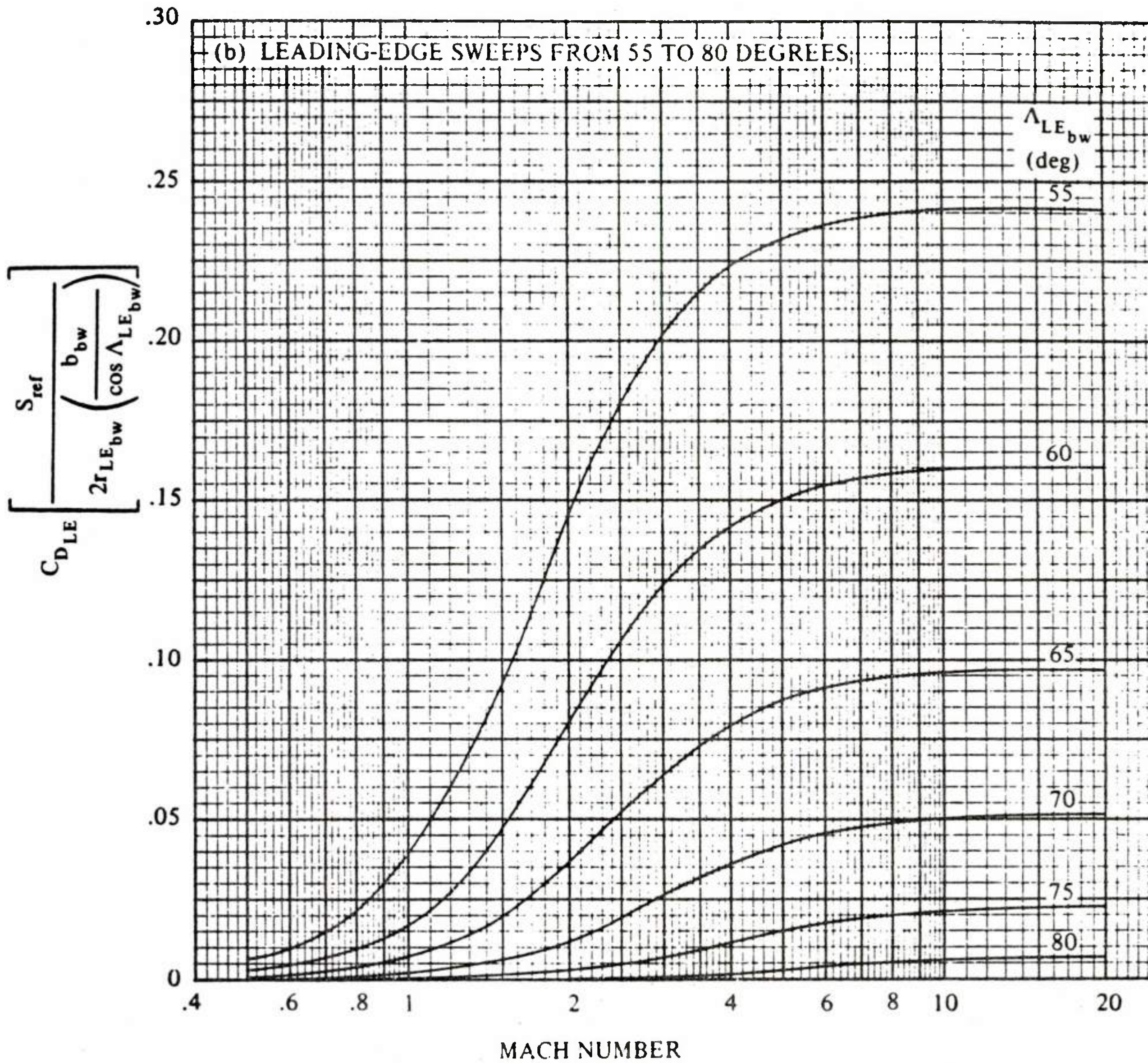

Figure 65. (continued)

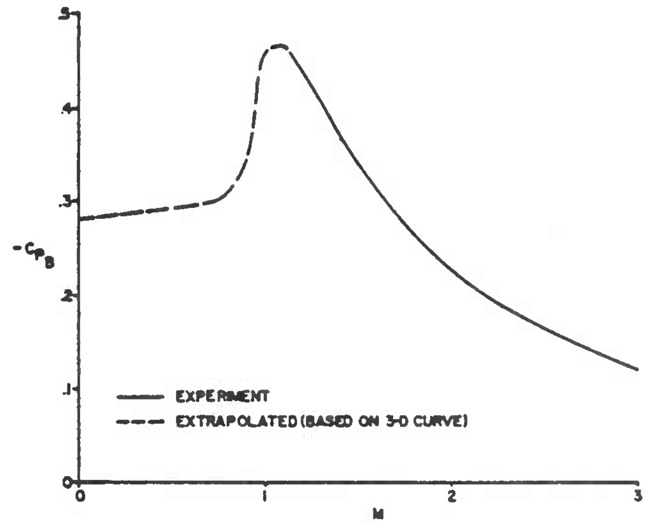

Figure 66. Two-Dimensional Base Drag Coefficient for Fins

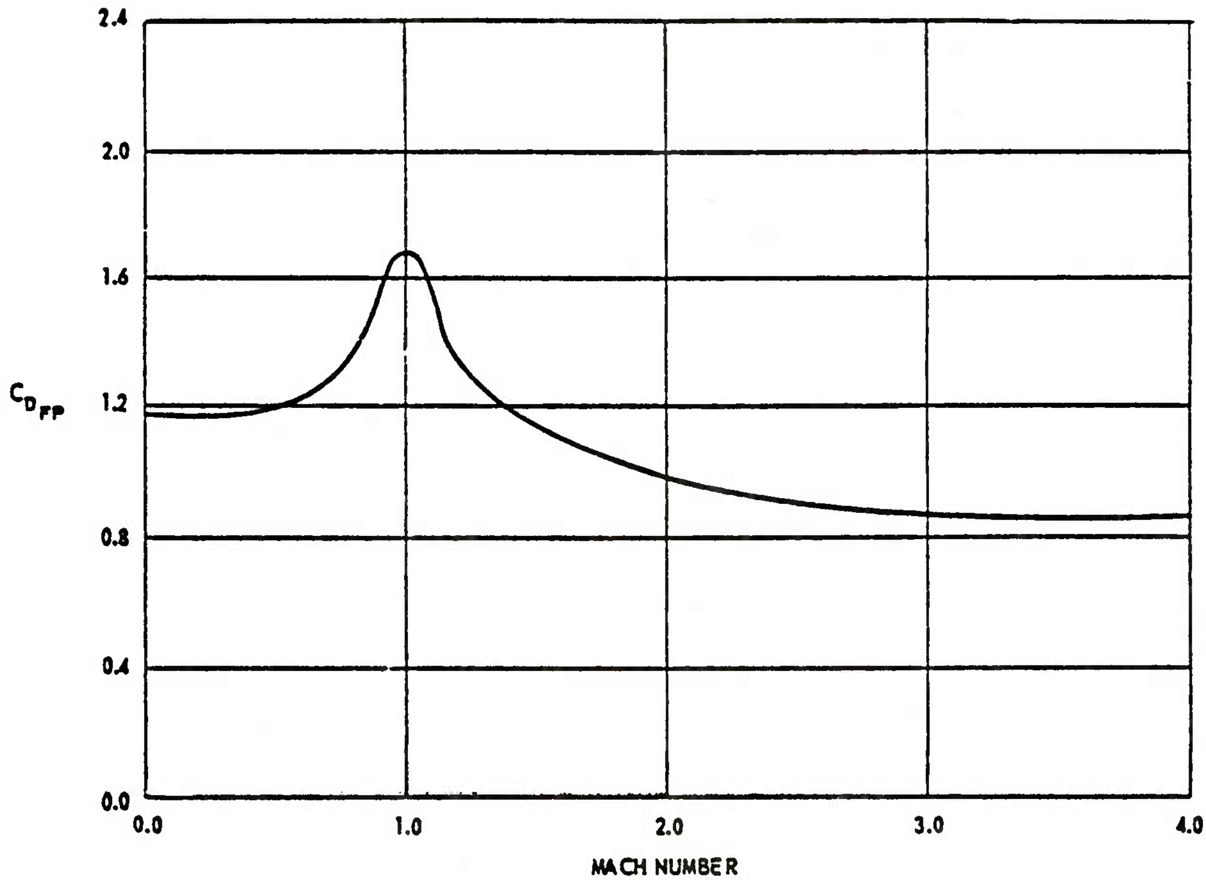

Figure 67. Drag Coefficient for a Flat Plate Normal to the Flow

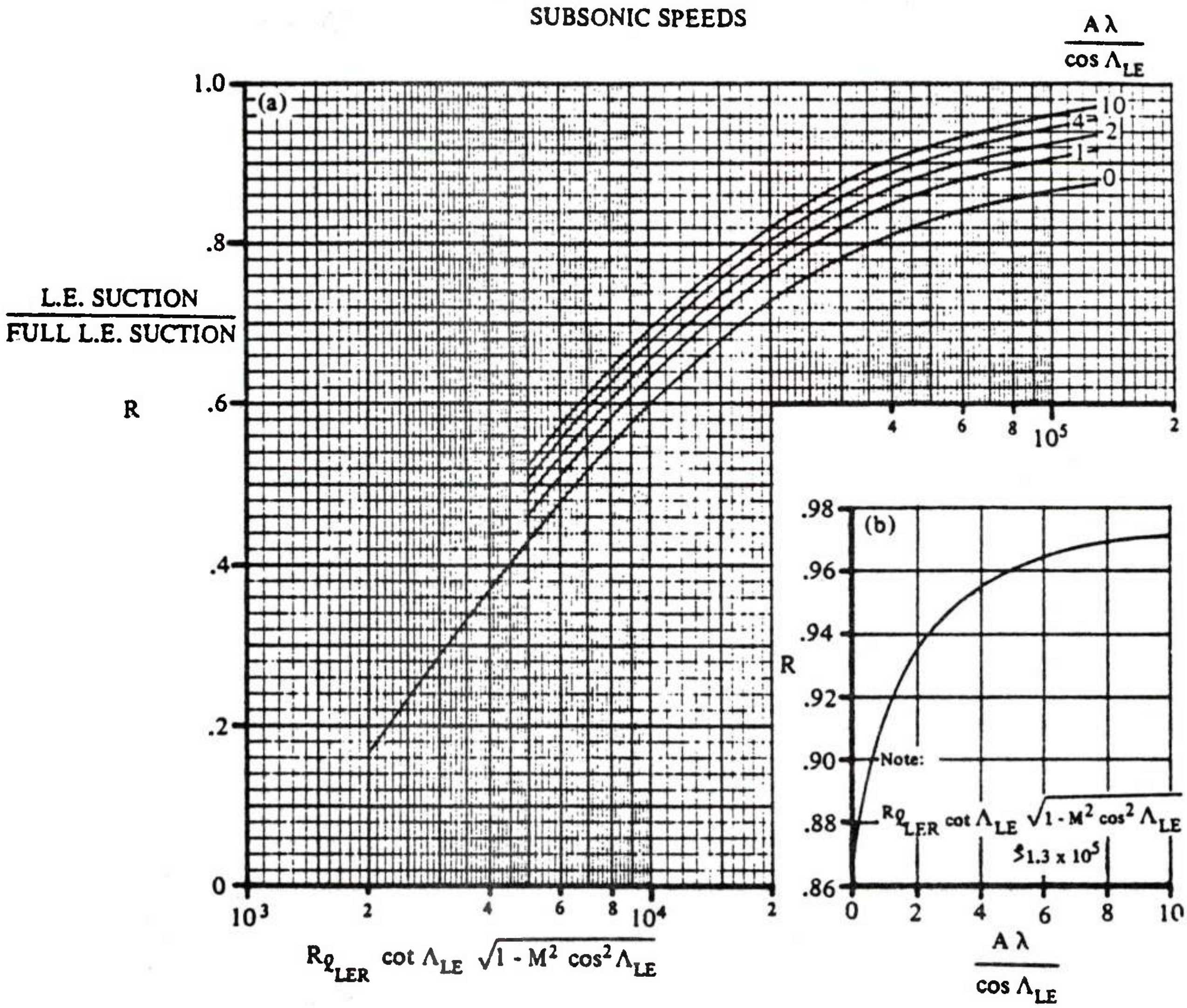

Figure 68. LEADING-EDGE SUCTION PARAMETER AT SUBSONIC SPEEDS. $M \leq 0.8$

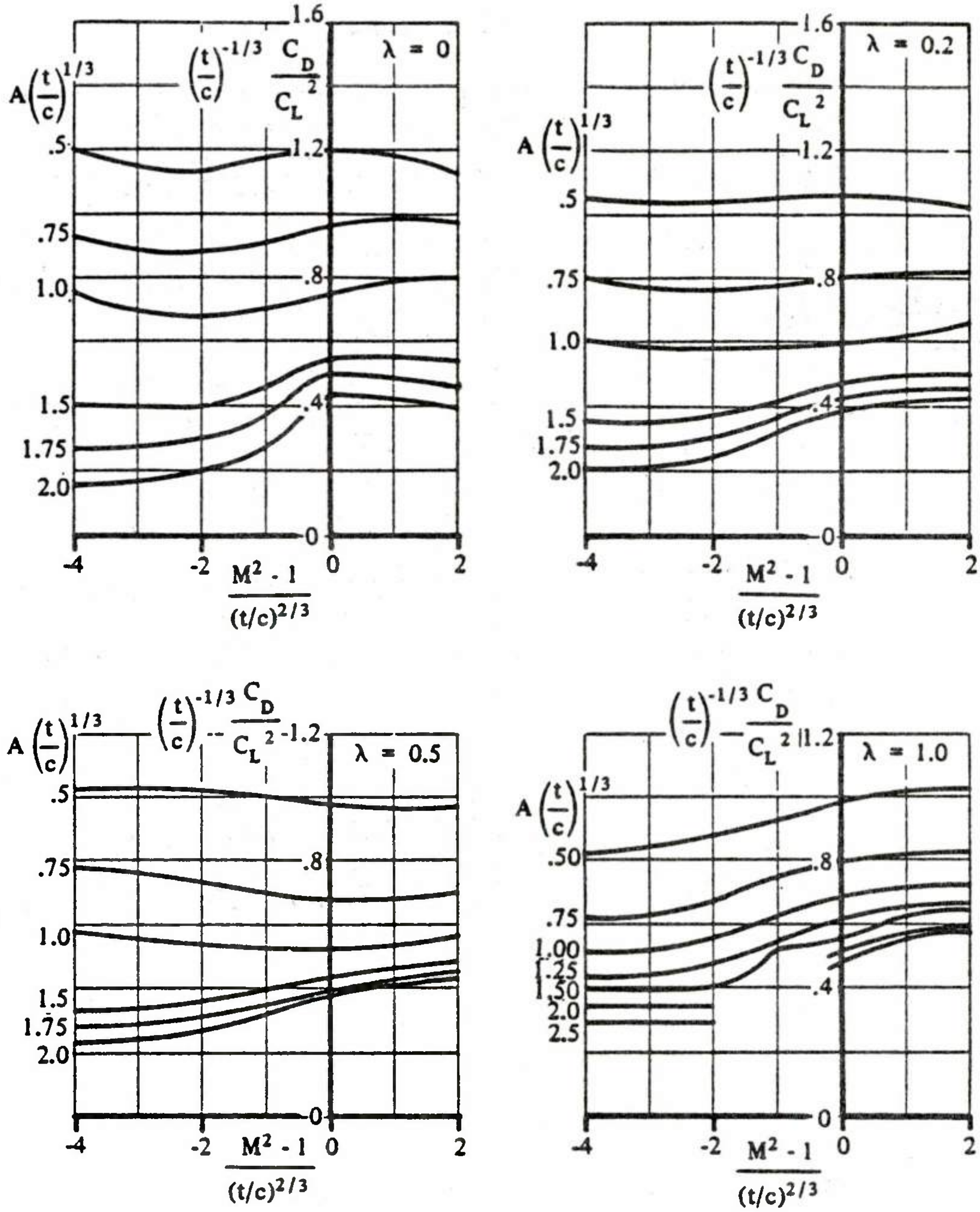

Figure 69. **TRANSONIC DRAG DUE TO LIFT**
(a) A TAN Λ_{LE} = 0

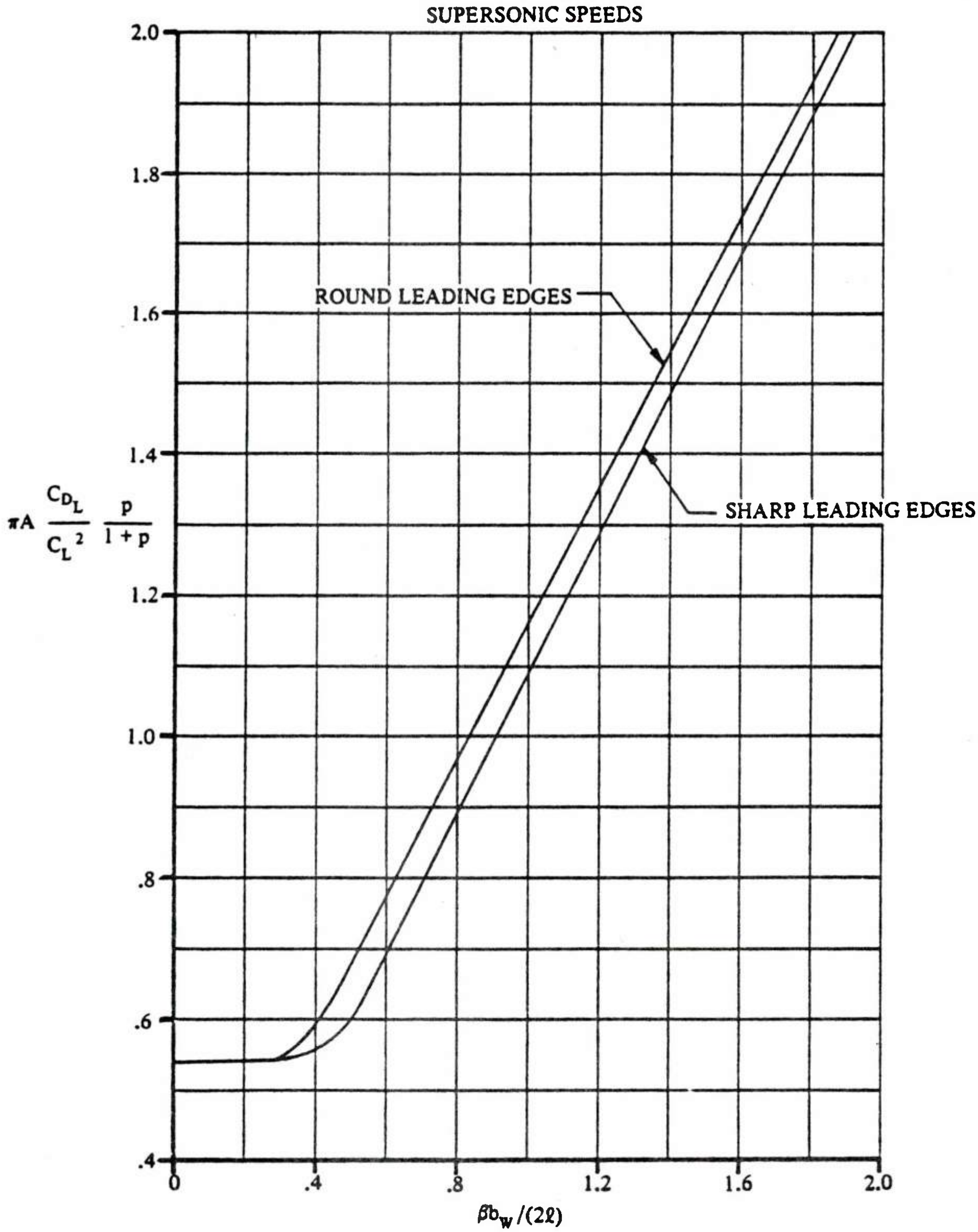

Figure 70. CORRELATION OF DRAG DUE TO LIFT OF STRAIGHT-TAPERED WINGS

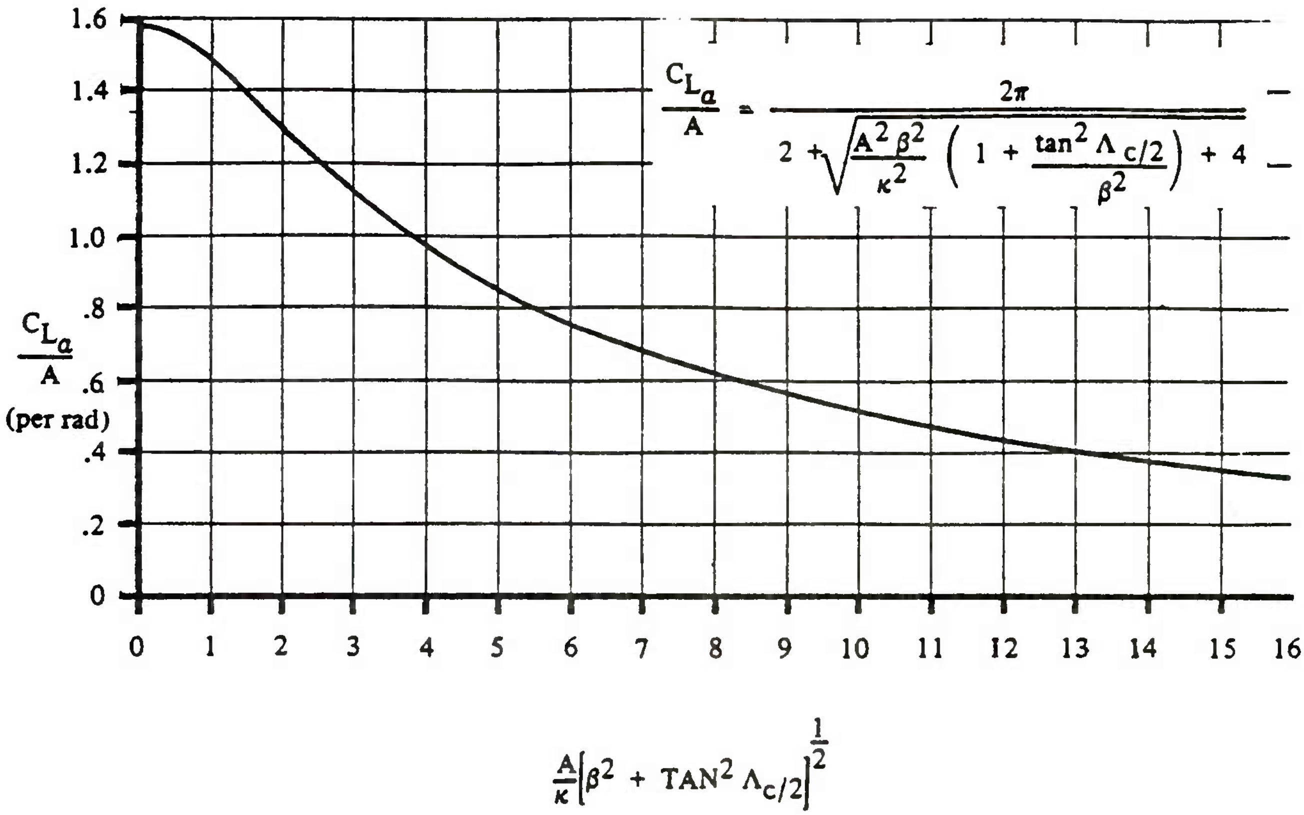

FIGURE 4.1.3.2-49 SUBSONIC WING LIFT-CURVE SLOPE

Theoretical section lift curve slope:

$$c_{\ell_\alpha} = 6.28 + 4.7\ t/c\left[1 + .00375\ \phi_{TE}\right]\ \text{(per rad)}$$

Section lift-curve slope corrected for viscous effects:

$$c_{\ell_\alpha} = \frac{1.05}{\beta}\left[\frac{c_{\ell_\alpha}}{\left(c_{\ell_\alpha}\right)_{theory}}\right]\left(c_{\ell_\alpha}\right)_{theory}$$

Subsonic Panel Lift-Curve-Slope

Figure 71. Subsonic Wing Lift-Curve Slope

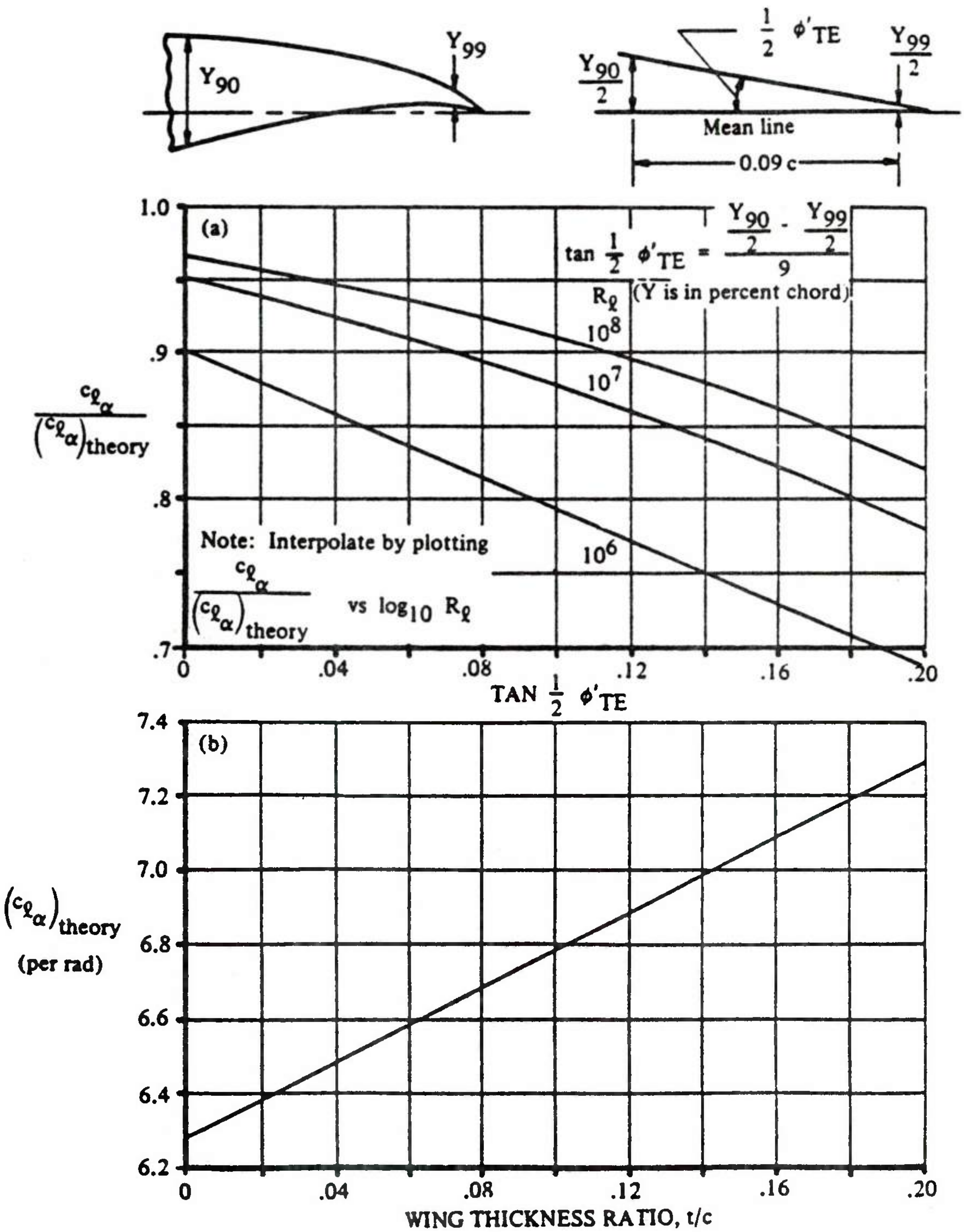

Figure 72. TWO-DIMENSIONAL LIFT-CURVE SLOPE

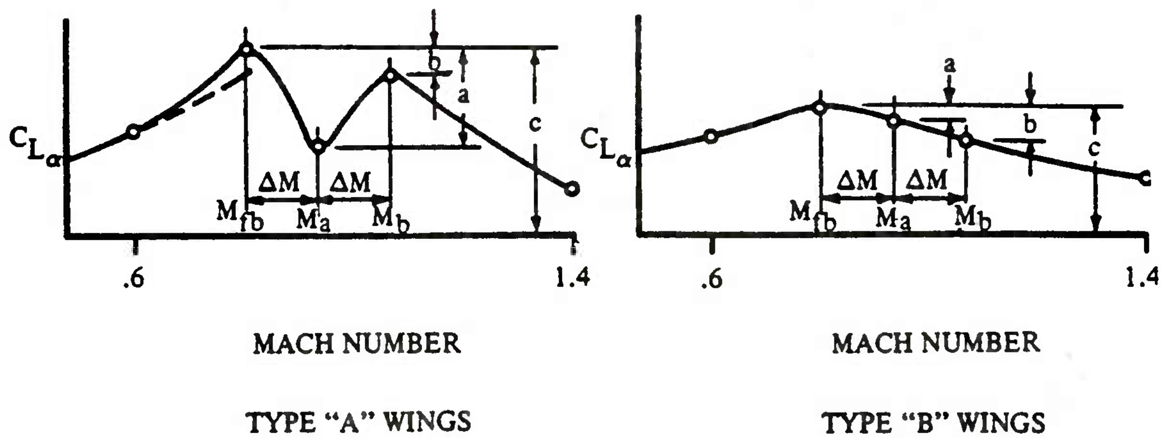

Figure 73. Wing Type Classification

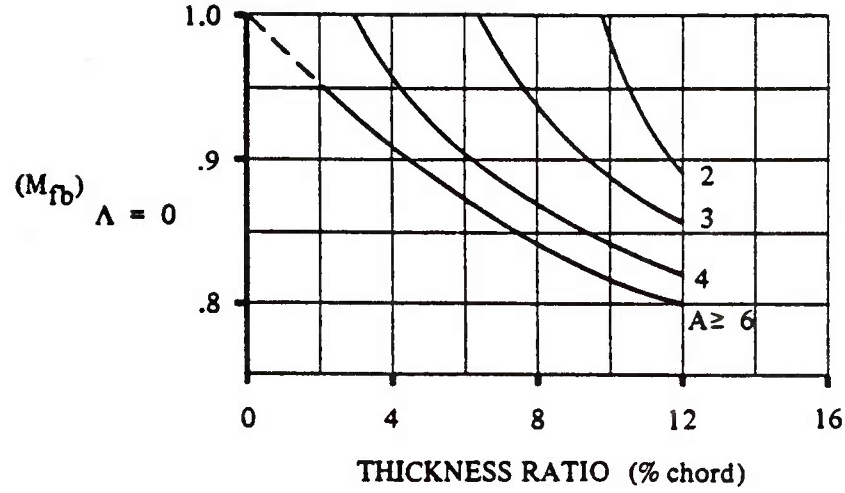

Figure 74. TRANSONIC FORCE-BREAK MACH NUMBER FOR ZERO SWEEP

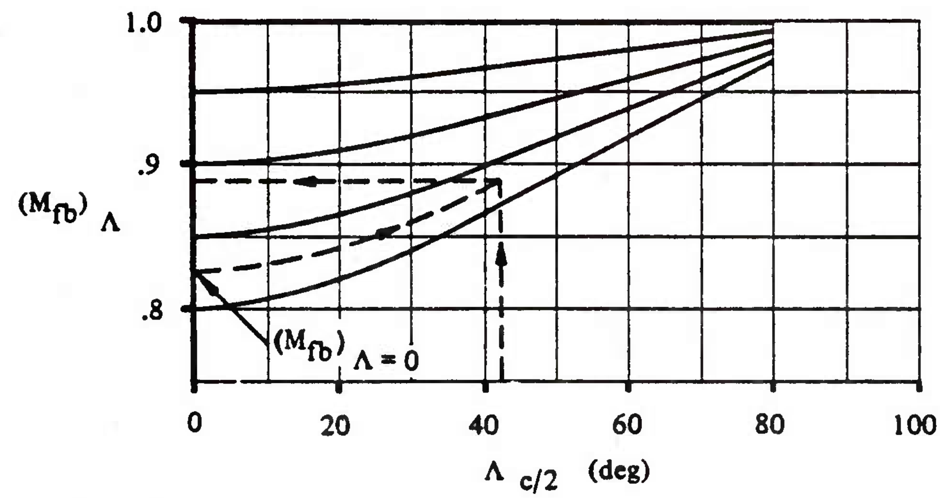

Figure 75. TRANSONIC SWEEP CORRECTION FOR FORCE-BREAK MACH NUMBER

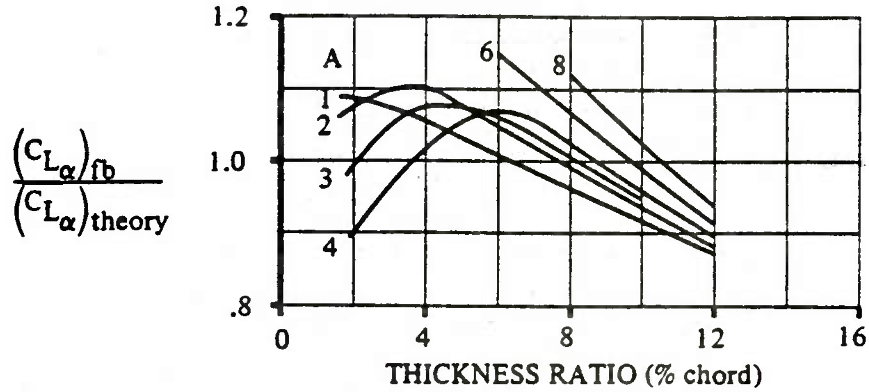

a) CORRECTION TO LIFT-CURVE SLOPE AT FORCE-BREAK MACH NUMBER

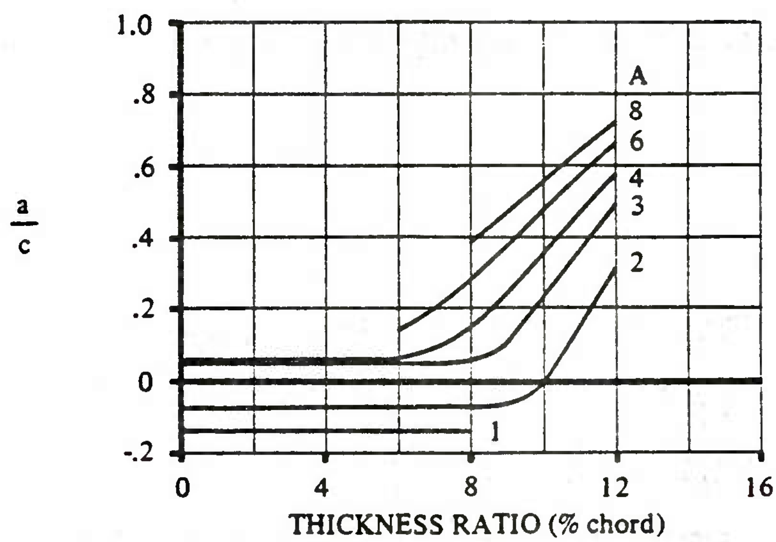

b) CHART FOR DETERMINING LIFT-CURVE SLOPE AT M_a

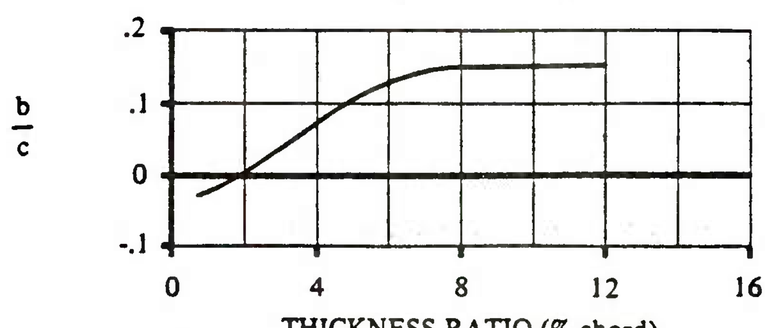

c) CHART FOR DETERMINING LIFT-CURVE SLOPE AT M_b

Figure 76. Datcom Transonic Fairing Parameter

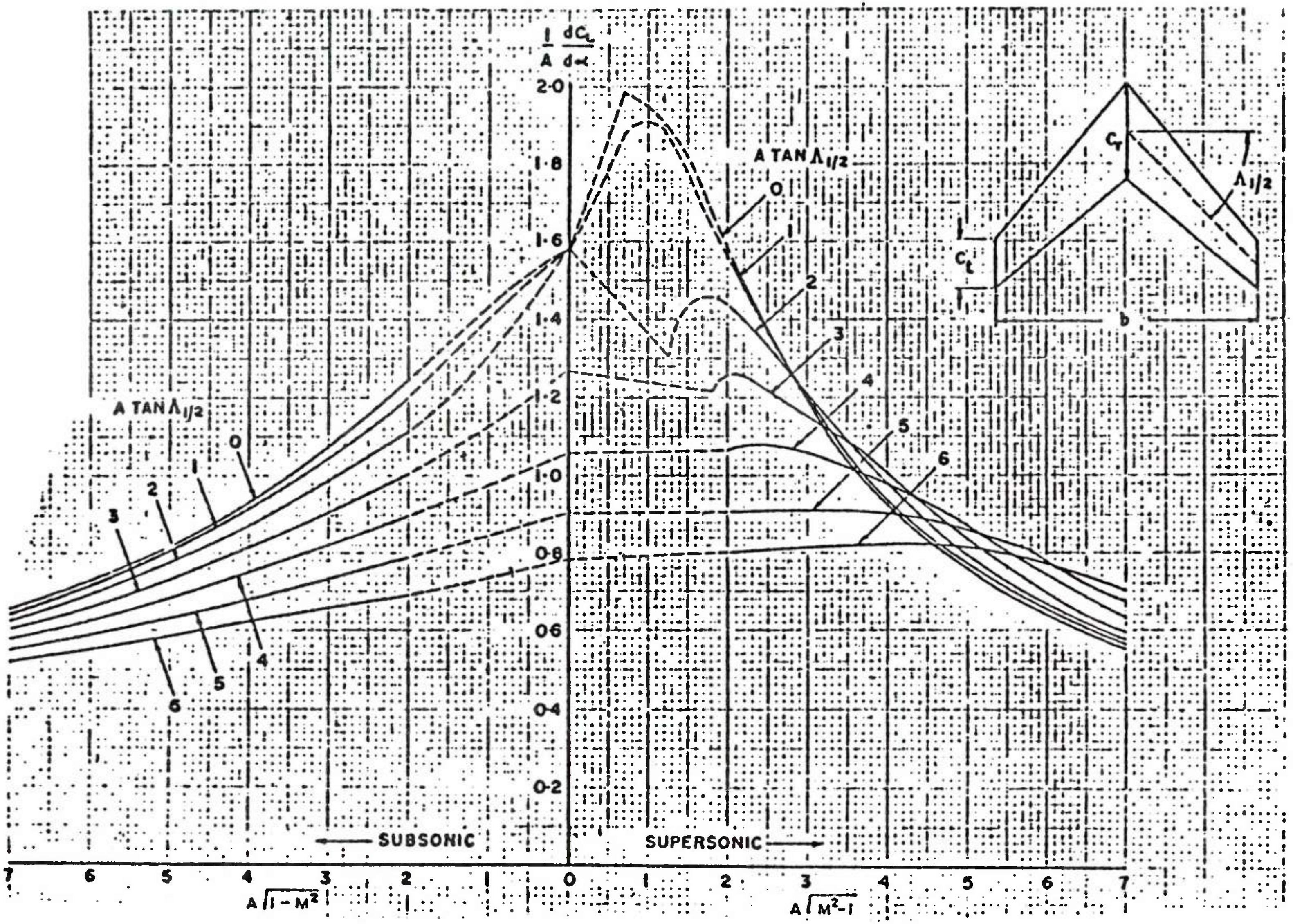

Figure 77. Panel Lift-Curve-Slope-R.A.S. Data Sheets

GENERALIZED FORMULAS FOR ΔC_p DISTRIBUTIONS CAUSED BY CONSTANT ANGLE OF ATTACK AND BY STEADY ROLLING

$$B\cot\Lambda \geq 1;\quad \left|B\cot\Lambda_{TE}\right| \geq 1;\quad BA \geq \frac{4B\cot\Lambda}{(1+\lambda)(1+B\cot\Lambda)}$$

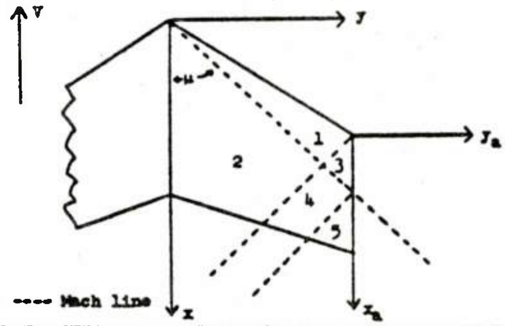

Region (see sketch)	Formula for ΔC_p contributed by α	Formula for ΔC_p contributed by p
1	$\frac{4\alpha m}{\sqrt{B^2m^2-1}}$	$\frac{4pm^2x(B^2m^2v-1)}{v(B^2m^2-1)^{3/2}}$
2	$\frac{4\alpha m}{\pi\sqrt{B^2m^2-1}}\left[\cos^{-1}\frac{1+B^2m^2v}{Bm(1+v)}+\cos^{-1}\frac{1-B^2m^2v}{Bm(1-v)}\right]$	$\frac{4pm^2x}{\pi v(B^2m^2-1)^{3/2}}\left[(1+B^2m^2v)\cos^{-1}\frac{1+B^2m^2v}{Bm(1+v)}-(1-B^2m^2v)\cos^{-1}\frac{1-B^2m^2v}{Bm(1-v)}\right]$
3	$\frac{4\alpha m}{\sqrt{B^2m^2-1}}+\left(\Delta C_{p_t}\right)_\alpha^*$	$\frac{4pm^2x(B^2m^2v-1)}{v(B^2m^2-1)^{3/2}}+\left(\Delta C_{p_t}\right)_p^*$
4	$\left(\Delta C_p\right)_{\text{Region 2}}+\left(\Delta C_{p_t}\right)_\alpha^*$	$\left(\Delta C_p\right)_{\text{Region 2}}+\left(\Delta C_{p_t}\right)_p^*$
5	$\frac{4\alpha m}{\pi\sqrt{B^2m^2-1}}\cos^{-1}\frac{mx_a-y_a(1-2Bm)+2h}{mx_a+y_a+2h}$	$\frac{4pm}{\pi v(B^2m^2-1)^{3/2}}\left\{\left[mx_a+B^2m^2y_a+h(B^2m^2+1)\right]\cos^{-1}\frac{mx_a-y_a(1-2Bm)+2h}{mx_a+y_a+2h}-2Bm\sqrt{-y_a(Bm-1)(mx_a+Bmy_a+2h)}\right\}$

NACA

$$^*\left(\Delta C_{p_t}\right)_\alpha = -\frac{4\alpha m}{\pi\sqrt{B^2m^2-1}}\cos^{-1}\frac{-\left[mx_a+y_a(2Bm+1)\right]}{mx_a-y_a}$$

$$\left(\Delta C_{p_t}\right)_p = \frac{4pm}{\pi v(B^2m^2-1)^{3/2}}\left\{\left[mx_a-B^2m^2y_a-h(B^2m^2-1)\right]\cos^{-1}\frac{-\left[mx_a+y_a(2Bm+1)\right]}{mx_a-y_a}-2Bm\sqrt{-my_a(x_a+By_a)(Bm+1)}\right\}$$

Notes: $B = \sqrt{M^2-1}$ $X_a = X - h/m$

$M = \cot\Lambda_{LE}$ $Y_a = Y - h$

$V = Y/(mx)$ h = semi-span

Figure 78. NACA TN 2114 Pressure Regions

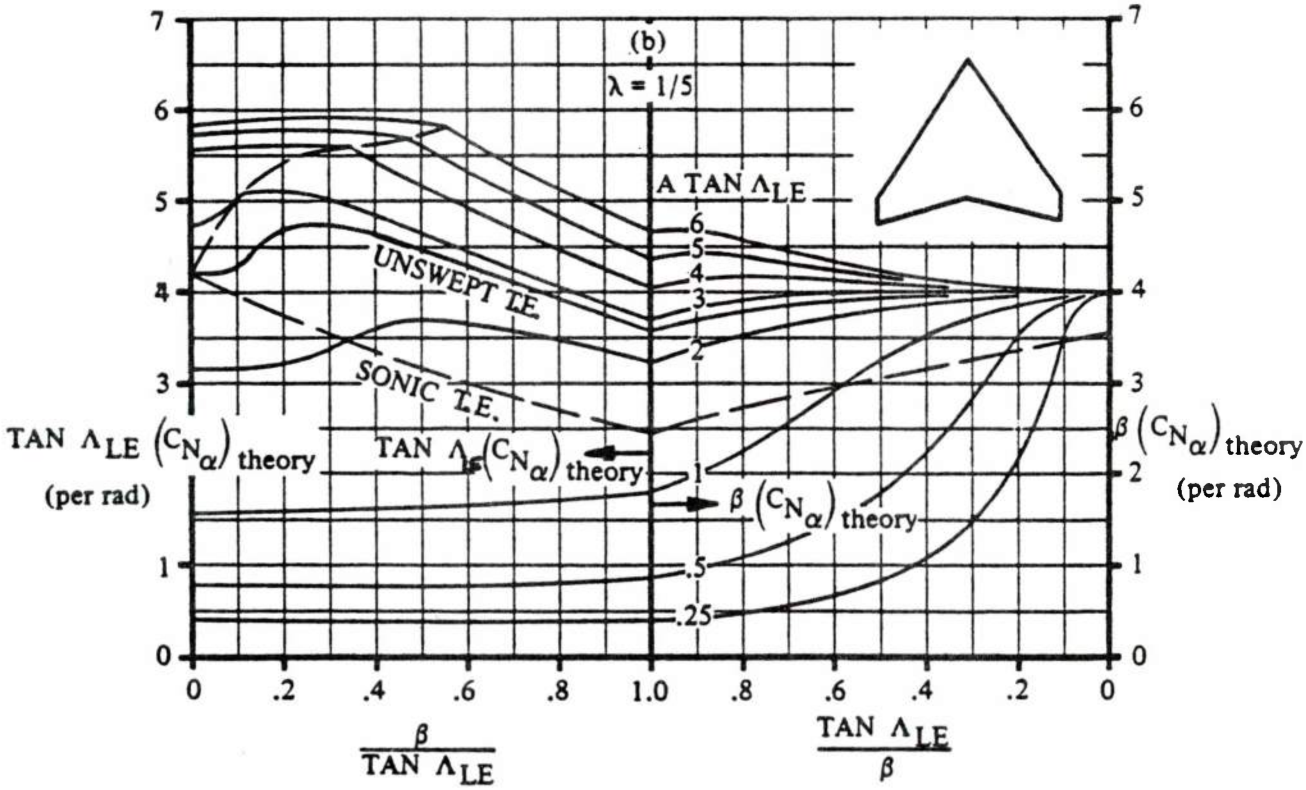

Figure 79. WING SUPERSONIC NORMAL-FORCE-CURVE SLOPE

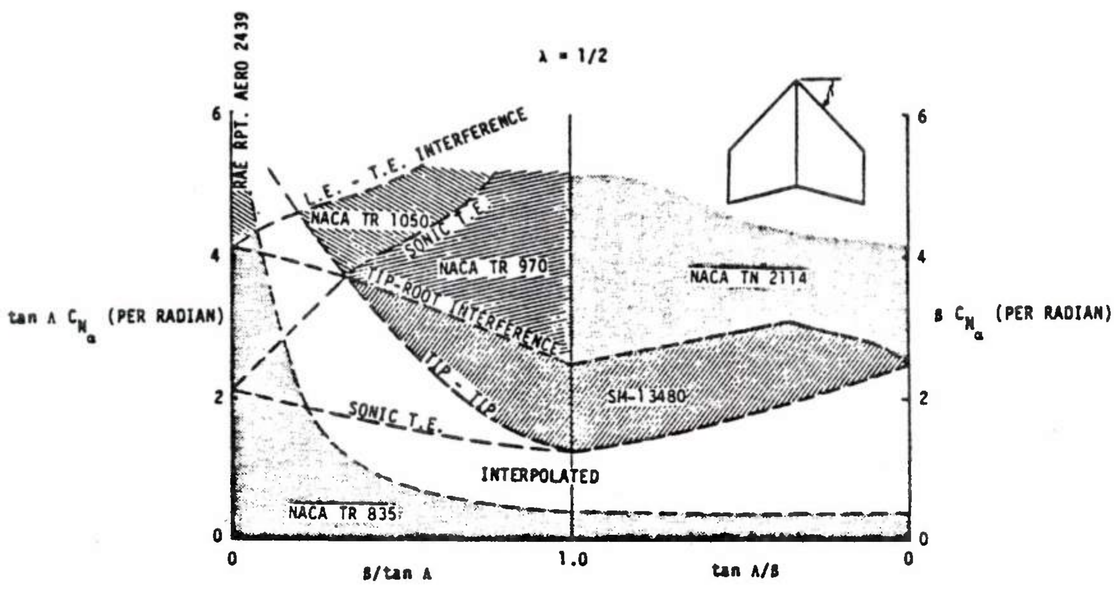

Figure 80. Datcom Normal Force Slope Design Chart Theoretical Sources

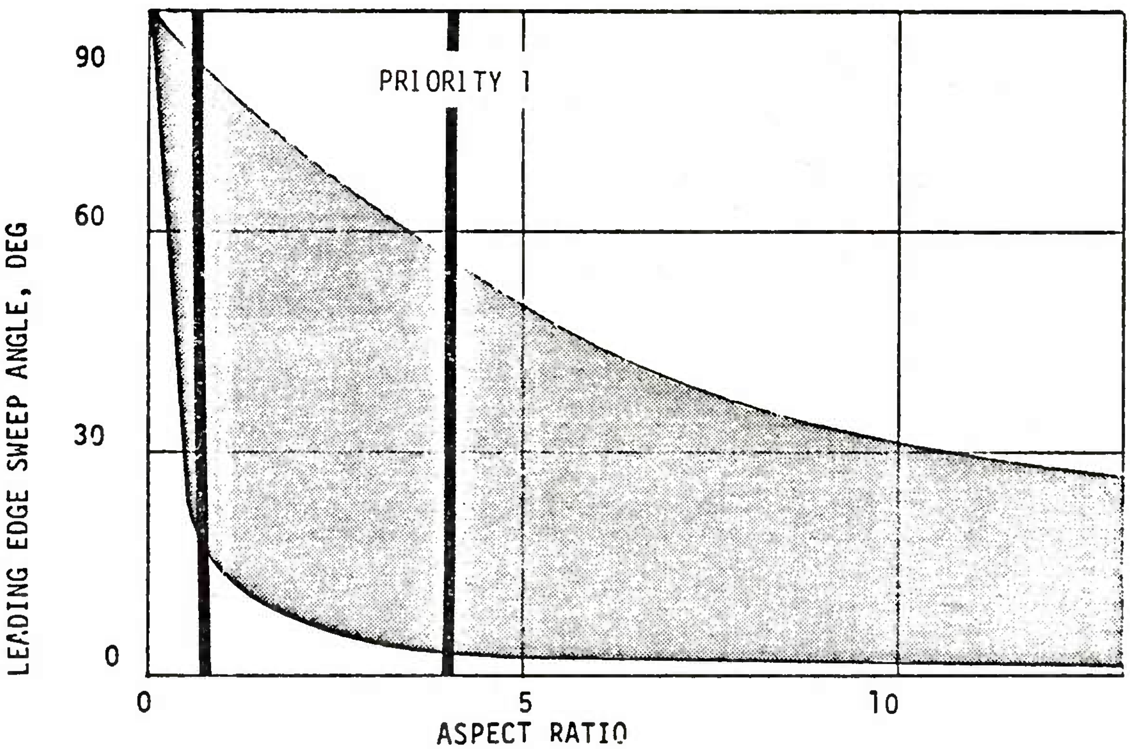

Figure 81. Applicability of Datcom Charts

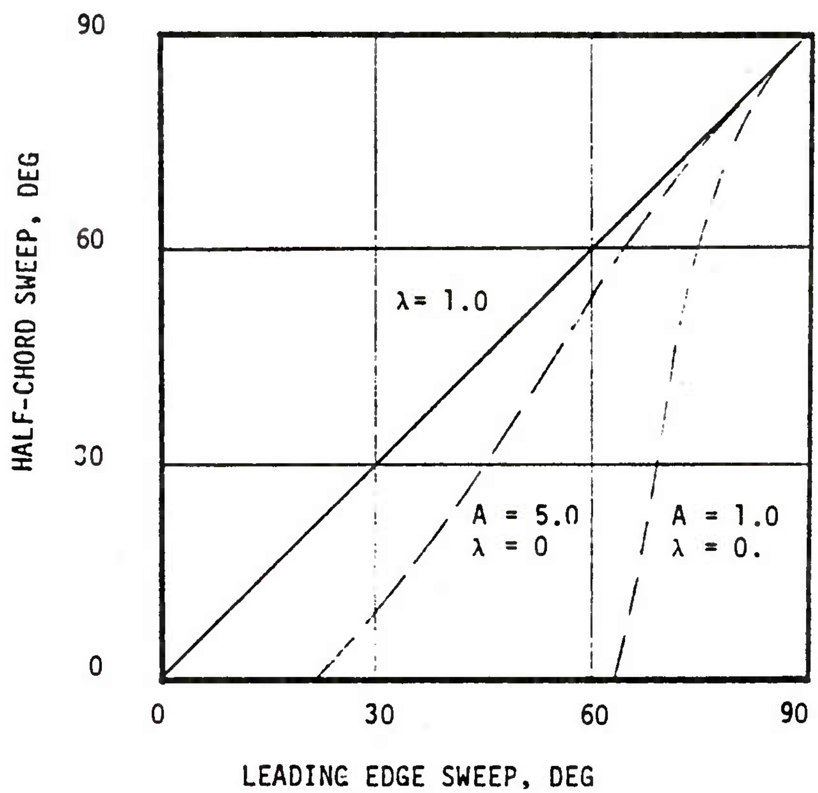

Figure 82. Comparison of Half-Chord and Leading Edge Sweep Angles for Straight-Tapered Panels

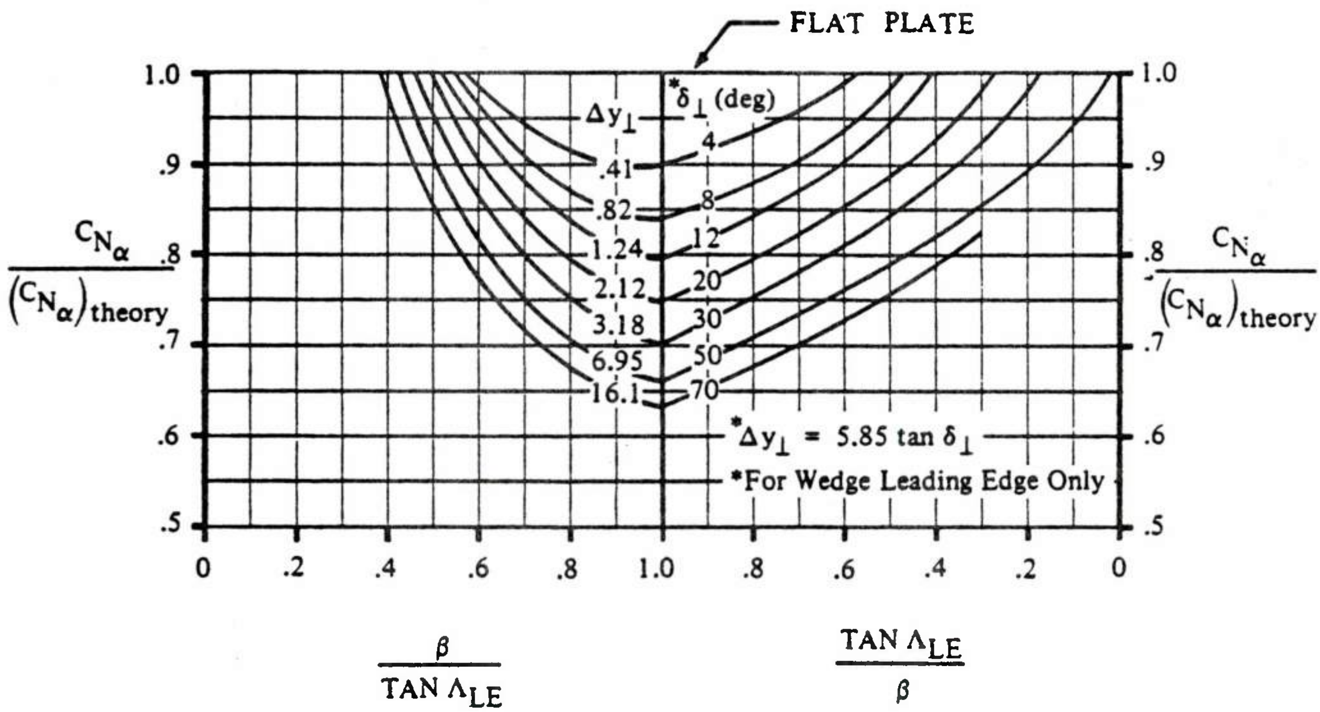

Figure 83. SUPERSONIC WING LIFT-CURVE-SLOPE CORRECTION FACTOR FOR SONIC-LEADING-EDGE REGION

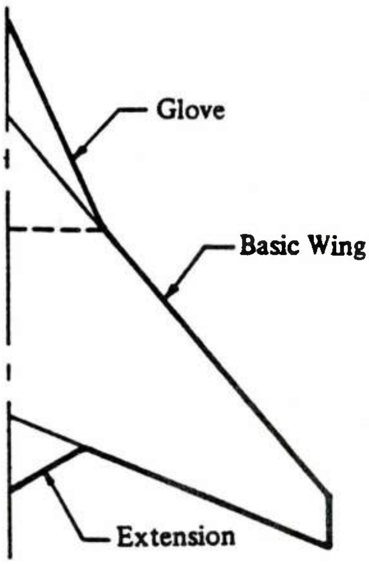

$$C_{N_\alpha} = K_L\left[\left(C_{N_\alpha}\right)_{bw}\frac{S_{bw}}{S_W}\left(C_{LE}\right)_{bw} + \left(C_{N_\alpha}\right)_g\frac{S_g}{S_W}\left(C_{LE}\right)_g + \left(C_{N_\alpha}\right)_E\frac{S_E}{S_W}\right]$$

$$\left(C_{N_\alpha}\right)_E\frac{S_E}{S_W} = \left[\left(\frac{C_{N_\alpha}}{A}\right)_1 - \left(\frac{C_{N_\alpha}}{A}\right)_2\right]\frac{b_E^{\,2}}{S_W}$$

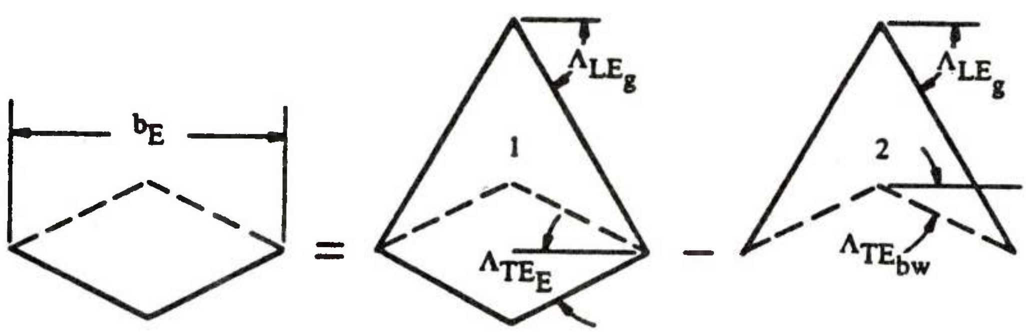

$$\left(C_{N_\alpha}\right)_E\frac{S_E}{S_W} = \left(C_{N_\alpha}\right)_1\frac{S_1}{S_W} - \left(C_{N_\alpha}\right)_2\frac{S_2}{S_W}$$

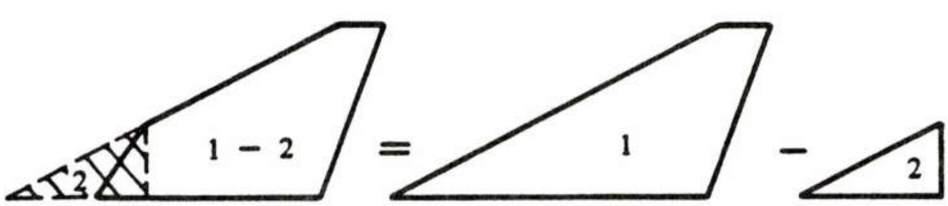

$$\left(C_{N_\alpha}\right)_{bw}\frac{S_{bw}}{S_W} = \left(C_{N_\alpha}\right)_1\frac{S_1}{S_W} - \left(C_{N_\alpha}\right)_2\frac{S_2}{S_W}$$

Figure 4.1.3.2-63 may also be applied with equal facility to obtain normal-force-curve slope of the glove. Using $(C_{N_\alpha}/A)_g$ from Figure 4.1.3.2-63

$$\left(C_{N_\alpha}\right)_g\frac{S_g}{S_W} = \left(\frac{C_{N_\alpha}}{A}\right)_g\frac{b_g^{\,2}}{S_W}$$

Figure 84. Datcom Method for Gloved Panels

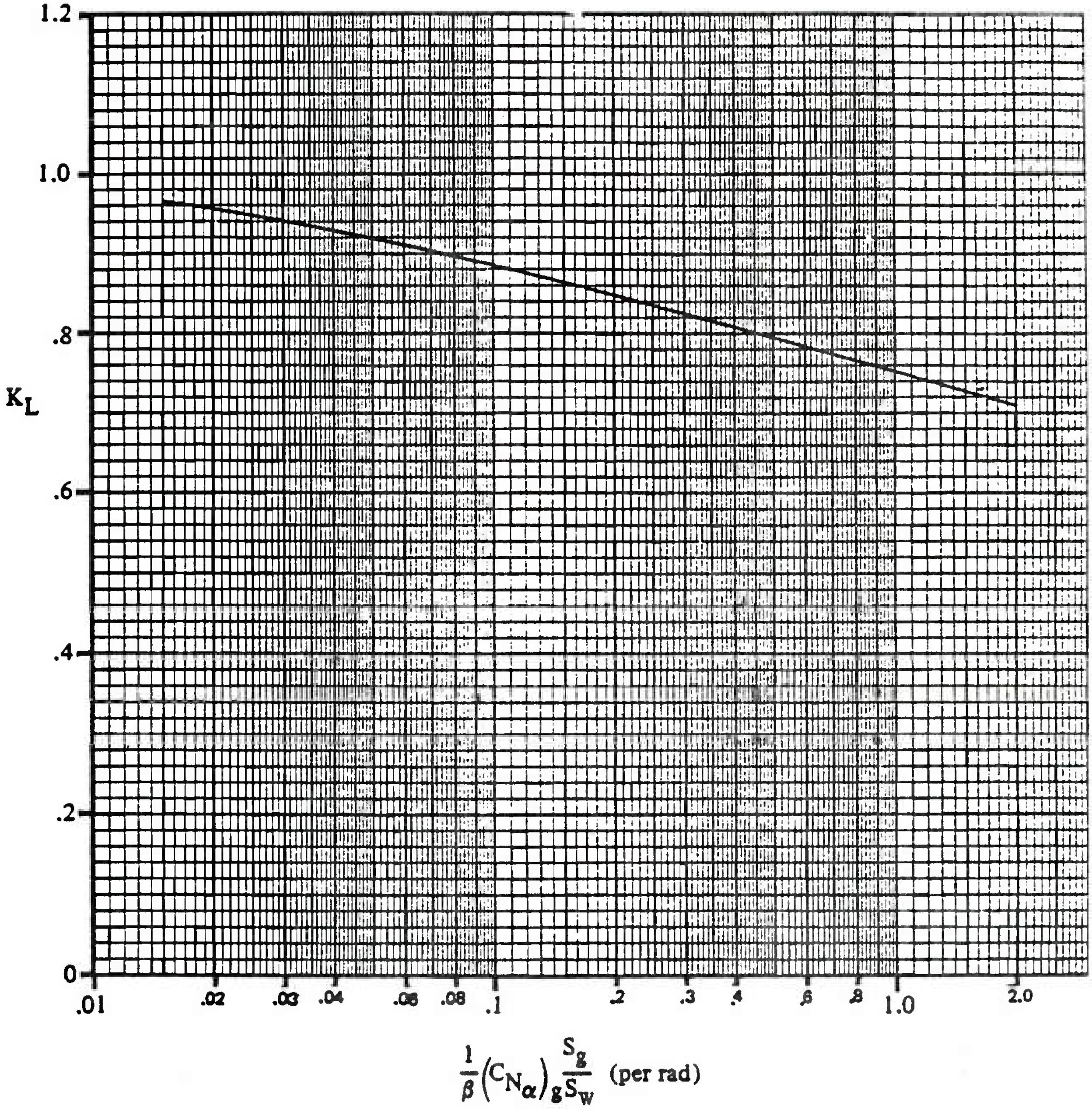

Figure 85. LIFT-INTERFERENCE FACTOR FOR NORMAL-FORCE-CURVE SLOPE AT SUPERSONIC SPEEDS

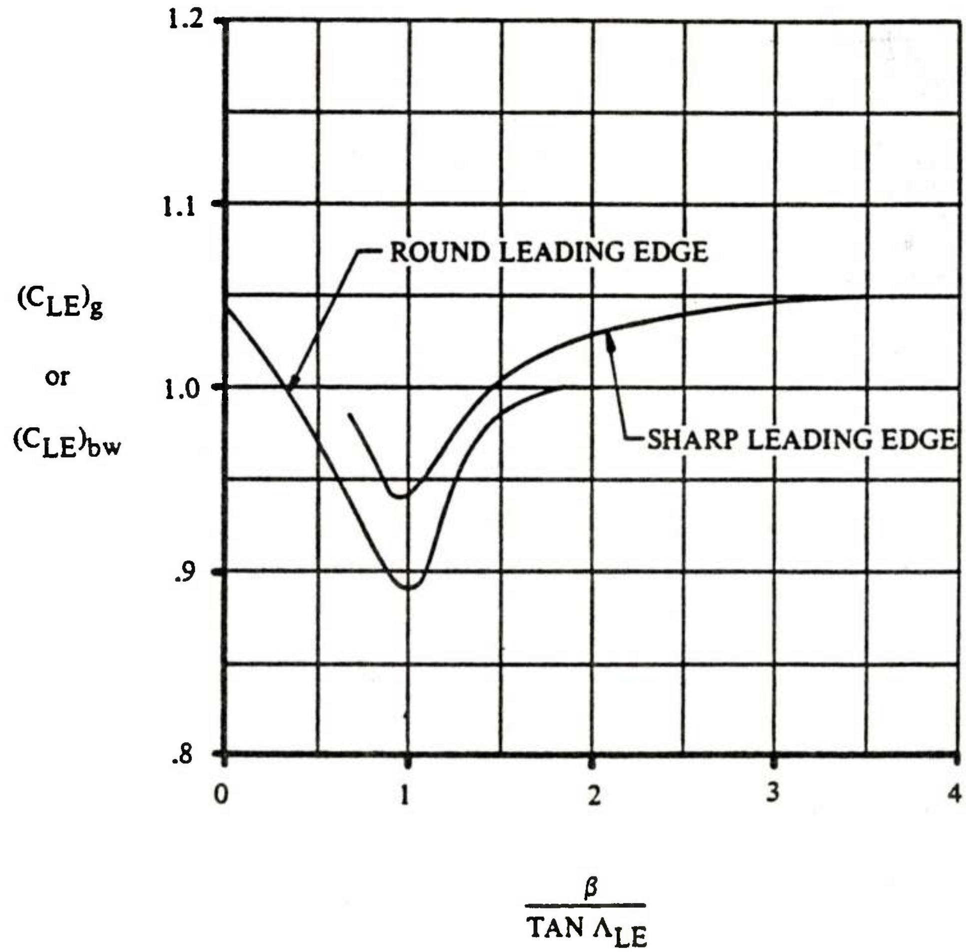

Figure 86. LEADING-EDGE-EFFECT FACTORS $(C_{LE})_g$ AND $(C_{LE})_{bw}$ FOR NORMAL-FORCE-CURVE SLOPE AT SUPERSONIC SPEEDS

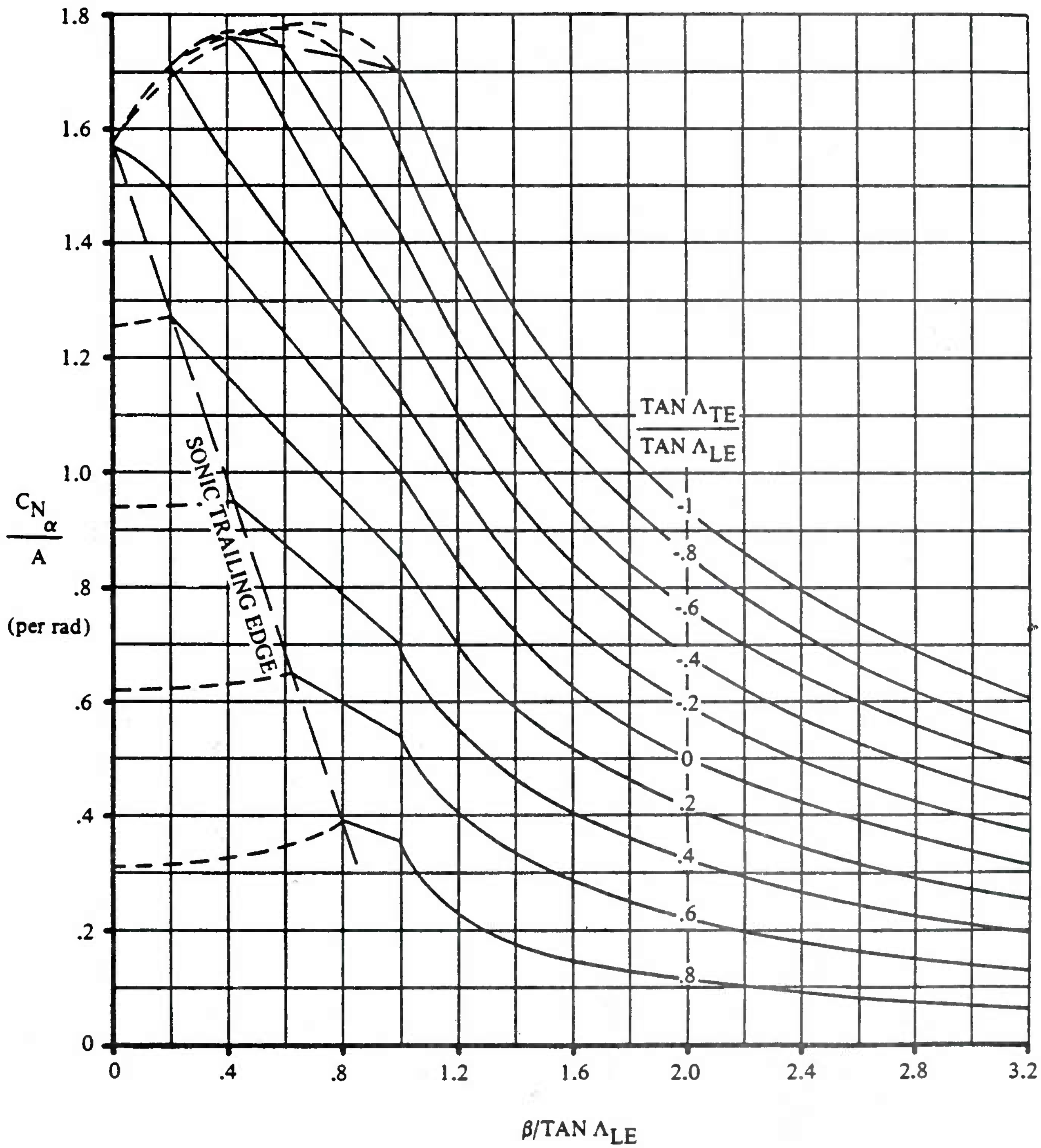

Figure 87. **WING SUPERSONIC NORMAL-FORCE-CURVE SLOPE,** $\lambda = 0$

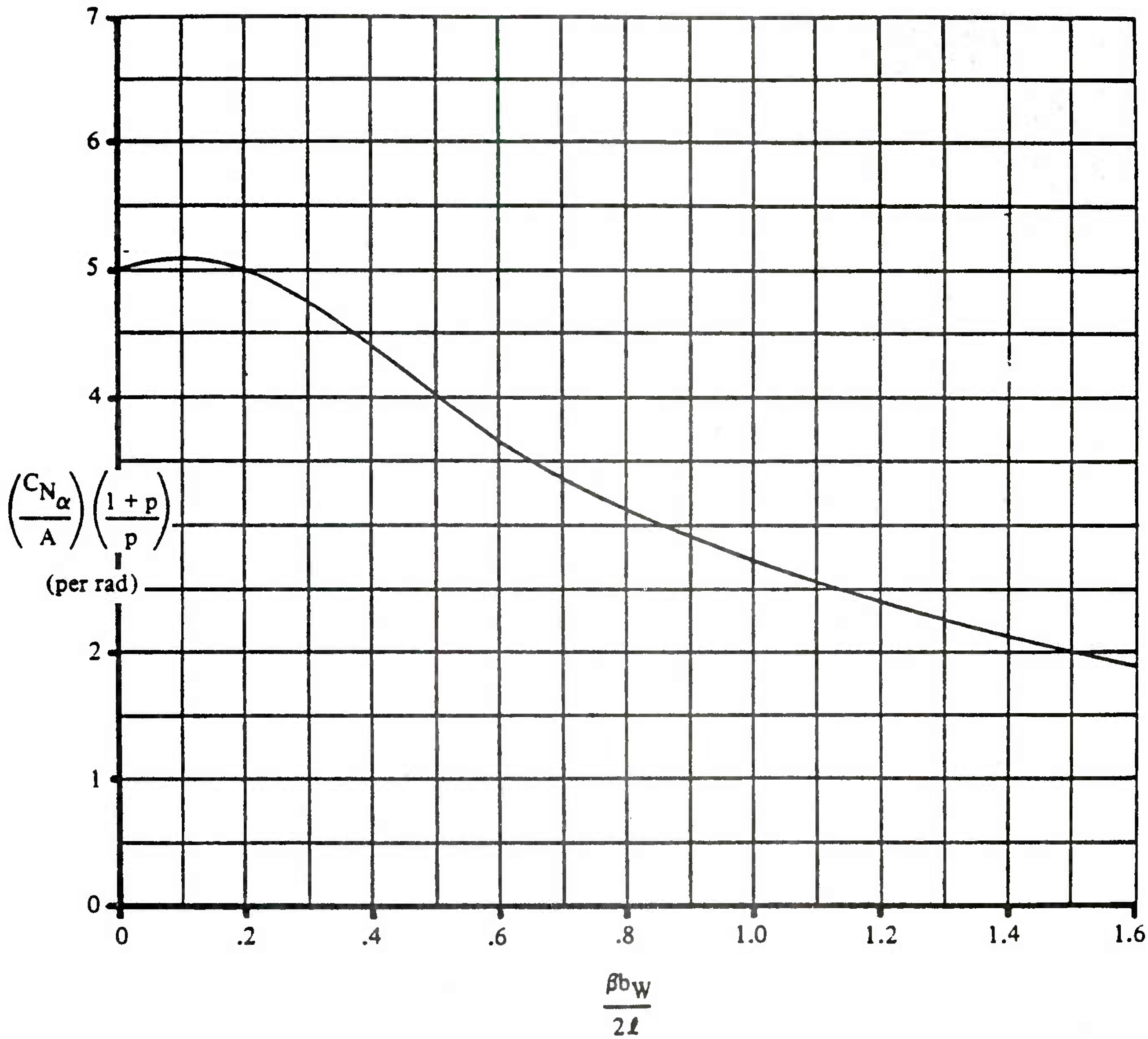

Figure 88. CORRELATION OF NORMAL-FORCE-CURVE SLOPE AT SUPERSONIC SPEEDS FOR GOTHIC AND OGEE PLANFORMS HAVING SHARP-NOSED AIRFOILS

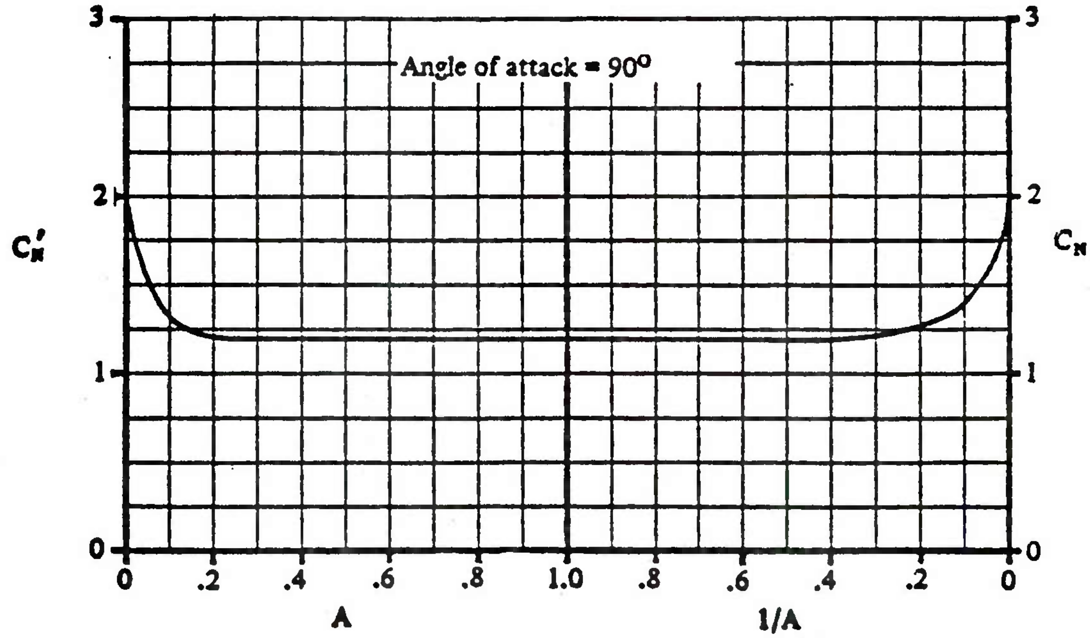

a) Subsonic Lift Variation with Wing Aspect Ratio at 90° Angle of Attack, Datcom.

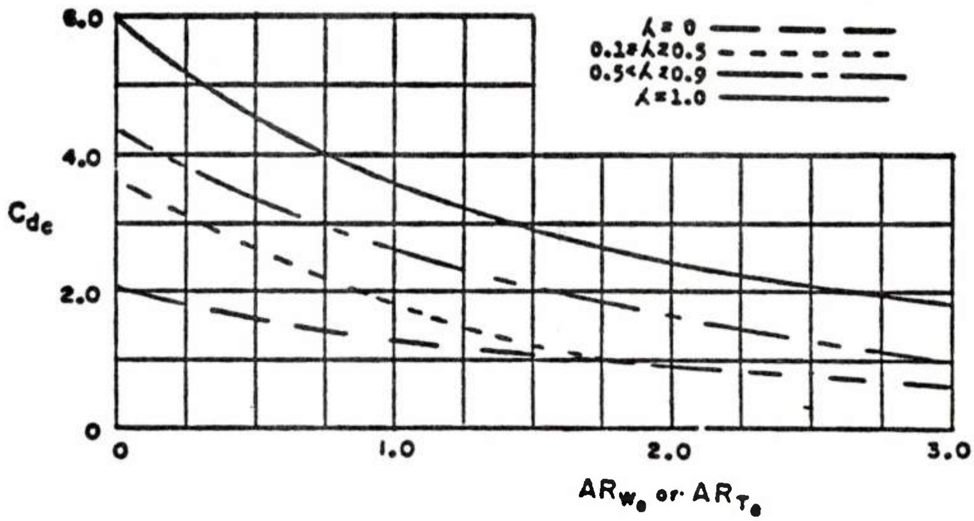

b) Eaton Fin Cross-Flow Drag

Figure 89. Methods for Fin Cross-Flow Drag

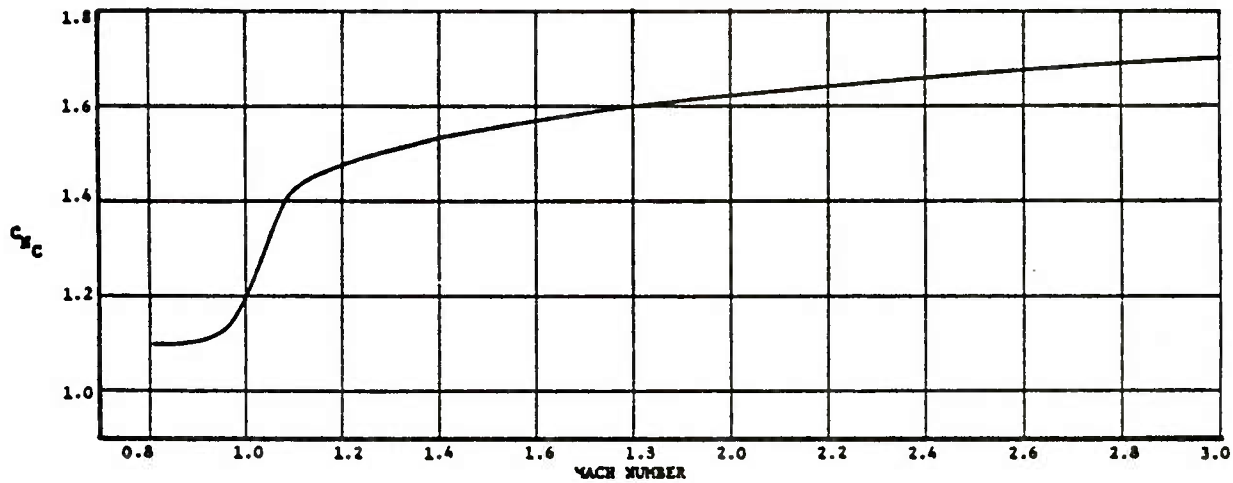

Variation of Fin Normal Force at α = 90 Degrees With Mach Number

c) Aiello Fin C_N in Normal Flow

Figure 89 (Continued)

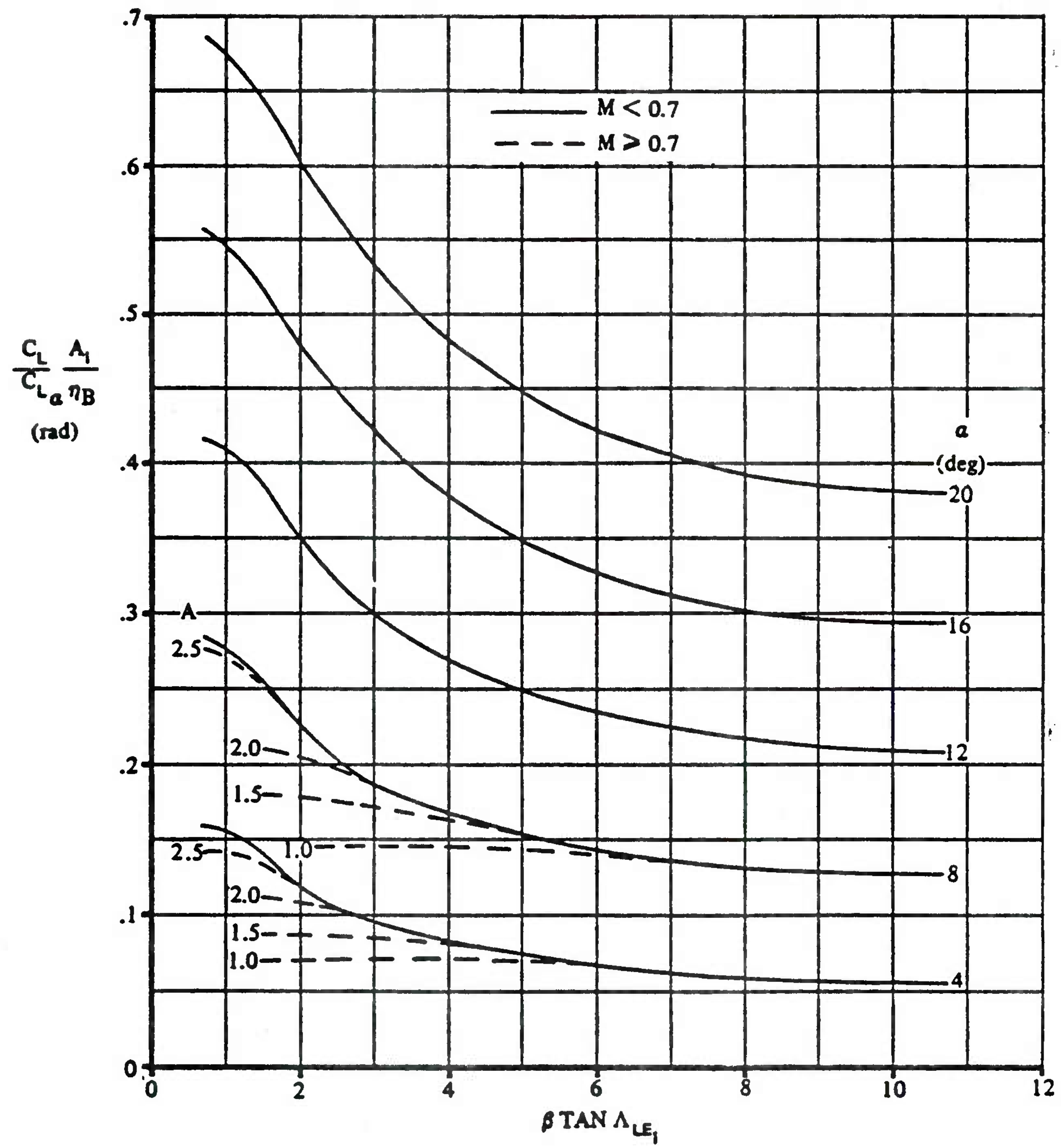

Figure 90. PREDICTION OF NONLINEAR LIFT OF DOUBLE-DELTA PLANFORMS AT SUBSONIC SPEEDS

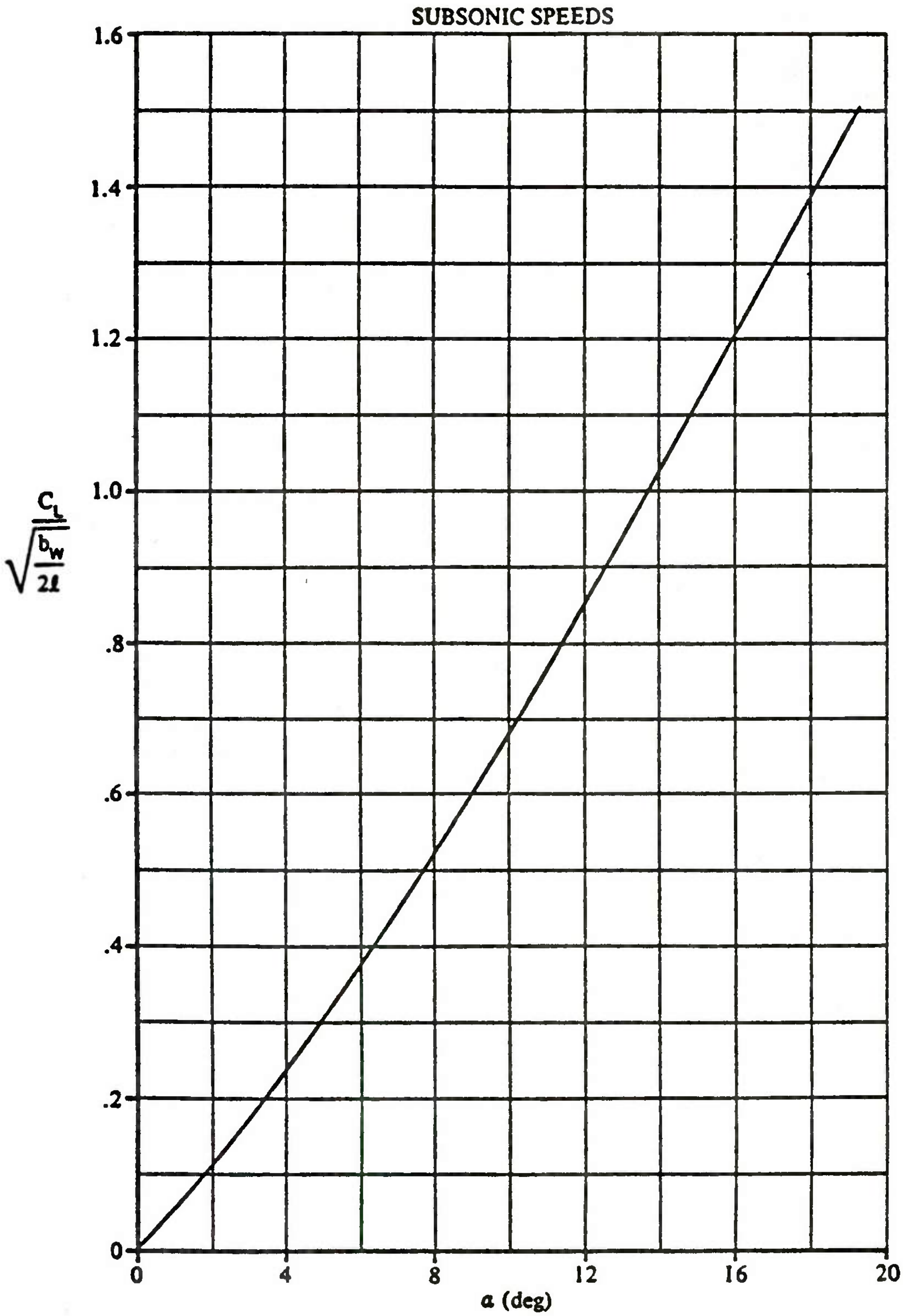

Figure 91. CORRELATION OF LIFT CURVES OF GOTHIC AND OGEE PLANFORMS

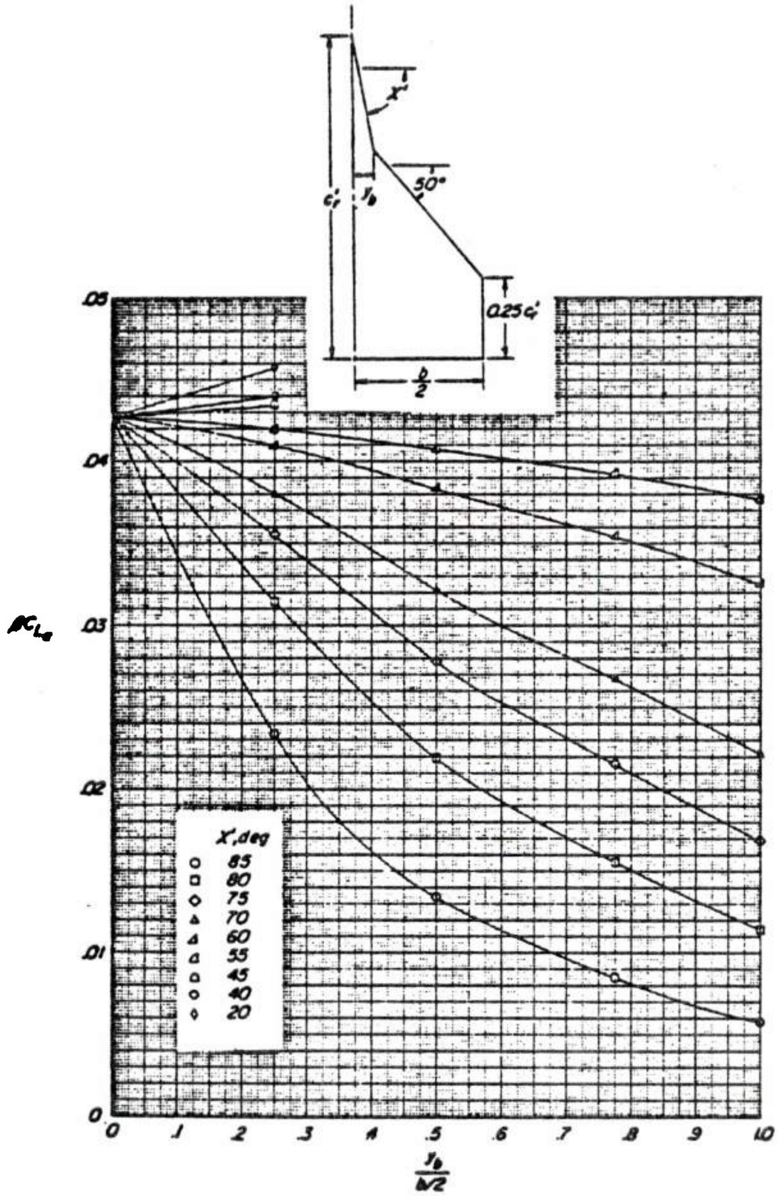

(b) Λ′ = 50°; λ = 0.25.

Figure 92. Subsonic Lift-Curve-Slope for Double-Delta Panels

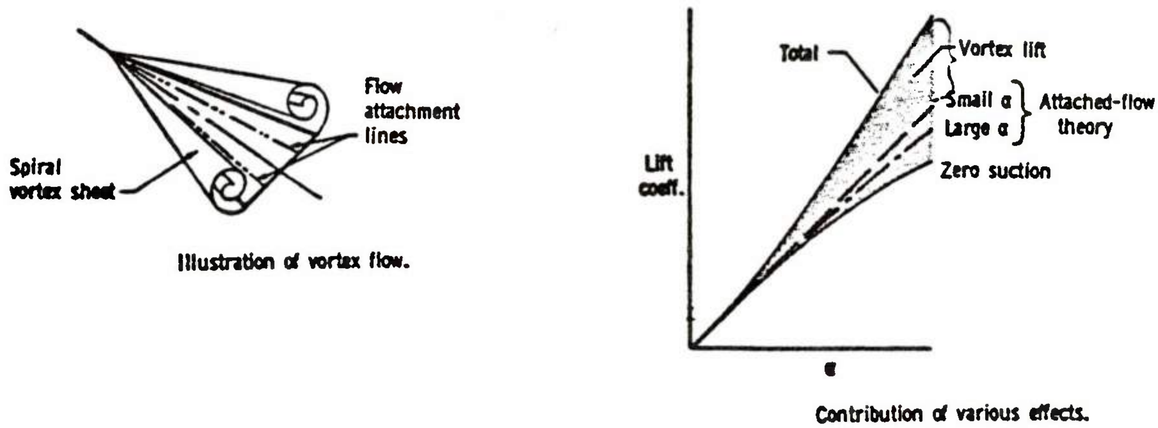

Illustration of vortex flow.

Contribution of various effects.

Figure 93. Polhamus Suction Analogy

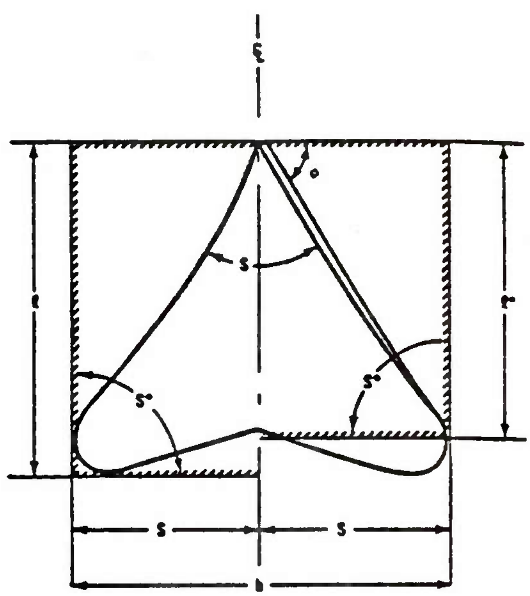

ρ:	ρ^*:
$\rho = \frac{S}{S^*}$ $S^* = b\ell$ ℓ = OVERALL LENGTH FROM APEX TO AFTMOST POINT ON TRAILING EDGE $\frac{s}{\ell}$ = WING SLENDERNESS PARAMETER $A = \frac{b^2}{S}$	$\rho^* = \frac{S}{S^*}$ $S^* = b\ell^* = \frac{b^2}{2} \tan\varphi$ ℓ^* = DISTANCE FROM APEX TO AFTMOST POINT OF MAXIMUM SPAN φ SWEEP OF SEMI SPAN DIAGONAL: $\tan\varphi = \frac{\ell^*}{s}$ $A = \frac{b^2}{S} = \frac{2}{\rho^* \tan\varphi}$

Figure 94. Panel Shape Parameter for "Goniometric Aerodynamics"

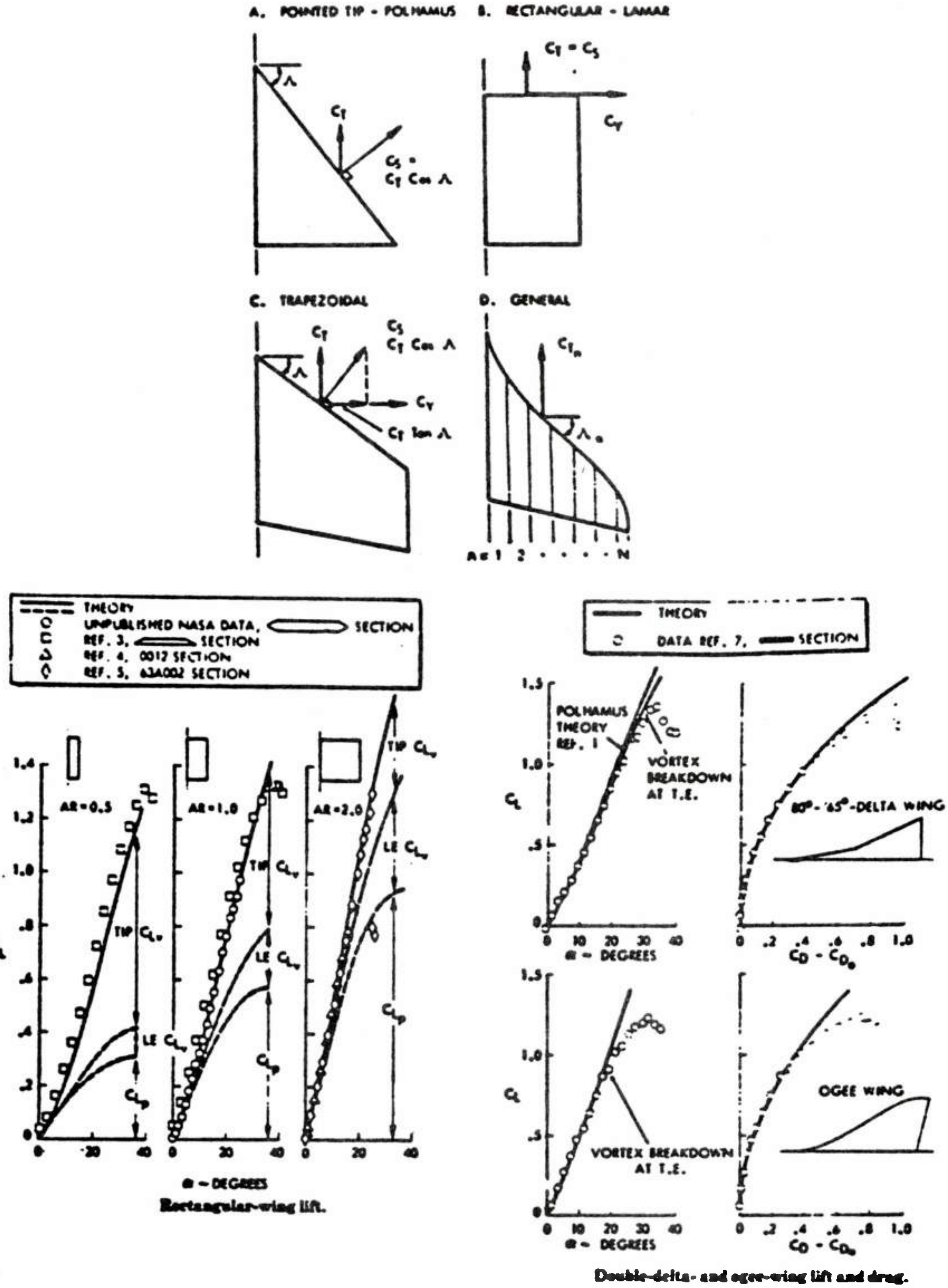

Figure 95. Results of Method From GD/Convair - Bradley

SUPERSONIC SPEEDS
SECTION CENTER OF PRESSURE

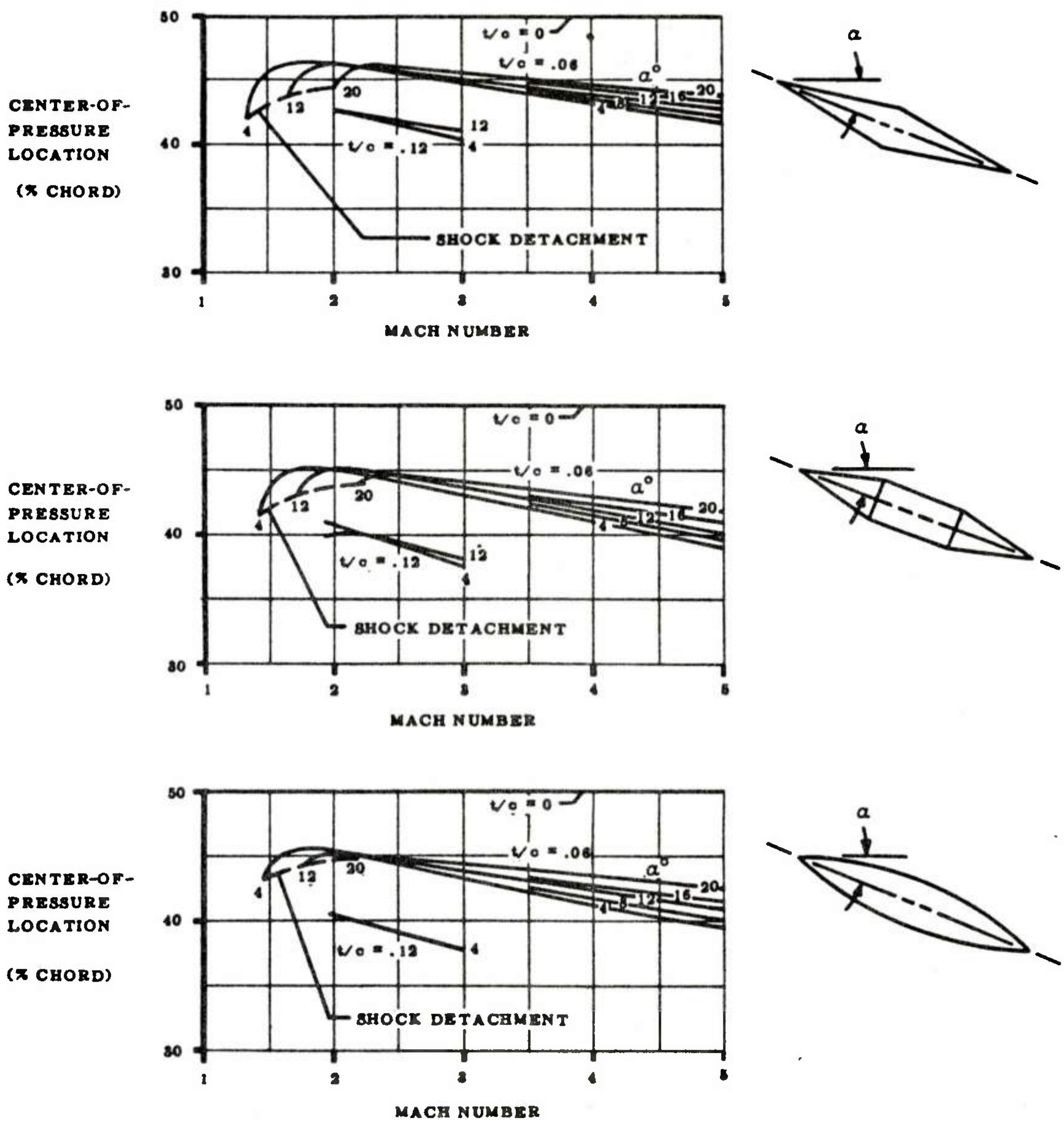

Figure 96. Effect of Thickness and Angle of Attack on Center of Pressure Location

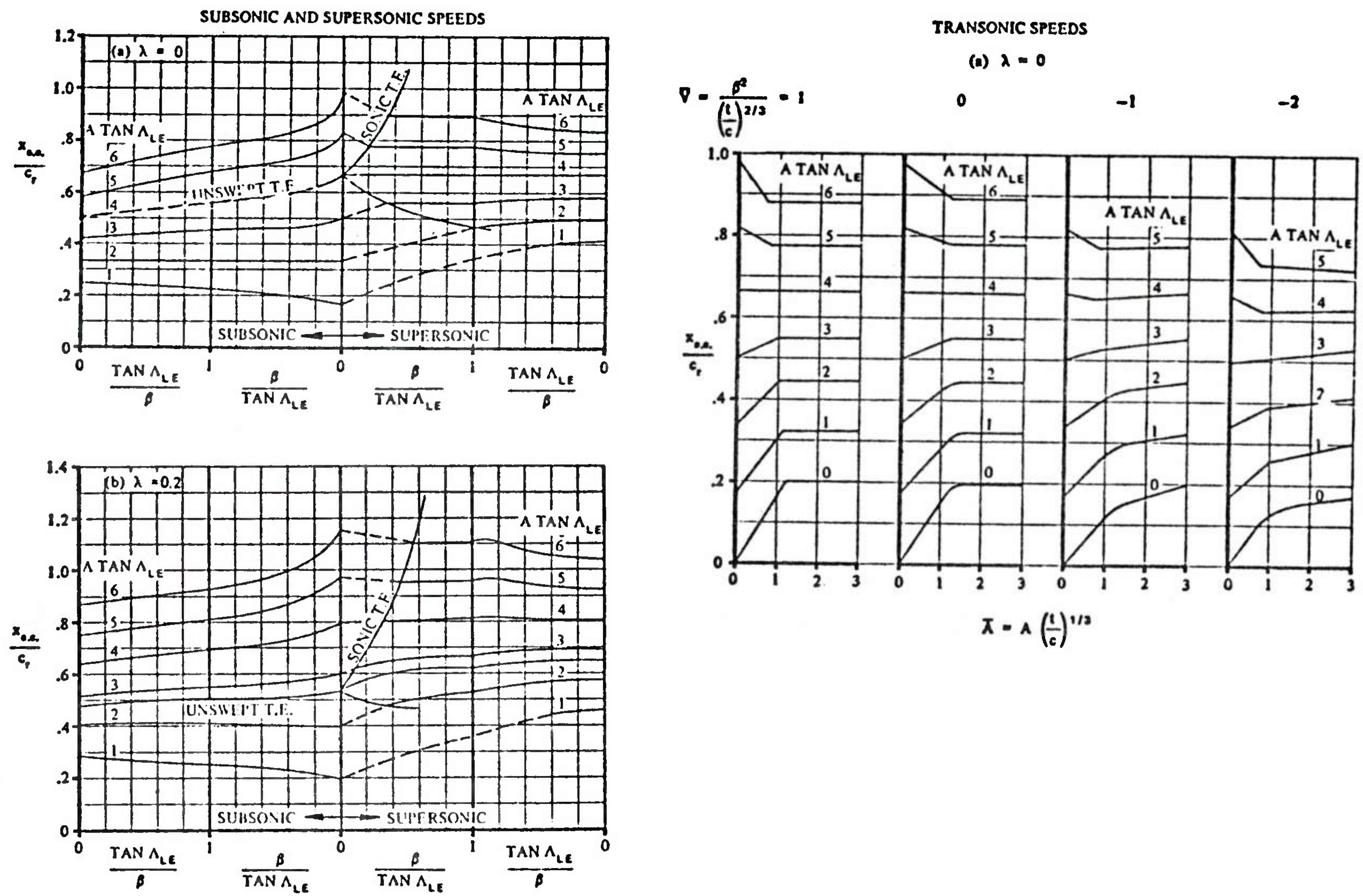

Figure 97. Datcom Charts for Panel Aerodynamic Center

SECTION 5
COMPONENT INTERFERENCE METHODOLOGY

5.1 INTRODUCTION

The component interference methodology is a critical concept in the build-up approach selected for Missile Datcom. These mutual interference effects are normally described as two separate phenomena, carryover interference and vortex interference. The methods available to evaluate each are discussed in the following sections.

5.2 CARRY-OVER INTERFERENCE

This section presents a summary of the methodologies for predicting non-vortical inteference effects on missile configurations. The interference prediction techniques available include body-fin and panel-panel interference for deflected and undeflected straight-tapered fins. Method development has emphasized interference effects on lift and center-of-pressure. However, some empirical methods model the effects of fin/afterbody combinations on axial force.

The development of prediction techniques for the interference among components of high speed missile designs began in the 1950's due to use of low aspect ratio fins on relatively large diameter bodies. The work of Pitts, Nielsen and Kaattari (PNK) published in 1957, Reference 167, presented an approach for calculating body-fin interference based on slender-body theory. The approach adopted for lift interference relates fin alone lift to combined body-fin lift by the factor K_C such that

$$K_C = (C_{L_\alpha})_{BW}/(C_{L_\alpha})_W$$

The interference factor K_C is handled by separately considering the interactions of the body and fin as a function of angle of attack and fin deflection. The individual interference effects are thus defined as

- $K_{W(B)}$ - fin interference due to body, variable angle of attack
- $K_{B(W)}$ - body interference due to fin, variable angle of attack
- $k_{W(B)}$ - fin interference due to body, variable fin incidence
- $k_{B(W)}$ - body interference due to wing, variable fin incidence

Figure 98 illustrates the influence regions used by PNK for a typical missile concept.

<u>Body/Wing Interference (no deflection)</u> - The angle of attack interference of the body on the wing is shown by slender body theory to be

$$K_{W(B)} = \frac{2}{\pi}\frac{\left\{\left(1+\frac{r^4}{s^4}\right)\left[\frac{1}{2}\tan^{-1}\frac{1}{2}\left(\frac{s}{r}-\frac{r}{s}\right)+\frac{\pi}{4}\right]-\frac{r^2}{s^2}\left[\left(\frac{s}{r}-\frac{r}{s}\right)+2\tan^{-1}\frac{r}{s}\right]\right\}}{\left(1-\frac{r}{s}\right)^2}$$

This factor is applicable at subsonic and supersonic speeds, small angle of attack (linear regime), and low aspect ratio fins of straight-tapered planform with non-swept trailing edges. To compute the fin influence on the body due to angle of attack, PNK derived a slender-body theory value of

$$K_{B(W)} = \frac{\left(1-\frac{r^2}{s^2}\right)^2-\frac{2}{\pi}\left\{\left(1+\frac{r^4}{s^4}\right)\left[\frac{1}{2}\tan^{-1}\frac{1}{2}\left(\frac{s}{r}-\frac{r}{s}\right)+\frac{\pi}{4}\right]-\frac{r^2}{s^2}\left[\left(\frac{s}{r}-\frac{r}{s}\right)+2\tan^{-1}\frac{r}{s}\right]\right\}}{\left(1-\frac{r}{s}\right)^2}$$

The interference factors $K_{W(B)}$ and $K_{B(W)}$ are shown in Figure 99 as determined by slender-body theory. It is interesting to note that whenever slender-body theory is used, the sum of these two factors can be expressed in terms of geometry by the relationship (Reference 171),

$$K_{W(B)} + K_{B(W)} = \left(\frac{d}{b} + 1\right)^2$$

When slender-body values were compared to the results from conical flow theory in supersonic flow for triangular, rectangular and trapezoidal planforms, differences were observed for certain Mach number/planform combinations. The conical lifting solutions were developed by assumming the planar model shown in Figure 100; the lift on the body was calculated by integrating pressures due to the half-fin over the influenced region of the infinite body. The resulting interference factor equation for a supersonic leading edge was found to be

$$K_{B(W)} = \frac{8\beta m}{\pi\sqrt{\beta^2m^2-1}\,(1+\lambda)\left(\beta\frac{d}{c_r}\right)\left(\frac{s}{r}-1\right)(\beta C_{L_\alpha})_W}\left\{\left(\frac{\beta m}{1+\beta m}\right)\left[\frac{(\beta m+1)\frac{\beta d}{c_r}+\beta m}{\beta m}\right]^2\cos^{-1}\left[\frac{1+(1+\beta m)\beta\frac{d}{c_r}}{\beta m+(\beta m+1)\frac{\beta d}{c_r}}\right]+\frac{\sqrt{\beta^2m^2-1}}{(\beta m+1)}\left[\sqrt{1+2\frac{\beta d}{c_r}}-1\right]-\frac{\sqrt{\beta^2m^2-1}}{\beta m}\left(\frac{\beta d}{c_r}\right)^2\cosh^{-1}\left(1+\frac{c_r}{\beta d}\right)-\frac{\beta m}{1+\beta m}\cos^{-1}\left(\frac{1}{\beta m}\right)\right\}$$

where

$m = \cot\Lambda_{LE}$

$m\beta > 1$

For subsonic leading edges the equation is

$$K_{B(W)} = \frac{16\left(\frac{\beta m}{1+m\beta}\right)^2}{\pi(1+\lambda)\left(\frac{\beta d}{c_r}\right)\left(\frac{s}{r}-1\right)(\beta C_{L_\alpha})_W}\left\{\left[\frac{\beta m+(1+m\beta)\frac{\beta d}{c_r}}{\beta m}\right]^{3/2}+\left[\frac{\beta m+(1+m\beta)\frac{\beta d}{c_r}}{\beta m}\right]^{1/2}-2-\left[\frac{(1+m\beta)\frac{\beta d}{c_r}}{m\beta}\right]^2\tanh^{-1}\sqrt{\frac{\beta m}{\beta m+(1+m\beta)\frac{\beta d}{c_r}}}\right\}$$

where

$m\beta<1$

When the body is cut at the fin trailing edge, the solution yields the following equations,

$$K_{B(W)}[\beta(C_{L_\alpha})_W](\lambda+1)\left(\frac{s}{r}-1\right)=$$

$$\frac{8}{\pi\sqrt{\beta^2m^2-1}}\left(\frac{\beta d}{c_r}\right)\left[\left(1+\frac{mc_r}{d}\right)^2\cos^{-1}\left(\frac{m\beta+\frac{c_r}{\beta d}}{1+\frac{mc_r}{d}}\right)-\right.$$

$$m^2\beta^2\left(\frac{c_r}{\beta d}\right)^2\cos^{-1}\left(\frac{1}{m\beta}\right)+m\beta\left(\frac{c_r}{\beta d}\right)^2\sqrt{m^2\beta^2-1}\,\sin^{-1}\frac{\beta d}{c_r}-$$

$$\left.\sqrt{m^2\beta^2-1}\,\cosh^{-1}\frac{c_r}{\beta d}\right];\ \beta m>1,\ \frac{c_r}{\beta}>d$$

$$K_{B(W)}[\beta(C_{L_\alpha})_W](\lambda+1)\left(\frac{s}{r}-1\right)=$$

$$\frac{16\sqrt{m\beta}}{\pi(m\beta+1)}\left(\frac{\beta d}{c_r}\right)\left\{\left(1+\frac{mc_r}{d}\right)\sqrt{\left(\frac{c_r}{\beta d}-1\right)\left(\frac{mc_r}{d}+1\right)}-\right.$$

$$\left(\frac{c_r}{\beta d}\right)^2(m\beta)^{3/2}+m\beta\left(\frac{c_r}{\beta d}\right)^2(\beta m+1)\left[\tan^{-1}\sqrt{\frac{1}{\beta m}}-\right.$$

$$\left.\tan^{-1}\sqrt{\left(\frac{c_r}{\beta d}-1\right)\Big/\left(\frac{mc_r}{d}+1\right)}\right]-\frac{(m\beta+1)}{\sqrt{m\beta}}\tanh^{-1}$$

$$\left.\sqrt{m\beta\left(\frac{c_r}{\beta d}-1\right)\Big/\left(\frac{mc_r}{d}+1\right)}\right\};\ \beta m<1,\ \frac{c_r}{\beta}>d$$

Design charts developed for these solutions are shown in Figure 101, for the full afterbody and the no afterbody conditions.

Since the assumption of conical flow assumes that no Mach lines emanating from the fin tip leading edge projects into the body region of fin interference, this condition then establishes the following criteria for selecting $K_{B(W)}$ between slender-body theory and conical flow theory for triangular and non-triangular planforms in supersonic flow:

TRIANGULAR PLANFORMS	$\beta A\leq 1$	Slender-body theory
	>1	Conical flow theory
NONTRIANGULAR PLANFORMS	$\beta A(1+\lambda)\left(\frac{1}{\beta m}+1\right)$	
	≤ 4	Slender-body theory
	>4	Conical Flow theory

The body-fin carryover interference for the case of a low aspect ratio delta wing mounted on a conical body has been determined by Spreiter, Reference 169. This slender-body theory solution correlates well with experimental data throughout the speed range. Figure 102 is reproduced from Datcom and presents the interference factor $K_{(WB)}$ such that

$$K_{(WB)} = (C_{L_\alpha})_{WB}/(C_{L_\alpha})_W$$

The work of PNK was extended by Vukelich and Williams, Reference 170, to avoid the inaccuracy of interpolating between full and no afterbody interference values. This was done by changing the conical flow theory integral limits to match the physical situation. The integral limits for general afterbodies are described in Figure 103.

<u>Body/Fin Interference (with deflection)</u> - PNK used slender-body theory to determine body interference on a fin for variable fin incidence at α=0 to be

$$k_{W(B)} = \frac{1}{\pi^2}\left[\frac{\pi^2}{4}\frac{(\tau+1)^2}{\tau^2} + \frac{\pi(\tau^2+1)^2}{\tau^2(\tau-1)^2}\sin^{-1}\frac{\tau^2-1}{\tau^2+1} - \frac{2\pi(\tau+1)}{\tau(\tau-1)} + \right.$$

$$\left.\frac{(\tau^2+1)^2}{\tau^2(\tau-1)^2}\left(\sin^{-1}\frac{\tau^2-1}{\tau^2+1}\right)^2 - \frac{4(\tau+1)}{\tau(\tau-1)}\sin^{-1}\frac{\tau^2-1}{\tau^2+1} + \frac{8}{(\tau-1)^2}\log\frac{\tau^2+1}{2\tau}\right]$$

The effect of fin incidence on body carryover lift is derived from the reciprocal theorem of Reference 150 which states that for cylindrical body/fin combinations the following equality is valid under the assumptions of slender-body theory,

$$k_{B(W)} = K_{W(B)} - k_{W(B)}$$

The slender-body values of incidence interference are presented in Figure 104. Corresponding linear theory values are shown in Figure 105 for rectangular fin-body combinations. Slender-body values are used for all fins except rectangular planforms where $\beta A>2$ in supersonic flow.

Empirical values of body-fin interference due to deflection (k_W) are available in tabular form (Reference 141) for the transonic Mach numbers (0.8-1.3) and is assumed constant for all deflections and fin characteristics due to lack of available data. Between Mach 1.3 and 3.36 the lack of data has led Nielsen to suggest the following relationships due to the similarity rule (SBT=slender-body theory):

If $K_W > (k_W)_{SBT}$ THEN $k_W = (k_W)_{SBT}$

If $K_W < (k_W)_{SBT}$ THEN $k_W = K_W$

Above Mach 3.36, slender-body $(K_W)_{SBT}$ values are always used.

<u>Center of Pressure</u> - The PNK theory assumes the fin center of pressure is unaffected by carryover except for two special cases for which solutions have been obtained. One case is for rectangular fins for which Figure 106 presents the center of pressure variation at supersonic speeds as derived by linear theory, Reference 167. This method is valid for $4 > \beta A > 2$. outside this range are considered equal to fin alone variations. Figure 107 presents the case of triangular planform fins with no trailing edge sweep as derived from slender-body theory.

The supersonic center of pressure on the body due to the presence of a fin was derived by PNK from conical flow theory. For supersonic fin leading edges, the result is

$$M_{B(W)} = \frac{4q_\infty \alpha_W m}{3\pi\beta} c_r^3 \Bigg\{ \sqrt{1+\frac{2\beta d}{c_r}} \left[\frac{2m\beta+5}{3(m\beta+1)^2} + \frac{\beta d/c_r}{3(m\beta+1)} - \frac{(\beta d/c_r)^2}{\beta m}\right] + \frac{1}{\sqrt{m^2\beta^2-1}} \left[\left(1+\frac{\beta d}{c_r}\right)^3 - \frac{(\beta d/c_r)^3}{m^2\beta^2} - \frac{1}{(1+m\beta)^2}\right] \cos^{-1}\left[\frac{1+\frac{\beta d}{c_r}(m\beta+1)}{m\beta+\frac{\beta d}{c_r}(m\beta+1)}\right] + \left(\frac{\beta d}{c_r}\right)^3 \frac{1}{m^2\beta^2} \cosh^{-1}\left(1+\frac{c_r}{\beta d}\right) - \left[\frac{2m\beta+5}{3(m\beta+1)^2}\right] - \frac{\left[1-\left(\frac{1}{m\beta+1}\right)^2\right]}{\sqrt{m^2\beta^2-1}} \cos^{-1}\frac{1}{m\beta} \Bigg\}$$

For wings with subsonic leading edges the relationship is,

$$M_{B(W)} = \frac{4q_\infty \alpha_W}{\pi\beta^2} c_r^3 \Bigg\{ \frac{\sqrt{m^2\beta^2 + m\beta(m\beta+1)\frac{\beta d}{c_r}}}{9m\beta(m\beta+1)^3} \left[(8m\beta+24)m^2\beta^2 + (14m\beta+6)(m\beta+1)m\beta\frac{\beta d}{c_r} + 3(m\beta-3)(m\beta+1)^2\left(\frac{\beta d}{c_r}\right)^2\right] - \frac{(8m\beta+24)m^2\beta^2}{9m\beta(m\beta+1)^3} - \frac{(m\beta-3)}{3m\beta}\left(\frac{\beta d}{c_r}\right)^3 \cosh^{-1}\sqrt{\frac{m\beta+(m\beta+1)\frac{\beta d}{c_r}}{(m\beta+1)\frac{\beta d}{c_r}}} \Bigg\}$$

Hence, the center of pressure for fin interference on the body is defined by

$$\left(\frac{\bar{x}}{c_r}\right)_{B(W)} = \frac{M_{B(W)}}{K_{B(W)} L_W c_r}$$

The PNK derived body interference center of pressure between full and no afterbody cases were improved for finite afterbodies by the same approach illustrated in Figure 103.

For subsonic body center of pressure due to the presence of a fin, PNK offers an approximate method based on lifting-line theory. This method projects an image quarter-chord line with elliptical loading onto the body in the cross-flow plane. The resulting equation is,

$$\bar{x}_{B(W)}=\frac{c_r}{4}+(s-r)\tan\Lambda_{1/4}\left[\frac{r}{r-s}+\frac{\sqrt{s(s-2r)}\cosh^{-1}\left(\frac{s-r}{r}\right)-(s-r)+\frac{\pi r}{2}}{\frac{(s-r)r}{\sqrt{s(s-2r)}}\cosh^{-1}\left(\frac{s-r}{r}\right)+\frac{(s-r)^2}{r}-\frac{\pi}{2}(s-r)}\right];s>2r$$

and is valid for $\beta A \geq 4.0$ and $r/s \leq 0.5$. Extrapolation up to $r/s=0.8$ gives good results. When $\beta A<4.0$, the interference center of pressure is obtained by interpolating from the slender-body value at $\beta A=0$. The theoretical $\beta A=0$ aerodynamic-center locations are shown in Figure 108 from Datcom. Other values are obtained from Figure 109.

The work of PNK is the basis for methods to determine body-fin interference for missile configurations today. An improvement to the method was made by Moore in Reference 172 when he extended the approach to handle fins with swept trailing edges. Figure 110 illustrates the procedure for determining interference lift using slender-body theory for swept trailing edge fins. The approach defines a pseudo-panel which can be analyzed using slender-body theory. It is assummed that the interference lift is concentrated at the wing root. Hence, the interference lift is directly proportional to the actual chord-to-pseudo-chord fraction. Although this seems like a rather sever assumption, there is good agreement with experimental data. The technique is described by the following equations:

$$[K_{B(W)}]_{II}=[K_{B(W)}]_I G$$

$$[K_{W(B)}]_{II}=1+([K_{W(B)}]_I-1)G \qquad G=C_{r_{II}}/C_{r_I}$$

$$[k_{W(B)}]_{II}=1+([k_{W(B)}]_I-1)G$$

$$[k_{B(W)}]_{II}=([K_{W(B)}]_I-[k_{W(B)}]_I)G$$

Although the PNK results are generally limited to angles of attack less than ten degrees, and deflection angles less than 15 degrees, it is recommended that they be used in lieu of empirical results. Adequate theoretical methods do not exist at higher angle of attack or deflection angles.

<u>Effect of Angle of Attack</u> - Empirical techniques for calculating fin-body interference have been developed. These approaches reduce appropriate increments for normal force and moment interference from test data of body and fin alone at angle of attack. Examples of this type approach are that of Baker (AEDC), Reference 74, Aiello (Martin Marietta), Reference 58, and Nielsen, Reference 141. These approaches are limited by the bounds of the data available which are summarized in Figure 111. It is important to note that these data do cover angles of attack well outside the linear range assumed

for slender-body and linear theory and thus provide the non-linear effect of angle of attack. Typical angle of attack effects on body-fin interference are shown in Figure 112. The trends are very nonlinear at intermediate angles of attack, even showing adverse interference on the wing at certain conditions. These effects must be handled empirically since no theoretical methods are available. The empirical data base should be expanded further to include a greater range of applicability.

Panel-Panel Interference - The theoretical methods described to this point assume planar fin orientation, and only reflect small angle of attack effects. The next step in the interference analysis determined the impact of cruciform fins and out of plane effects ($\beta,\phi \neq 0$). An approach to the analysis of arbitrarily deflected cruciform fins at angle of attack and roll has been developed by Nielsen, Reference 141 and is termed the "equivalent angle of attack" (α_{eq}) concept. The term α_{eq} is defined as that angle of attack of the fin alone for which its normal force is that of the "influenced" fin accounting for the various interference effects. The differences between planar and cruciform configurations is panel-panel interference which results from a coupling of the sidewash velocities due to angle of attack and sideslip.

The panel-panel interference due to fin deflection of other cruciform fins has been calculated using slender-body theory as an incremental α_{eq}, and is presented in Figure 113. All fins are assumed to be within each others region of influence at subsonic and transonic Mach numbers. For supersonic flow, a technique is provided that determines the ratio of area of influence of a fin to the total fin area. The application of the equivalent angle of attack approach to data within the data base has shown reasonable ability to duplicate fin nonlinearities at angle of attack and arbitrary roll as shown in Figure 114.

An approach similar in concept to α_{eq} is that of Oberkampf, Reference 159. Figure 115 defines the relevant geometry. An effective leading edge sweep angle is determined for each fin by the relationship,

$$\tilde{\Lambda}_{le} = \cos^{-1} (\cos^2 \phi \cos \Lambda_{le} - \sin \alpha_b \sin \phi \sin \Lambda_{le} + \cos \alpha_b \sin^2 \phi \cos \Lambda_{le})$$

This expression, and one for the trailing edge effective sweep angle, result is an effective aspect ratio defined by,

$$\bar{A} = \frac{4}{\frac{2\,c_r}{b_o - a}\left[\frac{\cos \Lambda_{\ell e}}{\cos \bar{\Lambda}_{\ell e}}\right]^2 + \tan \bar{\Lambda}_{te} - \tan \bar{\Lambda}_{\ell e}}$$

Oberkampf applied the effective aspect ratio to a subsonic lift technique based on the Polhamus Suction Analogy with mixed results. Figure 116 shows that the α_{eq} approach of Nielsen predicted better roll characteristics than the equivalent aspect ratio concept of Oberkampf in the roll angle regime of most interest. The α_{eq} approach is preferred.

Another multi-fin interference approach has been proposed by Darling, Reference 89. He suggests the lift increase due to the addition of fins to a cruciform arrangement should be,

	Subsonic	Supersonic
$(C_{N_\alpha})_{6FINS}/(C_{N_\alpha})_{4FINS}$	1.37	1.50
$(C_{N_\alpha})_{8FINS}/(C_{N_\alpha})_{4FINS}$	1.62	2.00

However, six or eight fin panels in combination are rare. Since the effect of body radius to span ratio can be substantial, it is recommended that these results be used as a first approximation.

Fin Gaps - Gaps between the fin root and the body mold line cannot be avoided with all movable control surfaces. Limited results from tests has shown that the decrease in body/fin carryover is relatively small for typical gap widths. No method is recommended to account for fin/body gaps, but reference to typical experimental results, as a design guide, are recommended for inclusion in Missile Datcom.

Body Ellipticity - Although the PNK results have been formulated for circular bodies, they are often applied to other body shapes as well. The body width at the fin panels is chosen as the body diameter for the carryover calculations. Krieger, Reference 49, has used the method of Jorgensen to determine the effect of elliptical bodies; the ratio $(C_{N_{WB}})_{ELLIP}/(C_{N_{WB}})_{CIR}$ was computed and has been shown to correlate well with test results. It is recommended that this approach be used in Missile Datcom.

Interference Drag - A limited amount of methodology is available for boattail-base-fin interference. Darling provides an approach to determine the effect of a boattail on subcaliber fin lift at subsonic speeds; a subcaliber fin is one whose span is less than the maximum body diameter, such as a small fin on a boattail. The fin effectiveness is reduced by a factor which depends on the fin nose bluntness. The fin lift is calculated using the boattail diameter for carryover purposes, then is modified empirically by the factor $K_{f(SC)}$ as shown in Figure 117.

Two empirical techniques are available that modify base drag due to the presence of tail fins. Reference 14 suggests the change in base drag is a function of fin thickness-to-chord ratio and Mach number such that

$$\Delta C_{D_{BASE}} = (t/c)_f \ (0.825/M^2 - 0.05/M)n$$

where n = number of fins

in the range $1.4 \leq M \leq 2.8$

Moore, Reference 172, gives the change in base drag to be

$$(\Delta C_{P_B})_f = -[(\Delta C_{P_B}/(t/c)]_{m=M_f}[(t/c) - 0.1x/c]; \qquad t/c \geq 0.1x/c$$

$$(\Delta C_{P_B})_f = 0; \qquad t/c < 0.1\,x/c$$

This approach is empirical and assumes the fins are flush with the base. Figure 118 shows the Mach number trend and the means to extrapolate the results for non-flush mounted fins. This method is recommended.

Summary - The primary areas of concern for methods development or improvement are in the area of high angle of attack carryover and panel-panel interference for generalized body-fin combinations. The theoretical methods presented here are generally applicable to typical missile configurations at angles of attack of 10° or less and fin deflection angles of 15° or less. The results of Hill and Kaattari, Reference 173, are presented in Figure 119, and shows the non-linear behavior at high angles of attack and incidence. Enough data is available to develop empirical nonlinear methods for typical low aspect ratio fin-body combinations. Additional data should be sought to extend the applicability of such a method even further. Being able to predict this nonlinear behavior is crucial to configuration stability and control

analysis at high angles of attack. Most configurations utilize the fully-movable panel for control and therefore require adequate definition of carry-over nonlinearities. In addition, only planar or curciform panels (panels 90 degrees apart) are treated. There are few methods available which describe the influence of other panel arrangements, such as tri-form or arbitrary dihedral angle cruciform panels. One may use the inertial coefficients derived by Nielsen in the text "Missile Aerodynamics", Reference 12, and determine the approximate effect from slender body theory. This has been done and the results are presented in Figure 120 in a ratioed form to that for a cruciform configuration in the "plus" orientation.

It is recommended that a mix of PNK theoretical and other empirically derived results for carryover be incorporated in Missile Datcom. The deficiency in methods due to high angle of attack or panel incidence should be corrected for maximum accuracy and utility of Missile Datcom.

Methods could not be found which address carryover interference of non-straight tapered panels or those panels which are swept-forward. These designs are not at all uncommon in missile design today. It is recommended that these deficiencies be corrected.

5.3 VORTEX INTERFERENCE

In analyzing configurations, the effect of vortices is an important aerodynamic consideration that cannot be neglected. Four specific tasks must be performed to analyze the vortex effects as follows:

a) Position of vortex shedding, either position on the body or span location on the wing

b) Wing produced flowfields; the wing flowfield can be modeled as a flat sheet downwash field, as a fully-rolled-up line vortex, or in combination.

c) Vortex tracking; mapping the vortex position through the flowfield and determining its proximity to the configuration

d) Vortex strength; determination of the vortex circulation strength

Figure 121 illustrates the number and type of vortex interactions which occur for a typical missile design. Vortices generated by the body influence any fins present (the effect on the body aft of the separation point is accounted for through use of viscous cross flow), whereas fin produced vortices influence both the body and any aft lifting surfaces. The system

of vortices can get extremely complex through addition of inlets, launch lugs, conduits or even body shape. Axisymmetric bodies without protuberances have been explored in sufficient detail to develop methodology to track and determine the strength of the body nose vortices. The method in Datcom Section 4.3.1.3 and the empirical correlations of Nielsen, briefly presented in Figure 122, illustrate the methods in use. No design methods are available for general shaped configurations.

The vortex effect of forward lifting surfaces has also been explored in detail. The first such efforts were presented by Sprieter and Sacks, Reference 175, in 1951 and Decker, Reference 174, in 1956. These methods considered the downwash behind wings and characterized the vortex effect as either a sheet or a fully-rolled up vortex core. The presence of a vortex sheet is dependent upon panel aspect ratio; the roll-up into a vortex is inversely proportional to aspect ratio and directly proportional to lift. For larger aspect ratio panels, or low lift coefficients, the wing will shed a trailing vortex sheet which slowly rolls into a fully developed vortex core at angle of attack. Since missile panels are frequently low aspect ratio, it is appropriate to consider only the fully-rolled vortex concept, which was explored in detail by Pitts, Nielsen and Kaattari in NACA 1307 (Reference 167). However, for cruise missiles, or other aircraft-type designs, the "sheet" concept is appropriate and the Datcom method should be retained for that purpose.

The method of NACA 1307 is highly appropriate for classical missile configurations. Single vortex cores are shed from each panel and trail aft approximately along the free-stream velocity vector and, hence, are dependent upon the total angle of attack. Since the method of NACA 1307 assumes fin panels on both sides of the body, the vortex effect on one panel at dihedral must be handled with care. A method available to perform this task is presented in Datcom and shown in Figure 123. This process assumes that superposition of multiple vortex effects can be performed. In reality, the vortices interact with each other and do not necessarily follow the free-stream velocity vector at angle of attack. Simulations of these vortex tracks should provide more accurate results. It has not been determined what degree of accuracy improvement is realized compared to computing costs. Such a determination is beyond the scope of this study, but should be quantified during the development efforts. Since the vortices tend to

follow the velocity vector, track nearly parallel to the chord of a lifting surface in close proximity, and continue aft, it may be possible to devise a simple but suitably accurate method using such observations, particularily for those configurations involving tandem lifting surfaces where otherwise the mathematics can be extremely complex.

As illustrated in Figure 124, a body at angle of attack sheds a number of vortices which have been observed to separate at predictable positions along the body. These body vortices can be significant for tail orientations other than cruciform "plus" or at mixed angle of attack and sideslip angle. Figure 125 illustrates the panel local angle of attack for both the vortex free and vortex present cases. For leeside flow conditions the total vortex effects results in as much as a 12 deg. change in local angle of attack. The magnitude of error induced in neglecting the afterbody vortices is unknown, though expected to be significant at the higher angles of attack. A more significant question in this highly empirical regime is the justification of its incorporation for design. Can a suitable design be evolved without its use? This question must be addressed in the Missile Datcom development. It is recommended that changes in local dynamic pressure at the lifting surfaces due to flow conditions (compressive or expansive flow) given in Datcom be retained and expanded for missile design purposes.

It is recommended that the wing vortex tracking and vortex strength methods of NACA 1307 and Datcom be used. It is also recommended that the empirical correlations of nose vortex strength and shedding position of Nielsen be adopted. Until the complex vortex tracking methods can be evaluated with respect to accuracy and cost, tracking along the velocity vector is recommended. Those recommended techniques are given in Table 16.

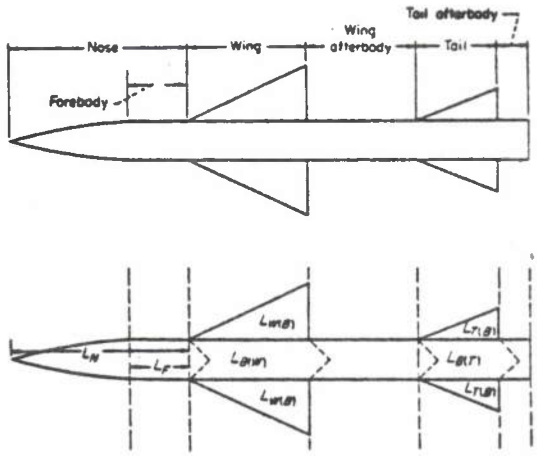

Figure 98. NACA 1307 Interference Regimes

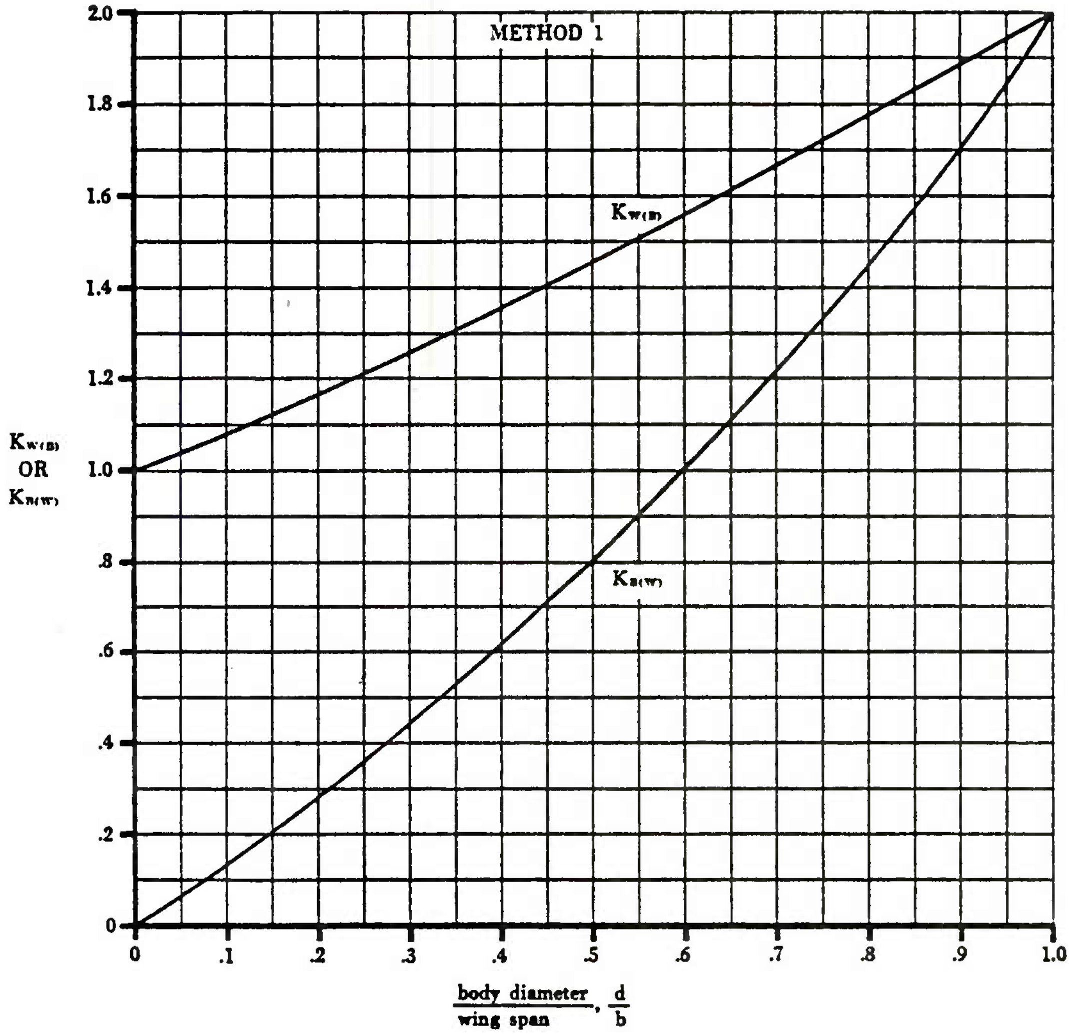

Figure 99. LIFT RATIOS $K_{W(B)}$ AND $K_{B(W)}$ —SLENDER-BODY THEORY—FIXED INCIDENCE—ALL SPEEDS

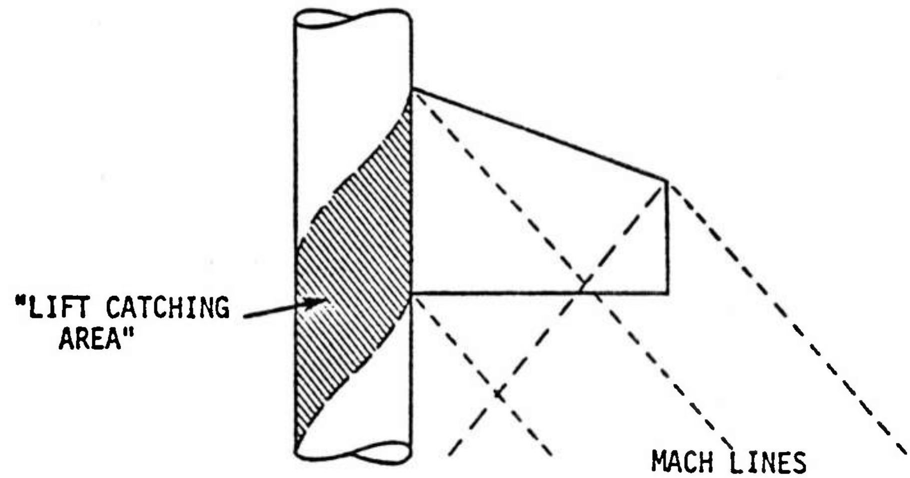

(a) NON-PLANAR MODEL

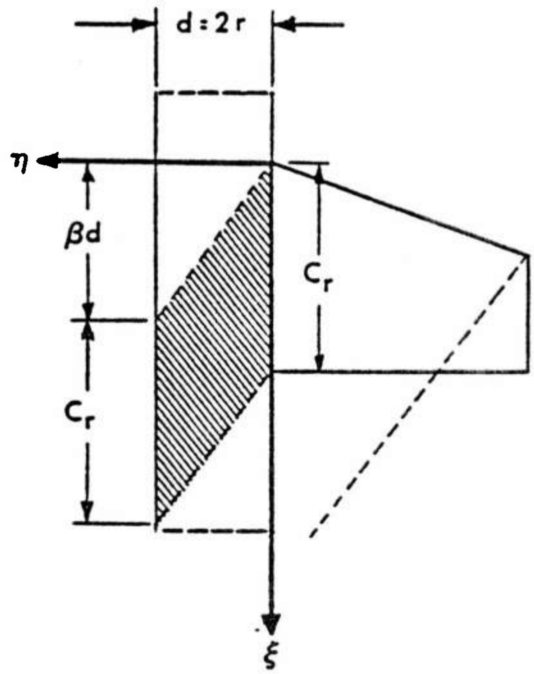

(b) PLANAR MODEL

Figure 100. Carry-Over Interference Model

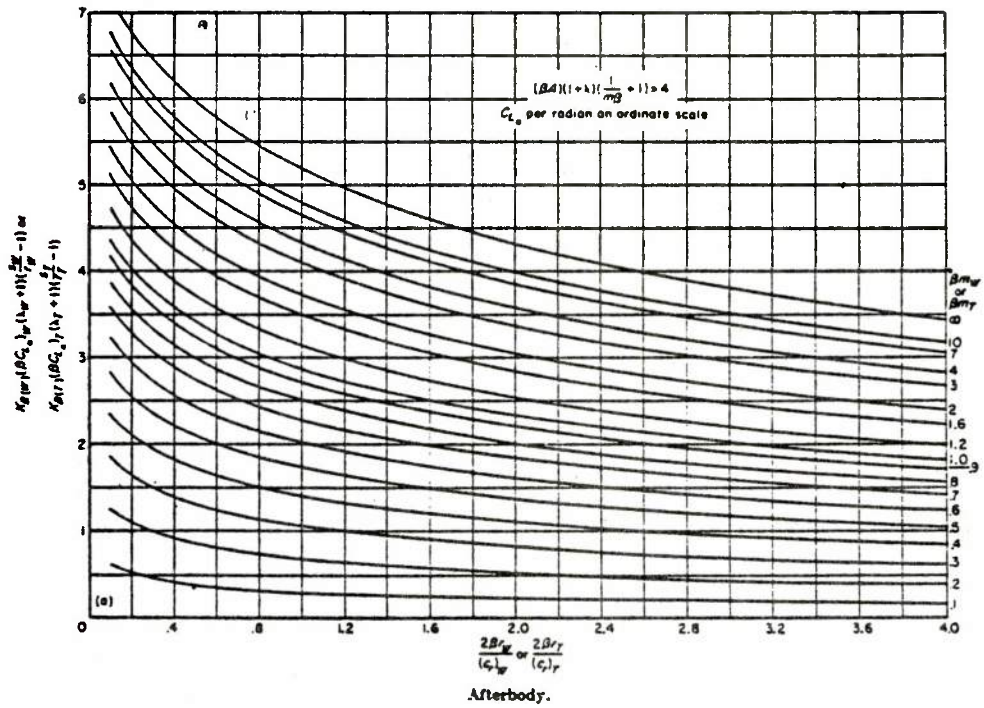

a) $K_{B(W)}$ Design Chart for Full Afterbody
(Conical Flow Theory)

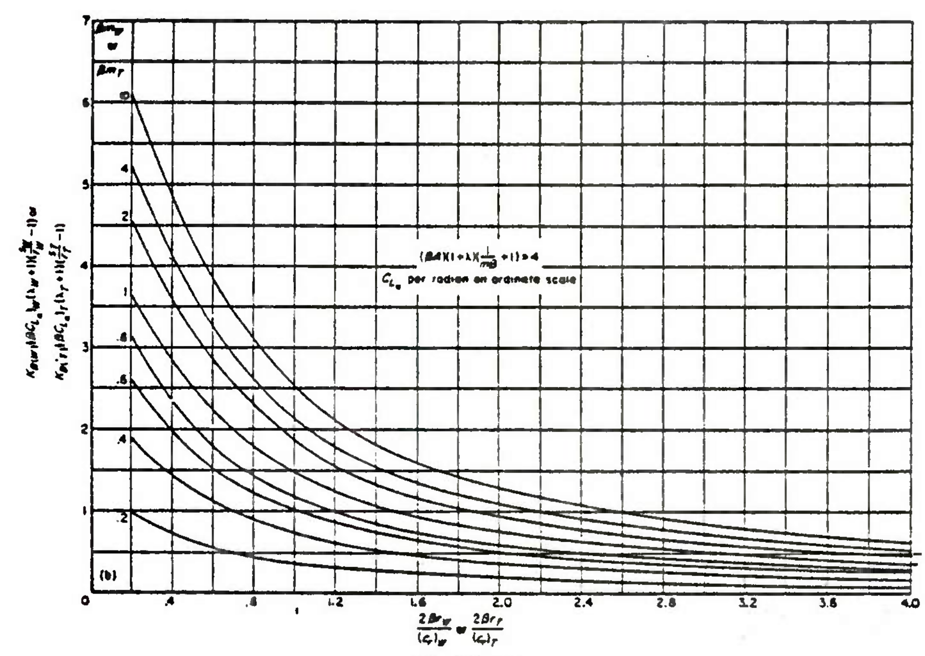

b) $K_{B(W)}$ Design Chart for No Afterbody
(Conical Flow Theory)

Figure 101. Body in Presence of Wing Carry-Over-Supersonic

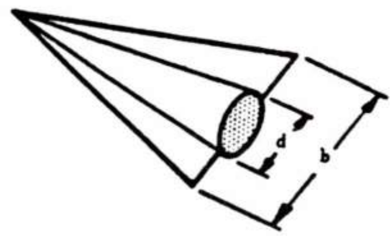

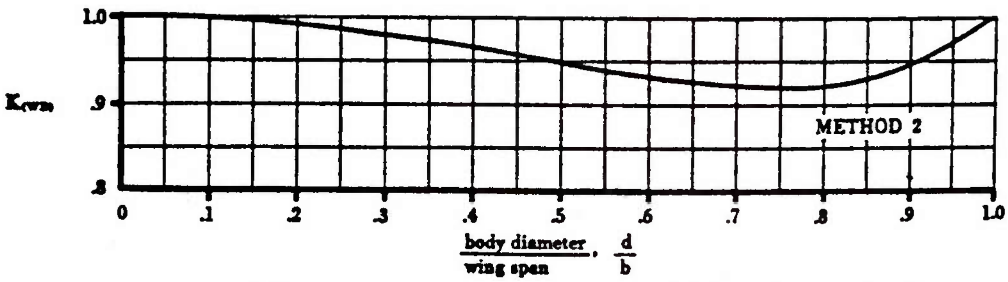

Figure 102. Spreiter cone-delta wing interference factor

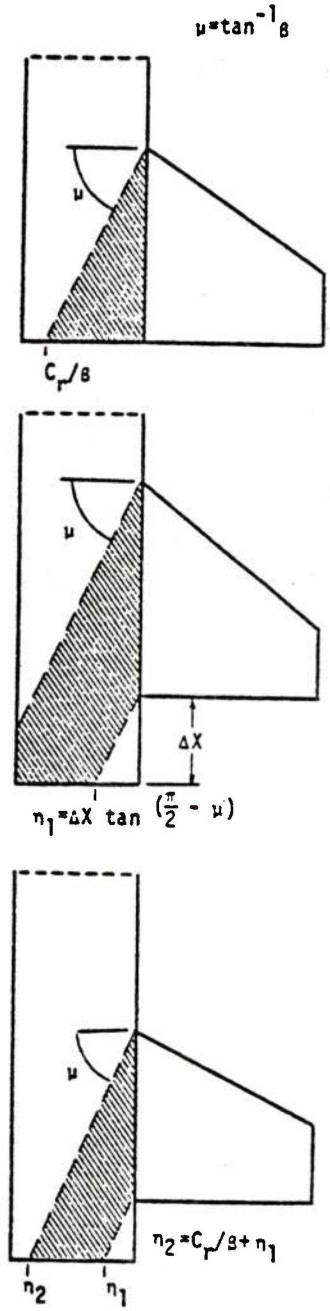

$$K_{B(W)} = \frac{2}{C_{L_\alpha} \alpha S_W} \int_{0}^{C_r/\beta} \int_{\beta\eta}^{C_r} P \, d\xi d\eta$$

CASE (A)

$$K_{B(W)} = \frac{2}{C_{L_\alpha} \alpha S_W} \left[\int_{0}^{\eta_1} \int_{\beta\eta}^{C_r+\beta\eta} P \, d\xi d\eta + \int_{\eta_1}^{d} \int_{\beta\eta}^{C_r+\Delta X} P \, d\xi d\eta \right]$$

CASE (B)

$$K_{B(W)} = \frac{2}{C_{L_\alpha} \alpha S_W} \left[\int_{0}^{\eta_1} \int_{\beta\eta}^{C_r+\beta\eta} P \, d\xi d\eta + \int_{\eta_1}^{\eta_2} \int_{\beta\eta}^{C_r+\Delta X} P \, d\xi d\eta \right]$$

CASE (C)

Figure 103. Integration Limits for General Afterbody Geometries

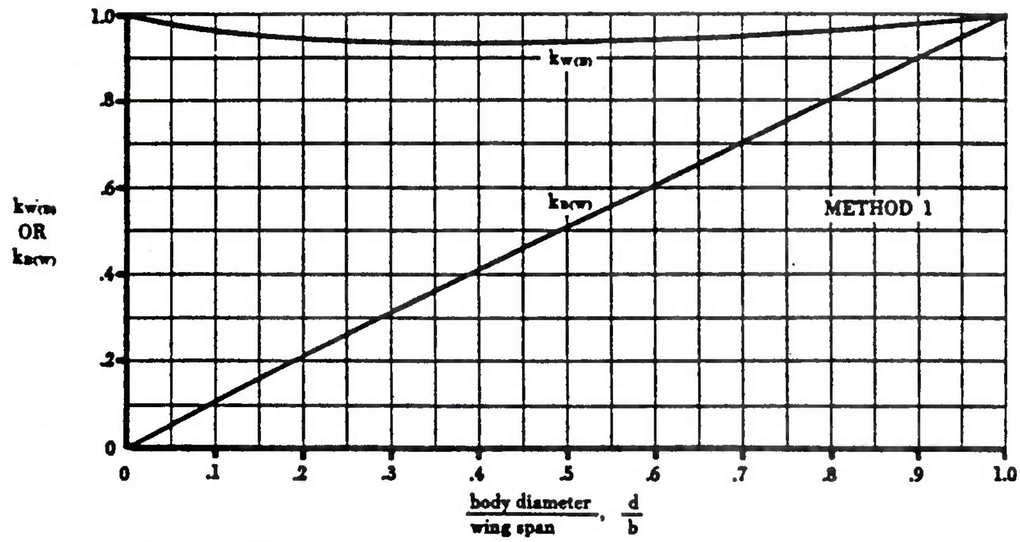

Figure 104. LIFT RATIOS $k_{W(B)}$ AND $k_{B(W)}$—SLENDER-BODY THEORY VARIABLE INCIDENCE—ALL SPEEDS

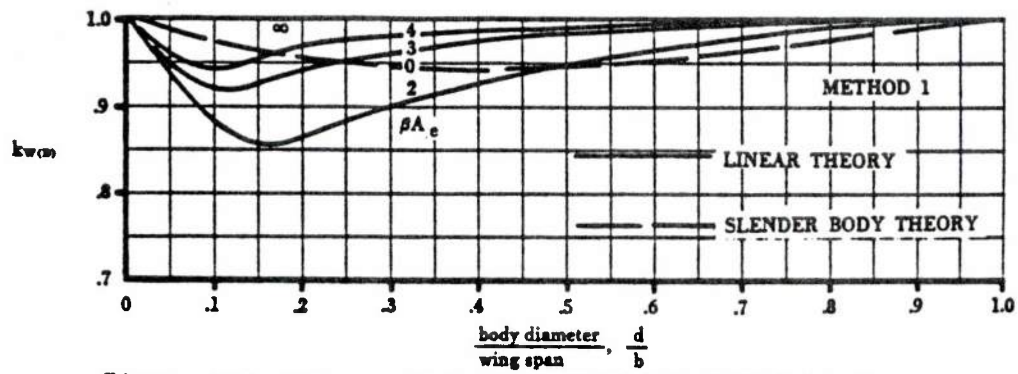

Figure 105. LIFT ON BODY IN PRESENCE OF WING—VARIABLE INCIDENCE SUPERSONIC SPEEDS

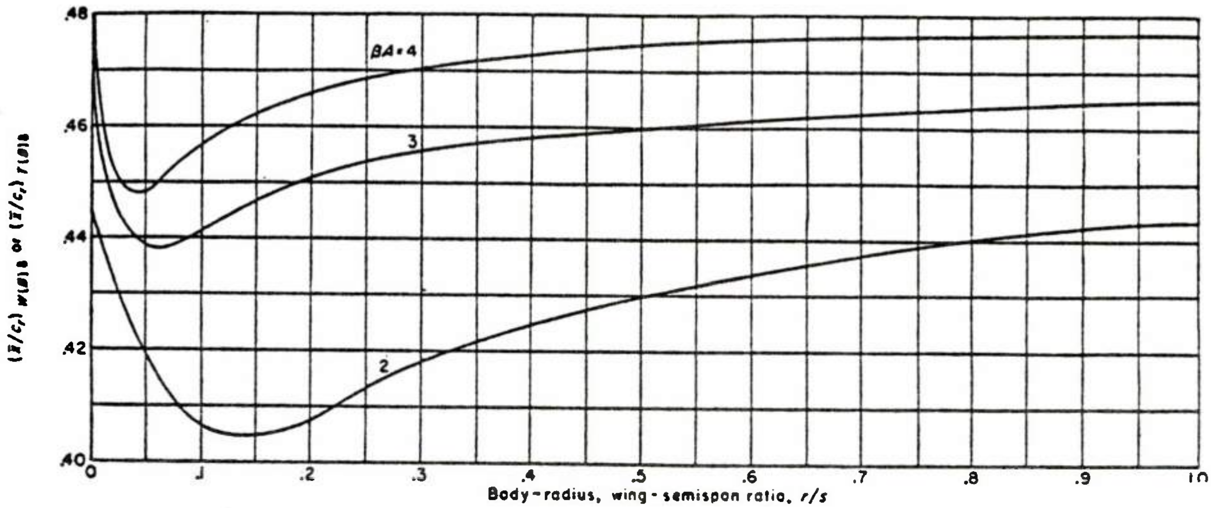

Figure 106. Rectangular Fin Center of Pressure Variation due to Incidence and Body Carryover at Supersonic Speeds
(Linear Theory)

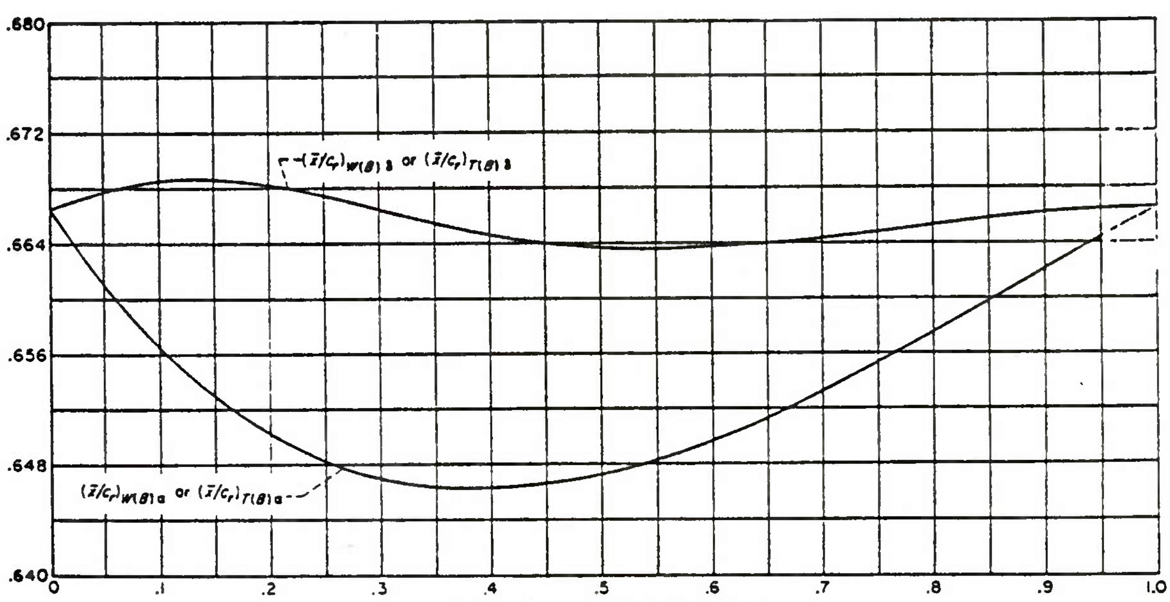

Figure 107. Triangular Fin Center of Pressure Variation due to Incidence and Body Carryover
(Slender-Body Theory)

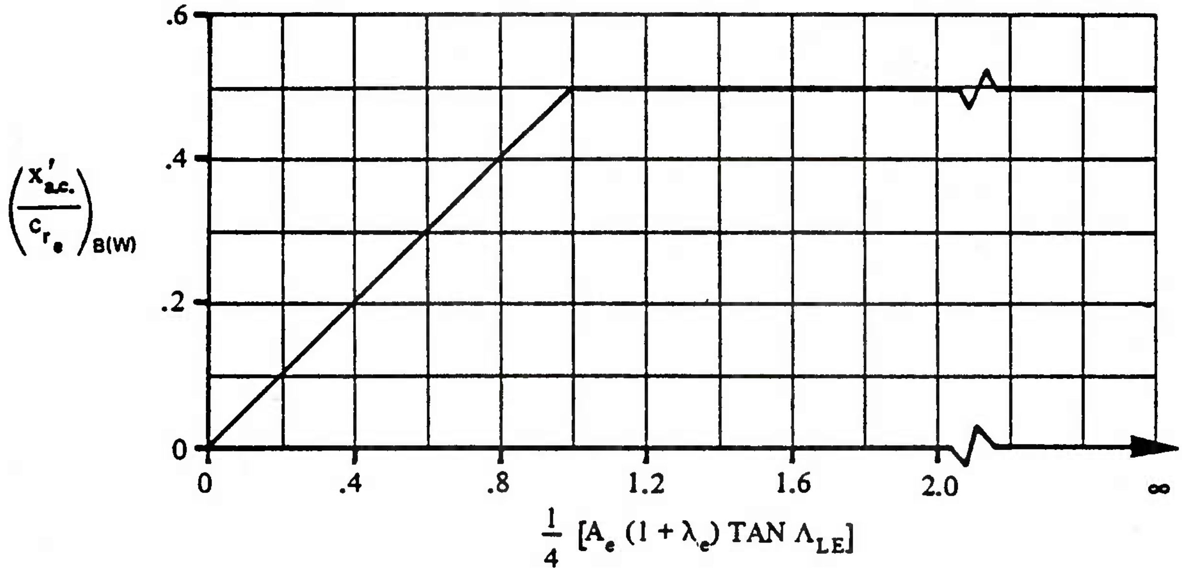

Figure 108. THEORETICAL AERODYNAMIC-CENTER LOCATIONS FOR $\beta A_e = 0$

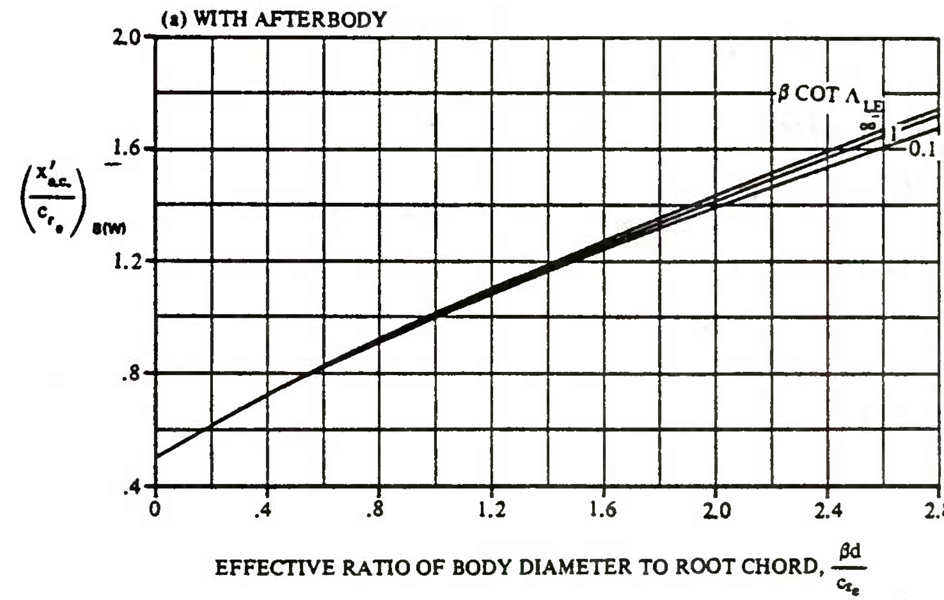

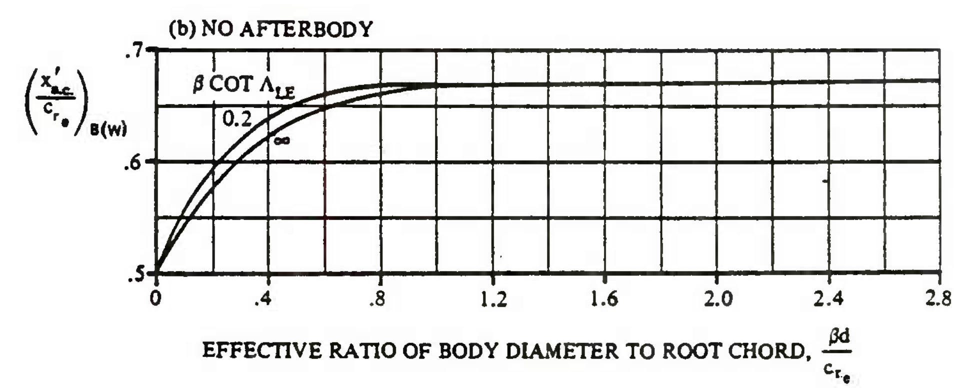

Figure 109. AERODYNAMIC-CENTER LOCATIONS FOR LIFT CARRYOVER OF WING ONTO BODY AT SUPERSONIC SPEEDS WHEN $\beta A_e (1 + \lambda_e) \left(1 + \frac{1}{\beta \text{ COT } \Lambda_{LE}}\right) > 4.0$

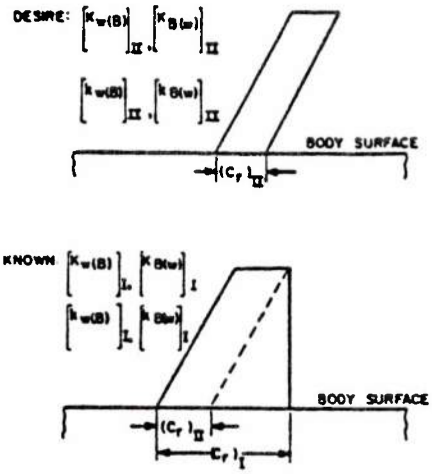

Procedure used to calculate interference lift for wings with sweptback trailing edges when slender body theory is used: a) wing for which interference lift is desired; b) assumed slender body representation.

Figure 110. Swept Trailing Edge Interference Approach By Moore

	Baker Ref. 74	Aiello Ref. 58	Nielsen Ref. 141
Mach Number	0.6-3.0	0.6-3.0	0.8-3.0
Angle of Attack (°)	0-180	0-30	0-45
r/s	0.3-0.5	0.3-0.5	0-0.5
A	0.5-2.0	0.5-2.0	0.5-2.0
λ	0-1.0	0-1.0	0-1.0

Figure 111. Empirical Interference Methods Data Base Limitations

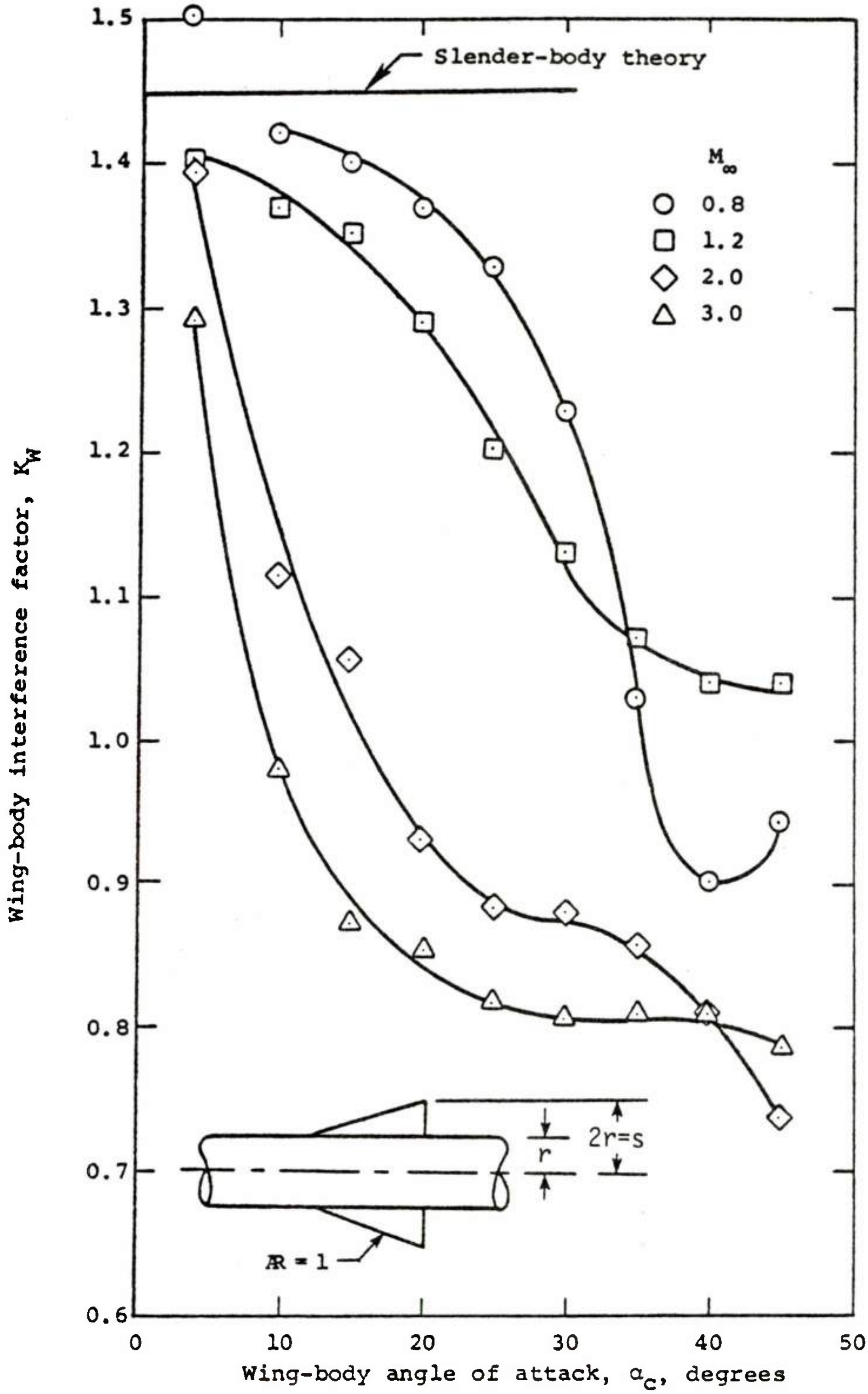

Figure 112. Effect of Angle of Attack on Body-Fin Interference

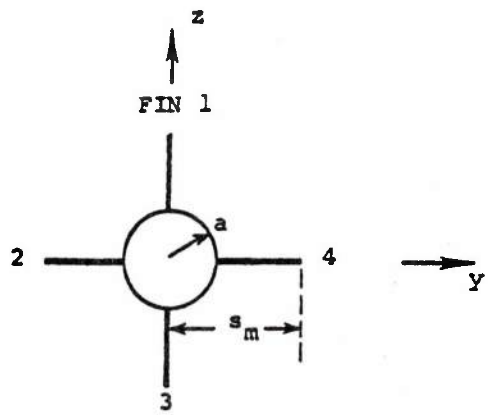

δ_4 = deflection of Fin 4

(a) Equivalent angles of attack

a/s_m	$\frac{\Delta(\alpha_{eq})_1}{\delta_4}$	$\frac{\Delta(\alpha_{eq})_2}{\delta_4}$	$\frac{\Delta(\alpha_{eq})_3}{\delta_4}$	$\frac{\Delta(\alpha_{eq})_4}{\delta_4}$
0	-.275	.0789	.275	.921
.1	-.230	.0731	.230	.890
.2	-.188	.0658	.188	.878
.3	-.149	.0567	.149	.879
.4	-.112	.0460	.112	.889
.5	-.0784	.0343	.0784	.905
.6	-.0498	.0230	.0498	.925
.7	-.0272	.0130	.0272	.946
.8	-.0115	.00566	.0115	.966
.9	-.0027	.00134	.0027	.984
1.0	0	0	.0	1.00

Figure 113. Panel-panel Interference due to deflection - Cruciform Fins (Slender-Body Theory)

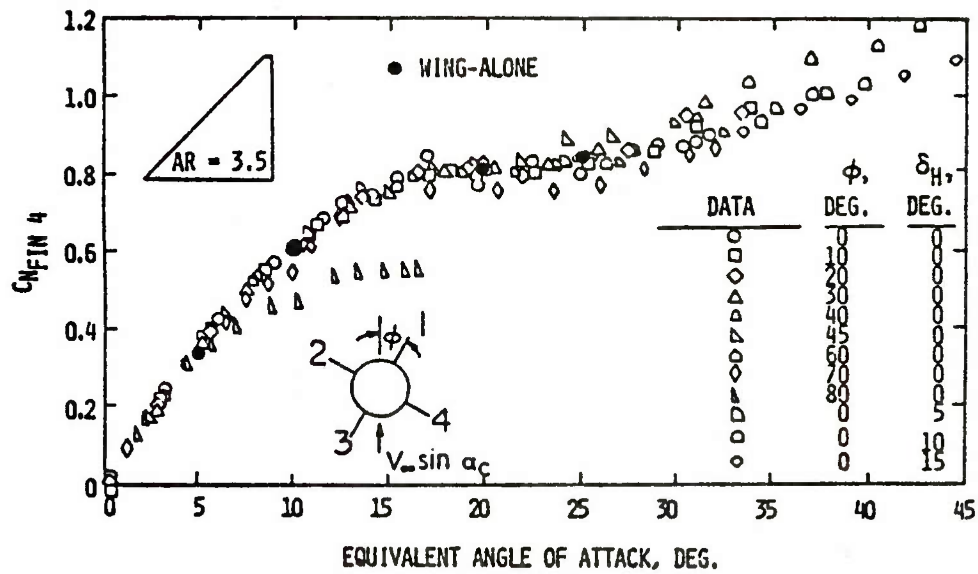

Figure 114. Equivalent Angle of Attack Concept Comparison

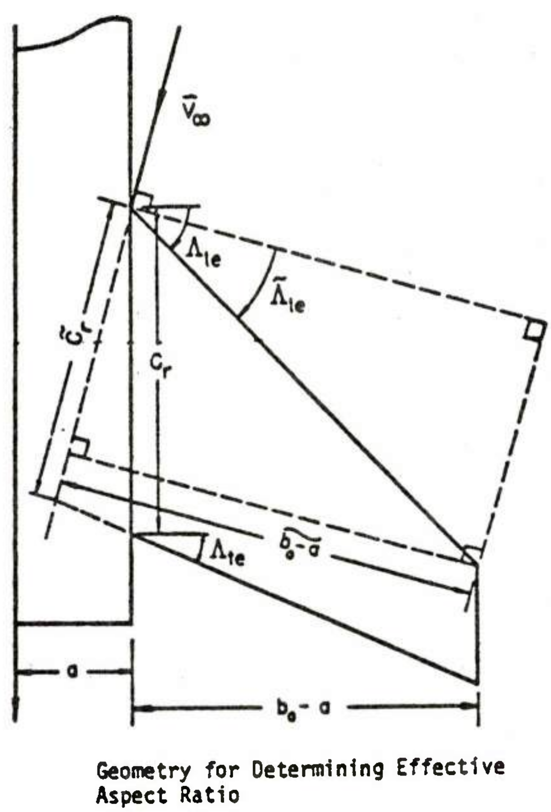

Figure 115. Oberkampf Geometry

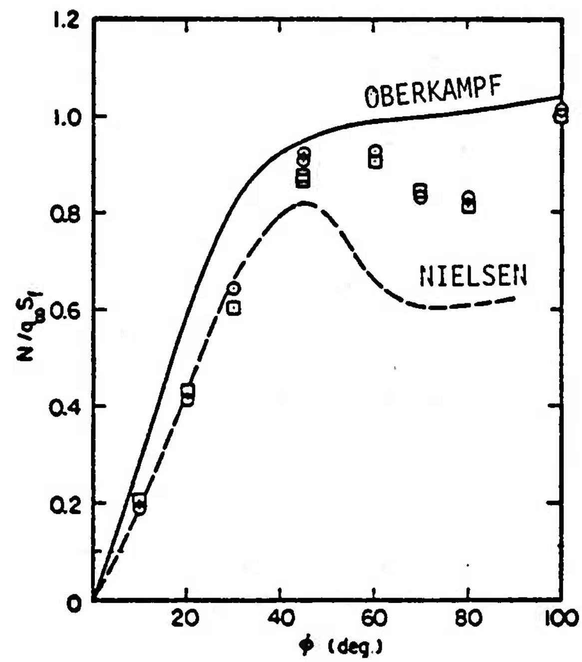

Figure 116. Comparisons of Nielsen vs Oberkampf Approaches

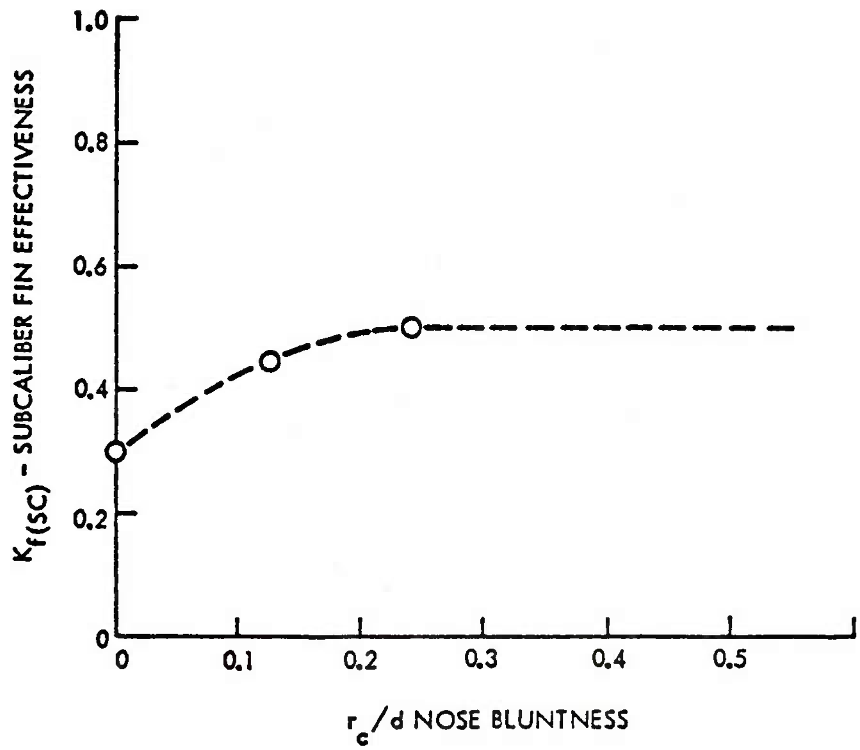

Figure 117. SUBCALIBER FIN EFFECTIVENESS FACTOR VARIATION WITH NOSE BLUNTNESS

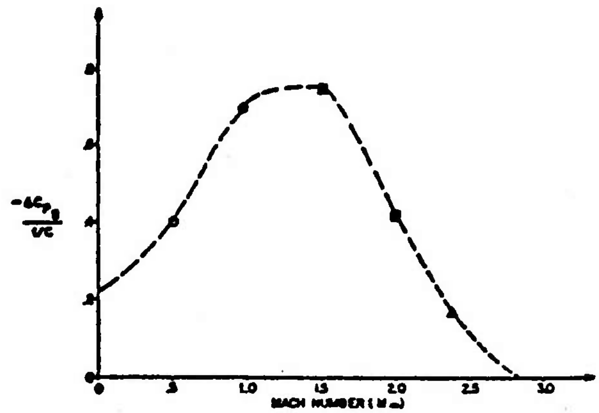

Base pressure coefficient change with fins located flush with base.

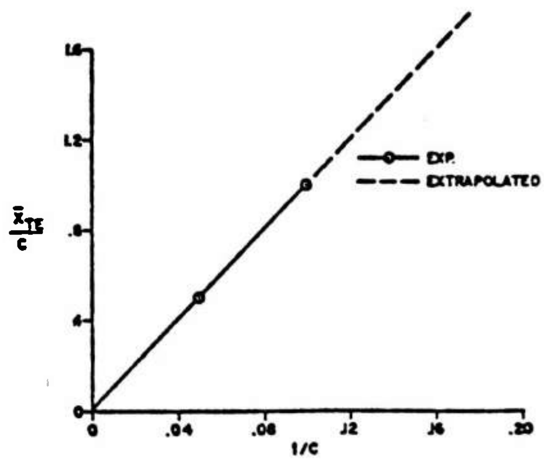

$\bar{X}_{TE}$ = distance from base to tail trailing edge where a fin of given thickness has no affect on base pressure.

Figure 118. Effect of Fins on Base Drag

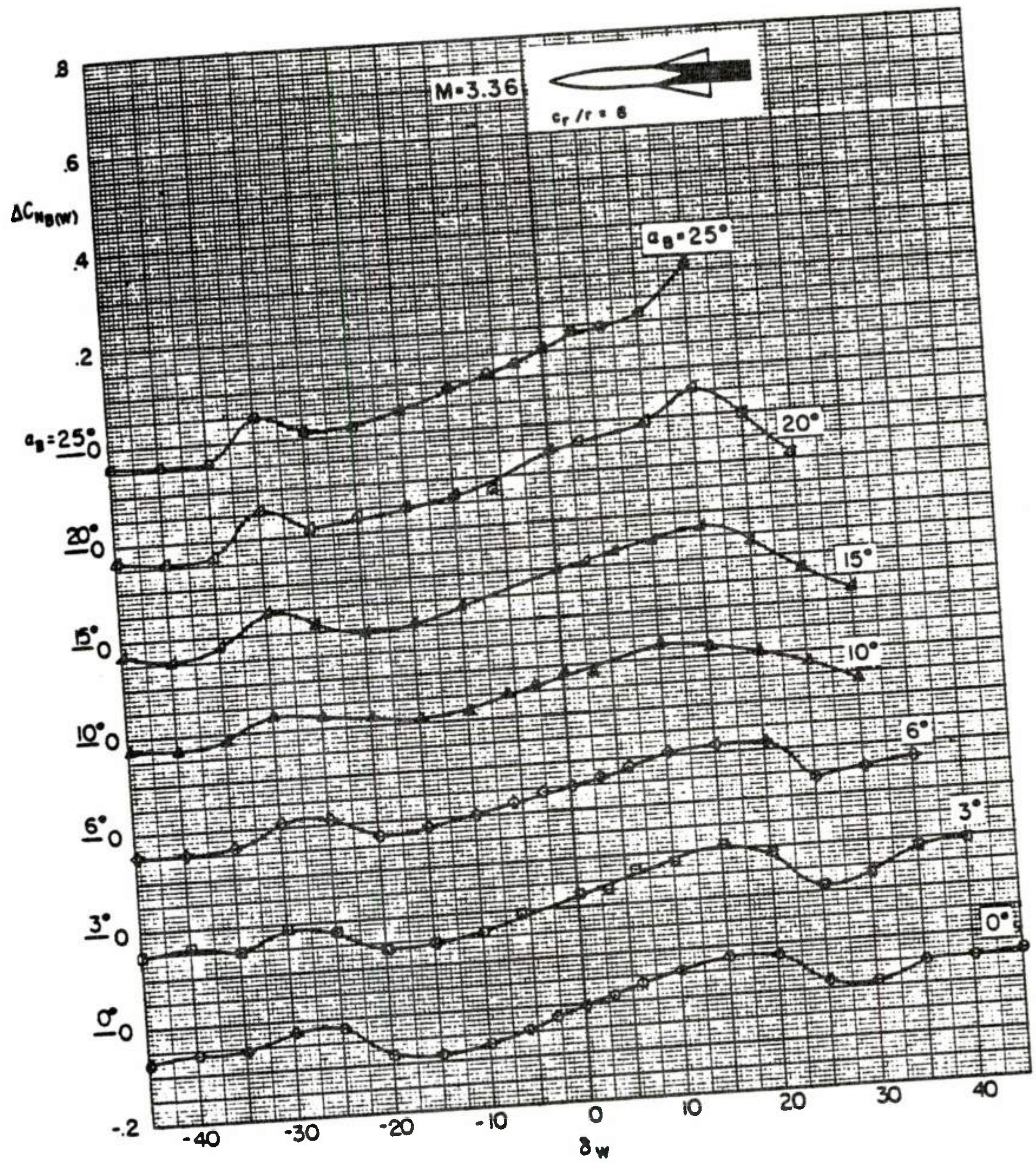

A = 1 triangular wing, r/s = 0.4.

Figure 119. Variation with Deflection angle of Interference Normal Force Coefficient for the Body in the Presence of the Wings.

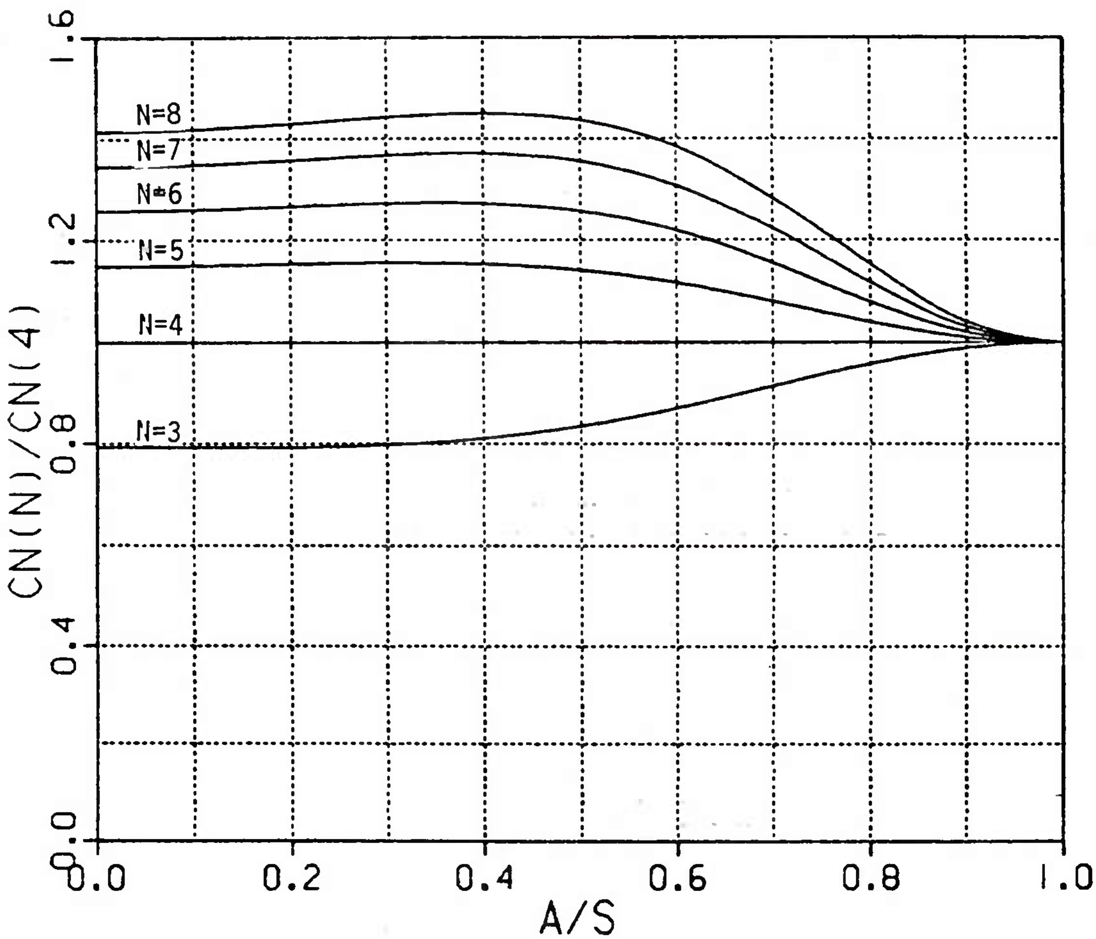

Figure 120. Apparent Mass Effect of Number of Fin Panels Versus Diameter to Span Ratio

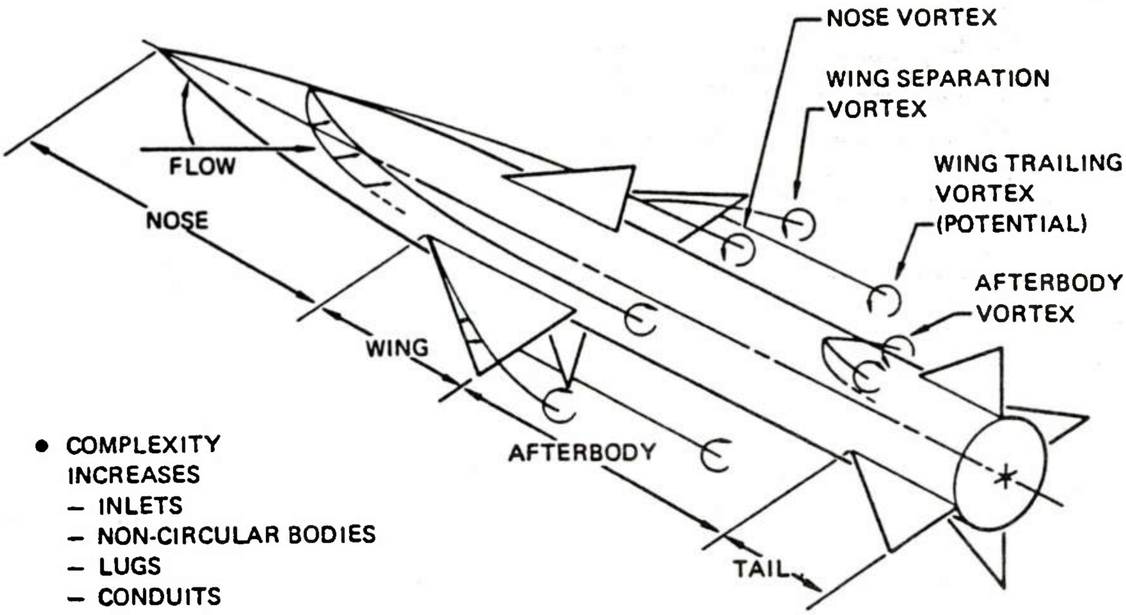

Figure 121. Vortices Present for a Typical Configuration

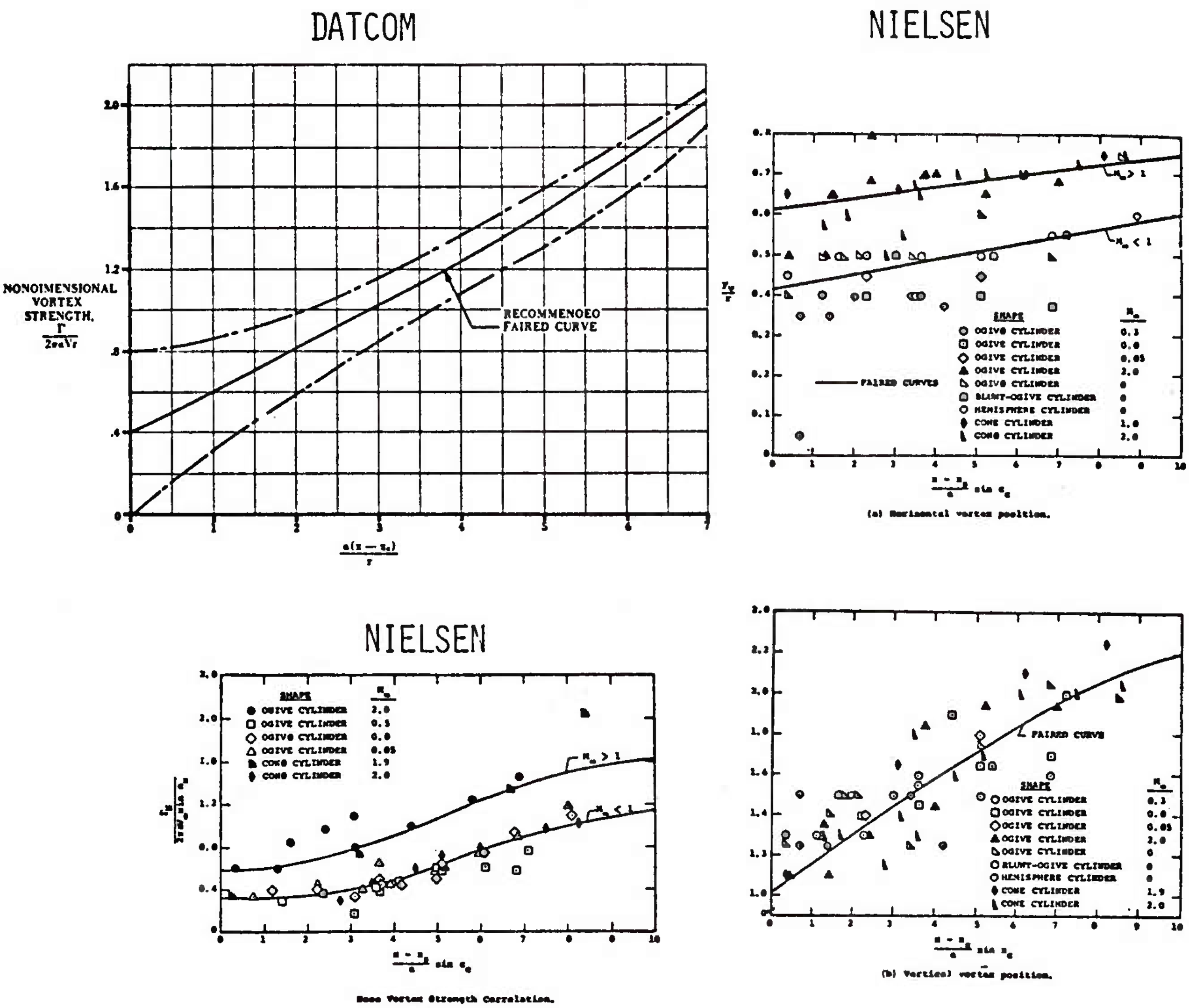

Figure 122. Body Nose Vortex Correlations

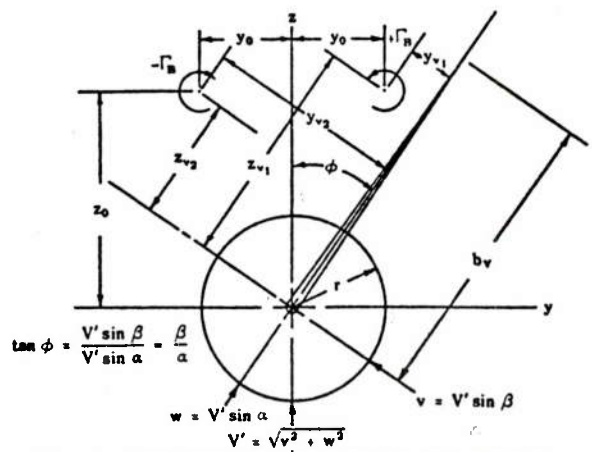

TYPICAL ORIENTATION OF BODY VORTICES WITH RESPECT TO TAIL PLANE FOR CONFIGURATION AT COMBINED ANGLES

$$\frac{z_{v_1}}{b_v} = \frac{r}{b_v}\left[\frac{z_0}{r}\cos\phi + \frac{y_0}{r}\sin\phi\right]$$

$$\frac{y_{v_1}}{b_v} = \frac{r}{b_v}\left[\frac{z_0}{r}\sin\phi - \frac{y_0}{r}\cos\phi\right]$$

$$\frac{z_{v_2}}{b_v} = \frac{r}{b_v}\left[\frac{z_0}{r}\cos\phi - \frac{y_0}{r}\sin\phi\right]$$

$$\frac{y_{v_2}}{b_v} = \frac{r}{b_v}\left[\frac{z_0}{r}\sin\phi + \frac{y_0}{r}\cos\phi\right]$$

where $\phi = \tan^{-1}\frac{\beta}{\alpha}$

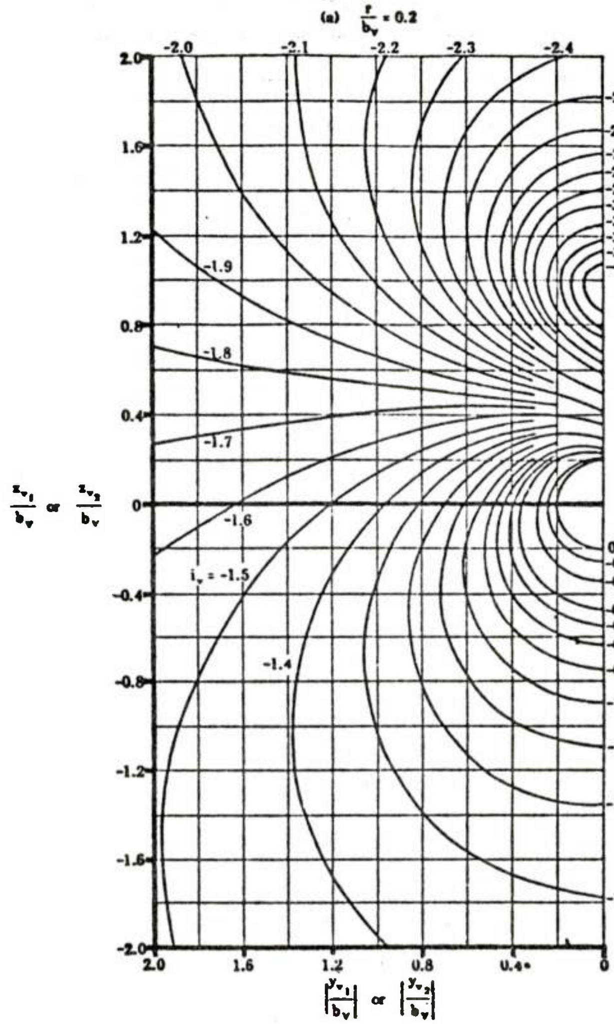

VORTEX INTERFERENCE FACTOR

Figure 123. Datcom Vortex Effect Due to Panel Orientation

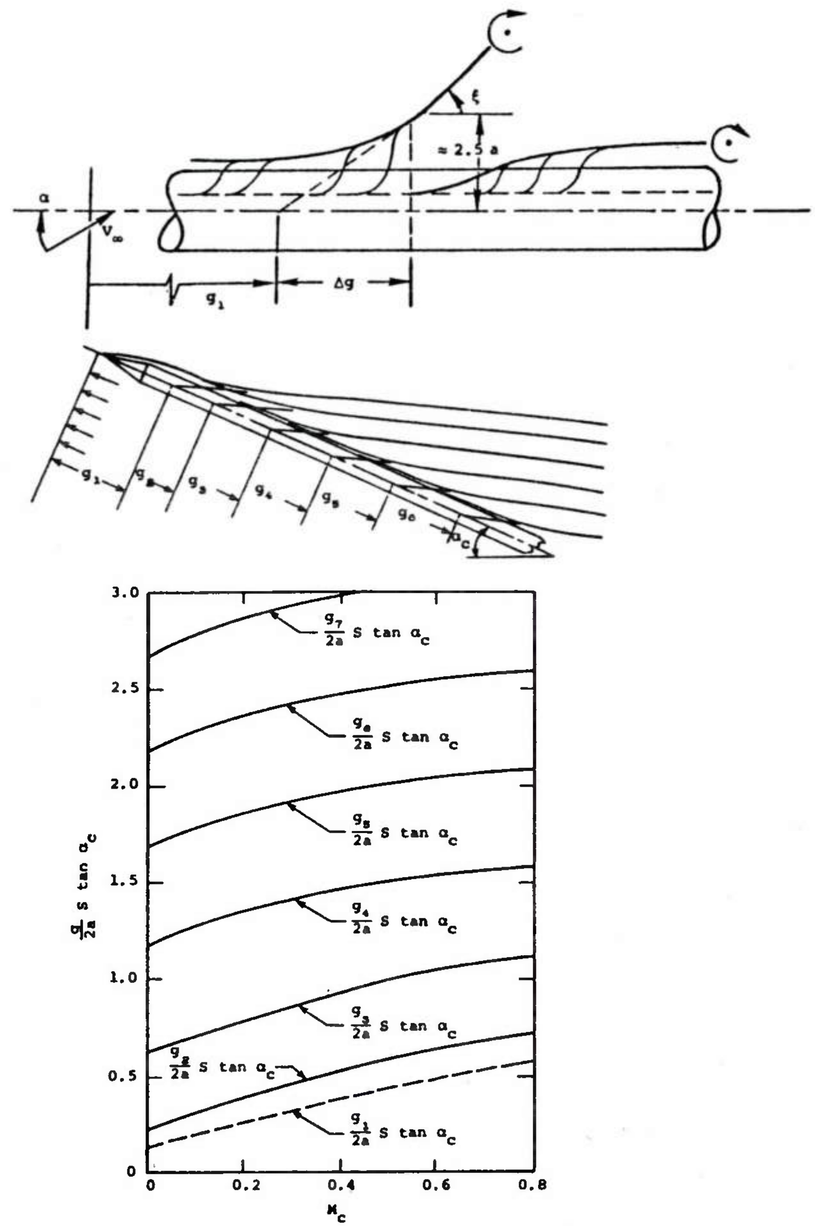

COMPUTATION PROCEDURE

- o DETERMINE STARTING POSITIONS
  - o COMBINE BODY CROSSFLOW
    - FREESTREAM
    - FIN VORTEX
  - o APPLY STARTING CRITERIA
    - TE FIN
    - $\frac{X_S}{a} = 2 + \frac{10°}{\alpha_{cr} - 4°}$ (α_{cr} averaged)
- o TRACK FOREBODY VORTICES OVER AFTBODY
  - o NOSE VORTEX
  - o FIN VORTEX
- o COMPUTE AFTERBODY VORTEX STRENGTH
  - o VORTEX IMPULSE THEOREM
  - o 2-D CROSSFLOW DRAG CORRELATIONS
- o AFTERBODY VORTEX DEVELOPMENT CHARACTERISTICS
  - o 2 POTENTIAL LINE VORTICES
  - o FOREBODY VORTICES INFLUENCES
- o THOMSONS MULTIPLE VORTICES CORRELATION

$$\frac{X_S}{a} = \frac{g_1}{a} + \frac{\Delta g}{a}$$

Figure 124. Afterbody Vortices Can be Well Predicted

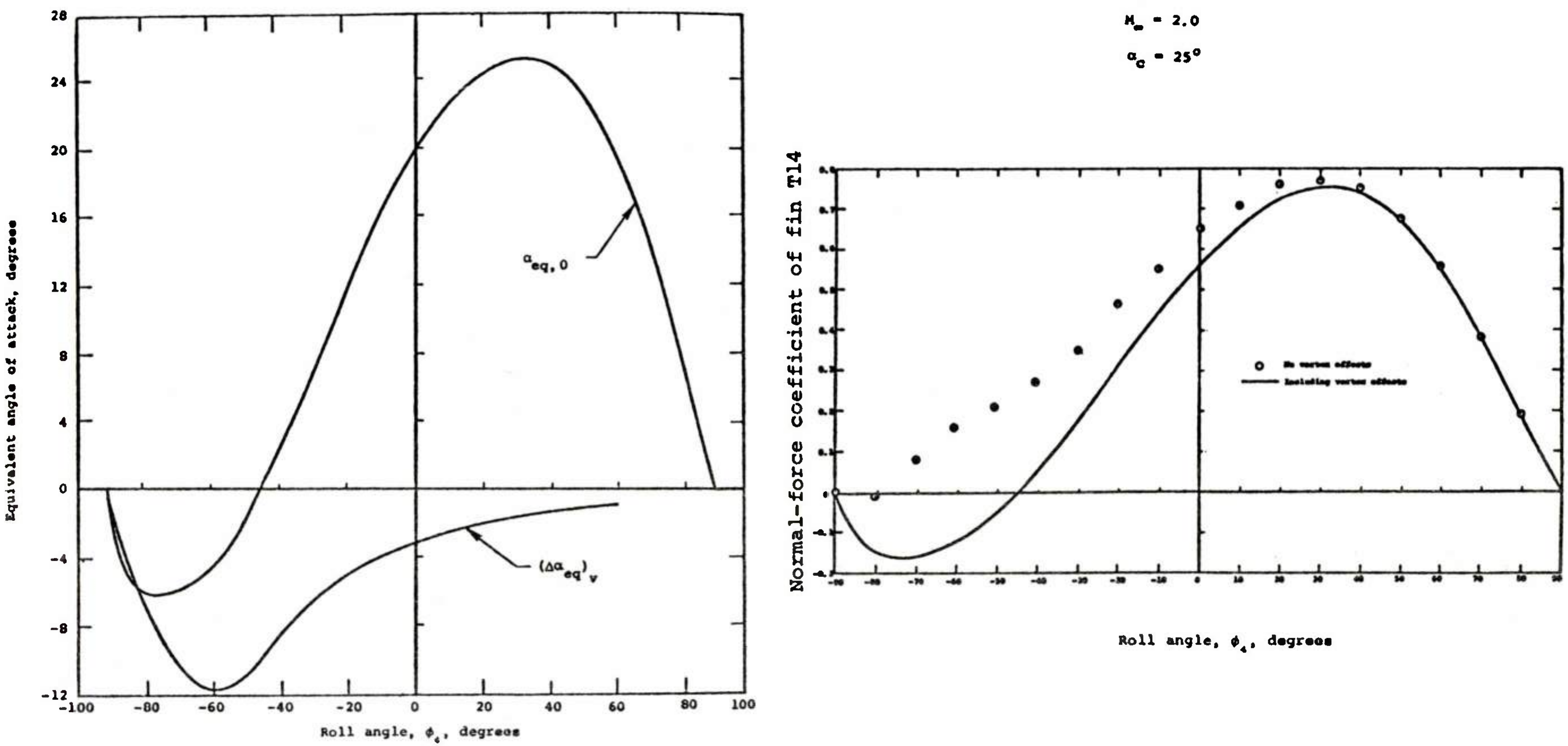

Figure 125. Effect of External Vortices on Panel Angle of Attack

TABLE 16 RECOMMENDED INTERFERENCE METHODOLOGY

COMPONENT \ MACH NUMBER REGION	SUBSONIC	TRANSONIC	SUPERSONIC
WING-BODY INTERFERENCE K,k	NACA 1307, EMPIRICAL		LINEAR THEORY, SLENDER BODY THEORY & EMPIRICAL
WING-TAIL INTERFERENCE	LINE VORTEX THEORY		
BODY BASE PRESSURE DRAG CAUSED BY TAIL FINS	EMPIRICAL		
JET INTERFERENCE	EMPIRICAL		
FIN/FIN INTERFERENCE	SLENDER BODY THEORY		

SECTION 6
CONFIGURATION SYNTHESIS

It is recommended that Missile Datcom utilize the component buildup approach for missile configuration synthesis. The equivalent angle of attack approach with a total angle of attack, bank angle coordinate system is recommended to facilitate interference calculations at arbitrary roll angles. The computer program should be structured so that user supplied experimental results available for a particular configuration component can be used. This then establishes the need for a modular program in which the aerodynamic computations are isolated in individual routines. The program structure would be similar to the Missile Datcom handbook outline presented in Section 2.

Configuration synthesis is the process of estimating the aerodynamic characteristics of a complete configuration. Typically, synthesis involves the summation of the aerodynamic characteristics of each of the configuration components and then adding mutual interference effects. Two approaches exist for combining components to obtain total configuration aerodynamics. Figure 126 classifies the two methods for normal force of a wing-body-tail configuration. The "classic" approach is the linear lift method presented in NACA 1307 extended to non-linear angles of attack. The carryover effects between wing/body and tail/body are represented as multipliers ($K_{W(B)}$, $K_{B(W)}$, $K_{T(B)}$, $K_{B(T)}$) to the panel alone characteristics. Since the body generates a pair of trailing nose vortices, these vortex effects, $I_{VW(B)}$ and $I_{VT(B)}$, on the panels are separately computed and summed with the wing vortex effect, $I_{VT(W)}$, on the tail surfaces. Although wing and tail vortices are present, their effect on the body is assummed negligible. The body nose vortex effect on the body is modeled using the viscous cross-flow procedure described by Allen and Perkins, and presented in Section 3.

The "equivalent angle of attack" concept by Nielsen (Reference 176) identifies the same interference contributors, but combines the effects of carryover and vortices on the panel local angle of attack. The sources of interference considered are 1) panel-panel interference, where the change in loading of one panel affects another, 2) nose vortex-fin interference, 3) wing vortex-tail interference, and 4) afterbody vortex-tail interference. All of these effects are evaluated as an incremental effect on equivalent angle of attack. Once the equivalent angle of attack has been evaluated, the panel normal force is obtained from the empirical or theoretical panel

alone characteristics. This technique is advantageous since at transonic speeds only empirical panel aerodynamic characteristics are available.

These two methods are easier to apply if aerodynamic characteristics are estimated as a function of total angle of attack and roll angle. Bank-to-turn and skid-to-turn missile configurations have different angle of attack and sideslip angle envelopes, as shown in Figure 127. The synthesis technique chosen must encompass the most extreme condition, such as 20 degrees of angle of attack and sideslip. For those cases, the "equivalent angle of attack" approach is the easiest to apply. The loads on the individual panels are directly determined; therefore, the panel hinge moment and bending moment can be computed. This system is best for the vortex calculations, since the vortex paths are related to the configuration total angle of attack. References 177-185 describe in detail the synthesis of configurations at angle of attack and bank angle and serve as excellent documentation for the effects of high body incidence. For arbitrary shaped bodies, an angle of attack/sideslip angle system is still required because of the non-axial symmetry of the body. It is difficult to obtain total angle of attack characteristics of arbitrary-shaped bodies throughout the required envelope.

CLASSIC APPROACH:

$$C_N = C_{N_{BODY}} + \left[K_{W(B)} + K_{B(W)}\right] C_{N_{WING}} + \left[K_{T(B)} + K_{B(T)}\right] C_{N_{TAIL}} + I_{V_{W(B)}} + I_{V_{T(B)}} + I_{V_{T(W)}}$$

NIELSEN EQUIVALENT ANGLE OF ATTACK APPROACH:

$$C_N = C_{N_{BODY}} + K_{B(W)}\, C_{N_{WING}} + K_{B(T)}\, C_{N_{TAIL}} \underbrace{+ \sum C_{N_{WING}} (\alpha_{EQ})_W + \sum C_{N_{TAIL}} (\alpha_{EQ})_T}_{\text{INCLUDES EFFECT OF } \alpha, \delta, \phi \text{ AND ALL EXTERNAL VORTICES (NOSE, AFTERBODY, WING)}}$$

Figure 126. Configuration Synthesis Concepts

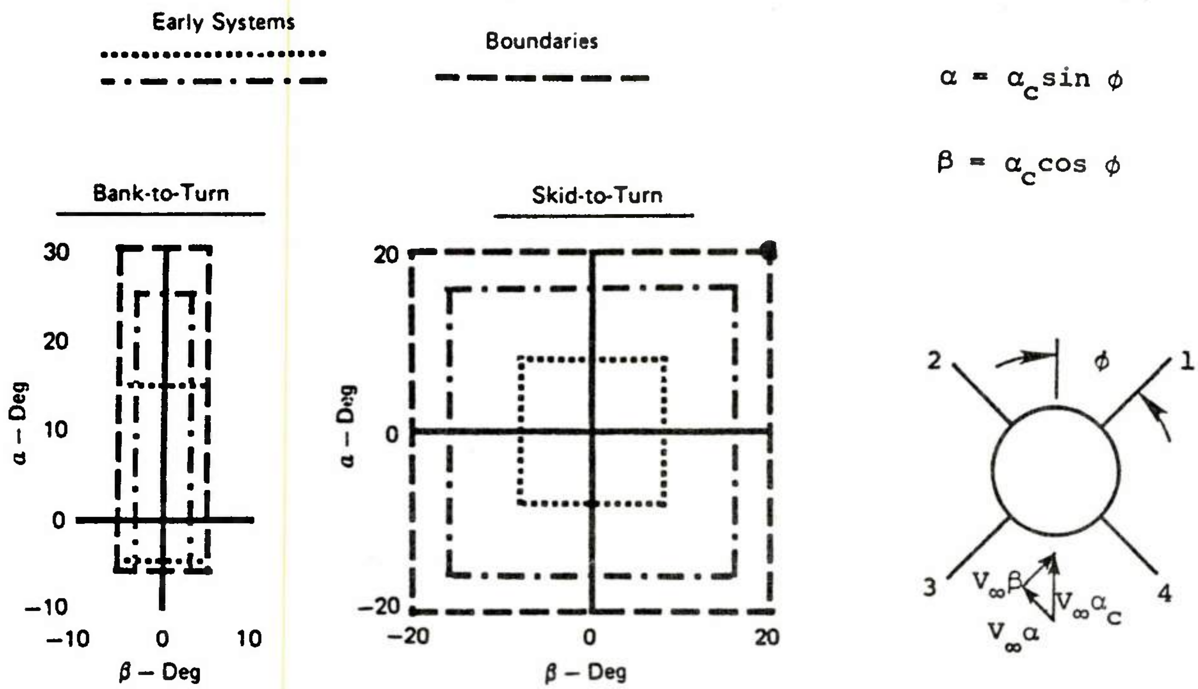

Figure 127. α and β Envelopes

SECTION 7
PROPULSION SYSTEM EFFECTS

Missiles generally use one of three propulsion system types: (a) rocket, (b) turbojet, or (c) ramjet. Propulsion system effects on aerodynamics is perhaps the least developed area in missile aerodynamics, due to the complexity and variety of propulsion systems. Many missile aerodynamic prediction codes ignore the propulsion effect on aerodynamics, although it is often significant. Section 3 has described the effect of jet plume/exhaust on boattail wave drag. This section will describe those other effects which will be required for Missile Datcom.

Plume/Airframe C_N, C_m - A major problem for the aerodynamicist are the plume/airframe interaction effects. As the vehicle climbs in altitude, the exhaust plume from a rocket will expand producing the effect illustrated in Figure 128. Normal force and pitching moment can be significantly altered. The classic means of solving this problem is to assume that the plume effect is similar to that of a transverse-jet control device, but requires detailed computations. The recommended approach is that presented by Aiello and Bateman, Reference 58, where the incremental body normal force, body center of pressure, and tail normal force, have been empirically correlated over the Mach range from 0.6 to 2.2 through 180 degrees angle of attack. The extrapolation of these results to higher and lower Mach numbers should be investigated. It will be necessary to obtain additional data for further method development.

For an airbreathing propulsion system, the effect of jet plume/airframe interaction should be minimal. The captured air will be exhausted at a pressure close to that for the free-stream, and pluming will be small. Operational airbreathing propulsion systems typically have high pressure recovery coefficients. For these propulsion systems the effect of plume/airframe interaction can be assumed to be negligible for preliminary design purposes.

Plume/Base Interaction - The base pressure methods described in Section 3 were for jet-off characteristics. The jet effects on base drag occur for all propulsion systems and were theoretically analyized by Addy, Reference 187, and Korst, Reference 188. These methods assume a strong plume/freestream interaction such as that for an over-expanded plume typical of rockets. However, they do not address the base aspiration effect typical to airbreathing missiles where

the plume may not interact strongly with the free-stream. Although therKorst technique is automated, Reference 189, it is a complex program; a method of characteristics computation is performed to determine the plume shape. Various simplified forms of the technique are available, one such method being that of Reference 190. This technique is recommended for rocket propulsion systems. The plume shape and pressure have been correlated into simple relationships, and the calculation of base pressure becomes a routine computation.

For airbreathing inlets, a simple approach is recommended. For turbojets and ramjets the power-on base drag is usually higher than that for power-off, but the annular base area is usually smaller than the power-off area. Therefore, the inaccuracy is using power-off base drag from Stoney, Reference 35, is usually small. If necessary a compendium of data and empirical techniques are available in Reference 32 for more detailed estimates.

Inlet Effect - Airbreathing inlets change the body shape to non-axisymmetric and are usually treated empirically. A limited number of methods are available in Reference 192 using empirical correlations. Generally, detailed analysis of the inlet components (e.g., cowl, duct, boundary layer diverter) involves a number of theoretical and empirical methods (which have been summarized in Reference 191 for several inlet types) similar to the component build-up approach for bodies. Use of sophisticated panel techniques have also been employed. The simple inlet/circular body build-up method is seen as an ideal candidate for preliminary design. A compendium of data for 2-D, axisymmetric and chin inlet designs is available to develop this technique. The chin inlet methods of Reference 58 are recommended for this task. A significant amount of test data has been obtained through a cooperative effort between NASA-Langley and the Naval Weapons Center in China Lake, CA. These data contain configuration build-up data for a missile configuration with the 2-D and axisymmetric inlet types. The inlets were mounted on the body in various longitudinal and circumferential positions. However, this data has yet to be put into a form suitable for engineering design purposes. It is recommended that an R&D task be funded specifically for the purpose of deriving preliminary and conceptual design methodology using this data base and the methods of References 58 and 191. In the interim, methods which have been derived from empirical results and presented in the "Ramjet Design

Handbook", Reference 192 should serve as excellent design methodology when data is unavailable.

It is recommended that the component build-up approach be applied to inlet effects on configuration aerodynamics. It is also recommended that the automated version of Missile Datcom employ a structure which will allow substitution of test data when it is available.

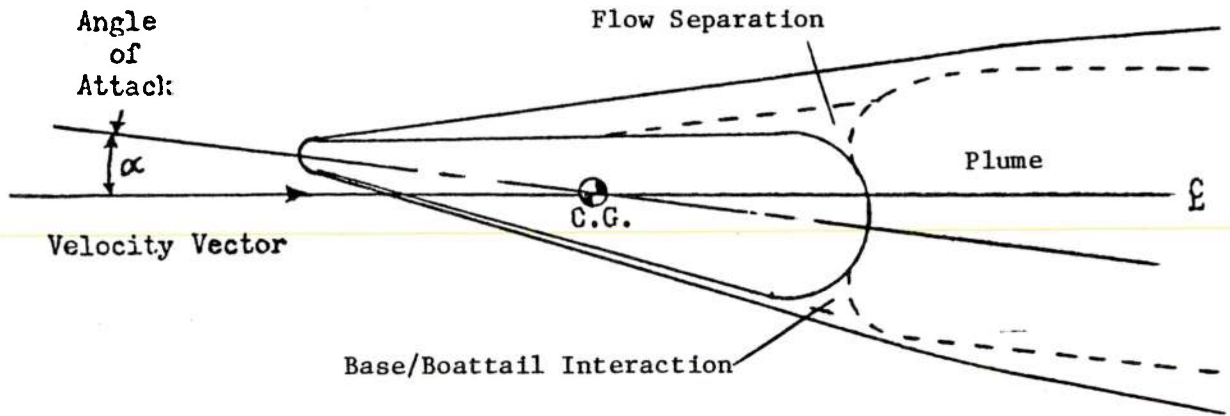

Postulated Effects:

a. Reduced Normal Force and Pitching Moment Coefficients

b. Modified Axial Force

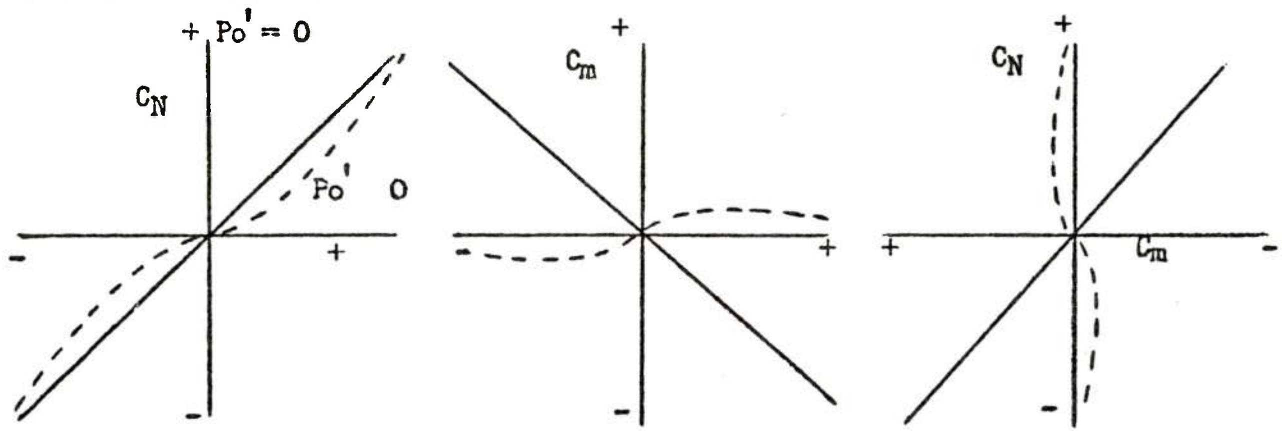

Figure 128. Plume/Airframe Interactions can Influence Aerodynamics

SECTION 8
CONTROL DEVICE METHODOLOGY

The method recommendations for control device methodology are as follows:

(a) Panel deflection, use of the "equivalent angle of attack" concept by Nielsen

(b) Plain flap; Datcom

(c) Hypersonic flaps; Datcom

(d) Transverse-jet control; Datcom

(e) Strakes; Aiello and Bateman

These methods are briefly summarized in this section.

Only the simplest of control devices are used in missile design because of cost and complexity constraints. The most often used control device is the all-movable surface with deflection ranges typically of ± 30 degrees. Other control devices less frequently used include thrust-vector-control (TVC), jet interaction/reaction jet control (JI/RJC), plain trailing edge flaps and body flaps. More sophisticated control devices such as split flaps, leading-edge flaps, or jet flaps are extremely rare and their inclusion is not recommended.

<u>Panel Deflection</u> - Section 5 on component interference described in detail the effect of high angle of attack and deflection on panel effectiveness, emphasizing the need for carry-over interference results beyond that obtained through slender-body or conical flow theory. Through use of the empirical results available for a variety of fin panel designs, sufficiently accruate results in the transonic and supersonic Mach regimes can be obtained. Effective use of the "equivalent angle of attack" concept by Nielsen allows determination of panel hinge moment and bending moment characteristics. Correlations with test results have shown acceptable accuracy for preliminary design.

<u>Plain Flaps</u> - The Datcom methods for plain flaps are recommended. Typical variation of the flap characteristics are presented in Figures 129-132. The method reference and limitations due to Mach number are as follows:

(a) Subsonic (Reference 136)

(b) Transonic (Approximate technique, Reference 1)

(c) Supersonic (Reference 193; supersonic leading edge and trailing edge and flap surfaces; control located on surface tip)

Typical design charts for the Datcom method are presented in Figures 133-141. The method results in Figure 142 show good correlation with test data.

Hypersonic Flap - The Datcom method for a plain flap at hypersonic speeds (Hypersonic Flap) is recommended. This technique is for Mach numbers greater than five and for the most part was taken from Reference 194. A qualitative variation of the pressure distribution is shown in Figure 143.

Transverse-Jet Control - The transverse-jet control methods of References 195-197 have been incorporated into the Datcom method. These methods are also recommended for inclusion in Missile Datcom. The methods presented in Datcom cover the Mach range from 2 to 20. A representative pressure distribution due to jet interaction with the flow is shown in Figure 144.

Strakes - Strakes are sometimes included for the purpose of enhancing control effectiveness. As shown in Figure 145, a strake produced vortex will sweep across the major lifting surface and result in increased lift effectiveness at much higher angles of attack. This phenomena benefits a bank-to-turn missile configuration due to increased pitch normal force as Figure 146 illustrates. A thorough discussion of these results is presented in References 198 and 199. There are no theoretical methods available to predict the favorable interference effect of wing strakes but the empirical (subsonic) lift methods in Datcom are available for cranked or double-delta panels (straked wings) for angles of attack to 20 degrees. Isolated strakes (i.e. not a physical part of a primary lifting surface) are also in common use to influence the stability characteristics. These isolated strakes may be treated through use of very low aspect ratio wing theory and wing-body carry-over interference. An empirically derived technique is available from Aiello and Bateman (Reference 58) and is shown in Figure 147. Body-strake aerodynamic effects are predicted as an increment to the body-alone aerodynamics. The criteria which defines those panels which are classified as "wings" or "fins" and those which are classed as "strakes" is lacking. A cut-off aspect ratio or span-to-diameter ratio should be defined to distinguish between the methods to be utilized. It is recommended that the Aiello method be compared with low aspect ratio wing theory and carry-over interference effects so that a method can be chosen. In addition, a criteria should be defined which specifies those surfaces which should be analyzed using wing theory or strake methodology. The Aiello and Bateman method is recommended, subject to a thorough quantiative analysis.

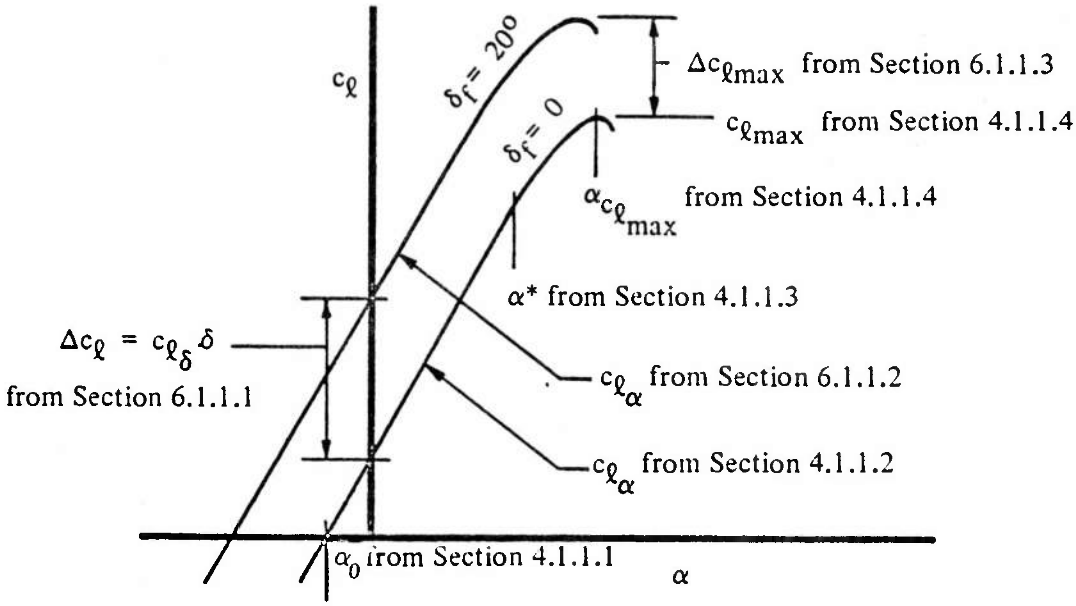

Figure 129. Panel Section Lift Due to Plain Flap, from Datcom

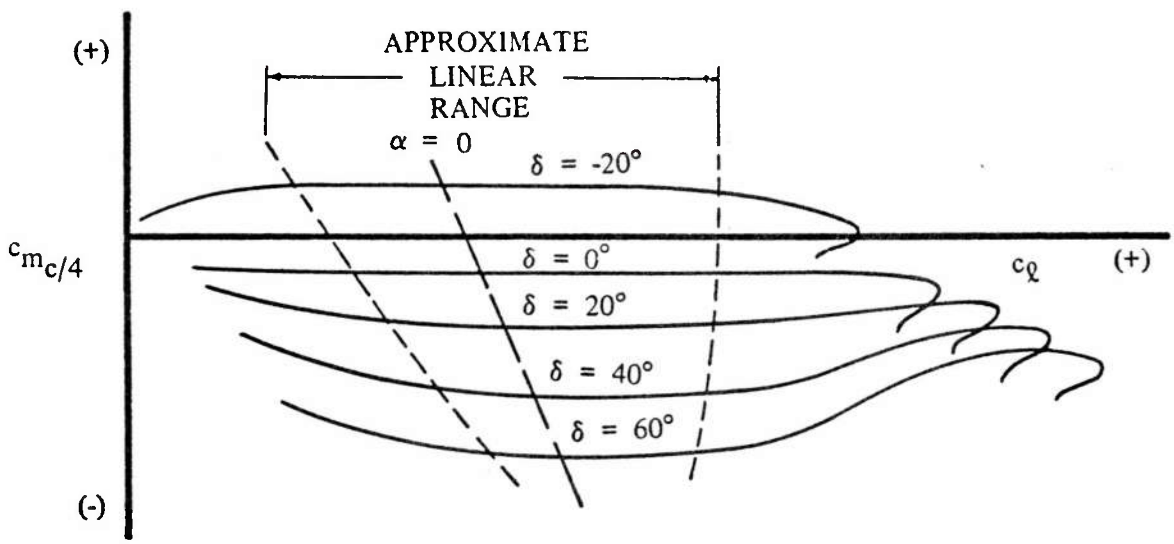

Figure 130. Panel Section Pitching Moment Linear Range, from Datcom

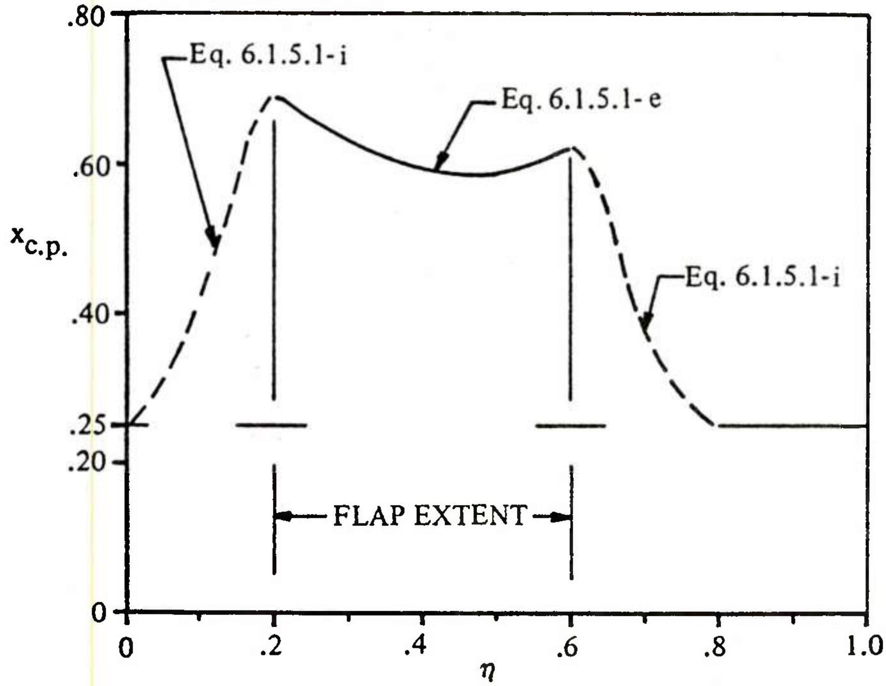

Figure 131. Center of Pressure Across a Flapped Surface, from Datcom

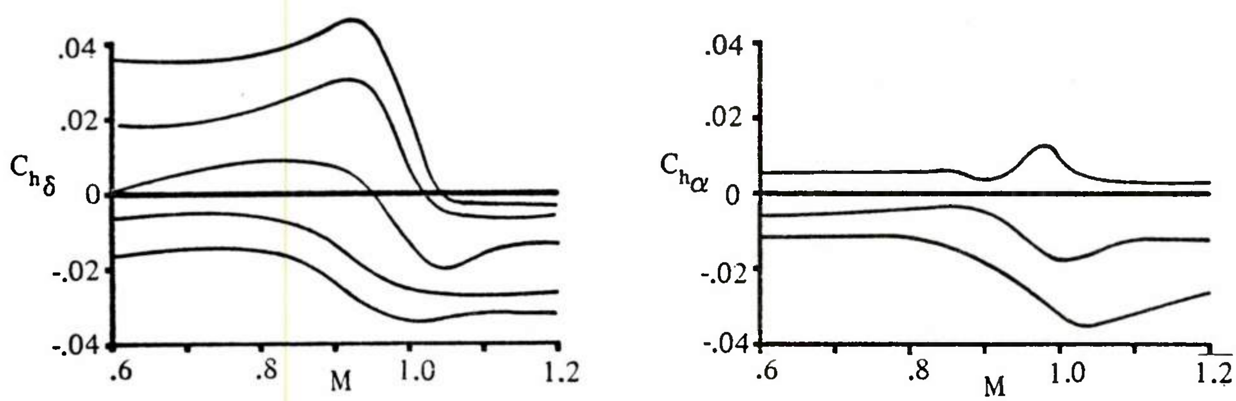

Figure 132. Typical Hinge Moment Results for A Plain Flap, from Datcom

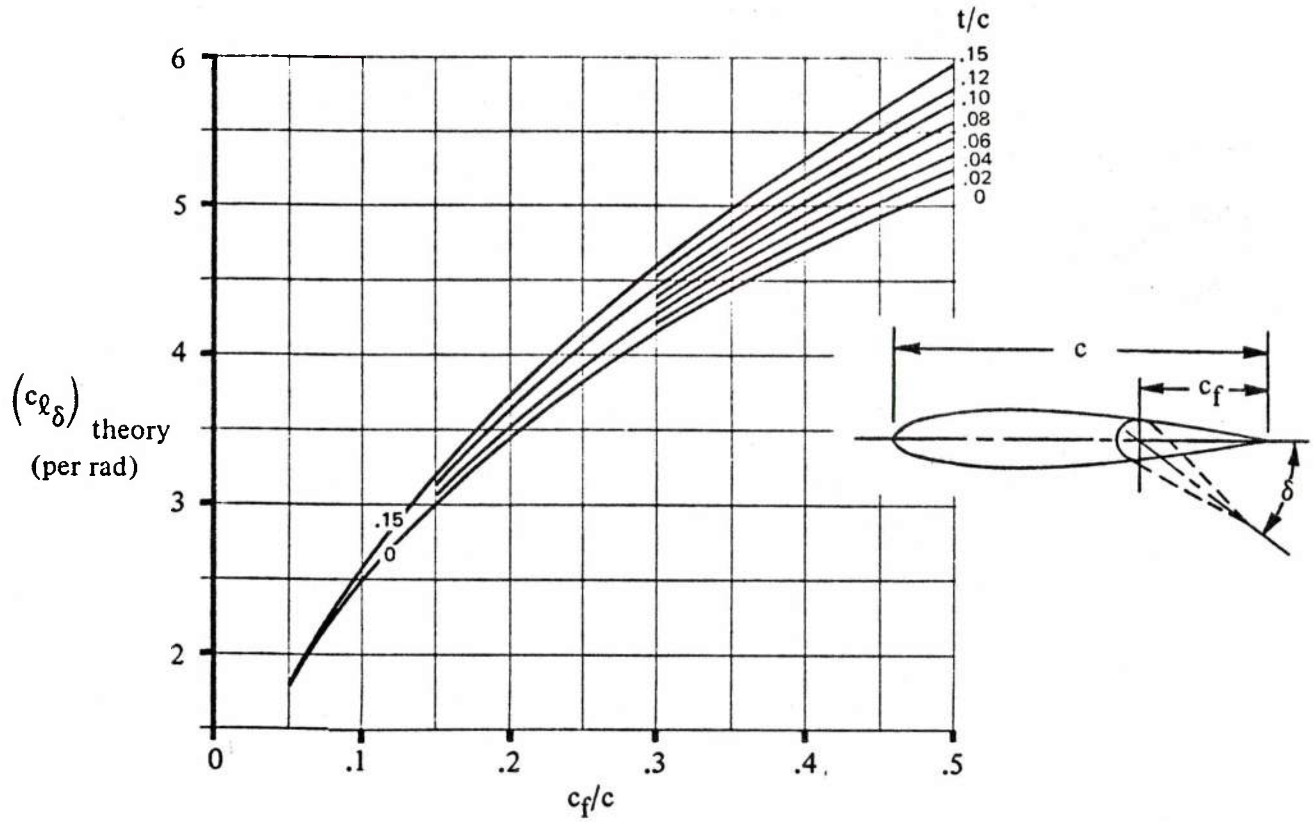

Figure 133. Theoretical Lift Effectiveness of Plain Trailing-Edge Flaps

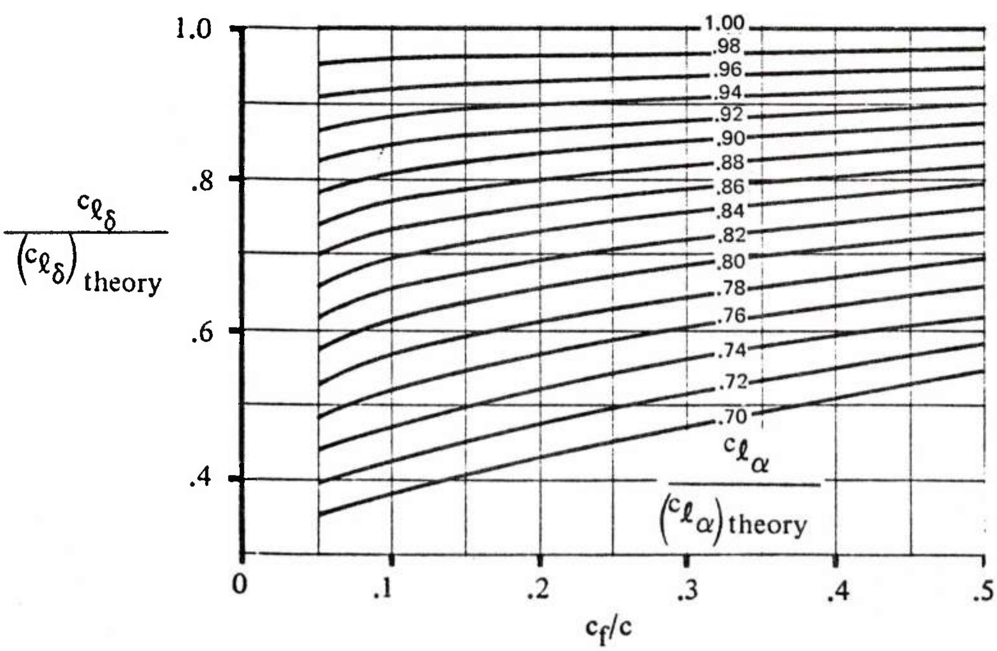

Figure 134. Empirical Correction for Lift Effectiveness of Plain Trailing-Edge Flaps

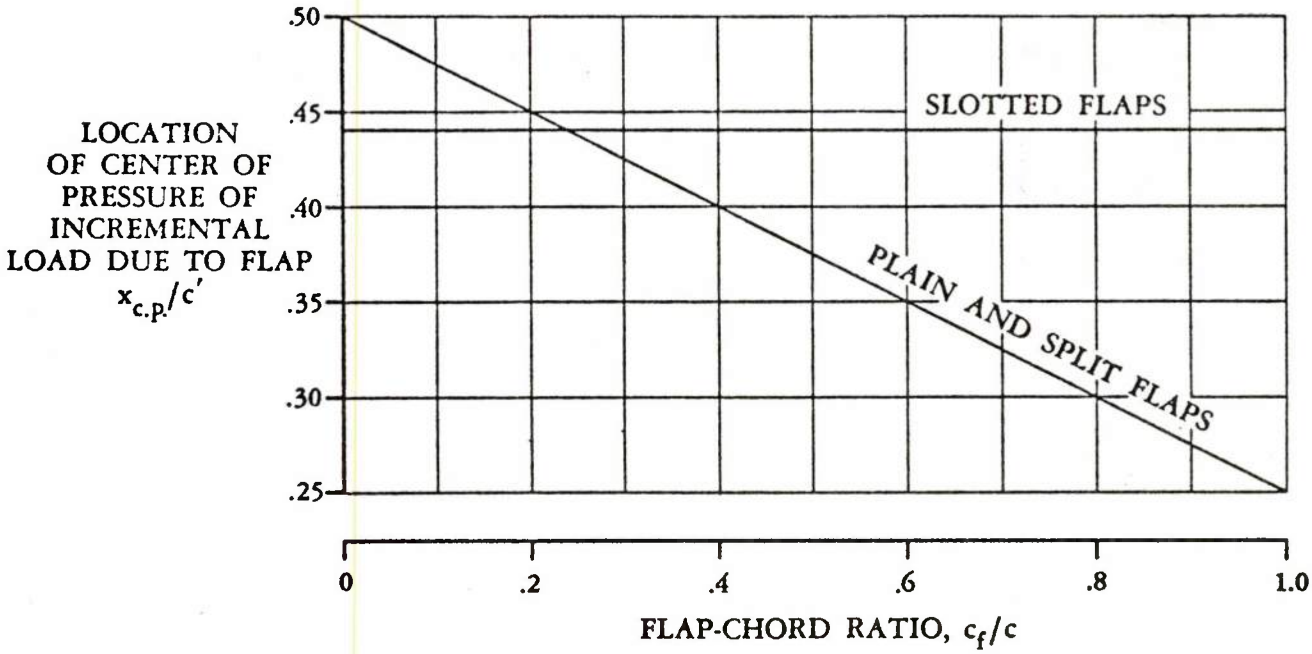

Figure 135. Empirical Location of Center of Pressure of Incremental Load due to Trailing-Edge, Mechanical Flaps

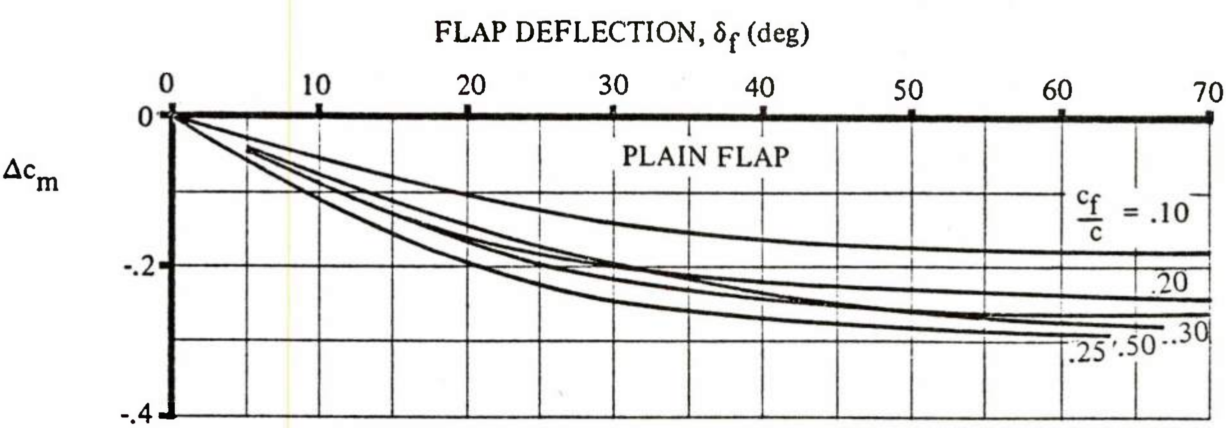

Figure 136. Effect of Trailing Edge Flap Deflection and Flap-Chord-to-Wing-Chord Ratio on Section Incremental Pitching Moment Due to Plain Flaps

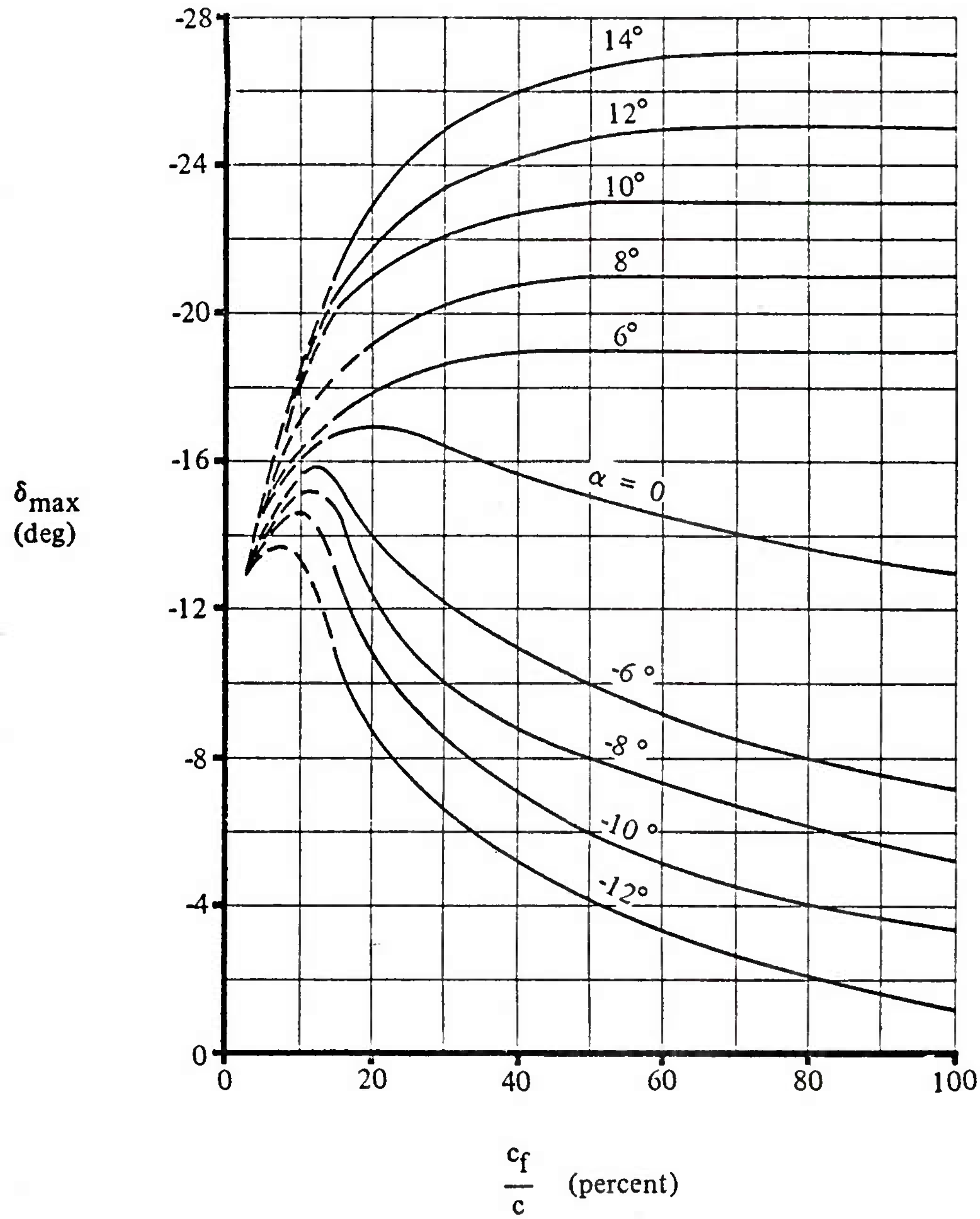

Figure 137. Approximate Maximum Control-Surface and Deflections for Linear Control Characteristics of a Plain, Sealed Flap (NACA 0009 Airfoil)

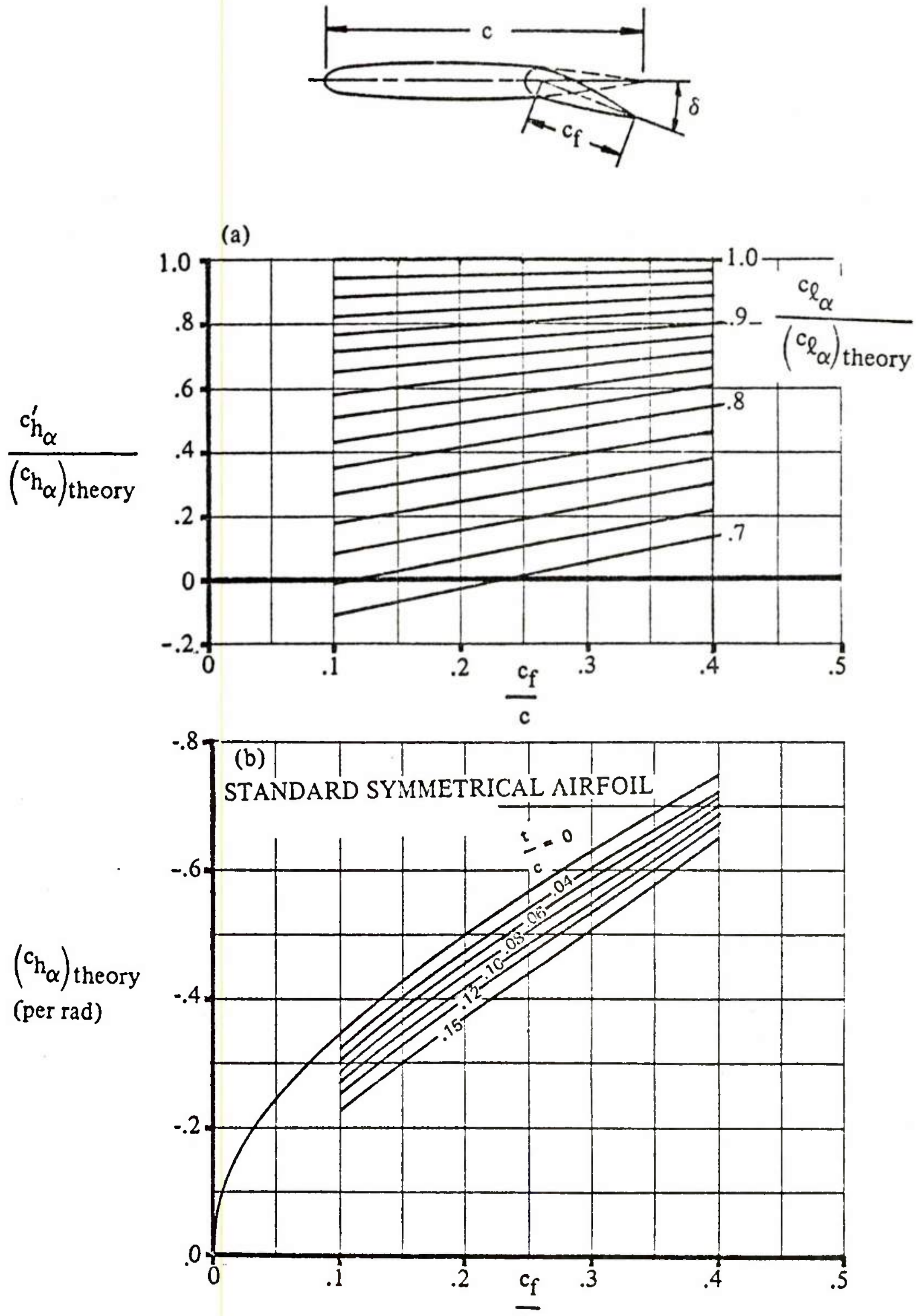

Figure 138. Rate of Change of Section Hinge Moment Coefficient With Angle of Attack for A Plain Flap

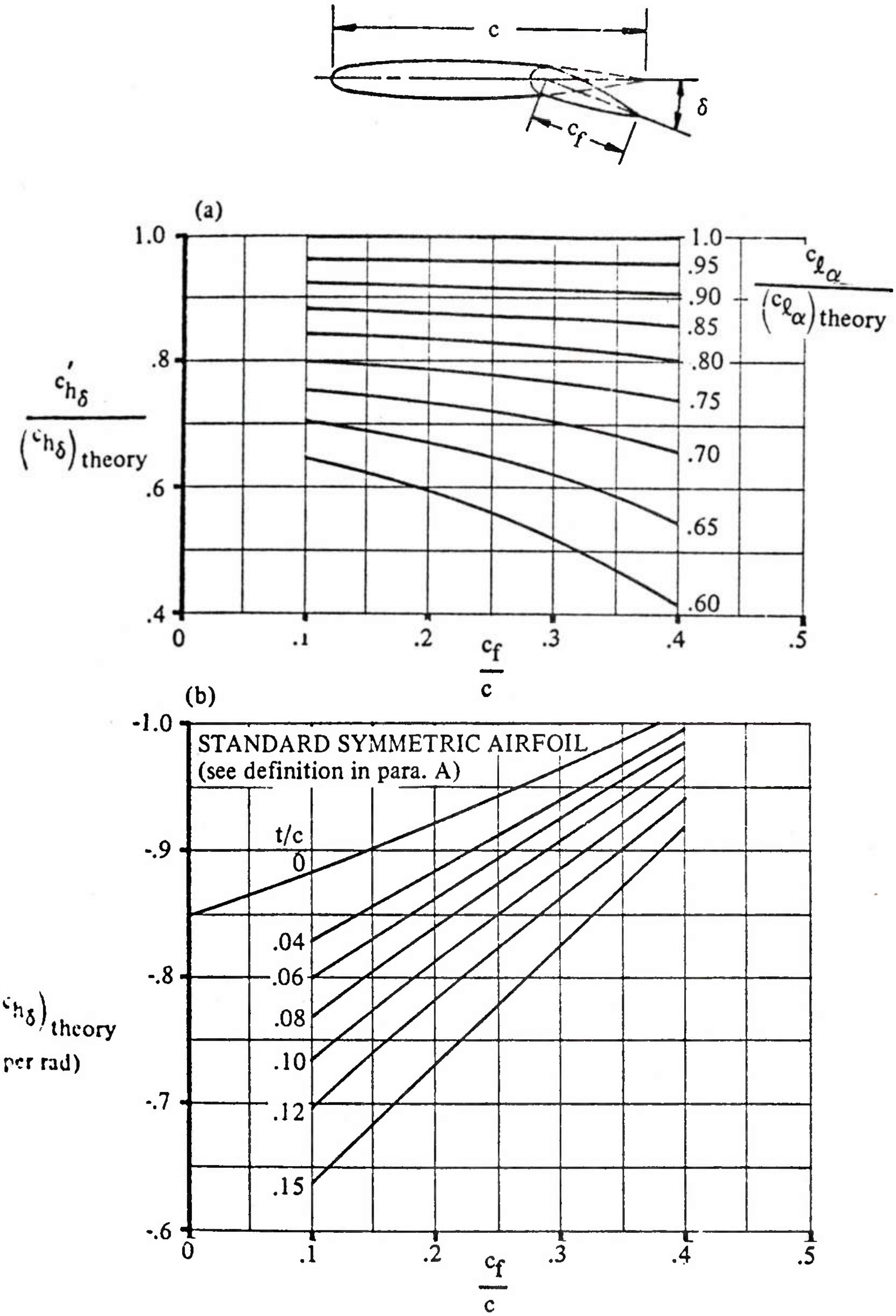

Figure 139. Rate of Change of Hinge-Moment Coefficient with Control Deflection for a Plain Flap

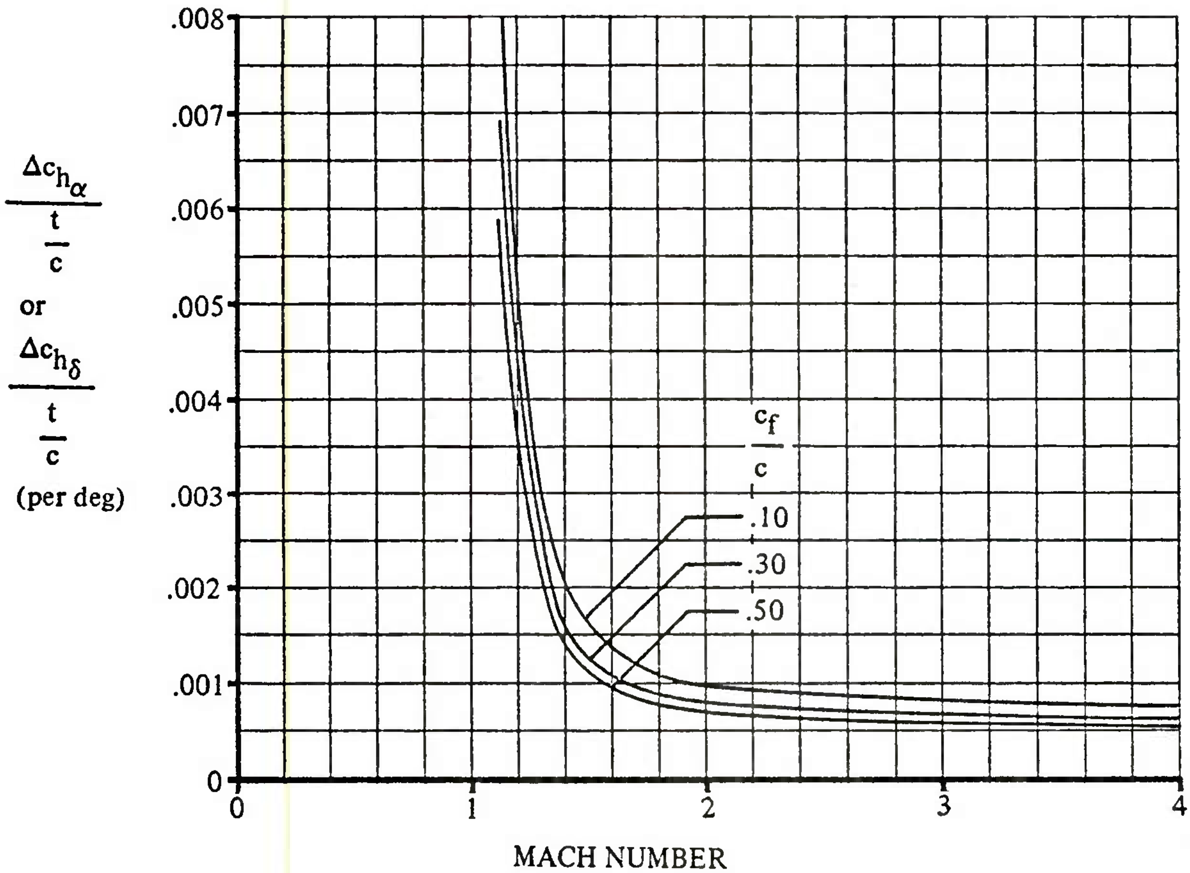

Figure 140. Thickness Correction Factor for Hinge-Moment Derivatives for Symmetric, Circular-Arc Airfoils

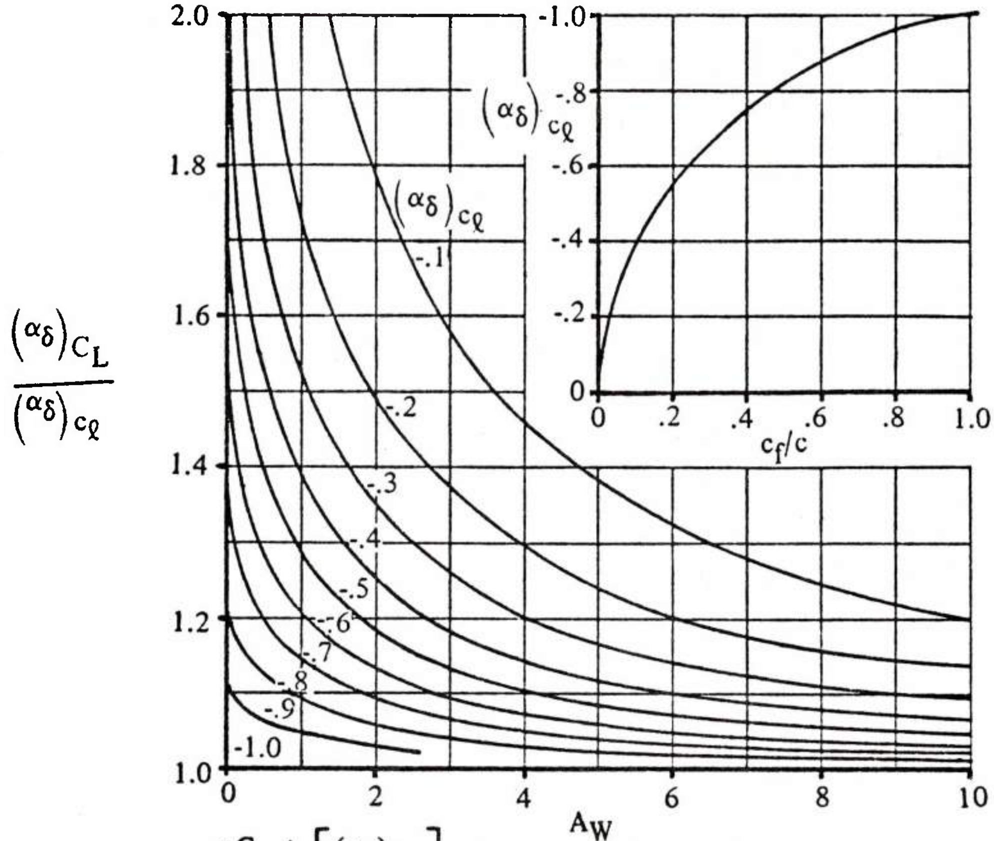

$$\Delta C_L = \Delta c_\ell \left(\frac{C_{L_\alpha}}{c_{\ell_\alpha}}\right)\left[\frac{(\alpha_\delta)_{C_L}}{(\alpha_\delta)_{c_\ell}}\right] K_b$$

Figure 141. Flap-Chord Factor

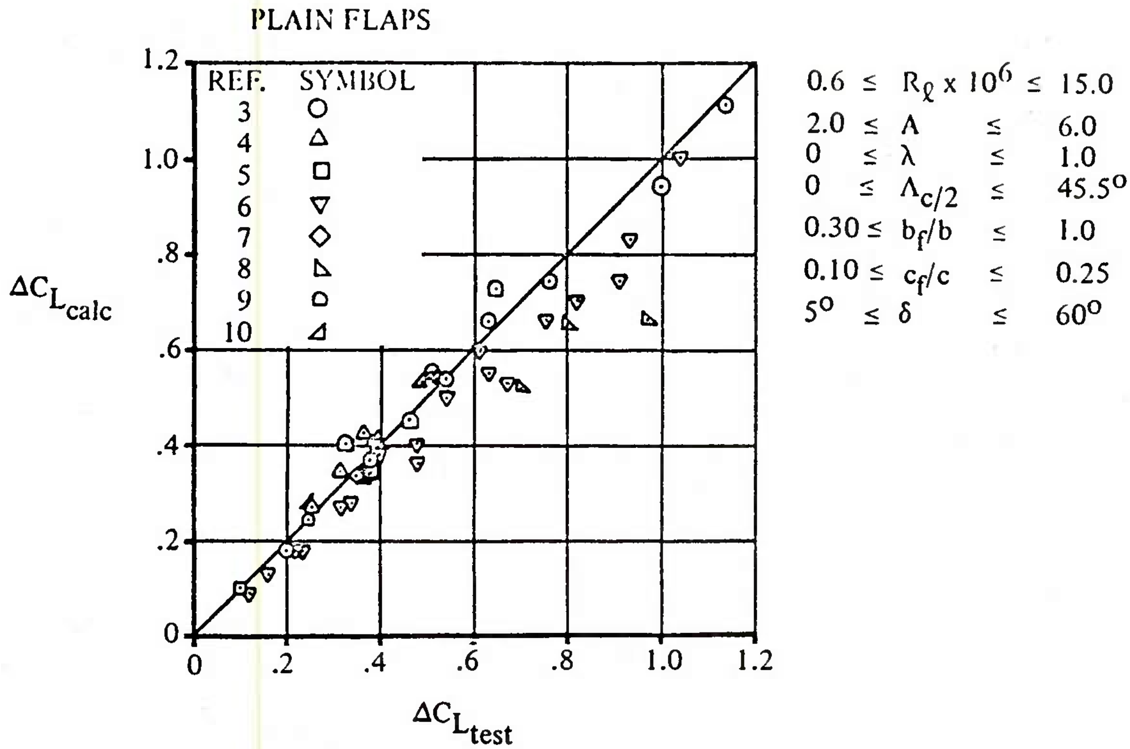

Figure 142. Correlation of Datcom Plain Flap Method for Lift With Test Data

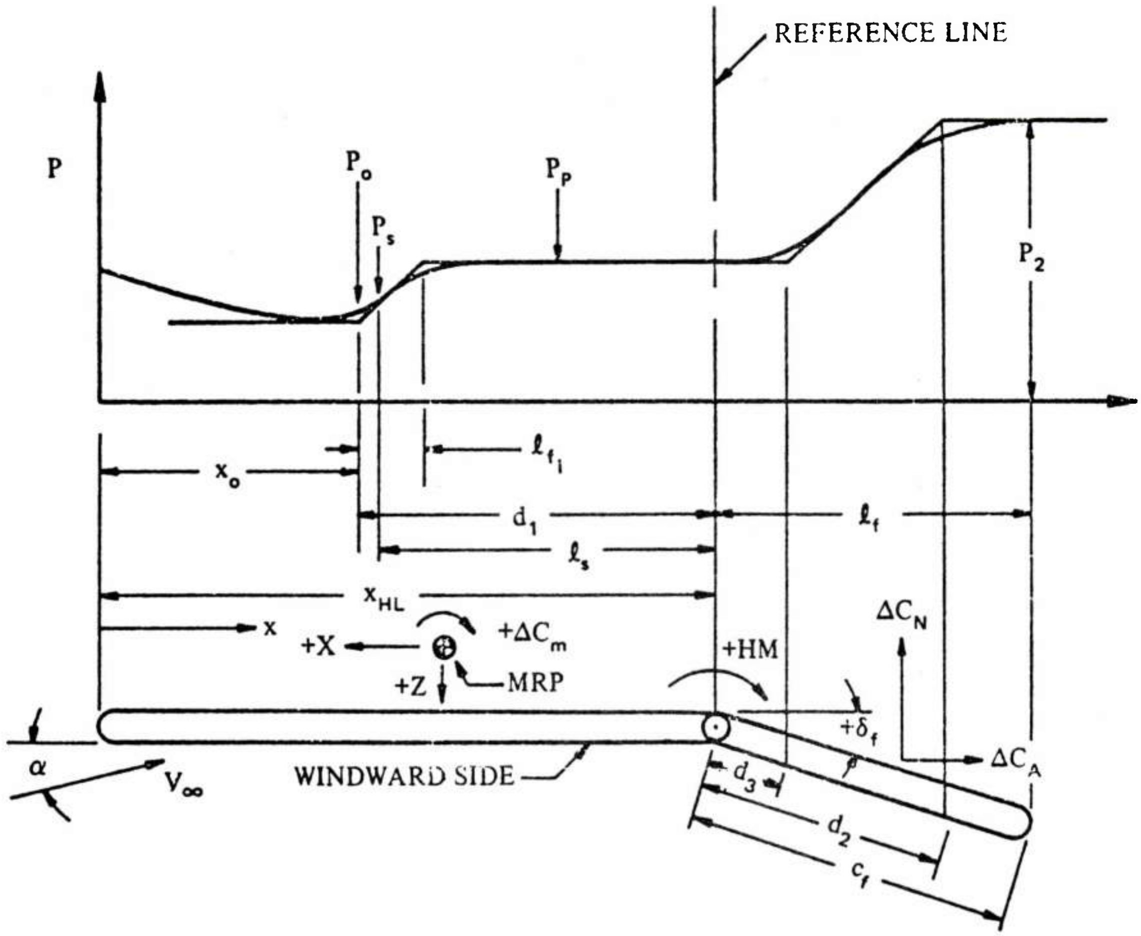

Figure 143. Pressure Distribution for a Plain Flap Panel at High Speed (Hypersonic Flap), from Datcom

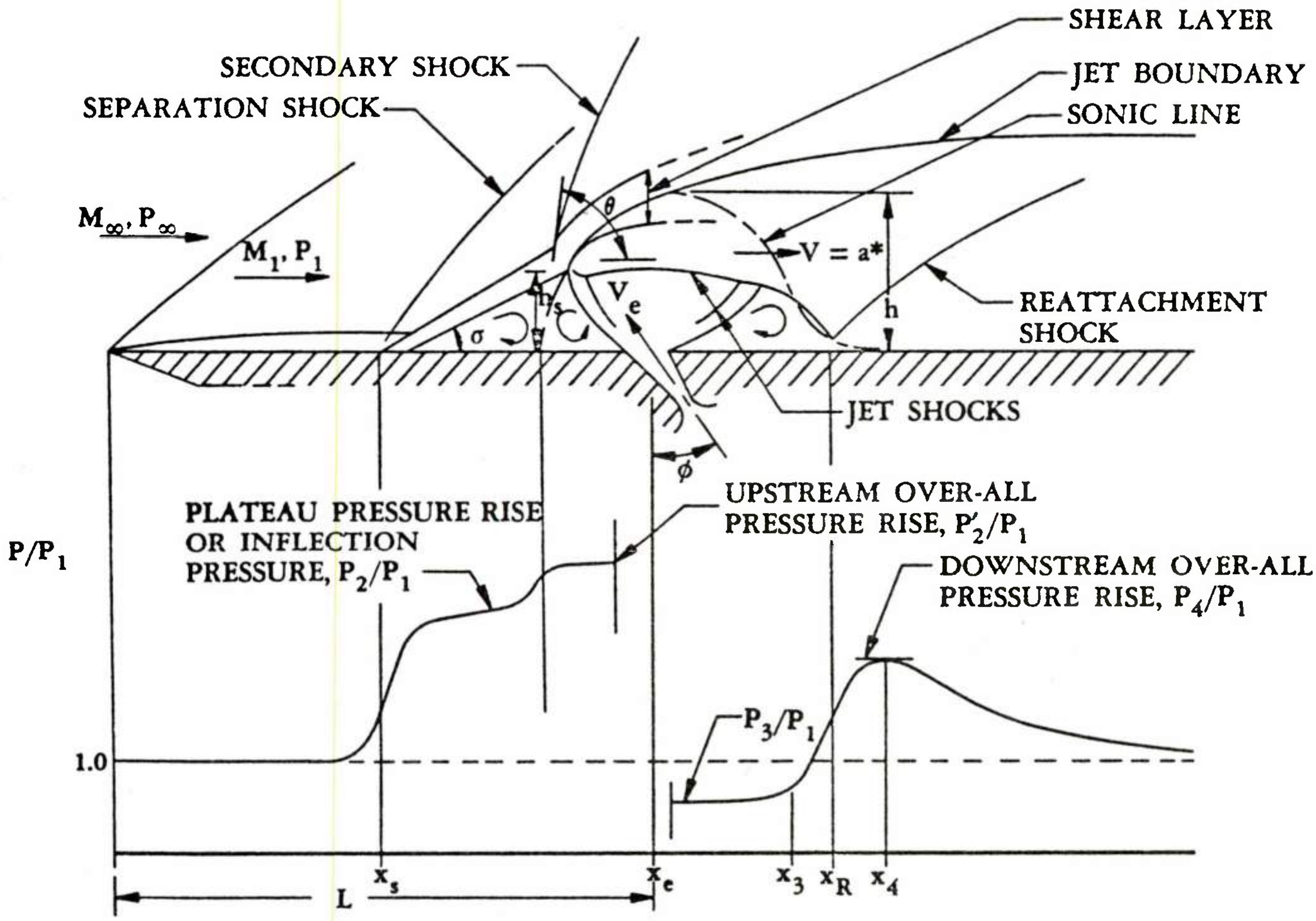

Figure 144. Pressure Distribution Due to Transverse-Jet Control, from Datcom

CONSIDERABLE BENEFIT TO BANK-TO-TURN MISSILES
- SWEEP BREAK SEVERS VORTEX FEEDING SHEETS
- SHED VORTICES INCREASE LIFT EFFECTIVENESS

Figure 145. Wing Strakes in Aerodynamics

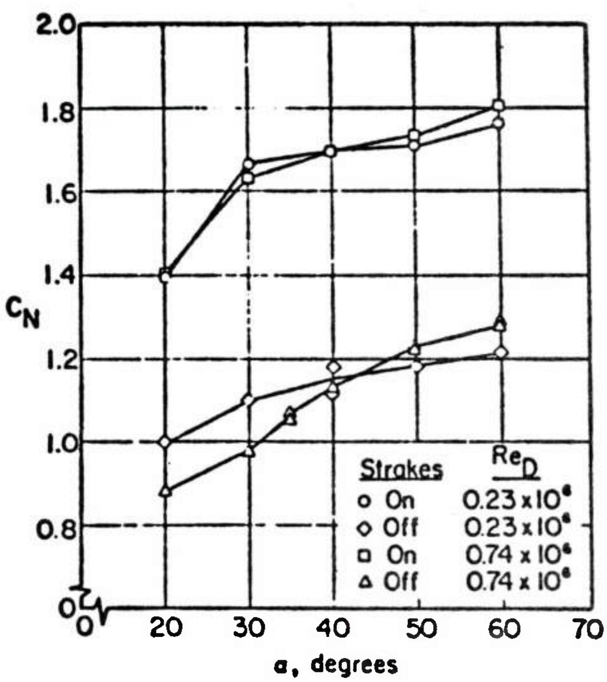

VORTICES TEND TO STABILIZE FLOW

DELAY SEPARATION

INCREASE LIFT, EVEN AT HIGH ALPHA

Figure 146. Benefit of Wing Strakes

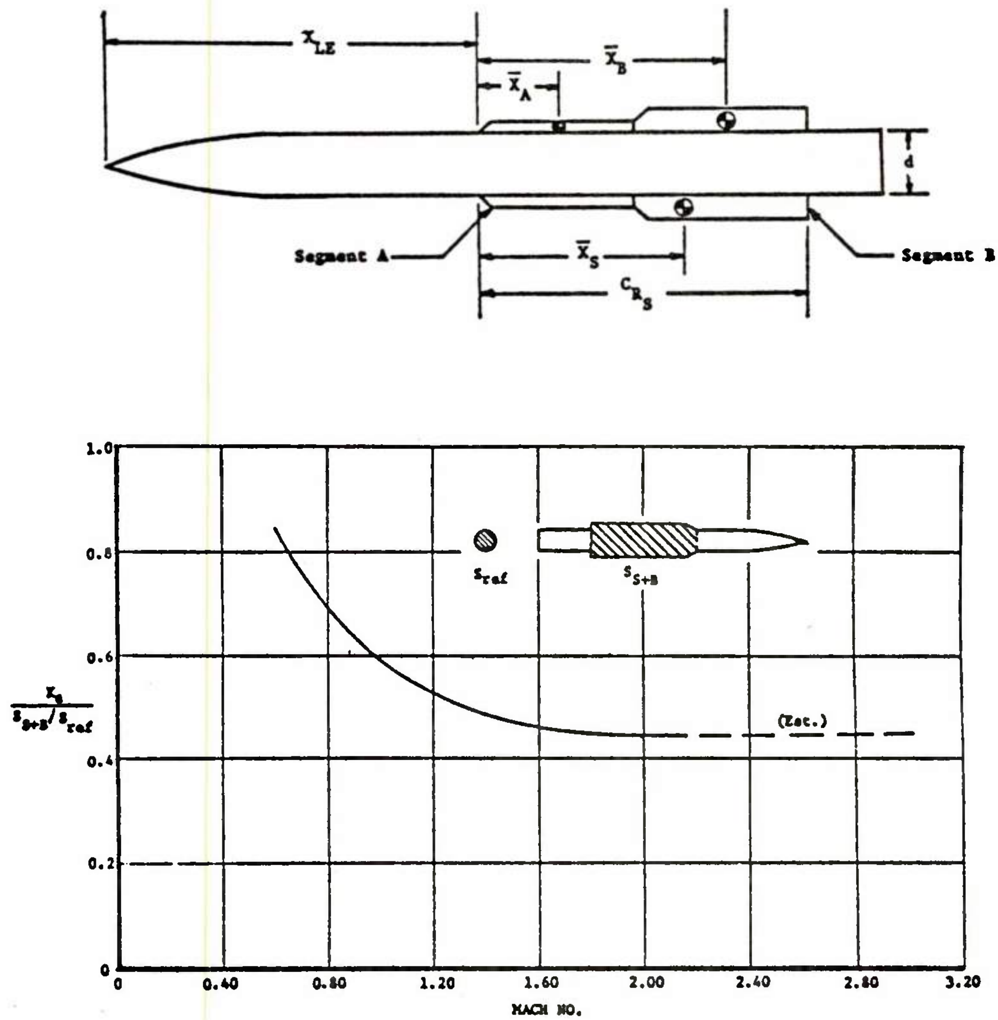

Figure 147. Aiello Strake Method

SECTION 9
DYNAMIC DERIVATIVE METHODOLOGY

The most comprehensive compendium of dynamic derivative methodology is that of Datcom which is valid only at low angles of attack with attached flow conditions. Few theoretical methods are available to compute the dynamic derivatives of configurations not covered by Datcom. The Datcom methods are summarized in Table 17. These techniques are presented in the stability-axes coordinate system. Transfer equations from stability to body axes have been recommended in Section 2 of this report. The Magnus effect is discussed in Section 10.

Body and Body Fin Configurations - Most of the available methodology for body configurations is derived from slender body theory (see for example References 12, 200, and 201), or correlations of large amounts of test results. Although rigorous numerical techniques are available, such as in References 92 and 201, their complexity is considered beyond the suitability for Missile Datcom. The recent works of Ericsson (Reference 204-206) have extended the simple slender body theory and Newtonian theory methods to more properly account for Mach number. The method suggested by Erricson for bodies is (from Reference 204)

$$C_{m_q} + C_{m_{\dot{\alpha}}} = -2(0.77 + 0.23\,M_\infty^2)\cos\alpha\,(\frac{\ell}{d} \quad 0.77 + 0.23\,M_\infty^2 - \frac{X_{CG}}{d})^2$$

based on

$$\frac{d}{V_\infty}$$

This method has shown acceptable accuracy to Mach 6.0 but further substantiation of the method is required. Comparison of results with experimental data and the empirical results for the SPINNER code (Reference 208) is shown in Figure 148. In Reference 206, Ericsson presented methods which give excellent results for body-wing pitch damping at all speeds. These methods are recommended techniques for Missile Datcom. Other theoretical methods summarized in Datcom are given in References 211-221.

Other Configurations - The methodology available can be summarized as follows:

o DATCOM - THEORY (SLENDER-BODY, LIFTING SURFACE) (* SUBSONIC ONLY)

WINGS - C_{N_q}, C_{m_q}, C_{A_q}*, C_{Y_p}, C_{ℓ_p}, C_{n_p}, C_{ℓ_r}*, C_{n_r}, $C_{N_{\dot{\alpha}}}$, $C_{A_{\dot{\alpha}}}$*

BODY - C_{N_q}, C_{m_q}, $C_{N_{\dot{\alpha}}}$, $C_{M_{\dot{\alpha}}}$

WING-BODY - C_{N_q}, C_{m_q}, C_{ℓ_q}, $C_{N_{\dot{\alpha}}}$, $C_{M_{\dot{\alpha}}}$

BODY-WING-TAIL - C_{N_q}, C_{m_q}, C_{A_q}, C_{ℓ_p}*, C_{n_p}*, C_{Y_p}*, C_{Y_r}*, C_{ℓ_r}*, C_{n_r}*, C_{N_α}, C_{m_α}, C_{A_α}*, $C_{Y_\beta}^*$, $C_{n_\beta}^*$, $C_{\ell_\beta}^*$

o "SPINNER" PROGRAM - EMPIRICAL

EMPIRICAL DATA BASE

$C_{m_q} + C_{m_{\dot{\alpha}}}$

C_{ℓ_p}

MAGNUS

A suitable means of predicting the effects of forward lifting surfaces on the dynamic derivatives of aft lifting surfaces are required for these configurations which employ multiple lifting surfaces. Direct summation of the contributions of the configuration components provide an adequate first-order approximation, but the interference effects between components can be substantial. The only comprehensive interference methods available are those presented in Datcom. It is recommended that they be employed.

Angle of Attack Effect - No methods are available. The primary disadvantage of dynamic derivative methodology is its restriction to low angle of attack, attached flow conditions. No methodology was found that specifically addresses the effect of body incidence.

Jet Effects - No methods are recommended. Although jet pluming can affect the dynamic stability of a missile, it cannot be evaluated. It is ignored in most preliminary or conceptual designs.

Jet effects on dynamic derivatives are rarely calculated in existing prediction codes. Not all derivatives are necessary for preliminary or conceptual design, but the major contributors to dynamic stability: C_{m_q}, C_{n_r}, $C_{m_{\dot{\alpha}}}$, $C_{n_{\dot{\beta}}}$, and C_{ℓ_p} should be included in Missile Datcom. An important consideration in the choice of necessary derivatives is the missile configuration type and guidance steering class. Langham, Reference 207, performed an analysis of two missile configurations: the Interlab Air-to-Air Technology (ILAAT) and

the Aerodynamic Data Correlation (ADC) configurations, to determine the sensitivity to the dynamic stability derivatives. The following parameters were found to cause variations in missile motion: C_{m_q}, $C_{m_{\dot{\alpha}}}$, C_{n_r}, C_{ℓ_p}, C_{ℓ_r} and C_{n_p}, the derivatives C_{m_r}, C_{L_q}, $C_{L_{\dot{\alpha}}}$, C_{Y_p}, and C_{Y_r} were deemed insignificant to motion for both bank-to-turn and skid-to-turn configurations. It is recommended that a complete compendium of dynamic stability methodology be included. Although the results of Langham will prove valuable for some design configurations, a thorough analysis of a specific configuration is required to quantify those derivatives which are design critical.

TABLE 17 SUMMARY OF DATCOM DYNAMIC DERIVATIVE METHODS

METHODS SUMMARY

DERIVATIVE	CONFIG.	SPEED REGIME	EQUATIONS FOR DERIVATIVE ESTIMATION (Datcom section for components indicated)	METHOD LIMITATIONS ASSOCIATED WITH EQUATION COMPONENTS
C_{L_q}	W	SUBSONIC	$C_{L_q} = \left(\frac{1}{2} + 2\underbrace{\frac{\bar{x}}{\bar{c}}}_{4.1.4.2}\right)\underbrace{C_{L_\alpha}}_{4.1.3.2}$ Eq. 7.1.1.1-a	$\frac{\bar{x}}{\bar{c}}$ 1. $M < 0.6$; however, for swept wings with $t/c < 0.04$, application to higher Mach numbers is acceptable 2. Linear-lift range C_{L_α} 3. No curved planforms 4. $M < 0.8$, $t/c < 0.1$, if cranked wings with round LE
		TRANSONIC	(Same as subsonic equation)	$\frac{\bar{x}}{\bar{c}}$ 1. Straight-tapered wings 2. No camber C_{L_α} 3. Conventional thickness distribution 4. $\alpha = 0$
		SUPERSONIC	$C_{L_q} = \underbrace{C_{L_q}'}_{7.1.1.1} + 2\underbrace{\left(\frac{\bar{x}}{\bar{c}}\right)}_{4.1.4.2}\underbrace{C_{N_\alpha}}_{4.1.3.2}$ Eq. 7.1.1.1-c	1. Straight-tapered wings C_{L_q}' (a) Subsonic LE ($\beta \cot \Lambda_{LE} < 1$) 2. Mach lines from TE vertex may not intersect LE 3. Wing-tip Mach lines may not intersect on wings nor intersect opposite wing tips (b) Supersonic LE ($\beta \cot \Lambda_{LE} > 1$) 4. Valid only if Mach lines from LE vertex intersect TE 5. Foremost Mach line from either wing tip may not intersect remote half of wing $\frac{\bar{x}}{\bar{c}}$ 6. Linear-lift range

TABLE 17. (CONTINUED)

METHODS SUMMARY

DERIVATIVE	CONFIG.	SPEED REGIME	EQUATIONS FOR DERIVATIVE ESTIMATION (Datcom section for components indicated)	METHOD LIMITATIONS ASSOCIATED WITH EQUATION COMPONENTS
C_{L_q} (Contd.)	W (Contd.)	SUPERSONIC (Contd.)		C_{N_α} 7. $M > 1.4$
	WB	SUBSONIC	$\left(C_{L_q}\right)_{WB} = \underbrace{\left[K_{W(B)} + K_{B(W)}\right]}_{4.3.1.2}\left(\frac{S_e}{S}\right)\left(\frac{\bar{c}_e}{\bar{c}}\right)\underbrace{\left(C_{L_q}\right)_e}_{7.1.1.1} + \underbrace{\left(C_{L_q}\right)_B}_{7.2.1.1}\left(\frac{S_b}{S}\right)\left(\frac{\ell_B}{\bar{c}}\right)$ Eq. 7.3.1.1-a	Method 1 (body diameter)/(wing span) is small (see 4.3.1.2 Sketch (d)) $\left(C_{L_q}\right)_e$ 1. No curved planforms 2. Linear-lift range 3. $M < 0.6$; however, for swept wings with $t/c < 0.04$, application to higher Mach numbers is acceptable 4. $M < 0.8$, $t/c < 0.1$, if cranked wing with round LE $\left(C_{L_q}\right)_B$ 5. Bodies of revolution
			$\left(C_{L_q}\right)_{WB} = \underbrace{K_{(WB)}}_{4.3.1.2}\underbrace{\left(C_{L_q}\right)_W}_{7.1.1.1} + \underbrace{\left(C_{L_q}\right)_B}_{7.2.1.1}\left(\frac{S_b}{S}\right)\left(\frac{\ell_B}{\bar{c}}\right)$ Eq. 7.3.1.1-b	Method 2 (body diameter)/(wing span) is large, with delta wing extending entire length of body (see 4.3.1.2 Sketch (c)) (same limitations as Method 1 above)
		TRANSONIC	(Same as subsonic equations)	Method 1 (body diameter)/(wing span) is small (see 4.3.1.2 Sketch (d)) $K_{B(W)}$ (based on exposed wing geometry) $\left(C_{L_q}\right)_e$ 1. Straight-tapered wings 2. No camber 3. Conventional thickness distribution 4. $\alpha = 0$ $\left(C_{L_q}\right)_B$ 5. Bodies of revolution
				Method 2 (body diameter)/(wing span) is large, with delta wing extending entire length of body (see 4.3.1.2 Sketch (c)) (same limitations as Method 1 above)
		SUPERSONIC	(Same as subsonic equations)	Method 1 (body diameter)/(wing span) is small (see 4.3.1.2 Sketch (d)) $K_{B(W)}$ (based on exposed wing geometry) $\left(C_{L_q}\right)_e$ 1. Straight-tapered wings 2. $M > 1.4$ 3. Linear-lift range

TABLE 17 (CONTINUED)
METHODS SUMMARY

DERIVATIVE	CONFIG.	SPEED REGIME	EQUATIONS FOR DERIVATIVE ESTIMATION (Datcom section for components indicated)	METHOD LIMITATIONS ASSOCIATED WITH EQUATION COMPONENTS
C_{L_q} (Contd.)	WB (Contd.)	SUPERSONIC (Contd.)		(a) Subsonic LE ($\beta \cot \Lambda_{LE} < 1$) 4. Mach lines from TE vertex may not intersect LE 5. Wing tip Mach lines may not intersect on wing nor intersect opposite wing tips (b) Supersonic LE ($\beta \cot \Lambda_{LE} > 1$) 6. Valid only if Mach lines from LE vertex intersect TE 7. Foremost Mach line from either wing tip may not intersect remote half of wing $\left(C_{L_q}\right)_B$ 8. Bodies of revolution
				Method 2 (body diameter)/(wing span) is large, with delta wing extending entire length of body (see 4.3.1.2 Sketch (c)) (same limitations as Method 1 above)
	WBT	SUBSONIC	$C_{L_q} = \underbrace{\left(C_{L_q}\right)_{WB}}_{7.3.1.1} + 2 \underbrace{\left[K_{W(B)} + K_{B(W)}\right]''}_{4.3.1.2} \left(\frac{S_e''}{S'}\right) \underbrace{\left(\frac{x_{c.g.} - x''}{\bar{c}'}\right)}_{4.5.2.1} \underbrace{\left(\frac{q''}{q_\infty}\right)}_{4.4.1} \underbrace{\left(C_{L_\alpha}\right)_e''}_{4.1.3.2}$ Eq. 7.4.1.1-a	Method 1 $b_W/b_H \geq 1.5$ $\left(C_{L_q}\right)_{WB}$ (based on exposed wing geometry) 1. Linear-lift range 2. No curved planforms 3. Bodies of revolution 4. $M \leq 0.6$; however, for swept wings with $t/c \leq 0.04$, application to higher Mach numbers is acceptable 5. $M \leq 0.8$, $t/c \leq 0.1$, if cranked wings with round LE $\frac{q''}{q_\infty}$ 6. Valid only on the plane of symmetry $\left(C_{L_\alpha}\right)_e''$ 7. Additional tail limitations are identical to Items 2 and 5 immediately above
			$C_{L_q} = \underbrace{\left(C_{L_q}\right)_{WB}}_{7.3.1.1} + 2 \underbrace{\frac{x_{c.g.} - x''}{\bar{c}'}}_{4.5.2.1} \left\{ \underbrace{\left[K_{W(B)} + K_{B(W)}\right]''}_{4.3.1.2} \left(\frac{S_e''}{S'}\right) \underbrace{\left(\frac{q''}{q_\infty}\right)}_{4.4.1} \underbrace{\left(C_{L_\alpha}\right)_e''}_{4.1.3.2} + \underbrace{\left(C_{L_\alpha}\right)_{W''(v)}}_{7.4.1.1} \right\}$ Eq. 7.4.1.1-b	Method 2 $b_W/b_H < 1.5$ (same limitations as Method 1 above) $\left(C_{L_q}\right)_{WB}$ and $\left(C_{L_\alpha}\right)_{W''(v)}$ (based on exposed wing geometry)
		TRANSONIC	(Same as subsonic equations)	Method 1 $b_W/b_H \geq 1.5$ $\left(C_{L_q}\right)_{WB}$ (based on exposed wing geometry) 1. Straight-tapered wings 2. No camber 3. Conventional thickness distribution 4. Bodies of revolution

TABLE 17 (CONTINUED)

METHODS SUMMARY

DERIVATIVE	CONFIG.	SPEED REGIME	EQUATIONS FOR DERIVATIVE ESTIMATION (Datcom section for components indicated)	METHOD LIMITATIONS ASSOCIATED WITH EQUATION COMPONENTS
C_{L_q} (Contd.)	WBT (Contd.)	TRANSONIC (Contd.)		5. $\alpha = 0$ $K_{a(W)}$ (based on exposed wing geometry) $\frac{q''}{q_\infty}$ 6. Conventional trapezoidal planforms 7. Valid only on the plane of symmetry $\left(C_{L_\alpha}\right)_e''$ 8. Additional tail limitations are identical to Items 2, 3, and 5 immediately above Method 2 $b_W/b_H < 1.5$ (same limitations as Method 1 above) $\left(C_{L_q}\right)_{WB}$, $K_{B(W)}$, and $\left(C_{L_\alpha}\right)_{W''(v)}$ (based on exposed wing geometry)
		SUPERSONIC	(Same as subsonic equations)	Method 1 $b_W/b_H \geq 1.5$ 1. Linear-lift range $\left(C_{L_q}\right)_{WB}$ (based on exposed wing geometry) 2. Straight-tapered wings 3. Bodies of revolution 4. $M \geq 1.4$ $K_{B(W)}$ (based on exposed wing geometry) (a) Subsonic LE ($\beta \cot \Lambda_{LE} < 1$) 5. Mach line from TE vertex may not intersect LE 6. Wing-tip Mach lines may not intersect on wing nor intersect opposite wing tips (b) Supersonic LE ($\beta \cot \Lambda_{LE} > 1$) 7. Valid only if Mach lines from LE vertex intersect TE 8. Foremost Mach line from either wing tip may not intersect remote half of wing $\frac{q''}{q_\infty}$ 9. If nonviscous flow field, limited to unswept wings 10. If viscous flow field, valid only on plane of symmetry $\left(C_{L_\alpha}\right)_e''$ 11. Additional tail limitations are identical to Items 1 and 4 immediately above Method 2 $b_W/b_H < 1.5$ (same limitations as Method 1 above) $\left(C_{L_q}\right)_{WB}$, $K_{B(W)}$, and $\left(C_{L_\alpha}\right)_{W''(v)}$ (based on exposed wing geometry)

TABLE 17 (CONTINUED)

METHODS SUMMARY

DERIVATIVE	CONFIG.	SPEED REGIME	EQUATIONS FOR DERIVATIVE ESTIMATION (Datcom section for components indicated)		METHOD LIMITATIONS ASSOCIATED WITH EQUATION COMPONENTS
C_{m_q}	W	SUBSONIC	$\left(C_{m_q}\right)_{M\approx 0.2} = -0.7\,\underbrace{c_{\ell_\alpha}}_{\substack{4.1.1\\4.1.1.2}}\cos\Lambda_{c/4}\left\{\frac{A\left[\frac{1}{2}\overbrace{\frac{\bar{x}}{c}}^{7.1.1.1}+2\overbrace{\left(\frac{\bar{x}}{c}\right)^2}^{7.1.1.1}\right]}{A+2\cos\Lambda_{c/4}}+\frac{1}{24}\left(\frac{A^3\tan^2\Lambda_{c/4}}{A+6\cos\Lambda_{c/4}}\right)+\frac{1}{8}\right\}$	Eq. 7.1.1.2-a	$\frac{\bar{x}}{c}$ 1. $M \leq 0.6$; however, for swept wings with $t/c \leq 0.04$, application to higher Mach numbers is acceptable 2. Linear-lift range
			$\left(C_{m_q}\right)_{M>0.2} = \left[\frac{\frac{A^3\tan^2\Lambda_{c/4}}{AB+6\cos\Lambda_{c/4}}+\frac{3}{B}}{\frac{A^3\tan^2\Lambda_{c/4}}{A+6\cos\Lambda_{c/4}}+3}\right]\underbrace{\left(C_{m_q}\right)_{M\approx 0.2}}_{7.1.1.2}$	Eq. 7.1.1.2-b	
		TRANSONIC	$C_{m_q} = \frac{\left(C_{L_\alpha}\right)_M-\left(C_{L_\alpha}\right)_{M_{cr}}}{\underbrace{\left(C_{L_\alpha}\right)_{M=1.2}}_{4.1.3.2}-\underbrace{\left(C_{L_\alpha}\right)_{M_{cr}}}_{4.1.3.2}}\left[\underbrace{\left(C_{m_q}\right)_{M=1.2}}_{7.1.1.2}-\underbrace{\left(C_{m_q}\right)_{M_{cr}}}_{7.1.1.2}\right]+\underbrace{\left(C_{m_q}\right)_{M_{cr}}}_{7.1.1.2}$	Eq. 7.1.1.2-c	C_{L_α} 1. Symmetric airfoils of conventional thickness distribution 2. $\alpha = 0$ $\left(C_{m_q}\right)_{M=1.2}$ 3. Straight-tapered wings (a) Subsonic LE ($\beta\cot\Lambda_{LE} < 1$) 4. Mach line from TE vertex may not intersect LE 5. Wing-tip Mach lines may not intersect on wings nor intersect opposite wing tips (b) Supersonic LE ($\beta\cot\Lambda_{LE} > 1$) 6. Valid only if Mach lines from LE vertex intersect TE 7. Foremost Mach line from either wing tip may not intersect remote half of wing
		SUPERSONIC	$C_{m_q} = \underbrace{C_{m_q}'}_{7.1.1.2}-\underbrace{\left(\frac{\bar{x}}{c}\right)}_{7.1.1.1}\underbrace{C_{L_q}}_{7.1.1.1}$	Eq. 7.1.1.2-d	C_{m_q}' (a) Subsonic LE ($\beta\cot\Lambda_{LE} < 1$) 1. Mach line from TE vertex may not intersect LE 2. Wing-tip Mach lines may not intersect on wings nor intersect opposite wing tips (b) Supersonic LE ($\beta\cot\Lambda_{LE} > 1$) 3. Valid only if Mach lines from LE vertex intersect TE 4. Foremost Mach line from either wing tip may not intersect remote half of wing C_{L_q} 5. Straight-tapered wings 6. $M > 1.4$ 7. Linear-lift range

TABLE 17 (CONTINUED)

METHODS SUMMARY

DERIVATIVE	CONFIG.	SPEED REGIME	EQUATIONS FOR DERIVATIVE ESTIMATION (Datcom section for components indicated)	METHOD LIMITATIONS ASSOCIATED WITH EQUATION COMPONENTS
C_{m_q} (Contd.)	WB	SUBSONIC	$\left(C_{m_q}\right)_{WB} = \underbrace{\left[K_{W(B)} + K_{B(W)}\right]}_{4.3.1.2} \left(\frac{S_e}{S}\right)\left(\frac{\bar{c}_e}{\bar{c}}\right)^2 \underbrace{\left(C_{m_q}\right)_e}_{7.1.1.2} + \underbrace{\left(C_{m_q}\right)_B}_{7.2.1.2} \left(\frac{S_b}{S}\right)\left(\frac{\ell_B}{\bar{c}}\right)^2$ Eq. 7.3.1.2-a	Method 1 (body diameter)/(wing span) is small (see 4.3.1.2 Sketch (d)) 1. Linear-lift range $\left(C_{m_q}\right)_e$ 2. M < 0.6; however, for swept wings with t/c < 0.04, application to higher Mach numbers is acceptable $\left(C_{m_q}\right)_B$ 3. Bodies of revolution
			$\left(C_{m_q}\right)_{WB} = \underbrace{K_{(WB)}}_{4.3.1.2} \underbrace{\left(C_{m_q}\right)_W}_{7.1.1.2} + \underbrace{\left(C_{m_q}\right)_B}_{7.2.1.2} \left(\frac{S_b}{S}\right)\left(\frac{\ell_B}{\bar{c}}\right)^2$ Eq. 7.3.1.2-b	Method 2 (body diameter)/(wing span) is large with delta wing extending entire length of body (see 4.3.1.2 Sketch (c)) (same limitations as Method 1 above)
		TRANSONIC	(Same as subsonic equations)	Method 1 (body diameter)/(wing span) is small (see 4.3.1.2 Sketch (d)) 1. Linear-lift range $K_{B(W)}$ (based on exposed wing geometry) $\left(C_{m_q}\right)_e$ 2. Straight-tapered wings 3. Symmetric airfoils of conventional thickness distribution 4. $\alpha = 0$ (a) Subsonic LE ($\beta \cot \Lambda_{LE} < 1$) 5. Mach line from TE vertex may not intersect LE 6. Wing-tip Mach lines may not intersect on wings nor intersect opposite wing tips (b) Supersonic LE ($\beta \cot \Lambda_{LE} > 1$) 7. Valid only if Mach lines from LE vertex intersect TE 8. Foremost Mach line from either wing tip may not interesect remote half of wing $\left(C_{m_q}\right)_B$ 9. Bodies of revolution
				Method 2 (body diameter)/(wing span) is large, with delta wing extending entire length of body (see 4.3.1.2 Sketch (c)) (same limitations as Method 1 above)

TABLE 17 (CONTINUED)
METHODS SUMMARY

DERIVATIVE	CONFIG.	SPEED REGIME	EQUATIONS FOR DERIVATIVE ESTIMATION (Datcom section for components indicated)	METHOD LIMITATIONS ASSOCIATED WITH EQUATION COMPONENTS
C_{m_q} (Contd.)	WB (Contd.)	SUPERSONIC	(Same as subsonic equations)	Method 1 (body diameter)/(wing span) is small (see 4.3.1.2 Sketch (d)) 1. Linear-lift range $K_{B(W)}$ (based on exposed wing geometry) $\left(C_{m_q}\right)_e$ 2. Straight-tapered wings 3. $M > 1.4$ (a) Subsonic LE ($\beta \cot \Lambda_{LE} < 1$) 4. Mach line from TE vertex may not intersect LE 5. Wing-tip Mach lines may not intersect on wings nor intersect opposite wing tips (b) Supersonic LE ($\beta \cot \Lambda_{LE} > 1$) 6. Valid only if Mach lines from LE vertex intersect TE 7. Foremost Mach line from either wing tip may not intersect remote half of wing $\left(C_{m_q}\right)_B$ 8. Bodies of revolution
				Method 2 (body diameter)/(wing span) is large with delta wing extending entire length of body (see Sketch (c) 4.3.1.2) (same limitations as Method 1 above)
	WBT	SUBSONIC	$$C_{m_q} = \underbrace{\left(C_{m_q}\right)_{WB}}_{7.3.1.2} - 2\underbrace{\left[K_{W(B)} + K_{B(W)}\right]''}_{4.3.1.2}\left(\frac{S_e''}{S'}\right)\underbrace{\left(\frac{x_{c.g.} - x''}{\bar{c}'}\right)^2}_{4.5.2.1}\underbrace{\left(\frac{q''}{q_\infty}\right)}_{4.4.1}\underbrace{\left(C_{L_\alpha}\right)_e''}_{4.1.3.2}$$ Eq. 7.4.1.2-a	Method 1 $b_W/b_H > 1.5$ $\left(C_{m_q}\right)_{WB}$ (based on exposed wing geometry) 1. Bodies of revolution 2. $M < 0.6$; however, if a swept wing with $t/c < 0.04$, application to higher Mach numbers is acceptable 3. Linear-lift range $\frac{q''}{q_\infty}$ 4. Valid only on the plane of symmetry $\left(C_{L_\alpha}\right)_e''$ 5. No curved planforms 6. $M < 0.8$, $t/c < 0.10$, if cranked planforms with round LE
			$$C_{m_q} = \underbrace{\left(C_{m_q}\right)_{WB}}_{7.3.1.2} - 2\underbrace{\left(\frac{x_{c.g.} - x''}{\bar{c}'}\right)^2}_{4.5.2.1}\left\{\underbrace{\left[K_{W(B)} + K_{B(W)}\right]''}_{4.3.1.2}\left(\frac{S_e''}{S'}\right)\underbrace{\left(\frac{q''}{q_\infty}\right)}_{4.4.1}\underbrace{\left(C_{L_\alpha}\right)_e''}_{4.1.3.2} + \underbrace{\left(C_{L_\alpha}\right)_{W'(v)}}_{4.5.1.1}\right\}$$ Eq. 7.4.1.2-b	Method 2 $b_W/b_H < 1.5$ (same limitations as Method 1 above) $\left(C_{m_q}\right)_{WB}$ and $\left(C_{L_\alpha}\right)_{W'(v)}$ (based on exposed wing geometry)

TABLE 17 (CONTINUED)

METHODS SUMMARY

DERIVATIVE	CONFIG.	SPEED REGIME	EQUATIONS FOR DERIVATIVE ESTIMATION (Datcom section for components indicated)	METHOD LIMITATIONS ASSOCIATED WITH EQUATION COMPONENTS
C_{m_q} (Contd.)	WBT (Contd.)	TRANSONIC	(Same as subsonic equations)	Method 1 $b_W/b_H \geq 1.5$ $\left(C_{m_q}\right)_{WB}$ (based on exposed wing geometry) 1. Straight-tapered wings 2. Symmetric airfoils of conventional thickness distribution 3. Bodies of revolution 4. $\alpha = 0$ (a) Subsonic LE ($\beta \cot \Lambda_{LE} < 1$) 5. Mach line from TE vertex may not intersect LE 6. Wing-tip Mach lines may not intersect on wings nor intersect opposite wing tips (b) Supersonic LE ($\beta \cot \Lambda_{LE} > 1$) 7. Valid only if Mach lines from LE vertex intersect TE 8. Foremost Mach line from either wing tip may not intersect remote half of wing $K_{B(W)}$ (based on exposed wing geometry) $\frac{q''}{q_\infty}$ 9. Conventional trapezoidal planforms 10. Valid only on the plane of symmetry $\left(C_{L_\alpha}\right)_e''$ 11. Additional tail limitations are identical to Items 2 and 4 immediately above
				Method 2 $b_W/b_H < 1.5$ (same limitations as Method 1 above) $\left(C_{m_q}\right)_{WB}$, $K_{B(W)}$, and $\left(C_{L_\alpha}\right)_{W''(v)}$ (based on exposed wing geometry)
		SUPERSONIC	(Same as subsonic equations)	Method 1 $b_W/b_H \geq 1.5$ $\left(C_{m_q}\right)_{WB}$ (based on exposed wing geometry) 1. Straight-tapered wings 2. Bodies of revolution 3. $M \geq 1.4$ 4. Linear-lift range $K_{B(W)}$ (based on exposed wing geometry) (a) Subsonic LE ($\beta \cot \Lambda_{LE} < 1$) 5. Mach line from TE vertex may not intersect LE 6. Wing-tip Mach lines may not intersect on wings nor intersect opposite wing tips (b) Supersonic LE ($\beta \cot \Lambda_{LE} > 1$) 7. Valid only if Mach lines from LE vertex intersect TE

TABLE 17 (CONTINUED)

METHODS SUMMARY

DERIVATIVE	CONFIG.	SPEED REGIME	EQUATIONS FOR DERIVATIVE ESTIMATION (Datcom section for components indicated)	METHOD LIMITATIONS ASSOCIATED WITH EQUATION COMPONENTS
C_{m_q} (Contd.)	WBT (Contd.)	SUPERSONIC (Contd.)		8. Foremost Mach line from either wing tip may not intersect remote half of wing $\frac{q''}{q_\infty}$ 9. If nonviscous flow field, limited to unswept wings 10. If viscous flow field, valid only on the plane of symmetry $\left(C_{L_\alpha}\right)''_e$ 11. Additional tail limitations are identical to Items 3 and 4 immediately above Method 2 $b_W/b_H < 1.5$ (same limitations as Method 1 above) $\left(C_{m_q}\right)_{WB}$, $K_{B(W)}$, and $\left(C_{L_\alpha}\right)_{W''(v)}$ (based on exposed wing geometry)
$C_{L_{\dot\alpha}}$	W	SUBSONIC	$C_{L_{\dot\alpha}} = 1.5 \underbrace{\left(\frac{x_{a.c.}}{c_r}\right)}_{4.1.4.2} \underbrace{C_{L_\alpha}}_{4.1.3.2} + 3 \underbrace{C_L(g)}_{7.1.4.1}$ Eq. 7.1.4.1-a	1. Triangular planforms 2. Linear-lift range $\frac{x_{a.c.}}{c_r}$ 3. $M < 0.6$; however, if swept wing with $t/c < 0.04$, application to higher Mach numbers is acceptable $C_L(g)$ 4. $0 < \beta A < 4$
		TRANSONIC	(Same as subsonic equation)	1. Triangular planforms 2. $M_{cr} < M < 1.0$ 3. Linear-lift range $\frac{x_{a.c.}}{c_r}$ 4. No camber C_{L_α} 5. Symmetric airfoils of conventional thickness distribution 6. $\alpha = 0$ $C_L(g)$ 7. $0 < \beta A < 4$
		SUPERSONIC	$C_{L_{\dot\alpha}} = -\frac{\pi A M^2}{2\beta^2}\left[-3\underbrace{G(\beta C)}_{7.1.1.1}\underbrace{F_3(N)}_{7.1.4.1} + 2\underbrace{E''(\beta C)}_{7.1.1.1}\underbrace{F_2(N)}_{7.1.4.1} + \frac{1}{M^2}\underbrace{E''(\beta C)}_{7.1.1.1}\underbrace{F_1(N)}_{7.1.4.1}\right]$ Eq. 7.1.4.1-b	Method 1 1. Straight-tapered wings 2. $\lambda = 0$ 3. Subsonic LE ($\beta \cot \Lambda_{LE} < 1$) 4. Mach line from TE vertex may not intersect LE

TABLE 17 (CONTINUED)
METHODS SUMMARY

DERIVATIVE	CONFIG.	SPEED REGIME	EQUATIONS FOR DERIVATIVE ESTIMATION (Datcom section for components indicated)	METHOD LIMITATIONS ASSOCIATED WITH EQUATION COMPONENTS
$C_{L_{\dot\alpha}}$ (Contd.)	W (Contd.)	SUPERSONIC (Contd.)		5. Wing-tip Mach lines may not intersect on wings nor intersect opposite wing tips 6. Linear-lift range
			$C_{L_{\dot\alpha}} = \frac{M^2}{\beta^2}\underbrace{\left(C_{L_{\dot\alpha}}\right)_1}_{7.1.4.1} - \frac{1}{\beta^2}\underbrace{\left(C_{L_{\dot\alpha}}\right)_2}_{7.1.4.1}$ Eq. 7.1.4.1-c	Method 2 1. Straight-tapered wings 2. Linear-lift range (a) Subsonic LE ($\beta \cot \Lambda_{LE} < 1$) 3. $0.25 \leq \lambda \leq 1.0$ 4. Mach line from TE vertex may not intersect LE 5. Wing-tip Mach lines may not intersect on wings nor intersect opposite wing tips (b) Supersonic LE ($\beta \cot \Lambda_{LE} > 1$) 6. Valid only if Mach lines from LE vertex intersect TE 7. Foremost Mach line from either wing tip may not intersect the remote half-wing
	WB	SUBSONIC	$\left(C_{L_{\dot\alpha}}\right)_{WB} = \underbrace{\left[K_{W(B)} + K_{B(W)}\right]}_{4.3.1.2}\left(\frac{S_e}{S}\right)\left(\frac{\bar{c}_e}{\bar{c}}\right)\underbrace{\left(C_{L_{\dot\alpha}}\right)_e}_{7.1.4.1} + \underbrace{\left(C_{L_{\dot\alpha}}\right)_B}_{7.2.2.1}\left(\frac{S_b}{S}\right)\left(\frac{\ell_B}{\bar{c}}\right)$ Eq. 7.3.4.1-a	Method 1 (body diameter)/(wing span) is small (see sketch (d) 4.3.1.2) 1. Linear-lift range $\left(C_{L_{\dot\alpha}}\right)_e$ 2. Triangular planforms 3. $0 < \beta A < 4$ 4. $M \leq 0.6$; however, if swept wing with $t/c \leq 0.04$, application to higher Mach numbers is acceptable $\left(C_{L_{\dot\alpha}}\right)_B$ 5. Bodies of revolution
			$\left(C_{L_{\dot\alpha}}\right)_{WB} = \underbrace{K_{(WB)}}_{4.3.1.2}\underbrace{\left(C_{L_{\dot\alpha}}\right)_W}_{7.1.4.1} + \underbrace{\left(C_{L_{\dot\alpha}}\right)_B}_{7.2.2.1}\left(\frac{S_b}{S}\right)\left(\frac{\ell_B}{\bar{c}}\right)$ Eq. 7.3.4.1-b	Method 2 (body diameter)/(wing span) is large with delta wing extending entire length of body (see Sketch (c) 4.3.1.2) (same limitations as Method 1 above)
		TRANSONIC	(Same as subsonic equations)	Method 1 (body diameter)/(wing span) is small (see Sketch (d) 4.3.1.2) 1. Linear-lift range $K_{B(W)}$ (based on exposed wing geometry) $\left(C_{L_{\dot\alpha}}\right)_e$ 2. Triangular planforms 3. Symmetric airfoils with conventional thickness distribution 4. $0 < \beta A < 4$ 5. $M_{cr} \leq M \leq 1.0$

TABLE 17 (CONTINUED)

METHODS SUMMARY

DERIVATIVE	CONFIG.	SPEED REGIME	EQUATIONS FOR DERIVATIVE ESTIMATION (Datcom section for components indicated)	METHOD LIMITATIONS ASSOCIATED WITH EQUATION COMPONENTS
$C_{L_{\dot{\alpha}}}$ (Contd.)	WB (Contd.)	TRANSONIC (Contd.)		$\left(C_{L_{\dot{\alpha}}}\right)_B$ 6. Bodies of revolution Method 2 (body diameter)/(wing span) is large with delta wing extending entire length of body (see Sketch (c) 4.3.1.2) (same limitations as Method 1 above)
		SUPERSONIC	(Same as subsonic equations)	Method 1 (body diameter)/(wing span) is small (see Sketch (d) 4.3.1.2) 1. Straight-tapered wing 2. Linear-lift range $K_{B(W)}$ (based on exposed wing geometry) $\left(C_{L_{\dot{\alpha}}}\right)_e$ (a) Subsonic LE ($\beta \cot \Lambda_{LE} < 1$) 3. Mach line from TE vertex may not intersect LE 4. Wing-tip Mach lines may not intersect on wings nor intersect opposite wing tips (b) Supersonic LE ($\beta \cot \Lambda_{LE} > 1$) 5. Valid only if Mach lines from LE vertex intersect TE 6. Foremost Mach line from either wing tip may not intersect remote half-wing $\left(C_{L_{\dot{\alpha}}}\right)_B$ 7. Bodies of revolution Method 2 (body diameter)/(wing span) is large with delta wing extending entire length of body (see Sketch (c) 4.3.1.2)(limitations of Method 1)
	WBT	SUBSONIC	$C_{L_{\dot{\alpha}}} = \underbrace{\left(C_{L_{\dot{\alpha}}}\right)_{WB}}_{7.3.4.1} + 2\underbrace{\left[K_{W(B)} + K_{B(W)}\right]''}_{4.3.1.2}\left(\frac{S_e''}{S'}\right)\underbrace{\left(\frac{x_{c.g.} - x''}{\bar{c}'}\right)}_{4.5.2.1}\underbrace{\left(\frac{q''}{q_\infty}\right)}_{4.4.1}\underbrace{\left(\frac{\partial\epsilon}{\partial\alpha}\right)}_{4.4.1}\underbrace{\left(C_{L_\alpha}\right)_e''}_{4.1.3.2}$ Eq. 7.4.4.1-a	Method 1 $h_W/b_H \geq 1.5$ 1. Linear-lift range $\left(C_{L_{\dot{\alpha}}}\right)_{WB}$ (based on exposed wing geometry) 2. Triangular planforms 3. $0 < \beta A < 4$ 4. Bodies of revolution 5. $M \leq 0.6$; however, if swept wing with $t/c \leq 0.04$, application to higher Mach numbers is acceptable $\frac{q''}{q_\infty}$ 6. Valid only on the plane of symmetry $\frac{\partial\epsilon}{\partial\alpha}$ 7. Limitations depend upon $\frac{\partial\epsilon}{\partial\alpha}$ prediction method

TABLE 17 (CONTINUED)
METHODS SUMMARY

DERIVATIVE	CONFIG.	SPEED REGIME	EQUATIONS FOR DERIVATIVE ESTIMATION (Datcom section for components indicated)	METHOD LIMITATIONS ASSOCIATED WITH EQUATION COMPONENTS
$C_{L_{\dot\alpha}}$ (Contd.)	WBT (Contd.)	SUBSONIC (Contd.)	$C_{L_{\dot\alpha}} = \underbrace{\left(C_{L_{\dot\alpha}}\right)_{WB}}_{7.3.4.1} - 2\underbrace{\left(\frac{x_{c.g.} - x''}{\bar{c}}\right)}_{4.5.2.1}\underbrace{\left(C_{L_\alpha}\right)_{W''(v)}}_{4.5.1.1}$ Eq. 7.4.4.1-b	Method 2 $b_W/b_H < 1.5$ (same limitations as Items 1 through 5 immediately above) $\left(C_{L_{\dot\alpha}}\right)_{WB}$ and $\left(C_{L_\alpha}\right)_{W''(v)}$ (based on exposed wing geometry)
		TRANSONIC	(Same as subsonic equations)	Method 1 $b_W/b_H > 1.5$ 1. Linear-lift range $\left(C_{L_{\dot\alpha}}\right)_{WB}$ (based on exposed wing geometry) 2. Triangular planforms 3. Symmetric airfoils with conventional thickness distribution 4. $0 < \beta A < 4$ 5. Bodies of revolution 6. $M_{cr} < M < 1.0$ $K_{B(W)}$ (based on exposed wing geometry) $\frac{q''}{q_\infty}$ 7. Conventional trapezoidal planforms 8. Valid only on the plane of symmetry $\frac{\partial\epsilon}{\partial\alpha}$ 9. Proportional to C_L $\left(C_{L_\alpha}\right)_e''$ 10. $\alpha = 0$ 11. Additional tail limitation is identical to Item 3 immediately above - - - - - - - - - - Method 2 $b_W/b_H < 1.5$ (same limitations as Items 1 through 6 immediately above) $\left(C_{L_{\dot\alpha}}\right)_{WB}$ and $\left(C_{L_\alpha}\right)_{W''(v)}$ (based on exposed wing geometry)
		SUPERSONIC	(Same as subsonic equations)	Method 1 $b_W/b_H > 1.5$ 1. Straight-tapered wing 2. Linear-lift range $K_{B(W)}$ (based on exposed wing geometry) $\left(C_{L_{\dot\alpha}}\right)_{WB}$ (based on exposed wing geometry) 3. Bodies of revolution (a) Subsonic LE ($\beta \cot \Lambda_{LE} < 1$) 4. Mach line from TE vertex may not intersect LE 5. Wing-tip Mach lines may not intersect on wings nor intersect opposite wing tips

TABLE 17 (CONTINUED)

METHODS SUMMARY

DERIVATIVE	CONFIG.	SPEED REGIME	EQUATIONS FOR DERIVATIVE ESTIMATION (Datcom section for components Indicated)	METHOD LIMITATIONS ASSOCIATED WITH EQUATION COMPONENTS
$C_{L_{\dot{\alpha}}}$ (Contd.)	WBT (Contd.)	SUPERSONIC (Contd.)		(b) Supersonic LE ($\beta \cot \Lambda_{LE} > 1$) 6. Valid only if Mach lines from LE vertex intersect TE 7. Foremost Mach line from either wing tip may not intersect remote half-wing $K_{B(W)}$ (based on exposed wing geometry) $\frac{q''}{q_\infty}$ 8. If nonviscous flow field, limited to unswept wings 9. If viscous flow field, valid only on the plane of symmetry $\frac{\partial \epsilon}{\partial \alpha}$ 10. Straight-tapered wings 11. Other limitations depend upon $\frac{\partial \epsilon}{\partial \alpha}$ prediction method $\left(C_{L_\alpha}\right)_e''$ 12. $M > 1.4$ - - - - - - - - - - Method 2 $b_W/b_H < 1.5$ (same limitations as Items 1 through 7 immediately above) $\left(C_{L_{\dot{\alpha}}}\right)_{WB}$ and $\left(C_{L_\alpha}\right)_{W'(v)}$ (based on exposed wing geometry)
$C_{m_{\dot{\alpha}}}$	W	SUBSONIC	$C_{m_{\dot{\alpha}}} = \underbrace{C_{m_{\dot{\alpha}}}''}_{7.1.4.2} + \left(\frac{x_{c.g.}}{\bar{c}}\right) \underbrace{C_{L_{\dot{\alpha}}}}_{7.1.4.1}$ Eq. 7.1.4.2-a	$C_{L_{\dot{\alpha}}}$ 1. Triangular planforms 2. $0 < \beta A < 4$ 3. $M < 0.6$; however, if swept wing with $t/c < 0.04$, application to higher Mach numbers is acceptable 4. Linear-lift range
		TRANSONIC	(Same as subsonic equation)	$C_{L_{\dot{\alpha}}}$ 1. Triangular planforms 2. Symmetric airfoils of conventional thickness distribution 3. $0 < \beta A < 4$ 4. $M_{cr} < M < 1.0$ 5. Linear-lift range
		SUPERSONIC	(Same as subsonic equation)	$C_{m_{\dot{\alpha}}}''$ (a) Subsonic LE ($\beta \cot \Lambda_{LE} < 1$) 1. Mach line from TE vertex may not intersect LE 2. Wing-tip Mach lines may not intersect on wings nor intersect opposite wing tips

TABLE 17 (CONTINUED)
METHODS SUMMARY

DERIVATIVE	CONFIG.	SPEED REGIME	EQUATIONS FOR DERIVATIVE ESTIMATION (Datcom section for components indicated)	METHOD LIMITATIONS ASSOCIATED WITH EQUATION COMPONENTS
$C_{m_{\dot\alpha}}$ (Contd.)	W (Contd.)	SUPERSONIC (Contd.)		(b) Supersonic LE ($\beta \cot \Lambda_{LE} > 1$) 3. Valid only if Mach lines from LE vertex intersect TE 4. Foremost Mach line from either wing tip may not intersect remote half-wing $C_{L_{\dot\alpha}}$ 5. Straight-tapered wings 6. Linear-lift range
	WB	SUBSONIC	$\left(C_{m_{\dot\alpha}}\right)_{WB} = \underbrace{\left[K_{W(B)} + K_{B(W)}\right]}_{4.3.1.2}\left(\frac{S_e}{S}\right)\left(\frac{\bar c_e}{\bar c}\right)^2 \underbrace{\left(C_{m_{\dot\alpha}}\right)_e}_{7.1.4.2} + \underbrace{\left(C_{m_{\dot\alpha}}\right)_B}_{7.2.2.2}\left(\frac{S_b}{S}\right)\left(\frac{\ell_B}{\bar c}\right)^2$ Eq. 7.3.4.2-a	Method 1 (body diameter)/(wing span) is small (see 4.3.1.2 Sketch (d)) 1. Linear-lift range $\left(C_{m_{\dot\alpha}}\right)_e$ 2. Triangular planforms $\left[\text{due to } \left(C_{L_{\dot\alpha}}\right)_e\right]$ 3. $0 < \beta A < 4$ 4. $M \le 0.6$; however, if swept wing with $t/c \le 0.04$, application to higher Mach numbers is acceptable $\left(C_{m_{\dot\alpha}}\right)_B$ 5. Bodies of revolution
			$\left(C_{m_{\dot\alpha}}\right)_{WB} = \underbrace{K_{(WB)}}_{4.3.1.2} \underbrace{\left(C_{m_{\dot\alpha}}\right)_W}_{7.1.4.2} + \underbrace{\left(C_{m_{\dot\alpha}}\right)_B}_{7.2.2.2}\left(\frac{S_b}{S}\right)\left(\frac{\ell_B}{\bar c}\right)^2$ Eq. 7.3.4.2-b	Method 2 (body diameter)/(wing span) is large, with delta wing extending over entire length of body (see 4.3.1.2 Sketch (c)) (same limitations as Method 1 above)
		TRANSONIC	(Same as subsonic equations)	Method 1 (body diameter)/(wing span) is small (see 4.3.1.2 Sketch (d)) 1. Linear-lift range $K_{B(W)}$ (based on exposed wing geometry) $\left(C_{m_{\dot\alpha}}\right)_e$ 2. Triangular planforms $\left[\text{due to } \left(C_{L_{\dot\alpha}}\right)_e\right]$ 3. Symmetric airfoils of conventional thickness distribution 4. $0 < \beta A < 4$ 5. $M_{cr} \le M \le 1.0$ $\left(C_{m_{\dot\alpha}}\right)_B$ 6. Bodies of revolution
				Method 2 (body diameter)/(wing span) is large, with delta wing extending entire length of body (see 4.3.1.2 Sketch (c)) (same limitations as Method 1 above)
		SUPERSONIC	(Same as subsonic equations)	Method 1 (body diameter)/(wing span) is small (see 4.3.1.2 Sketch (d)) 1. Straight-tapered wings 2. Linear-lift range

TABLE 17 (CONTINUED)

METHODS SUMMARY

DERIVATIVE	CONFIG.	SPEED REGIME	EQUATIONS FOR DERIVATIVE ESTIMATION (Datcom section for components indicated)	METHOD LIMITATIONS ASSOCIATED WITH EQUATION COMPONENTS
$C_{m_{\dot{\alpha}}}$ (Contd.)	WB (Contd.)	SUPERSONIC (Contd.)		$K_{B(W)}$ (based on exposed wing geometry) $\left(C_{m_{\dot{\alpha}}}\right)_e$ (a) Subsonic LE ($\beta \cot \Lambda_{LE} < 1$) 3. Mach line from TE vertex may not intersect LE 4. Wing-tip Mach lines may not intersect on wings nor intersect opposite wing tips (b) Supersonic LE ($\beta \cot \Lambda_{LE} > 1$) 5. Valid only if Mach lines from LE vertex intersect TE 6. Foremost Mach line from either wing tip may not intersect remote half-wing $\left(C_{m_{\dot{\alpha}}}\right)_B$ 7. Bodies of revolution
				Method 2 (body diameter)/(wing span) is large, with delta wing extending entire length of body (see 4.3.1.2 Sketch (c)) (same limitations as Method 1 above)
	WBT	SUBSONIC	$C_{m_{\dot{\alpha}}} = \underbrace{\left(C_{m_{\dot{\alpha}}}\right)_{WB}}_{7.3.4.2} - 2\underbrace{\left[K_{W(B)} + K_{B(W)}\right]}_{4.3.1.2}\left(\frac{S_e''}{S'}\right)\underbrace{\left(\frac{x_{c.g.} - x''}{\bar{c}'}\right)^2}_{4.5.2.1}\underbrace{\left(\frac{q''}{q_\infty}\right)}_{4.4.1}\underbrace{\left(\frac{\partial\epsilon}{\partial\alpha}\right)}_{4.4.1}\underbrace{\left(C_{L_\alpha}\right)_e''}_{4.1.3.2}$ Eq. 7.4.4.2-a	Method 1 $b_W/b_H > 1.5$ 1. Linear-lift range $\left(C_{m_{\dot{\alpha}}}\right)_{WB}$ (based on exposed wing geometry) 2. Triangular planforms $\left[\text{due to } \left(C_{L_{\dot{\alpha}}}\right)_e\right]$ 3. $0 < \beta A < 4$ 4. Bodies of revolution 5. $M < 0.6$; however, if swept wing with $t/c < 0.04$, application to higher Mach numbers is acceptable $\frac{q''}{q_\infty}$ 6. Valid only on the plane of symmetry $\frac{\partial\epsilon}{\partial\alpha}$ 7. Limitations depend upon $\frac{\partial\epsilon}{\partial\alpha}$ prediction method
			$C_{m_{\dot{\alpha}}} = \underbrace{\left(C_{m_{\dot{\alpha}}}\right)_{WB}}_{7.3.4.2} + 2\underbrace{\left(\frac{x_{c.g.} - x''}{\bar{c}'}\right)^2}_{4.5.2.1}\underbrace{\left(C_{L_\alpha}\right)_{W''(v)}}_{4.5.1.1}$ Eq. 7.4.4.2-b	Method 2 $b_W/b_H < 1.5$ (same limitations as Items 1 through 5 immediately above) $\left(C_{m_{\dot{\alpha}}}\right)_{WB}$ and $\left(C_{L_\alpha}\right)_{W''(v)}$ (based on exposed wing geometry)
		TRANSONIC	(Same as subsonic equations)	Method 1 $h_W/b_H > 1.5$ 1. Linear-lift range

TABLE 17 (CONTINUED)

METHODS SUMMARY

DERIVATIVE	CONFIG.	SPEED REGIME	EQUATIONS FOR DERIVATIVE ESTIMATION (Datcom section for components indicated)	METHOD LIMITATIONS ASSOCIATED WITH EQUATION COMPONENTS
$C_{m_{\dot{\alpha}}}$ (Contd.)	WBT (Contd.)	TRANSONIC (Contd.)		$\left(C_{m_{\dot{\alpha}}}\right)_{WB}$ (based on exposed wing geometry) 2. Triangular planforms $\left[\text{due to } \left(C_{L_{\dot{\alpha}}}\right)_e\right]$ 3. Symmetric airfoils of conventional thickness distribution 4. $0 < \beta A < 1.0$ 5. Bodies of revolution 6. $M_{cr} < M < 1.0$ $K_{B(W)}$ (based on exposed wing geometry) $\frac{q''}{q_\infty}$ 7. Conventional trapezoidal planforms 8. Valid only on the plane of symmetry $\frac{\partial \epsilon}{\partial \alpha}$ 9. Proportional to C_{L_α} $\left(C_{L_\alpha}\right)''_e$ 10. $\alpha = 0$ 11. Additional tail limitation is identical to Item 3 immediately above
				Method 2 $b_W/b_H < 1.5$ (same limitations as Items 1 through 6 immediately above) $\left(C_{m_{\dot{\alpha}}}\right)_{WB}$ and $\left(C_{L_\alpha}\right)_{W''(v)}$ (based on exposed wing geometry)
		SUPERSONIC	(Same as subsonic equations)	Method 1 $b_W/b_H > 1.5$ 1. Straight-tapered wings 2. Linear-lift range $\left(C_{m_{\dot{\alpha}}}\right)_{WB}$ (based on exposed wing geometry) 3. Bodies of revolution (a) Subsonic LE ($\beta \cot \Lambda_{LE} < 1$) 4. Mach line from TE vertex may not intersect LE 5. Wing-tip Mach lines may not intersect on wings nor intersect opposite wing tips (b) Supersonic LE ($\beta \cot \Lambda_{LE} > 1$) 6. Valid only if Mach lines from LE vertex intersect TE 7. Foremost Mach line from either wing tip may not intersect the remote half-wing $K_{B(W)}$ (based on exposed wing geometry) $\frac{q''}{q_\infty}$ 8. If nonviscous flow field, limited to unswept wings 9. If viscous flow field, valid only on the plane of symmetry

TABLE 17 (CONTINUED)
METHODS SUMMARY

DERIVATIVE	CONFIG.	SPEED REGIME	EQUATIONS FOR DERIVATIVE ESTIMATION (Datcom section for components indicated)	METHOD LIMITATIONS ASSOCIATED WITH EQUATION COMPONENTS
$C_{m_{\dot{\alpha}}}$ (Contd.)	WBT (Contd.)	SUPERSONIC (Contd.)		$\frac{\partial\epsilon}{\partial\alpha}$ 10. Limitations depend upon $\frac{\partial\epsilon}{\partial\alpha}$ prediction method $(C_{N_\alpha})_e^*$ 11. $M > 1.4$ Method 2 $b_W/b_H < 1.5$ (same limitations as Items 1 through 7 immediately above) $(C_{m_{\dot{\alpha}}})_{WB}$ and $(C_{L_\alpha})_{W'(v)}$ (based on exposed wing geometry)
C_{Y_p}	W	SUBSONIC	$C_{Y_p} = \underbrace{K}_{7.1.2.1} \left[\underbrace{\left(\frac{C_{Y_p}}{C_L}\right)_{\substack{C_L=0\\M}}}_{7.1.2.1} C_L \right] + \underbrace{(\Delta C_{Y_p})_\Gamma}_{7.1.2.1}$ Eq. 7.1.2.1-a	K 1. $\alpha < \alpha_{stall}$ 2. Test data for lift and drag $\left(\frac{C_{Y_p}}{C_L}\right)_{\substack{C_L=0\\M}}$ 3. $M < M_{cr}$
		TRANSONIC	(No method)	
		SUPERSONIC	Figure 7.1.2.1-10	1. Thin, sweptback, tapered wings with streamwise tips 2. Low lift coefficients
	WB	SUBSONIC	$C_{Y_p} = \underbrace{K}_{7.1.2.1} \left[\underbrace{\left(\frac{C_{Y_p}}{C_L}\right)_{\substack{C_L=0\\M}}}_{7.1.2.1} C_L \right] + \underbrace{(\Delta C_{Y_p})_\Gamma}_{7.1.2.1}$ Eq. 7.1.2.1-a	K 1. (Body diameter)/(wing span) < 0.3 2. $\alpha < \alpha_{stall}$ 3. Test data for lift and drag

TABLE 17 (CONTINUED)
METHODS SUMMARY

DERIVATIVE	CONFIG.	SPEED REGIME	EQUATIONS FOR DERIVATIVE ESTIMATION (Datcom section for components indicated)		METHOD LIMITATIONS ASSOCIATED WITH EQUATION COMPONENTS
C_{Y_p} (Contd.)	WB (Contd.)	SUBSONIC (Contd.)			$\left(\frac{C_{Y_p}}{C_L}\right)_{\substack{C_L=0\\M}}$ 4. $M < M_{cr}$
		TRANSONIC	(No method)		
		SUPERSONIC	Figure 7.1.2.1-10		1. Thin, sweptback, tapered wings with streamwise tips 2. (Body diameter)/(wing span) ≤ 0.3 3. Low lift coefficients
	WBT	SUBSONIC	$C_{Y_p} = \underbrace{\left(C_{Y_p}\right)_{WB}}_{7.3.2.1} + 2\left[\frac{z - z_p}{b_W}\right]\underbrace{\left(\Delta C_{Y_\beta}\right)_{V(WBH)}}_{5.3.1.1}$	Eq. 7.4.2.1-a	Method 1 (conventionally located vertical tails) $\left(C_{Y_p}\right)_{WB}$ 1. (body diameter)/(wing span) ≤ 0.3 2. $\alpha < \alpha_{stall}$ 3. Test data for lift and drag 4. $M < M_{cr}$ $\left(\Delta C_{Y_\beta}\right)_{V(WBH)}$ 5. Additional or identical tail limitations depend on $\left(\Delta C_{Y_\beta}\right)_{V(WBH)}$ prediction method
			$C_{Y_p} = \underbrace{\left(C_{Y_p}\right)_{WB}}_{7.3.2.1} + \left[\frac{2z - z_p}{b_W}\right]\underbrace{\left(\Delta C_{Y_\beta}\right)_{V(WBH)}}_{5.3.1.1}$	Eq. 7.4.2.1-c	Method 2 (vertical tail directly above, or above and slightly behind wing) (same limitations as Method 1 above)
		TRANSONIC	(No method)		
		SUPERSONIC	(No method)		
C_{l_p}	W	SUBSONIC	$C_{l_p} = \underbrace{\left(\frac{\beta C_{l_p}}{\kappa}\right)_{C_L=0}}_{7.1.2.2}\underbrace{\left(\frac{\kappa}{\beta}\right)}_{4.1.1.2}\frac{\overbrace{\left(C_{L_\alpha}\right)_{C_L}}^{4.1.3.3}}{\underbrace{\left(C_{L_\alpha}\right)_{C_L=0}}_{4.1.3.2}}\underbrace{\frac{\left(C_{l_p}\right)_\Gamma}{\left(C_{l_p}\right)_{\Gamma=0}}}_{7.1.2.2} + \underbrace{\left(\Delta C_{l_p}\right)_{drag}}_{7.1.2.2}$	Eq. 7.1.2.2-a	1. $M < M_{cr}$ $\left(C_{L_\alpha}\right)_{C_L}$ 2. Symmetric airfoils 3. $1 \times 10^6 \leq R_\ell \leq 15 \times 10^6$ based on MAC $\left(C_{L_\alpha}\right)_{C_L=0}$ 4. Straight-tapered wings
		TRANSONIC	(No method)		

TABLE 17 (CONTINUED)

METHODS SUMMARY

DERIVATIVE	CONFIG.	SPEED REGIME	EQUATIONS FOR DERIVATIVE ESTIMATION (Datcom section for components indicated)	METHOD LIMITATIONS ASSOCIATED WITH EQUATION COMPONENTS
C_{l_p} (Contd.)	W (Contd.)	SUPERSONIC	$C_{l_p} = \underbrace{\left[\frac{\left(C_{l_p}\right)_{theory}}{A}\right]}_{7.1.2.2} A \frac{C_{l_p}}{\underbrace{\left(C_{l_p}\right)_{theory}}_{7.1.2.2}}$ Eq. 7.1.2.2-d	1. Straight-tapered wings 2. Wing tips parallel to free stream 3. Foremost Mach line from tip may not intersect remote half-wing 4. Supersonic TE
	WB	SUBSONIC	$C_{l_p} = \underbrace{\left(\frac{\beta C_{l_p}}{\kappa}\right)_{C_L=0}}_{7.1.2.2} \underbrace{\left(\frac{\kappa}{\beta}\right)}_{4.1.1.2} \frac{\overbrace{\left(C_{L_\alpha}\right)_{C_L}}^{4.1.3.3}}{\underbrace{\left(C_{L_\alpha}\right)_{C_L=0}}_{4.1.3.2}} \frac{\left(C_{l_p}\right)_{\Gamma}}{\underbrace{\left(C_{l_p}\right)_{\Gamma=0}}_{7.1.2.2}} + \underbrace{\left(\Delta C_{l_p}\right)_{drag}}_{7.1.2.2}$ Eq. 7.1.2.2-a	1. (Body diameter)/(wing span) < 0.3 2. $M < M_{cr}$ $\left(C_{L_\alpha}\right)_{C_L}$ 3. Symmetric airfoils 4. $1 \times 10^6 < R_\ell < 15 \times 10^6$ based on MAC $\left(C_{L_\alpha}\right)_{C_L=0}$ 5. Straight-tapered wings
		TRANSONIC	(No method)	
		SUPERSONIC	$\left(C_{l_p}\right)_{WB} = \underbrace{\left(C_{l_p}\right)_W}_{7.1.2.2} \frac{C_{l_p}}{\underbrace{\left(C_{l_p}\right)_{d/b=0}}_{7.3.2.2}}$ Eq. 7.3.2.2-a	1. Straight-tapered wings. If (body diameter)/(wing span) > 0.3, valid only for triangular wings) 2. Cylindrical or nearly cylindrical bodies $\left(C_{l_p}\right)_W$ 3. Wing tips parallel to free stream 4. Foremost Mach line from tip may not intersect remote half-wing 5. Supersonic TE
	WBT	SUBSONIC	$C_{l_p} = \underbrace{\left(C_{l_p}\right)_{WB}}_{7.1.2.2} + 0.5 \underbrace{\left(C_{l_p}\right)_H}_{7.1.2.2} \left(\frac{S_H}{S_W}\right)\left(\frac{b_H}{b_W}\right)^2 + \left\lvert 2\left(\frac{z}{b_W}\right)\left[\frac{z - z_p}{b_W}\right]\right\rvert \underbrace{\left(\Delta C_{Y_\beta}\right)_{V(WBH)}}_{5.3.1.1}$ Eq. 7.4.2.2-a	Method 1 (conventionally located vertical tails) $\left(C_{l_p}\right)_{WB}$ and $\left(C_{l_p}\right)_H$ 1. Straight-tapered planforms 2. Symmetric airfoils 3. (Body diameter)/(wing span) < 0.3 4. $M < M_{cr}$ 5. $1 \times 10^6 < R_\ell < 15 \times 10^6$ based on MAC $\left(\Delta C_{Y_\beta}\right)_{V(WBH)}$ 6. Additional or identical tail limitationa depend on $\left(\Delta C_{Y_\beta}\right)_{V(WBH)}$ prediction method

TABLE 17 (CONTINUED)
METHODS SUMMARY

DERIVATIVE	CONFIG.	SPEED REGIME	EQUATIONS FOR DERIVATIVE ESTIMATION (Datcom section for components indicated)	METHOD LIMITATIONS ASSOCIATED WITH EQUATION COMPONENTS
C_{l_p} (Contd.)	WBT (Contd.)	SUBSONIC (Contd.)	$C_{l_p} = \underbrace{\left(C_{l_p}\right)_{WB}}_{7.1.2.2} + 0.5 \underbrace{\left(C_{l_p}\right)_H}_{7.1.2.2} \left(\frac{S_H}{S_W}\right)\left(\frac{b_H}{b_W}\right)^2 + \left\lvert \frac{z}{b_W}\left[\frac{2z - z_p}{b_W}\right]\right\rvert \underbrace{\left(\Delta C_{Y_\beta}\right)_{V(WBH)}}_{5.3.1.1}$ Eq. 7.4.2.2-b	Method 2 (vertical tail located directly above, or above and slightly behind wing) (same limitations as Method 1 above)
		TRANSONIC	(No method)	
		SUPERSONIC	(No method)	
C_{n_p}	W	SUBSONIC	$C_{n_p} = -\underbrace{C_{l_p}}_{7.1.2.2} \tan\alpha - \underbrace{K}_{7.1.2.3}\left[-\underbrace{C_{l_p}}_{7.1.2.2} \tan\alpha - \underbrace{\left(\frac{C_{n_p}}{C_L}\right)_{\substack{C_L=0 \\ M}}}_{7.1.2.3} C_L\right] + \underbrace{\left(\frac{\Delta C_{n_p}}{\theta}\right)}_{7.1.2.3}\theta + \underbrace{\left[\frac{\Delta C_{n_p}}{\left(\frac{\partial\alpha}{\partial\delta}\right)_f \delta_f}\right]}_{7.1.2.3}\underbrace{\left(\frac{\partial\alpha}{\partial\delta}\right)_f}_{6.1.1.1}\delta_f$ Eq. 7.1.2.3-a	1. $M < M_{cr}$ 2. Lift coefficients up to stall (if reliable lift and drag data are available) C_{l_p} 3. Straight-tapered wings 4. Symmetric airfoils 5. $1 \times 10^6 < R_\ell < 15 \times 10^6$ based on MAC
		TRANSONIC	(No method)	
		SUPERSONIC	$\frac{C_{n_p}}{\alpha} = \underbrace{\left(\frac{C_{n_p}}{\alpha}\right)_{\substack{\text{body}\\ \text{axis}}}}_{7.1.2.3} + \frac{2x_{c.g.}}{A(1+\lambda)}\underbrace{\left(\frac{C_{Y_p}}{\alpha}\right)}_{7.1.2.1} - \left(\underbrace{C_{l_p}}_{7.1.2.2} - \underbrace{C_{n_r}}_{7.1.3.3}\right)$ Eq. 7.1.2.3-e	Method 1 (Subsonic leading edges ($\beta \cot\Lambda_{LE} < 1$) 1. Straight-tapered wings 2. Streamwise wing tips 3. Low lift coefficients C_{l_p} 4. Foremost Mach line from tip may not intersect remote half-wing 5. Supersonic TE
			$\frac{C_{n_p}}{\alpha} = \underbrace{\left(\frac{C_{n_p}}{\alpha}\right)_{\substack{\text{body}\\ \text{axis}}}}_{7.1.2.3} + \left[\frac{2x_{c.g.}}{A(1+\lambda)} - \frac{1}{2}\tan\Lambda_{LE}\right]\underbrace{\frac{C_{Y_p}}{\alpha}}_{7.1.2.1} - \underbrace{C_{l_p}}_{7.1.2.2}$ Eq. 7.1.2.3-g	Method 2 (Supersonic leading edges ($\beta \cot\Lambda_{LE} > 1$) (same limitations as Method 1 above)
	WB	SUBSONIC	$C_{n_p} = -\underbrace{C_{l_p}}_{7.1.2.2}\tan\alpha - \underbrace{K}_{7.1.2.3}\left[-\underbrace{C_{l_p}}_{7.1.2.2}\tan\alpha - \underbrace{\left(\frac{C_{n_p}}{C_L}\right)_{\substack{C_L=0\\ M}}}_{7.1.2.3} C_L\right]$ $+\underbrace{\left(\frac{\Delta C_{n_p}}{\theta}\right)}_{7.1.2.3}\theta + \underbrace{\left[\frac{\Delta C_{n_p}}{\left(\frac{\partial\alpha}{\partial\delta}\right)_f \delta_f}\right]}_{7.1.2.3}\underbrace{\left(\frac{\partial\alpha}{\partial\delta}\right)_f}_{6.1.1.1}\delta_f$ Eq. 7.1.2.3-a	1. (Body diameter)/(wing span) ≤ 0.3 2. $M < M_{cr}$ 3. Lift coefficients up to stall (if reliable lift and drag data are available) C_{l_p} 4. Straight-tapered wings 5. Symmetric airfoils 6. $1 \times 10^6 < R_\ell < 15 \times 10^6$ based on MAC

TABLE 17 (CONTINUED)
METHODS SUMMARY

DERIVATIVE	CONFIG.	SPEED REGIME	EQUATIONS FOR DERIVATIVE ESTIMATION (Datcom section for components indicated)		METHOD LIMITATIONS ASSOCIATED WITH EQUATION COMPONENTS
C_{n_p} (Contd.)	WB (Contd.)	TRANSONIC	(No method)		
		SUPERSONIC	$\frac{C_{n_p}}{\alpha} = \underbrace{\left(\frac{C_{n_p}}{\alpha}\right)_{\substack{body\\axis}}}_{7.1.2.3} + \frac{2x_{c.g.}}{A(1+\lambda)} \underbrace{\left(\frac{C_{Y_p}}{\alpha}\right)}_{7.1.2.1} - \left(\underbrace{C_{l_p}}_{7.1.2.2} - \underbrace{C_{n_r}}_{7.1.3.3}\right)$	Eq. 7.1.2.3-e	Method 1 Subsonic leading edges ($\beta \cot \Lambda_{LE} < 1$) 1. Straight-tapered wings 2. Streamwise wing tips 3. (Body diameter)/(wing span) ≤ 0.3 4. Lift coefficients where C_{n_p} varies linearly with C_L C_{l_p} 5. Foremost Mach line from tip may not intersect remote half-wing 6. Supersonic TE
			$\frac{C_{n_p}}{\alpha} = \underbrace{\left(\frac{C_{n_p}}{\alpha}\right)_{\substack{body\\axis}}}_{7.1.2.3} + \left[\frac{2x_{c.g.}}{A(1+\lambda)} - \frac{1}{2}\tan\Lambda_{LE}\right] \underbrace{\frac{C_{Y_p}}{\alpha}}_{7.1.2.1} - \underbrace{C_{l_p}}_{7.1.2.2}$	Eq. 7.1.2.3-g	Method 2 Supersonic leading edges ($\beta \cot \Lambda_{LE} > 1$) (same limitations as Method 1 above)
	WBT	SUBSONIC	$C_{n_p} = \underbrace{\left(C_{n_p}\right)_{WB}}_{7.3.2.3} - \frac{2}{b_W}\left(\ell_p \cos\alpha + z_p \sin\alpha\right)\left[\frac{z - z_p}{b_W}\right] \underbrace{\left(\Delta C_{Y_\beta}\right)_{V(WBH)}}_{5.3.1.1}$	Eq. 7.4.2.3-a	Method 1 (conventionally located vertical tails) $\left(C_{n_p}\right)_{WB}$ 1. Straight-tapered wings 2. Symmetric airfoils 3. (Body diameter)/(wing span) ≤ 0.3 4. $M \leq M_{cr}$ 5. $1 \times 10^6 \leq R_\ell \leq 15 \times 10^6$ based on MAC 6. Lift coefficients up to stall (if reliable lift and drag data are available) $\left(\Delta C_{Y_\beta}\right)_{V(WBH)}$ 7. Additional or identical tail limitations depend on $\left(\Delta C_{Y_\beta}\right)_{V(WBH)}$ prediction method
			$C_{n_p} = \underbrace{\left(C_{n_p}\right)_{WB}}_{7.3.2.3} + 2\left[\frac{z - z_p}{b_W}\right]\left(\Delta C_{n_\beta}\right)_p$	Eq. 7.4.2.3-b	(same limitations as for Eq. 7.4.2.3-a above) $\left(\Delta C_{n_\beta}\right)_p$ 1. Test data
			$C_{n_p} = \underbrace{\left(C_{n_p}\right)_{WB}}_{7.3.2.3} - \left[\frac{\ell_p \cos\alpha + z_p \sin\alpha}{b_W}\right]\left[\frac{2z - z_p}{b_W}\right] \underbrace{\left(\Delta C_{Y_\beta}\right)_{V(WBH)}}_{5.3.1.1}$	Eq. 7.4.2.3-c	Method 2 (vertical tails located directly above, or above and slightly behind wing) (same limitations as for Eq. 7.4.2.3-a above)
			$C_{n_p} = \underbrace{\left(C_{n_p}\right)_{WB}}_{7.3.2.3} + \left[\frac{2z - z_p}{b_W}\right]\left(\Delta C_{n_\beta}\right)_p$	Eq. 7.4.2.3-d	(same limitations as Method 1 above)

TABLE 17 (CONTINUED)

METHODS SUMMARY

DERIVATIVE	CONFIG.	SPEED REGIME	EQUATIONS FOR DERIVATIVE ESTIMATION (Datcom section for components indicated)	METHOD LIMITATIONS ASSOCIATED WITH EQUATION COMPONENTS
C_{n_p} (Contd.)	WBT (Contd.)	TRANSONIC	(No method)	
		SUPERSONIC	(No method)	
C_{Y_r}	W	SUBSONIC	(No method)	
		TRANSONIC	(No method)	
		SUPERSONIC	(No method)	
	WB	SUBSONIC	(No method)	
		TRANSONIC	(No method)	
		SUPERSONIC	(No method)	
	WBT	SUBSONIC	$C_{Y_r} = \left(C_{Y_r}\right)_{WB} - \frac{2}{b_W}\left(\ell_p \cos\alpha + z_p \sin\alpha\right)\underbrace{\left(\Delta C_{Y_\beta}\right)_{V(WBH)}}_{5.3.1.1}$ Eq. 7.4.3.1-a	$\left(C_{Y_r}\right)_{WB}$ 1. Aperiodic mode only $\left(\Delta C_{Y_\beta}\right)_{V(WBH)}$ 2. Test data 3. Additional tail limitations depend on $\left(\Delta C_{Y_\beta}\right)_{V(WBH)}$ prediction method
			$C_{Y_r} = \left(C_{Y_r}\right)_{WB} + 2\left(\Delta C_{n_\beta}\right)_p$ Eq. 7.4.3.1-b	$\left(C_{Y_r}\right)_{WB}$ and $\left(\Delta C_{n_\beta}\right)_p$ 1. Test data
		TRANSONIC	(No method)	
		SUPERSONIC	(No method)	
C_{l_r}	W	SUBSONIC	$C_{l_r} = C_L \underbrace{\left(\frac{C_{l_r}}{C_L}\right)_{\substack{C_L=0\\M}}}_{7.1.3.2} + \underbrace{\left(\Delta C_{l_r}\right)_{C_L}}_{7.1.3.2} + \underbrace{\left(\frac{\Delta C_{l_r}}{\Gamma}\right)\Gamma}_{7.1.3.2} + \underbrace{\left(\frac{\Delta C_{l_r}}{\theta}\right)\theta}_{7.1.3.2} + \underbrace{\left[\frac{\Delta C_{l_r}}{\left(\frac{\partial\alpha}{\partial\delta}\right)_f \delta_f}\right]}_{7.1.3.2}\underbrace{\left(\frac{\partial\alpha}{\partial\delta}\right)_f}_{6.1.1.1}\delta_f$ Eq. 7.1.3.2-a	1. $M \leq M_{cr}$ $\left(\Delta C_{l_r}\right)_{C_L}$ 2. No curved planforms 3. No twist or dihedral, if non-straight-tapered wings 4. $t/c \leq 0.1$ if cranked wing with round LE 5. $M \leq 0.6$ 6. Linear-lift range 7. $-5^\circ \leq \beta \leq +5^\circ$
		TRANSONIC	(No method)	
		SUPERSONIC	(No method)	

TABLE 17 (CONTINUED)

METHODS SUMMARY

DERIVATIVE	CONFIG.	SPEED REGIME	EQUATIONS FOR DERIVATIVE ESTIMATION (Datcom section for components indicated)	METHOD LIMITATIONS ASSOCIATED WITH EQUATION COMPONENTS
C_{l_r} (Contd.)	WB	SUBSONIC	$C_{l_r} = \underbrace{C_L \left(\frac{C_{l_r}}{C_L}\right)_{\substack{C_L=0 \\ M}}}_{7.1.3.2} + \underbrace{\left(\Delta C_{l_r}\right)_{C_L}}_{7.1.3.2} + \underbrace{\left(\frac{\Delta C_{l_r}}{\Gamma}\right)}_{7.1.3.2} \Gamma + \underbrace{\left(\frac{\Delta C_{l_r}}{\theta}\right)}_{7.1.3.2} \theta + \underbrace{\left[\frac{\Delta C_{l_r}}{\left(\frac{\partial\alpha}{\partial\delta}\right)_f \delta_f}\right]}_{7.1.3.2} \underbrace{\left(\frac{\partial\alpha}{\partial\delta}\right)_f}_{6.1.1.1} \delta_f$ Eq. 7.1.3.2-a	1. (Body diameter)/(wing span) $\leq$ 0.3 2. $M \leq M_{cr}$ $\left(\Delta C_{l_r}\right)_{C_L}$ 3. No curved planforms 4. No twist or dihedral, if non-straight-tapered wing 5. $t/c \leq 0.1$ if cranked wing with round LE 6. $M \leq 0.6$ 7. Linear-lift range 8. $-5° \leq \beta \leq +5°$
		TRANSONIC	(No method)	
		SUPERSONIC	(No method)	
	WBT	SUBSONIC	$C_{l_r} = \underbrace{\left(C_{l_r}\right)_{WB}}_{7.3.3.2} - \frac{2}{b_W^2}\left(\ell_p \cos\alpha + z_p \sin\alpha\right)\left(z_p \cos\alpha - \ell_p \sin\alpha\right)\underbrace{\left(\Delta C_{Y_\beta}\right)_{V(WBH)}}_{5.3.1.1}$ Eq. 7.4.3.2-a	$\left(C_{l_r}\right)_{WB}$ 1. No curved planforms 2. No twist or dihedral, if non-straight-tapered wing 3. $t/c \leq 0.1$ if cranked wing with round LE 4. (Body diameter)/(wing span) $\leq$ 0.3 5. $M \leq 0.6$ 6. $M \leq M_{cr}$ 7. Linear-lift range 8. $-5° \leq \beta \leq +5°$ $\left(\Delta C_{Y_\beta}\right)_{V(WBH)}$ 9. Additional or identical tail limitations depend on $\left(\Delta C_{Y_\beta}\right)_{V(WBH)}$ prediction method
			$C_{l_r} = \underbrace{\left(C_{l_r}\right)_{WB}}_{7.3.3.2} - \frac{2}{b_W}\left(\ell_p \cos\alpha + z_p \sin\alpha\right)\left(\Delta C_{l_\beta}\right)_p$ Eq. 7.4.3.2-b	$\left(C_{l_r}\right)_{WB}$ (same limitations as for Eq. 7.4.3.2-a) $\left(\Delta C_{l_\beta}\right)_p$ 1. Test data
			$C_{l_r} = \underbrace{\left(C_{l_r}\right)_{WB}}_{7.3.3.2} + 2\,\frac{\left(\Delta C_{n_\beta}\right)_p}{\underbrace{\left(\Delta C_{Y_\beta}\right)_{V(WBH)}}_{5.3.1.1}}\left(\Delta C_{l_\beta}\right)_p$ Eq. 7.4.3.2-c	$\left(C_{l_r}\right)_{WB}$ (same limitations as for Eq. 7.4.3.2-a) $\left(\Delta C_{n_\beta}\right)_p$, $\left(\Delta C_{Y_\beta}\right)_{V(WBH)}$, and $\left(\Delta C_{l_\beta}\right)_p$ 1. Test data
		TRANSONIC	(No method)	

TABLE 17 (CONTINUED)

METHODS SUMMARY

DERIVATIVE	CONFIG.	SPEED REGIME	EQUATIONS FOR DERIVATIVE ESTIMATION (Datcom section for components indicated)	METHOD LIMITATIONS ASSOCIATED WITH EQUATION COMPONENTS
C_{l_r} (Contd.)	WBT (Contd.)	SUPERSONIC	(No method)	
C_{n_r}	W	SUBSONIC	$C_{n_r} = \underbrace{\left(\frac{C_{n_r}}{C_L^2}\right)}_{7.1.3.3} C_L^2 + \underbrace{\left(\frac{C_{n_r}}{C_{D_0}}\right)}_{7.1.3.3} C_{D_0}$ Eq. 7.1.3.3-a	1. No twist nor dihedral 2. Lift-coefficient range for which C_{n_r} varies linearly with C_L
		TRANSONIC	(No method)	
		SUPERSONIC	(No method)	
	WB	SUBSONIC	$C_{n_r} = \underbrace{\left(\frac{C_{n_r}}{C_L^2}\right)}_{7.1.3.3} C_L^2 + \underbrace{\left(\frac{C_{n_r}}{C_{D_0}}\right)}_{7.1.3.3} C_{D_0}$ Eq. 7.1.3.3-a	1. No twist nor dihedral 2. Lift coefficient range for which C_{n_r} varies linearly with C_L
		TRANSONIC	(No method)	
		SUPERSONIC	(No method)	
	WBT	SUBSONIC	$C_{n_r} = \underbrace{\left(C_{n_r}\right)_{WB}}_{7.3.3.3} + \frac{2}{b_W^2}\left(\ell_p \cos\alpha + z_p \sin\alpha\right)^2 \underbrace{\left(\Delta C_{Y_\beta}\right)_{V(WBH)}}_{5.3.1.1}$ Eq. 7.4.3.3-a	1. Aperiodic mode only $\left(C_{n_r}\right)_{WB}$ 2. No twist nor dihedral 3. Lift-coefficient range for which C_{n_r} varies linearly with C_L $\left(\Delta C_{Y_\beta}\right)_{V(WBH)}$ 4. Additional tail limitations depend upon $\left(\Delta C_{Y_\beta}\right)_{V(WBH)}$ prediction method
			$C_{n_r} = \underbrace{\left(C_{n_r}\right)_{WB}}_{7.3.3.3} + 2 \frac{\left(\Delta C_{n_\beta}\right)_p^2}{\underbrace{\left(\Delta C_{Y_\beta}\right)_{V(WBH)}}_{5.3.1.1}}$ Eq. 7.4.3.3-b	(same limitations as for Eq. 7.4.3.3-a above) $\left(\Delta C_{n_\beta}\right)_p$ 1. Test data
		TRANSONIC	(No method)	
		SUPERSONIC	(No method)	

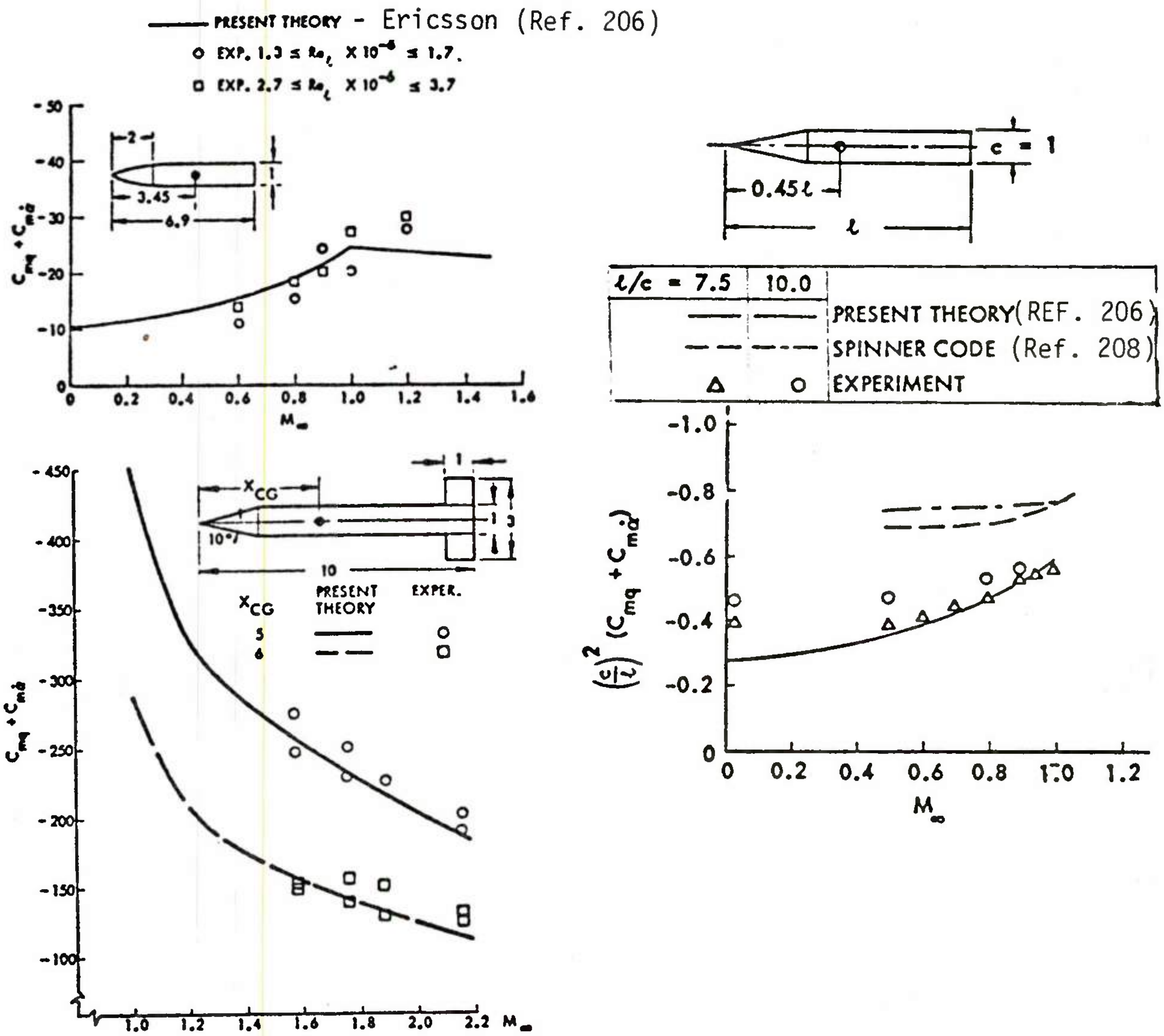

Figure 148. Ericsson Method Comparison

SECTION 10
SPECIALIZED METHODOLOGY

Section 9 of the Missile Datcom Outline, Table 3, covers "specialized" areas of missile aerodynamic analysis. Two specific areas were identified for inclusion, (1) tumbling motion, and (2) spinning motion. Although not required for typical missile aerodynamic design, these techniques will supply methodology to support projectile design (Magnus effect) and test range safety analysis of jettisoned components (tumbling motion).

Tumbling Motion - The simplest techniques found were empirically derived equations and charts to compute the average tumbling drag coefficient of plates, cubes, spheres and cylinders. This technique was assembled by MDAC-HB in Reference 32 and is the recommended approach. Other data available is summarized in Reference 252.

Magnus Effect - The effect of spinning motion has been the subject of comprehensive investigations (References 175, 253-255). A computer program (SPINNER, Reference 208) is available to numerically predict the Magnus effect. A number of theoretical methods include an angle of attack dependency. It is recommended that resalts from the theoretical and semi-empirical techniques be compared with the SPINNER code and test results for accuracy. A method selection can be made once this quantitative analysis is conducted. No specific recommendation is made at this time.

SECTION 11
CONCLUSIONS AND DEVELOPMENT RECOMMENDATIONS

11.1 Feasibility and Development

Based upon established realistic requirements the development of Missile Datcom is feasible. Methodology is available to perform preliminary or conceptual missile aerodynamic design. There is no comprehensive collection of missile design methods available. The assembly and publication of such methods as a handbook is seen as a major requirement to fill this important void.

Existing computer programs are available but they are often limited in applicability, poorly programmed, too complex, or are substantially undocumented. To overcome these problems Missile Datcom should be developed as follows:

a) A handbook and its companion computer program should be developed in parallel. The handbook should include: (1) A brief, but thorough discussion of the physical phenomena being modeled, including a summary of the techniques available and the reasons for choosing the recommended technique. (2) A description of the selected technique including all equations, tables and charts necessary for its use. This description is expected to include the geometric and flight condition range of applicability, data/theory comparisons, and specific recommendations for method interpolation and extrapolation. (3) A bibliography to allow more sophisticated analysis if required.

b) The computer program, developed concurrently with the handbook, should reflect as a minimum the same capability as the handbook. Where methods have been selected for the program, that are more sophisticated, or iterative, a description of the differences between the handbook and programmed techniques should be documented. The program should have the following characteristics: (1) It should be written to conform with the current American National Standards Institute (ANSI) standard FORTRAN computer code for easy use on many computer systems, (2) The code should be structured using the concepts of structured programming as applied to the FORTRAN language. This will insure code readability. (3) The program should be well documented internally, with liberal but effective use of comment cards. This will aid in code development and increase its utility. (4) The program should be modular with the capability

to interchange subroutines. Each subroutine should perform one specific task, such as computing panel lift curve slope at subsonic speeds. A group of routines which perform related computations, such as wing lift at angle of attack and Mach number, should be assembled within the same program segment. This concept will allow easy substitution of alternate methodology or experimental results.

(5) The program should be structured to minimize the number of user inputs required. The input scheme should be easy to use.

(6) The program should be structured to minimize computer execution time and core requirements, thus inexpensive to operate. Setting the maximum computer core at 100,000 octal words, as is presently done for Digital Datcom, is a realistic goal. (7) Finally, a user's manual should be developed which defines the inputs required and the outputs available. It should reference the handbook where possible. All extrapolations of the methods should be clearly identified.

11.2 Recommended Tasks

Those areas which require further method development are summarized in Table 18. The following tasks in decending order of priority should be performed to eliminate major deficiences in missile aerodynamic prediction at the conceptual and preliminary design levels.

A) Development of analytic methods for estimating the stability and control effects of airbreathing inlets. Present and future missile designs emphasize the need for longer cruise range. This requires the use of airbreathing propulsion systems. Section 7 details the present methodology status.

B) Development of analytical methods to determine mutual interference effects at all Mach numbers for the following conditions or configurations:

(1) angle of attack and panel deflection angles recommended in Table 2 where slender-body or conical flow theory is no longer valid. The available theoretical and empirical methods are discussed in Section 5.

(2) swept trailing-edge straight-tapered panels; method substantiation required.

(3) swept forward panels, such as for oblique wings employed on cruise missile class vehicles; no methods available.

(4) non-straight-tapered panels; no methods available

(5) fin panel mutual interference for other than planar or cruciform fin arrangements; no methods available.

C) Development of analytical techniques to determine fin panel normal force and center of pressure at high angles of attack, at all Mach numbers. No theoretical methods are available. Empirical results are limited.

D) Development of easily applied techniques to determine the stability and control characteristics of arbitrary shaped geometries at all speeds. Present methods are too expensive or too difficult to use.

E) Development of analytical techniques to determine the wave/pressure drag of nose shapes other than axisymmetric tangent ogives or cones. Data availability is limited at transonic Mach numbers.

F) Development of analytical techniques to determine the effect of angle of attack, panel deflection and jet exhaust on configuration dynamic stability. Very few methods are available.

The listed deficiencies cause significant shortcomings in missile aerodynamic prediction capability. It is important that these deficiencies be corrected as quickly as possible. Such an effort requires the leadership and support of the United States Air Force.

TABLE 18 GAPS IN METHODOLOGY

- INSTALLED INLET EFFECT AT ALL SPEEDS
- MUTUAL INTERFERENCE FOR SWEPT TRAILING EDGE FINS OR SWEPT FORWARD PANELS
- FIN CHARACTERISTICS AT HIGH ANGLE OF ATTACK
- BODY C_{N_0}, C_{M_0} AT ALL SPEEDS
- ARBITRARY CROSS-SECTION BODIES AT TRANSONIC AND SUPERSONIC SPEEDS
- EFFECT OF NOSE SHAPE ON PRESSURE/WAVE DRAG
- DYNAMICS AT ANGLE OF ATTACK OR PANEL INCIDENCE
- JET EFFECTS ON DYNAMIC DERIVATIVES

NOMENCLATURE

SYMBOL	DEFINITION
LOWER CASE	
a	Body radius
b	Fin span
c	Fin Chord
d	Body diameter; also reference length
e	Oswald's wing efficiency factor
g	Gravitation constant
h	Altitude
i	Interference factor; also fin incidence angle
p	Planform shape parameter; also roll rate, pressure
q	Pitch rate; also dynamic pressure
r	Yaw rate; also body radius
s	Fin span
t	Airfoil thickness
u	Axial component of velocity
v	Lateral component of velocity
w	Vertical component of velocity
x	Longitudinal distance
y	Lateral distance
z	Vertical distance
CAPITALS	
B	Mach similarity parameter
D	Maximum body diameter; also reference length
E	Elliptic integral of the second kind
I	Vortex interference factor
K	Constant of proportionality
M	Mach number
P	Pressure
R_e	Reynolds Number
S	Reference Area
V	Velocity

SYMBOL	DEFINITION
COEFFICIENTS	
C_A	Axial force coefficient; body axis
C_D	Drag coefficient; wind axis
C_f	Local skin friction coefficient
C_{f_i}	Incompressible skin friction coefficient
C_F	Total (average) skin friction coefficient
C_h	Hinge moment Coefficient
C_L	Lift coefficient; wind axis
C_ℓ	Section lift coefficient; wind axis
C_m	Pitching moment coefficient
C_N	Normal force coefficient; body axis
C_n	Yawing moment coefficient; wind axis
C_S	Leading-edge suction coefficient
C_T	Leading-edge thrust coefficient
C_Y	Side force coefficient; wind axis
GREEK	
α	Angle of attack
α_o	Zero lift angle of attack
α^*	Angle of attack limit for linear lift
α'	Total angle of attack
β	Sideslip angle
δ	Deflection angle, or surface slope
γ	Ratio of specific heats for a gas; 1.4 for air
λ	Panel taper ratio; tip chord/root chord
Θ	Panel twist angle
ϕ	Roll angle; or bank angle

SYMBOL	DEFINITION
GENERAL SUBSCRIPTS	
A.C.	Aerodynamic Center
B	Body
(B)	In presence of body
C.P.	Center of pressure
T	Tail
(T)	In presence of tail
Theo	Theoretical
W	Wing
(W)	In presence of wing
WB	Wing-body combination
∞	At free-stream conditions

NON-DIMENSIONAL FACTORS

All forces and moments are non-dimensionalized by the free-stream dynamic pressure and the reference area. The reference area is the maximum cross-sectional area of the body. In addition, the moments are non-dimensionalized by the body maximum diameter. The reference area and length is the same for both longitudinal and lateral-directional aerodynamic coefficients.

The dynamic derivatives are non-dimensionalized by the free-stream dynamic pressure, the reference area and the reference length. In addition, the rate derivatives are non-dimensionalized using the free-stream velocity and the reference length. For example, the dynamic derivative C_{m_q} is non-dimensionalized using

$$\frac{\partial(C_m)}{\partial(\frac{qd}{V})}$$

REFERENCES AND
BIBLIOGRAPHY

1. Hoak, D.E., et al, "USAF Stability and Control Datcom", McDonnell Douglas Corp., Revised, 1978.
2. Pretty, R.T., "Jane's Weapon Systems, 1979-1980", Tenth Edition, 1979.
3. Briggs, M.M., et al, "Aeromechanics Survey and Evaluation", NSWC/DL TR-3772, Vols. I, II and III, October, 1977.
4. Wright, J., "A Compilation of Aerodynamic Nomenclature and Axis Systems", NOLTR-1241, 1962.
5. Hopkin, H.R., "A Scheme of Notation and Nomenclature for Aircraft Dynamics and Associated Aerodynamics", British R&M 3562, Part 4, 1970.
6. Etkin, B., "Dynamics of Flight", John Wiley and Sons, Inc., New York
7. Lessing, H.C., and Butler, J.K., "Wind Tunnel Investigation at Subsonic and Supersonic Speeds of the Static and Dynamic Stability Derivatives of and Airplane Model with an Unswept Wing and a High Horizontal Tail", NASA-MEMO-6-5-59A, 1959.
8. Thelander, J.A., "Aircraft Motion Analysis," FDL-TDR-64-70, 1964.
9. Chemical Propulsion Information Agency, "Airbreathing Propulsion Manual", CPIA/M6, 1977.
10. COESA, "U.S. Standard Atmosphere, 1962", December 1962.
11. Schlichting, H., "Boundary Layer Theory", McGraw Book Company, Inc.
12. Nielsen, J.N., "Missile Aerodynamics", McGraw Hill Book Company, Inc.
13. Peterson, J.B., "A Comparison of Experimental and Theoretical Results for the Compressible Turbulent-Boundary-Layer Skin Friction with Zero Pressure Gradient.", NASA TND-1795, March 1963.
14. Faro, Jone, D.V., "Handbook of Supersonic Aerodynamics,"NAVWEPS Report 1488, Vol. 3, October 1961.
15. Komar, J.J.,"Improved Turbulent Skin-Friction Coefficient Predictions Utilizing the Spalding-Chi Method," Douglas Report DAC-59801 November 1966.
16. Van Driest, E.R., "Turbulent Boundary Layer in Compressible Fluids." J. Aero. Sci., Vol. 18, pp 145-160, March 1951.
17. Van Driest, E.R., "Calculation of the Stability of the Laminar Boundary Layer in a Compressible Fluid on a Flat Plate with Heat Transfer," J. Aero., Sci., Vol. 19, pp 801-812, December 1952.

18. Clutter, D.W., "Charts for Determining Skin-Friction Coefficients on Smooth and on Rough Flat Plates at Mach Numbers up to 5.0 With and Without Heat Transfer," Douglas Aircraft Company Report No. ES29074, April 1959.
19. Clay, J.T., and Sieron, T.R., "Study to Determine Skin-Friction Drag in Hypersonic Low-Density Flow,"ASD-TR-61-433, Vol. 1 April 1962.
20. Dunn, D.W., and Lin, C.C., "On The Stability of the Laminar Boundary Layer in a Compressible Fluid", J. Aero Sci., Vol. 22, pp 455-477, July 1955.
21. Gazeley, C., "Boundary Layer Stability and Transition in Subsonic and Supersonic Flow", J. Aero. Sci., Vol. 20, pp 19-28, January 1953.
22. Landis, F., Fink, M.R., and Rosenberg, M.H., "Boundary-Layer Transition Measurements at Mach Numbers from 5.4 to 7.4", J. Aero. Sci., Vol. 27, pp 719-920, April 1060.
23. Van Driest, E.R., and Boison, J.C., "Experiments on Boundary Layer Transition at Supersonic Speeds", J. Aero. Sci., Vol. 24, pp 885-899, December 1957.
24. Emmons, H.W., "The Laminar-Turbulent Transition in a Boundary-Layer - Part I", J. Aero. Sci., Vol. 18, pp 490-498, July 1951.
25. Probstein R.F., and Elliot, D., "The Transverse Curvature Effect in Compressible Axially Symmetric Laminar Boundary-Layer Flow", J. Aero. Sci., Vol. 23, pp 208-224, March 1956.
26. Eckstrom, D.J., "Engineering Analysis of Boundary Layers and Skin Friction on Bodies of Revolution at Zero Angle of Attack", LMSC/805162 TM 55-21-21, May 1965.
27. Foley, J.E., "CCMD Computer Program for the Computation of Non-Linear Normal Force and Pitching Moment Coefficients by Kelly's Viscous Crossflow Method", ADB-TN-13-64, July 1964.
28. Sternberg, J. "A Free-Flight Investigation of the Possibility of High Reynolds Number Supersonic Laminar Boundary Layers", J. Aero. Sci., Vol. 19, No. 11, pp 721-733, November 1952.
29. Eckert, H. U., "Simplified Treatment of the Turbulent Boundary Layer Along a Cylinder in Compressible Flow ," J. Aero. Sci., Vol. 19, pp 23-28 January 1952.
30. Clark, E., "Aerodynamic Characteristics of the Hemisphere at Supersonic and Hypersonic Mach Numbers," Vol. 7, No. 7, AIAA Journal, Technical Note, 1969, pp 1385.

31. Prandtl, L. and Schlichting, H., "Sas Widerstandsgesetz rauher Platten", Werft-Reederei Hafen, January 1, 1934, No. 1, pp 1-4.
32. MDAC-West, "Aerodynamics Design Handbook," M 8.080-CD, October 1972.
33. Eaton, P.T., "A Method for Predicting the Static Aerodynamic Characteristics of Low-Aspect-Ratio Configurations", DTMB Report 2216, June 1966.
34. Chapman, D.R., and Kester, R.H., "Turbulent Boundary Layer and Skin Friction Measurements in Axial Flow Along Cylinders at Mach Numbers Between 0.5 and 3.6", NACA TN 3097.
35. Stoney, W.E., Jr., "Collection of Zero-Lift Drag Data on Bodies of Revolution from Free-Flight Investigations," NASA TR R-100.
36. Hoerner, S.F., "Fluid Dynamic Drag," Published by Author, 1965.
37. Nichols, J.O., and Nierengarten, E.A., "Aerodynamic Characteristics of Blunt Bodies," JPL TR-32-677, 1965.
38. Owens, R.V., Aerodynamic Characteristics of Spherically Blunted Cones at Mach Numbers from 0.5 to 5.0," NASA TN-D-3088, 1965.
39. Foster, A.D., "A Compilation of Longitudinal Aerodynamic Characteristics Including Pressure Information for Sharp and Blunt Nose Cones Having Flat and Modified Bases," Sandia Corp. Monograph SC-R-64-1311, 1965.
40. DeLeo, R.V., "The Effect of Nose Shape on Missile Nose Drag", Univ. of Minnesota Institute of Technology, 1950.
41. Perkins, E.W., Jorgensen, L.H., and Sommer, S.C., "Investigation of the Drag of Various Axially Symmetric Nose Shapes of Finess Ratio 3 for Mach Numbers from 1.24 to 7.4", NACA Report 1386, 1958.
42. Laurenson, D.I., "A Semi-Empirical Method for Preliminary Estimation of the Drag of Axisymmetric Ballistic Re-Entry Vehicles", General Electric Aerodynamic Data Memorandum 1:24, July 1960.
43. Chaussee, D.S., "Improved Transonic Nose Drag Estimates for the NSWC Missile Aerodynamic Computer Program", NSWC/DL TR-3830, April 1978.
44. Syvertson, C.A., and Dennis, D.H., "A Second-Order Shock Expansion Method Applicable to Bodies of Revolution near Zero Lift", NACA Report 1328, 1957.
45. Kosher, M.M., Cobb, E.R., et.al., "Missile Synthesis and Performance Computer Program (CAMS)", OR 11,245, August 1971.
46. Perkins, E.W., and Jorgensen, L.H., "Investigation of the Drag of Various Axially Symmetric Nose Shapes of Fineness Ratio 3 for Mach Numbers from 1.24 to 3.67", NACA RM A52H28, November, 1952.

47. Jorgensen, L.H., "Prediction of Static Aerodynamic Characteristics for Space Shuttle Like and Other Bodies at Angles of Attack from 0° to 180°", NASA TN-D-6996, 1973.

48. Gentry, A.E., Smyth, D.N., and Oliver, W.R., "The Mark IV Supersonic-Hypersonic Arbitrary Body Program", AFFDL-TR-73-159, November 1973.

49. Krieger, R. J., et al., "Aerodynamic Standard Routine Handbook," MDC-E1630, 1977.

50. Schwartz, L., "Comment on 'Empirical Expressions for Drag Coefficients of Cones at Supersonic Speeds'", AIAA Journal Vol. 7, No. 3 Comments, 1969, p. 572.

51. Moore, F.G., "Body Alone Aerodynamics of Guided and Unguided Projectiles at Subsonic, Transonic and Supersonic Mach Numbers," NWL TR-2796, 1972.

52. Bonney, A.E., "Engineering Supersonic Aerodynamics", McGraw-Hill Book Company, Inc., 1950.

53. Payne, P.R., Hartley, R.M., and Taylor, R.M., "Afterbody Drag", DTNSRDC/ASED-80/10, May, 1980, ASED-80/12, June, 1980.

54. Aoyama, Kinya, and Wu, Jain-Ming, "On Transonic Flow Field Around Ogive Bodies", AIAA Paper 70-189, January, 1970.

55. Jack, J.R., "Theoretical Pressure Distributions and Wave Drags for Conical Boattails", NACA TN-2972, July 1953.

56. Butler, S.F.J., Editor, "Aerodynamic Drag," AGARD-CP-124, 1973, Paper 2.

57. Love, E.S., "Base Pressure at Supersonic Speeds on Two-Dimensional Air-flows and on Bodies of Revolution, With and Without Fins, having Turbulent Boundary Layers," NACA TN-3819, 1957.

58. Aiello, G.F., and Bateman, M.C., "Aerodynamic Stability Technology for Maneuverable Missiles", AFFDL-TR-76-55, Vol. I and II, March 1979.

59. Dow, E.C., and Sarver, R.H., "The Effects of Protuberances and Scaling Parameters on the Aerodynamic Characteristics of an Air-to-Air Cruciform Missile", AIAA Paper 72-969.

60. Williams, J.E., and Vukelich, S.R., "Analysis of Datcom Methods as Applied to Modern Configurations", MDC E2265, May, 1980.

61. Munk, M.M., "The Aerodynamic Forces on Airship Hulls," NACA TN-184, 1924.

62. Lamb, H., "Hydrodynamics," Dover Publications, New York, 1945.

63. Ward, G.N., "Supersonic Flow Past Slender Pointed Bodies," Quart. Journal Mechanics and Appl. Math., Vol. 2, Pt. 1, March 1949.

64. Allen, H.J., "Estimation of Forces and Moments Acting on Inclined Bodies of Revolution of High Fineness Ratio", NACA RM A9126, 1949.

65. Allen, H.J., "Estimation of Forces and Moments Acting on Inclined Bodies of Revolution," NACA RM A50L07, 1951
66. Allen, H.J., and Perkins, E.W., "A study of Effects of Viscosity on Flow over Slender Inclined Bodies of Revolution", NACA Report 1048, 1951.

67. Van Dyke, M.D., "Practical Calculation of Second-Order Supersonic Flow Past Nonlifting Bodies of Revolution," NACA TN-2744, 1952.
68. Van Dyke, M.D., "A Study of Second-Order Supersonic Flow Theory," NACA Report 1081, 1952.
69. Von Karman, T., "The Problem of Resistance in Compressible Fluids", Proc. of Fifth Volta Congress, Rome, 1935.
70. Taylor, G.I., and Maccoll, J.W., "The Air Pressure on a Cone Moving at High Speeds," Proc. Roy. Soc. London, Vol. 139, Series A, 1933.
71. Kopal, Z., et al, "Tables of Supersonic Flow Around Cones," TR No. 1, MIT, 1947.
72. Fenter, F.W., "An Approximate Method for Calculation of the Aerodynamic Characteristics of Ogive-Cylinders near Zero-Lift," Report 390, Defense Research Laboratory, Univ. of Texas, 1957.
73. Goldstein, S., "Modern Developments in Fluid Dynamics," The Charendon Press, Oxford, 1938.
74. Baker, W.B., "Static Aerodynamic Characteristics of a Series of Generalized Slender Bodies With and Without Fins at Mach Numbers from 0.6 to 3.0," AEDC-TR-75-124, 1976.
75. Hill, J.A.F., "Forces on Slender Bodies at Angles of Attack," MIT NSL R-a-100-59, 1950.
76. Kelly, H.R., "The Estimation of Normal Force and Pitching Moment Coefficients for Blunt-Based Bodies of Revolution at Large Angles of Attack," NOTS TM 998, 1953.
77. Schwabe, M., "Pressure Distribution for Nonuniform Two-Dimensional Flow," NACA TM 1039, 1943.
78. Sarpkaya, T., "Separated Flow About Lifting Bodies and Impulsive Flow About Lifting Bodies and Impulsive Flow About Cylinders," AIAA Journal, Vol. 4, No. 3, 1966.
79. Perkins, E.W., and Jorgensen, L.H., "Comparison of Experimental and Theoretical Normal Force Distribtuions on an Ogive-Cylinder Body at Mach Number 1.98," NACA TN-3716, 1956.

80. Mello, J.F., "Investigation of Normal Force Distributions and Wake Vortex Characteristics of Bodies of Revolution at Supersonic Speeds", J. Aero. Space Sci., Vol. 25, No. 3, 1959.

81. Wardlaw, A.B., and Morrison, A.M., "Induced Side Forces at High Angles of Attack," AIAA J. Spacecraft and Rockets, Vol. 13, No. 10, 1976.

82. Wardlaw, A.B., "High Angle of Attack Missile Aerodynamics," AGARD Lecture Series 98, 1979.

83. Fleeman, E.L., and Nelson, R.C., "Aerodynamic Forces and Moments on a Slender Body with a Jet Plume for Angles of Attack up to 180°," AIAA Paper 74-110, 1974.

84. Reding, J.P. and Ericson, L.E., "Minimum Side Forces and Associated Yawing Moments on Slender Bodies", AIAA Paper 79-1647, 1979.

85. Dahlem, V., "Semi-Empirical Prediction Method for Induced Side Forces on Missiles at High Angles of Attack," AIAA Paper 79-25, 1979.

86. Jorgensen, L.H., "A Method for Estimating Static Aerodynamic Characteristics for Slender Bodies of Circular and Non-Circular Cross Sections Alone with Lifting Surfaces at Angles of Attack from 0° to 180°," NASA TN-D-7228, 1973.

87. Jorgensen, L.H., "Prediction of Static Aerodynamic Characteristics for Slender Bodies Alone and With Lifting Surfaces to Very High Angles of Attack", NASA TR-R-474, 1977.

88. Macha, J.M., "Drag of Circular Cylinders at Transonic Mach Numbers," AIAA J. Aircraft, Vol. 14, No. 6, 1977, p.605

89. Darling, J.A., "Handbook of Blunt-Body Aerodynamics, Volume I, Static Stability," NOL-TR-73-225, December 1973.

90. Smith, A.M.O., and Pierce, J., "Exact Solution of the Neumann Problem. Calculation of Non-Circulatory Plane and Axially Symmetric Flows About or Within Arbitrary Boundaries", DAC Report ES 26988, April, 1958.

91. Hess, J.L., and Smith, A.M.O., "Calculation of Non-Lifting Potential Flow About Arbitrary Three-Dimensional Bodies", DAC Report ES 40622, March, 1962.

92. Woodward, F.A., "An Improved Method for the Aerodynamic Analysis of Wing-Body-Tail Configurations in Subsonic and Supersonic Flow", NASA CR-2228, May, 1973.

93. Klopfer, G.H., and Chaussee, D.S., "Numerical Solution of Three Dimensional Transonic Flows around Axisymmetric Bodies at Angle of Attack," NEAR TR-176, February 1979.

94. Van Dyke, M.D., "Practical Calculation of Second-Order Supersonic Flow Past Nonlifting Bodies of Revolution," NACA TN-2744, 1952.

95. Van Dyke, M.D., "A Study of Second-Order Supersonic Flow Theory," NACA Report 1081, 1952.

96. Taylor, G.I., and Maccoll, J.W., "The Air Pressure on a Cone Moving at High Speeds," Proc. Roy. Soc. London, Vol. 139, Series A, 1933.

97. Kopal, Z., et al, "Tables of Supersonic Flow Around Cones," TR No. 1, MIT, 1947.

98. Ames Research Staff, "Equations, Tables, and Charts for Compressible Flow," NACA Report 1135, 1953.

99. Fenter, F.W., "An Approximate Method for the Calculation of the Aerodynamic Characteristics of Ogive-Cylinders near Zero Lift," Report 390, Defense Research Laboratory, Univ. of Texas, 1957.

100. Forehand, J.C., "Method of Exterior Characteristics (JB21)," DAC Memo A2-260-CES-JB21-1, April 1961.

101. Shapiro, A.H., "The Dynamics and Thermodynamics of Compressible Fluid Flow," The Ronald Press, New York, 1953.

102. Polhamus, E.C., "A Concept of the Vortex Lift of Sharp-Edge Delta Wings Based on the Leading-Edge-Suction Analogy", NACA TN D-3767, 1966.

103. Nelms, W.P., Jr., "Effects of Body Shape on the Aerodynamic Characteristics of an All-Body Hypersonic Aircraft Configuration at Mach Numbers from 0.65 to 10.6," NASA TN-D-6821, 1922.

104. Spencer, B., and Phillips, W.P., "Transonic Aerodynamic Characteristics of a Series of Bodies Having Variations in Fineness Ratio and Cross-Sectional Ellipticity," NASA TN-D-2622, 1965.

105. Spencer, B., "Transonic Aerodynamic Characteristics of a Series of Related Bodies with Cross-Sectional Ellipticity," NASA TN-D-3203, 1966.

106. Fournier, R.H., and Spencer, B., "Supersonic Aerodynamic Characteristics of a Series of Related Bodies with Cross-Sectional Ellipticity," NASA TN-D-3539, 1966.

107. Fuller, D.E., Shaw, D.S., and Wassum, D.L., "Effect of Cross-Section Shape on the Aerodynamic Characteristics of Bodies at Mach Numbers from 2.50 to 4.63," NASA TN-D-1620, 1963.

108. Williams, L.J., "Estimated Aerodynamics of All-Body Hypersonic Aircraft Configurations", NASA TM-X-2091, 1971.

109. Sidwell, K.W., and Baruah, P.K., "Pan Air - A Computer Program for Predicting Subsonic or Supersonic Linear Potential Flows About Arbitrary Configurations Using a Higher Order Panel Method," NASA-CR-3552, 1980.

110. Gregoire, J.E., and Krieger, R.J., "Aerodynamic Prediction Rationale for Advanced Arbitrarily Shaped Missile Concepts," AIAA Paper 80-0256, 1980.

111. Landrum, E.J., and Miller, D.S., "Assessment of Analytic Methods for the Prediction of Aerodynamic Characteristics of Arbitrary Bodies at Supersonic Speeds," AIAA Paper 80-071, 1980.

112. Chapman, D.R., "An Analysis of Base Pressure At Supersonic Velocities and Comparison with Experiments", NACA Report 1051, 1951.

113. Cubbage, J.M., Jr., "Jet Effects on Base and Afterbody Pressures of a Cylindrical Afterbody at Transonic Speeds," NACA RML56C21, May 1956.

114. Cubbage, J.M., Jr., "Jet Effects on the Drag of Conical Afterbodies for Mach Numbers of 0.6 to 1.28", NACA RM L57B21, April 1957.

115. Maise, G., "Wave Drag of Optimum and Other Boattails," AIAA J.A., Vol. 7, No. 5, 1970.

116. Winter, K.G., and Gaudet, L., "Turbulent Boundary-Layer Studies at High Reynolds Numbers at Mach numbers between 0.2 and 2.8", RAE Technical Report 70251, 1970.

117. Barkhem, A., "Skin Friction Formula for Tapered and Delta Wings," AIAA J. Aircraft, Vol. 6, No. 3, 1969, p. 284

118. Vondrasek, D., "Combined Skin Friction and EN-30 Wave Drag Program for Advanced Design," Memo 241-4940, 11 Mar 75.

119. Benepe, D.B., Kouri, B.G., Webb, J.B., et al, "Aerodynamic Characteristics of Non-Straight-Tapered Wings", AFFDL-TR-66-73, 1966.

120. Bonney, E.A., "Aerodynamic Characteristics of Rectangular Wings at Supersonic Speeds," Jour, Aero Sci., Vol. 14, No. 2, Feb 1947.

121. Puckett, A.E., and Stewart, H.J., "Aerodynamic Performance of Delta Wings at Supersonic Speeds," Jour. Aero. Sci., Vol. 14, No. 10, Oct 1947.

122. Beane, B., "The Characteristics of Supersonic Wings Having Biconvex Sections", Jour. Aero Sci., Vol. 18, No. 1, Jan 1951.
123. Puckett, A.E., "Supersonic Wave Drag of Thin Airfoils", Jour, Aero Sci., Vol. 13, No. 9, Sept. 1946.
124. Margolis, K., "Supersonic Wave Drag of Nonlifting Sweptback Tapered Wings with Mach Lines behind the Line of Maximum Thickness," NACA TN 1672, 1948.
125. Bishop, R.A., and Cane, E.G., "Charts of the Theoretical Wave Drag of Wings at Zero-Lift," RAE, TN 2421, 1956.
126. Jones, R.T., "Thin Oblique Airfoils at Supersonic Speed," NACA TN 1107, 1946.
127. R.A.S. Data Sheets: Wings, S.00.03.04.
128. Carafoli, Elie, "Wing Theory in Supersonic Flow", Pergamon Press, 1969.
129. R.A.S. Data Sheets: Wings, S.02.03.01.
130. Pike, J., "Moments and Forces on General Convex Bodies in Hypersonic Flow," AIAA J., Vol. 12, No. 9, p. 1241, 1974.
131. Moore, F.G., "Static Aerodynamics of Missile Configurations for Mach 0. to 3.0" AIAA J.A., 1975, Vol. 12, No. 10, pp 797-806.
132. Crosthwait, E.L., "Drag of Two-Dimensional Cylindrical Leading Edges," General Dynamics, F/W Rpt. AIM No. 50, 1966.
133. R.A.S. Data Sheets: Wings S.02.03.10.
134. Chapman, D.R., Wimbrow, W.R., and Kester, R.H., "Experimental Investigation of Base Pressure on Blunt-Trailing-Edge Wings at Supersonic Velocities," NACA Rpt. 1109, 1952.
135. Saffell, B.F., Howard, M.L., and Brooks, E.N., "A Method for Predicting the Static Aerodynamic Characteristics of Typical Missile Configurations for Angles of Attack to 180 degrees", NSRDC Aero Report 1168, 1971.
136. Lowry, J.G., and Polhamus, E., "A Method for Predicting Lift Increments Due to Flap Deflection at Low Angles of Attack in Incompressible Flow," NACA TR 3911, 1957.
137. Abbott, I.H., and Van Doenhoff, A.E., "Theory of Wing Sections," Dover Publications, 1959.
138. Multhopp, H., "Methods for Calculating Lift Distribution of Wings", ARC R&M 2884, 1950.
139. Moore, F.G., "Aerodynamics of Guided and Unguided Weapons", NWL-TR-3018, 1973.

140. Spencer, B.J., "A Simplified Method for Estimating Subsonic Lift-Curve Slope at Low Angles of Attack for Irregular Planform Wings," NASA TMX-525, 1961.

141. Nielsen, J.N., Hemsch, M.J., and Smith, C.A., 'Preliminary Method for Calculating the Aerodynamic Characteristics of Cruciform Missiles to High Angles of Attack Including Effects of Roll Angle and Control Deflections," NEAR TR-152, 1977.

142. Stallings, R.L., and Lamb, M., "Wing Alone Aerodynamic Characteristics at High Angles of Attack", AIAA Paper 81-008, 1981.

143. Harmon, S.M., and Jeffreys, I., "Theoretical Lift and Damping in Roll of Thin Wings with Arbitrary Sweep and Taper at Supersonic Speeds. Supersonic Leading and Trailing Edges," NACA TN 2114, 1950.

144. Malvestuto, F.S., Margolis, K., and Ribner, H.S., "Theoretical Lift and Damping in Roll at Supersonic Speeds of Thin Sweptback Tapered Wings with Streamwise Tips, Subsonic Leading Edges, and Supersonic Trailing Edges," NACA TR 970, 1950.

145. Lapin, E., "Charts for the Computation of Lift and Drag of Finite Wings at Supersonic Speeds," Douglas Aircraft Company Report SM-13480, 1949.

146. Cohen, D., "Formulas for the Supersonic Leading, Lift, and Drag of Flat Sweptback Wings with Leading Edges Behind the Mach Lines," NACA TR 1050, 1951.

147. Jones, R.T., "Properties of Low-Aspect-Ratio Pointed Wings at Speeds Below and Above the Speed Sound," NACA TR 835, 1946.

148. Mangler, K.W., "Calculation of the Pressure Distribution Over a Wing at Sonic Speeds," ARC R&M 2888, 1955.

149. Mirels, H., "Aerodynamics of Slender Wings and Wing-Body Combinations Having Swept Trailing Edges," NACA TN 3105. 1954.

150. Heaslet, M.A., and Spreiter, J.R., "Reciprocity Relations in Aerodynamics", NACA TR 1119, 1953.

151. Squire, L.C., "Some Applications of Not-So-Slender Wing Theory to Wings with Curved Leading Edges," ARC R&M 3278, 1962.

152. Lamar, J.E., "Design Charts of Static and Rotary Stability Derivatives for Cropped Double-Delta Wings in Subsonic Compressible Flow", NASA TN D-5661, 1970.

153. Polhamus, E.C., "Application of the Leading-Edge-Suction Analogy of Vortex Lift to the Drag Due to Lift of Sharp-Edge Delta Wings," NASA TN D-4739.

154. Polhamus, E.C., "Predictions of Vortex-Lift Characteristics by a Leading-Edge Suction Analogy," AIAA J. of Aircraft, Vol. 8, No. 4, April 1971.
155. Lamar, J.E., "A Modified Multhopp Approach for Predicting Lifting Pressures and Camber Shape for Composite Planforms in Subsonic Flow," NASA TN D-4427, 1968.
156. Lamar, J.E., "Prediction of Vortex Flow Characteristics of Wings at Subsonic and Transonic Speeds," AIAA Paper 75-249, January, 1975.
157. Polhamus, E.C., "Charts for Predicting the Subsonic Vortex-Lift Characteristics of Arrow, Delta, and Diamond Wings", NASA TN D-6243, 1971.
158. Lecat, R., and Rietschlin, J., "Goniometric Aerodynamics; A Different Perspective: Description - Applications", AIAA Paper 79-1650.
159. Oberkampf, W.L., "Prediction of Forces and Moments on Finned Missiles in Subsonic Flow", AIAA Paper 79-365.
160. Bradley, R.G., et al, "Vortex-Lift Prediction for Complex Wing Planforms", AIAA J. of Aircraft, Vol. 10, No. 6, June 1973, pp. 379-381.
161. Meyer, R.D., "Wrap Around Fins: Design Considerations", AIAA Paper 76-942.
162. Dahlke, C.W., and Craft, J.C., "Aerodynamic Characteristics of Wrap Around Fins Mounted on Bodies of Revolution and their Influence on the Missile Static Stability at Mach Numbers from 0.3 to 1.3," RD-TM-72-1, Army Missile Command, March 1972.
163. Dunkin, O.L., "Effects of Fin Folding Angle and Leading-Edge Sweep Angle on the Aerodynamic Characteristics of Missiles Equipped with Wrap Around Fins at Mach Numbers from 0.5 to 1.3", AEDC-TR-73-191.
164. Fournier, R.H., "Supersonic Aerodynamic Characteristics of a Series of Wrap-Around-Fin Missile Configurations", NASA-TM-X-3451, March 1977.
165. Humphrey, J.A., and Dahlke, C.W., "Summary of Aerodynamic Characteristics for Wrap-Around Fins from Mach 0.3 to 3.0," Army Research and Development Report TD-77-55, March, 1977.
166. Hill, W.A., "Experimental Lift of Low-Aspect Ratio Triangular Wings at Large Angles of Attack and Supersonic Speeds," NACA RM A57I17, 1957.
167. Pitts, W.C., Nielsen, J.N., Kaattari, G.E., "Lift and Center of Pressure of Wing-Body-Tail Combinations at Subsonic, Transonic, and Supersonic Speeds," NACA-RPT-1307, 1959.
168. Graham, R.E., and McDowell, J.L., "Simplification of the Wing-Body Interference Problem", Jour. of Aircraft Vol. 9, No. 10, October 1972.

169. Spreiter, J., "The Aerodynamic Forces on Slender Plane and Cruciform Wing and Body Combinations," NACA TR 962, 1950.

170. Vukelich, S.R, and Williams, J.E., "Wing-Body Carry-Over at Supersonic Speeds with Finite Afterbodies," AIAA Journal, Vol. 19, No. 5, May 1981, p. 661

171. Nielsen, J.N., and Pitts, W.C., "Wing-Body Interference at Supersonic Speeds with An Application to Combinations with Rectangular Wings," NACA TN 2677, 1952.

172. Moore, F.G., and Swanson, R.C., "Aerodynamics of Tactical Weapons to Mach Number 3 and Angle of Attack 15^{0}, Part I - Theory and Application," NSWC/DL TR-3584, 1977.

173. Hill, W.A., and Kaattari, G.E., "Force and Pressure - Distribution Investigation to High Angles of Attack on All-Movable Triangular and Rectangular Wings in Combination with a Body at Supersonic Speeds," NACA RM A56C12, July 1956.

174. Decker, J.L., "Prediction of Downwash at Various Angles of Attack for Arbitrary Tail Locations," Aeronautical Engineering Review, Vol. 15, No. 8, 1956.

175. Spreiter, J.R., and Sacks, A.H., "The Rolling-up of the Trailing Vortex Sheet and Its Effect on the Downwash Behind Wings", Journal of the Aeronautical Sciences, January 1951.

176. Hemsch, M.J. et.al., "Component Aerodynamic Characteristics of Banked Cruciform Missiles with Arbitrary Control Deflections," AIAA Paper 77-1153.

177. Dillenius, M.F.E., and Nielsen, J.N., "Supersonic Lifting Surface Program for Cruciform Wing-Body Combinations in Combined Pitch and Sideslip," NEAR TR-74.

178. Hemsch, M.J., Nielsen, J.N., and Dillenius, M.F.E., "Method for Calculating Induced Rolling Moments for Cruciform Canard Missiles At Angles of Attack Up to 20°," NWC TP-5761 (NEAR TR 85).

179. Dillenius, M.F.E., and Nielsen, J.N., "Prediction of Aerodynamics of Missiles at High Angles of Attack In Supersonic Flow," NEAR TR 99.

180. Hemsch, M.J., et al, "Calculation of Component Forces and Moments of Arbitrarily Banked Cruciform Missiles with Control Deflection," ONR-CR215-226-3.

181. Spahr, J.R., "Contribution of the Wing Panels to the Forces and Moments of Supersonic Wing-Body Combination at Combined Angles", NACA TN 4146
182. Mendenhall, M.R., and Nielsen, J.N., "Effect of Symmetrical Vortex Shedding On the Longitudinal Aerodynamic Characteristics of Wing-Body-Tail Combinations," NASA CR-2473
183. Dillenius, M.F.E., and Nielsen, J.N., "Computer Programs For Calculating Pressure Distributions Including Vortex Effects On Supersonic Monoplane or Cruciform Wing-Body-Tail Combinations With Round or Elliptical Bodies", NASA CR-3122.
184. Flaherty, J. I., "An Analysis of High Angle of Attack Missile Aerodynamics at Subsonic Flow Mach Numbers," AIAA Paper 70-1648.
185. Thomson, K. D., and Morrison, D. F., "The Spacing, Position and Strength of Vorticies in the Wake of Slender Cylindrical Bodies at Large Incidence," J. Fluid Mech., Vol. 50, part 4, pp 751-783.
186. Chapman, D. R., "Laminar Mixing of a Compressible Fluid," NACA Report 958, 1950.
187. Addy, A. L., "Experimental Theoretical Correlation of Supersonic Jet-On Base Pressure for Cylindrical Afterbodies," AIAA Journal of Aircraft, 1970, p. 474.
188. Korst, H. H., et al, "Research on Transonic and Supersonic Flow of a Real Fluid at Abrupt Increases in Cross Section," University of Illinois Report ME-TN-392-5, 1959.
189. Addy, A. L., "Analysis of the Axisymmetric Base-Pressure and Base-Temperature Probelm with Supersonic Interacting Freestream-Nozzle Flows Based on the Flow Model of Korst, et al; Part 1: A Computer Program and Representative Results for Cylindrical Afterbodies," Report RD-TR-69-12, U.S. Army Missile Command, July, 1969.
190. Krieger, R. J., "Simplified Base Pressure Prediction Technique," MDAC-E Memorandum E241-160, August 1970.
191. McMillan, O. J., Perkins, S. C., Perkins, E. W., and Kuhn, G. D., "Data Base for the Prediction of Airbreathing Missile Airframe/Propulsion System Interference Effects (U)," NWC-TP-6136, April 1980 (Confidential)
192. Kinroth, G. D., and Anderson, W. R., "Ramjet Design Handbook," CPIA-319, February 1980. (AFWAL TR-80-2003).

193. Goin, K. L., "Equations and Charts for the Rapid Estimation of Hinge Moment and Effectiveness Parameters for Trailing-Edge Controls Having Leading and Trailing Edges Swept Ahead of the Mach Lines," NACA TR-1041, 1951.

194. Popinski, Z., and Ehrlich, C. F., "Development of Design Methods for Predicting Hypersonic Aerodynamic Control Characteristics," AFFDL-TR-66-85, 1966.

195. Barnes, J. W., Davis, J. G., and Tang, H. H., "Control Effectiveness of Transverse Jets Interacting with a High-Speed Free Stream,"AFFDL-TR-67-90, 1967.

196. Grunnet, J., "Factors Affecting the Magnitude of Jet Interaction Forces," AIAA J. of Spacecraft and Rockets, Vol. 8, No. 2, 1971, pp. 1234-1235.

197. Nunn, R., "Jet Interaction Wrap-Around on Bodies of Revolution," AIAA J. of Spacecraft and Rockets, Vol. 7, No. 3, 1970, p. 334.

198. Spangler, S. B., and Mendenhall, M. R., "Further Studies of Aerodynamic Loads at Spin Entry," ONR-CR 212-225-3 (NEAR TR-141), July 1977.

199. Nielsen, J. N., "Nonlinearities in Missile Aerodynamics," AIAA Paper 78-20, 1978.

200. Bryson, A. E., "Stability Derivatives for a Slender Missile with Application to a Wing-Body-Vertical-Tail Configuration," J.A.S., Vol. 20, No. 5, May 1953, pp. 297-308.

201. Sacks, A. H., "Aerodynamic Forces, Moments and Stability Derivatives for Slender Bodies of General Cross Section," NACA TN-3283.

202. Liu, D. D., Platzer, M. F., and Ruo, S. Y., "On the Calculation of Static and Dynamic Stability Derivatives for Bodies of Revolution at Subsonic and Transonic Speeds," AIAA Paper 70-190, 1970.

203. Moore, F. G., and Swanson, R. C., "Dynamic Derivatives for Missile Configurations to Mach Number Three," J. of Spacecraft and Rockets, Vol. 15, No. 2, 1978, pp. 65-66.

204. Ericsson, L. E., "Effect of Mach Number on Slender Vehicle Dynamics," AIAA Paper 80-0362, 1980.

205. Ericsson, L. E., "Viscous Effects on Missile Aerodynamics at Low Angles of Attack," AIAA Paper 80-1378, 1980.

206. Ericsson, L. E., "Wing-Body Pitch Damping at Arbitrary Mach Number," AIAA Paper 80-1801, 1980.
207. Langham, T. F., "Missile Motion Sensitivity to Dynamic Stability Derivatives," AEDC-TR-80-11, September 1980.
208. Whyte, R. H., "Spinner - A Computer Program for Predicting the Aerodynamic Coefficients of Spin Stabilized Projectiles," General Electric Class 2 Reports, 1966.
209. Royal Aeronautical Society Data Sheets: Wings 5.08.03.02.
210. Toll, T. A., and Queijo, M. J., "Approximate Relations and Charts for Low-Speed Stability Derivatives of Swept Wings," NACA TN-1581, 1948.
211. Dorrance, W. H. "Nonsteady Supersonic Flow About Pointed Bodies of Revolution," Jour. of Aero. Sci., Vol. 18, No. 8, 1951.
212. Ohman, L. H. "A Surface Flow Solution and Stability Derivatives for Bodies of Revolution in Complex Supersonic Flow, Part 1 - Theory and Some Representative Results," NRL LR-418, 1964.
213. Ohman, L. H. "A Surface Flow Solution and Stability Derivatives for Bodies of Revolution in Complex Supersonic Flow, Part II - Results for Two Families of Bodies of Revolution for $1.1 \leq M \leq 5$," NRL LR-419, 1964
214. Platzer, M. F., and Sherer, A. D., "Dynamic Stability Analysis of Bodies of Revolution in Supersonic Flow," AIAA Paper 67-607, 1967.
215. Platz, M. F., and Hoffman, G. H., "Quasi-Slender Body Theory for Slowly Oscillating Bodies of Revolution in Supersonic Flow," NASA TN D-3440, 1966.
216. Smith, C. B., and Beane, B. J.,"Damping in Pitch of Bodies of Revolution at Supersonic Speeds," IAS Preprint 311, 1951.
217. Wood, R.M., and Murphy, C.H., "Aerodynamic Derivatives for Both Steady and Nonsteady Motion of Slender Bodies," Jour. of Aero. Sci., Vol. 22, No. 12, 1955.
218. Fisher, L. R., "Equations and Charts for Determining the Hypersonic Stability Derivatives of Combinations of Cone Frustums Computed by Newtonian Impact Theory," NASA TN D-149, 1959.
219. Kind, R. J., and Orlik-Ruckermann, K, "Stability Derivatives of Sharp Cones in Viscous Hypersonic Flow," NRC LR-427. 1965.
220. Quinn, B., "The Hypersonic Roll Damping Derivative of a Blunt Cone," ARL 68-0137, 1968.

221. Walchner, O., and Clay, J. T., "Hypersonic Stability Derivatives of Blunted Slender Cones," AIAA Journal, Vol. 8. No. 4, April 1965.
222. Bird, J. D., "Some Theoretical Low-Speed Span Loading Characteristics of Swept Wings in Roll and Sideslip," NACA TN 1938, 1949.
223. Bird, J. D., "Some Theoretical Low-Speed Span Loading Characteristics of Swept Wings in Roll and Sideslip," NACA TR 969, 1950.
224. Fisher, L. R., "Approximate Corrections for the Effects of Compressibility on the Subsonic Stability Derivatives of Swept Wings," NACA TN 1854, 1949.
225. Landahl, M. T., "The Flow Around Oscillating Low Aspect Ratio Wings at Transonic Speeds," Royal Institude of Technology, KTH Aero TN 40, 1954.
226. Polhamus, E. C., "A Simple Method of Estimating the Subsonic Lift and Damping in Roll of Sweptback Wings," NACA TN 1862, 1949.
227. Tobak, M., and Lessing, H. C., "Estimation of Rotary Stability Derivatives at Subsonic and Transonic Speeds," AGARD Report 343, 1961.
228. Hui, W. H., "Stability Derivatives of Sharp Wedges in Viscous Hypersonic Flow Including the Effects of Thickness and Wave Reflection," University of Southampton, AASU Rept. 278, 1967.
229. Lehrian, D. E., "Calculation of Stability Derivatives for Oscillating Wings," ARC R&M 2922, 1956.
230. Pearson, H. A., and Jones, R. T., "Theoretical Stability and Control Characteristics of Wings with Various Amounts of Taper and Twist," NACA TR 635, 1938.
231. Cole, I. J., and Margolis, K., "Lift and Pitching Moment at Supersonic Speeds Due to Constant Vertical Acceleration for Thin Sweptback Tapered Wings with Streamwise Tips. Supersonic Leading and Trailing Edges," NACA TN 3196, 1954.
232. Brown, C. E., and Adams, M. C., " Damping in Pitch and Roll of Triangular Wings at Supersonic Speeds," NACA TR 892, 1948.
233. Harmon, S. M., "Stability Derivatives at Supersonic Speeds of Thin Rectangular Wings with Diagonals Ahead of Tip Mach Lines," NACA TR 925, 1949.
234. Harmon, S. M., "Stability Derivatives of Thin Rectangular Wings at Supersonic Speeds," NACA TN 1706, 1948.

235. Harmon, S. M., and Jeffreys, I., "Theoretical Lift and Damping in Roll of Thin Wings with Arbitrary Sweep and Taper at Supersonic Speeds - Supersonic Leading and Trailing Edges," NACA TN 2114, 1950.
236. Henderson, A., Jr., "Pitching-Moment Derivatives C_{m_q} and C_{m_α} at Supersonic Speeds for a Slender-Delta-Wing and Slender-Body Combination and Approximate Solutions for Broad-Delta-Wing and Slender-Body Combinations," NACA TN 2553, 1951.
237. Hoerner, S., "Forces and Moments on a Yawed Airfoil,"NACA TM906, 1939
238. Ribner, H., "The Stability Derivatives of Low-Aspect-Ratio Triangular Wings at Subsonic and Supersonic Speeds," NACA TN 1423, 1947.
239. Ribner, H., "The Stability Derivatives of Low-Aspect-Ratio Triangular Wings at Subsonic and Supersonic Speeds," NACA TN 1423, 1947.
240. Ribner, H. S., and Malvestuto, F. S., Jr., "Stability Derivatives of Triangular Wings at Supersonic Speeds," NACA TR 908, 1948.
241. Malvestuto, F. S., Jr. Margolis, K., and Ribner, H. S., "Theoretical Lift and Damping in Roll of Thin Sweptback Wings of Arbitrary Taper and Sweep at Supersonic Speeds - Subsonic Leading Edges and Supersonic Trailing Edges," NACA TN 1860, 1950.
242. Malvestuto, F. S., Jr., and Margolis, K., "Theoretical Stability Derivatives of Thin Sweptback Wings Tapered to a Point with Swept-forward Trailing Edges for a Limited Range of Supersonic Speeds," NACA TR971, 1950.
243. Mangler, K. W., "A Method of Calculating the Short-Period Longitudinal Stability Derivatives of a Wing in Linearized Unsteady Compressible Flow," ARC R&M 2924, 1947.
244. Margolis, K., and Babbitt, P. J., "Theoretical Calculations of the Stability Derivatives at Supersonic Speeds for a High-Speed Airplane Configuration," NACA RM L53G17, 1953.
245. Martin, J. C., Margolis, K., and Jeffreys, I., "Calculation of Lift and Pitching Moments Due to Angle of Attack and Steady Pitching Velocity at Supersonic Speeds for Thin Sweptback Tapered Wings with Streamwise Tips and Supersonic Leading and Trailing Edges," NACA TN 2699, 1952.
246. Martina, A. P., "Method for Calculating the Rolling and Yawing Moments Due to Rolling for Unswept Wings with or Without Flaps or Ailerons by Use of Nonlinear Section Lift Data," NACA TN 2937., 1953.

247. Malvestuto, F. S., Jr., and Hoover, D. M.," Lift and Pitching Derivatives of Thin Sweptback Tapered Wings with Streamwise Tips and Subsonic Leading Edges at Supersonic Speeds," NACA TN 2294, 1951.

248. Malvestuto, F. S., Jr., and Hoover, D. M., "Supersonic Lift and Pitching Moment of Thin Sweptback Tapered Wings Produced by Constant Vertical Acceleration - Subsonic Leading Edges and Supersonic Trailing Edges," NACA TN 2315, 1951.

249. Malvestuto, F. S., Jr., Margolis, K., and Ribner, H. S., "Theoretical Lift and Damping in Roll at Supersonic Speeds of Thin Sweptback Tapered Wings with Streamwise Tips, Subsonic Leading Edges, and Supersonic Trailing Edges," NACA TR 970, 1950.

250. Jones, A. L., and Alksne, A., "The Damping Due to Roll of Triangular, Trapezoidal, and Related Plan Forms in Supersonic Flow," NACA TN 1548, 1948.

251. Piland, R. O., "Summary of the Theoretical Lift, Damping-in-Roll, and Center-of-Pressure Characteristics of Various Wing Plan Forms at Supersonic Speeds," NACA TN 1977, 1949.

252. Wortman, A., "Aerodynamics of Randomly Tumbling Bodies," AIAA J.S.R., Vol. 6, No. 2, 1964, p. 205.

253. Power, H., and Iverson, J., "Magnus Effect on Spinning Bodies of Revolution," AIAA J., Vol, 11, No. 4, 1973, p. 417.

254. Vaught, H., and Reis, G., "A Magnus Theory," AIAA J., Vol. 11, No. 10, 1973, p. 1396.

255. Iverson, J. D., "Correlation of Magnus Force Data for Slender Spinning Cylinders," AIAA JSR, VOl. 10, 1973, No. 4, p. 268.

☆U.S.Government Printing Office: 1983 — 659-006/3013